# A THREE-DIMENSIONAL MODEL OF ATMOSPHERIC $CO_2$ TRANSPORT BASED ON OBSERVED WINDS: 1. ANALYSIS OF OBSERVATIONAL DATA

Charles D. Keeling[1], R. B. Bacastow[1], A. F. Carter[1], S. C. Piper[1], Timothy P. Whorf[1], Martin Heimann[2], Willem G. Mook[3] and Hans Roeloffzen[3]

*Abstract.* Temporal and spatial patterns of atmospheric carbon dioxide elucidate the global carbon cycle as it functions on time scales ranging from days to decades. In preparation for interpreting these patterns with a three-dimensional model of atmospheric tracer transport, we have summarized $CO_2$ measurements obtained by the Scripps Institution of Oceanography since 1957 from an array of stations between the Arctic Basin and the South Pole. Ten stations contributed to the array, supplemented by sampling on ships and ice floes. After applying consistent calibrating criteria to the full set of data, we have decomposed each record into an annually periodic signal and a seasonally adjusted time series, smoothed to emphasize interannual variations. We have computed harmonic coefficients to express the average seasonal cycle. We have determined seasonally adjusted concentrations for 1962, 1968, and annually from 1978 to 1986, to reflect slowly varying characteristics of the carbon cycle, and we have assembled these data in north-to-south profiles to reveal spatial patterns. We have similarly assembled isotopic data derived from measurements of the $^{13}C/^{12}C$ isotopic ratio of atmospheric $CO_2$, made always on the same air measured for its $CO_2$ concentration. We have extended the data sets for stations at Mauna Loa Observatory, Hawaii and the South Pole through 1988 to create a continuous time series which approximates the global change in $CO_2$ concentration over 32 years and the isotopic ratio over 11 years. To establish interannual changes in the carbon cycle, we have developed a compartment model which treats the transfers of carbon between global atmospheric and terrestrial biospheric carbon pools, and between these pools and a world ocean in which vertical transport occurs by diffusion. In a variant to this model the oceanic submodel was replaced with a three-dimensional oceanic transport model. Both the concentration and isotopic ratio of $CO_2$ show clearly defined seasonal cycles and evidence that the carbon cycle responds to El Niño events that recur in the records approximately every 4 years. According to the isotopic data, oscillations in $CO_2$ associated with El Niño events are produced by opposing oceanic and biospheric fluxes several times larger than the net fluxes inferred from the $CO_2$ concentration data alone. On a longer time scale the concentration data show a weak, approximately 11 year, cycle possibly driven by variations in solar irradiance. On a still longer time scale the data indicate that a larger apparent fraction of $CO_2$ from fossil fuel combustion has been retained in the air during the past 14 years than formerly, in spite of a reduced acceleration in worldwide fuel consumption which, according to the compartment model, should have led to a lesser retention in the air after 1974. The isotopic records suggest that this increased retention is partially a result of ocean warming, but is predominantly caused by an accelerated release of $CO_2$ by the terrestrial biosphere.

## 1. Introduction

At locations remote from fossil fuel combustion and vigorous plant activity, direct measurements of atmospheric carbon dioxide show evidence of a persistent increase in concentration from year to year. At most locations a superimposed seasonal oscillation is also observed.

One of the longest records, at Mauna Loa Observatory, Hawaii, shows a 12 percent increase in the mean annual concentration in 31 years, from 315 parts per million by volume of dry air (ppm) in 1958 to 352 ppm in 1989. Similar increases are seen elsewhere. The rise, which is evidently global in extent, is mainly due to the combustion of fossil fuels. The seasonal oscillation, whose peak to peak amplitude varies regionally from 1 to 15 ppm, is mainly a result of the photosynthesis and respiration of the land biota.

Less obvious are interannual variations in the observations which neither correlate with the combustion of fossil fuels nor reflect the average seasonal cycle of plants. These variations, although sometimes only a few tenths ppm, nevertheless reflect significant transfers of carbon to and from the atmosphere. Study of these variations may reveal important characteristics of the global carbon cycle such as changing agricultural and forestry practices and responses to climate.

In addition to temporal variations small spatial variations in $CO_2$ are seen when mean annual or long-term averaged atmospheric data from remote stations are compared. A prominent feature at present is a concentration difference of 3 ppm between the South Pole and the Arctic Basin. In part it exists because fossil fuels are combusted mainly in the northern hemisphere, but its magnitude

[1]Scripps Institution of Oceanography, La Jolla, California 92093, U.S.A.
[2]Max-Planck-Institut für Meteorologie, Bundesstrasse 55 D-2000 Hamburg 13, FRG
[3]Laboratorium voor Algemene Natuurkunde, Rijksuniversiteit, Westersingel 34 9718 CM Groningen, The Netherlands

and time variation are not readily explained by fossil fuel combustion alone. Other smaller scale spatial features are also not readily attributed to fuel combustion.

It is worthwhile to identify the causes of these small systematic variations in $CO_2$ concentration which must be produced by $CO_2$ gas exchanging with either the land biota (the "terrestrial biosphere") or with the oceans. Although nature has not provided us with a direct means to distinguish between biospheric and oceanic exchanges, some help is afforded by rare, but stable, isotopic carbon-13. This isotope is strongly fractionated kinetically, relative to the abundant isotope, carbon-12, when land plants withdraw $CO_2$ from the air during photosynthesis, but it is passed back to the air with little or no further fractionation when these plants and their degradation products in soils respire $CO_2$. Therefore $CO_2$ of plant origin is isotopically distinct from atmospheric $CO_2$. On the other hand when $CO_2$ passes between the air and the oceans, kinetic isotopic fractionation is a factor of 10 smaller than photosynthetic fractionation. Thus airborne $CO_2$ of oceanic origin is hardly distinguishable isotopically from atmospheric $CO_2$. By measuring both the concentration and isotopic ratio of atmospheric $CO_2$ on the same samples of air, it is therefore possible to determine whether variations in concentration are a result of gains and losses of $CO_2$ of plant origin or oceanic origin. With respect to the stable isotopes, $CO_2$ from fossil fuel is indistinguishable from plant carbon, however, so that independent knowledge of industrial $CO_2$ sources is needed before the contribution of biospheric processes to $CO_2$ variations can be established.

Until recently, very few isotopic measurements of atmospheric $CO_2$ accompanied concentration measurements, and even now only a few isotopic records are long enough to establish interannual variations in conjunction with concentration variations. The data are adequate, however, to establish broadly how the mean annual isotopic ratio and isotopic seasonal oscillation vary spatially, at least with latitude. The more extensive $CO_2$ concentration records, on the other hand, better reveal long-term and global patterns. Therefore we used these records, even if they lack isotopic data.

To interpret atmospheric $CO_2$ data realistically requires that its transport be accounted for. We must predict how the atmospheric circulation modifies the $CO_2$ distribution produced locally by oceanic and terrestrial biospheric exchanges. In an article which follows, Heimann and Keeling [this volume] describe a three-dimensional tracer transport model which addresses this need. Two additional companion articles employ this tracer model to explain the observational data which we present here. In the first of these [Heimann et al., this volume], synoptic variations and the seasonal cycle of $CO_2$ are investigated, and in the second [Keeling et al., this volume], the mean annual distribution with emphasis on north-south variations is explored.

This tracer model does not explicitly represent the capacities of the terrestrial biosphere and oceans to store carbon, and it consequently cannot treat interannual variations in $CO_2$ mechanistically. As an adaptation to this limitation we have employed the model as though the carbon cycle were quasi-stationary, varying only on time scales of one year or less. To allow for the reality of interannual variations, we have defined a series of quasi-stationary states each representing the carbon cycle averaged over approximately 2 years. This approach is adequate to examine features of the cycle which vary on time scales significantly longer than the longest scale of atmospheric transport, i.e., appreciably longer than the one year exchange time of air between the northern and southern hemispheres. The model can thus address changes in the carbon cycle from decade to decade, and even with some success from one 5-year period to the next.

With a more realistic formulation of the biosphere and oceans the three-dimensional tracer model could simulate shorter-term interannual variations as well. In preparation for this extended study, and better to appreciate the limitations of the quasi-stationary model, we have attempted to explain relatively rapid interannual variations seen in the $CO_2$ records, especially fluctuations associated with El Niño events. For this purpose we employ a simple compartment model of the carbon cycle which prescribes the storage capacities of the major active carbon reservoirs and their rates of exchange for all time scales greater than 1 year. This model is useful also for examining slower, decadal scale changes, and even changes over a century or more, as seen in observations of air collected from polar ice cores. Still further, it provides estimates of the global integrals of the sources and sinks required in the definition of the quasi-stationary states of the three-dimensional model.

## 2. Measurements of Atmospheric $CO_2$ Concentration

### *2.1 Source of Data*

The $CO_2$ data which we have adopted as the principal basis for three-dimensional modeling were obtained as part of a study of the carbon cycle carried out at the Scripps Institution of Oceanography (SIO) from 1958 through 1985. Beginning in 1977, isotopic measurements have been included in this program. Where appropriate we also have used still preliminary data gathered since 1985.

Since 1970 the World Meteorological Organization (WMO) has supported a world-wide program to measure atmospheric $CO_2$ mainly through their affiliated national weather services [WMO, 1984]. Daily $CO_2$ concentrations are summarized in yearly reports [e.g., WMO, 1985]. Systematic corrections still need to be applied to these data to bring them to a common concentration scale. When comparing model predictions with direct observations, we have, therefore, generally refrained from combining our data sets with data from other laboratories (for example, the world-wide surface data reported by Komhyr et al. [1985], Conway et al. [1988], and Thoning et al. [1989]; shipboard, aircraft, and antarctic surface data by Tanaka et al. [1987a, b, c]; and surface and aircraft data in the southern hemisphere by Fraser et al. [1983], Pearman and Beardsmore [1984], and Beardsmore and Pearman [1987]. Some of these data, however, are discussed in the accompanying article by Heimann et al. [this volume].

Daily averages of measurements of $CO_2$ concentration for all locations are listed in a report by Keeling et al. [1989] available on microfiche.[4] This report cites all previous published literature pertaining to the listed data. Many of these data, however, have not been previously published. A similar report, with a complete listing of isotopic data, is in preparation, but will not be available in time to accompany the report by Keeling et al. [1989].

[4]Report containing daily averaged data obtained in the study carried out at the Scripps Institution of Oceanography is available on microfiche. Order from American Geophysical Union, 2000 Florida Avenue, N.W., Washington, D.C. 20009.

### 2.2 *Strategy of Data Analysis*

The observed variations in atmospheric $CO_2$ reflect time scales from minutes to decades. In the present study we address three time scales:

(1) A *synoptic* scale in which similar $CO_2$ variations occur over a broad area, e.g., owing to the influence of weather events. Although synoptic weather reporting can involve time scales as short as 1 hour, the shortest synoptic time scale for atmospheric $CO_2$ near the earth's surface is approximately 1 day owing to local diurnal scale fluctuations which must be suppressed to obtain regionally comparable data.

(2) A *seasonal* scale in which synoptic variations have been removed to produce time records which vary smoothly from month to month. Variations related to individual weather events no longer are seen on this scale when data are compared regionally.

(3) An *interannual* scale in which the seasonal cycle has been removed to produce a slowly varying residual. Time variations on this scale are similar over the entire globe, because the mixing time for a passive atmospheric tracer such as $CO_2$ is similar to, or less than, the time scales retained in the data.

The sites for $CO_2$ sampling of the SIO program were chosen to be close to an ocean or on barren ground where local sources and sinks of $CO_2$ are weak or absent. Except for Mauna Loa Observatory which, after selection as a station, was found to have a pronounced diurnal $CO_2$ cycle, instantaneous observations at these stations approximate data on the synoptic time scale. At Mauna Loa a selection process produces data on this scale [Keeling et al., 1976a]. At most locations data were collected so infrequently, however, that synoptic scale variations are not apparent, and thus only seasonal and interannual scale variations are seen in the time series. Besides at Mauna Loa Observatory, where data were obtained almost every day, synoptic scale variations are evident only at the north Pacific Ocean Station P, where samples were collected twice per week for some years, and at La Jolla, California, during selected periods, not considered in this article, when continuous measurements were made.

Almost everywhere, except at low latitudes of the southern hemisphere, the $CO_2$ records of the SIO program show clear evidence of a seasonal cycle, but the cycle does not repeat so faithfully from year to year that the separation of annual and interannual variations is made simple. A mathematically well defined separation of these time scales is afforded by digital filtering. Enting [1987], for example, has band-pass filtered the daily data of Mauna Loa Observatory to obtain a seasonal cycle which varies interannually in both phase and amplitude.

Securing a mathematically precise formulation of the seasonal cycle does not, however, produce a separation of the disparate contributions to the $CO_2$ seasonal cycle arising from the individual oceanic and terrestrial sources and sinks of $CO_2$. Two- and three-dimensional models, on the other hand, are useful in this regard, especially if the model analysis involves isotopic data as well as concentration data, and if the precise specification of interannual variations in phase and amplitude is not required. Therefore, as described in Appendix A, we have characterized interannual variations in the seasonal cycle only with respect to the most obvious feature in the atmospheric data: a slow, approximately linear, increase in amplitude with time. We define the seasonal function to be determined from the data for a given location by the general formula

$$C_{obs\ seas}(t) = (1+\gamma t)\sum_{k=1}^{m}(a_k \sin \omega_k t + b_k \cos \omega_k t) \qquad (2.1)$$

where $\gamma$ (a "gain factor") and the $a_k$ and $b_k$ denote constants obtained via a fit to the data, $t$ denotes the time, $\omega_k$ the angular frequency, equal to $2\pi k$ with $t$ expressed in years, and $m$ the number of harmonics, usually chosen to be 4.

The residual variations in $CO_2$ concentration remaining after removal of this harmonic function, we express two ways: by

(1) a discrete series of time averages which contain all of the variability not removed by subtraction of the harmonic function (2.1); and by

(2) a continuous function consisting of an exponential term, that captures most of the long-term trend associated with injection of industrial $CO_2$ into the air, summed with a spline function that provides a smoothed version of the remaining variation.

This residual continuous function (or "observed remainder") is defined by the expression

$$C_{obs\ rem}(t) = C_1 + C_2 \exp(C_3 t) + R \qquad (2.2)$$

where $C_1$, $C_2$ and $C_3$ are constants obtained by a nonlinear fit to the data and $R$ denotes the spline function, whose coefficients are determined by the same fit [Keeling et al., 1989]. The unsmoothed series of averages then consist of the sum of $C_{obs\ rem}(t)$ and a "noise" term $\overline{\varepsilon_{obs}(t)}$ which includes that part of the synoptic variability and other residual variability not removed by time averaging. We have selected one month for the period of averaging, to suppress diurnal and synoptic scale variations, but still to retain sufficient data to compute a four harmonic seasonal cycle. The $CO_2$ concentration at any station, expressed as monthly averages, $\overline{C_{obs}(t)}$, is thus given by the sum of three terms

$$\overline{C_{obs}(t)} = C_{obs\ rem}(t) + C_{obs\ seas}(t) + \overline{\varepsilon_{obs}(t)} \qquad (2.3)$$

Alternatively, we have in some instances computed daily averages. Here the "noise" term effectively is replaced by a synoptic scale term $C_{syn}(t)$ and a smaller noise term, $\varepsilon_{obs}(t)$, representing contributions to the daily averages from local diurnal scale variability and instrumental errors. The $CO_2$ concentration is then expressed as daily averages, $C_{obs}(t)$, given by the sum of four terms

$$C_{obs}(t) = C_{obs\ rem}(t) + C_{obs\ seas}(t) + C_{syn}(t) + \varepsilon_{obs}(t) \qquad (2.4)$$

In displaying longer term variations we will usually show seasonally adjusted monthly averages, $C_{obs\ rem}(t) + \overline{\varepsilon_{obs}(t)}$, as well as the continuous function $C_{obs\ rem}(t)$, so that no relevant information is suppressed in the plots. We will henceforth refer to $C_{obs\ seas}$ as the "seasonal variation" and $C_{obs\ rem}$ as the "seasonally adjusted concentration." Similar terminology will apply to the isotopic data. Synoptic variations are not further discussed in this article, but are examined by Heimann et al. [this volume].

Interannual variations on time scales of a few years are largely masked in the $CO_2$ records by the persistent rise in concentration associated with fossil fuel combustion. This persistent rise can be removed from the records in various ways. We have chosen to subtract a constant fraction of the cumulative input from industrial $CO_2$, $f_{abf}$, a factor which we will call an "airborne fraction." We thus sometimes separate the seasonally adjusted concentration, $C_{obs\ rem}(t)$ into two terms such that

$$C_{obs\ rem}(t) = (f_{abf} \int_{t_o}^{t} F_{IND}(t)\, dt) + C_{anom}(t) \qquad (2.5)$$

where $F_{IND}(t)$ denotes the rate of input of industrial $CO_2$ into the atmosphere. The time integral of $F_{IND}$ from the beginning of the industrial era, $t_o$, thus expresses the cumulative industrial input, while $C_{anom}(t)$ represents an "anomaly" with respect to a constant airborne fraction of this input.

To evaluate $f_{abf}$ two dates, $t_1$ and $t_2$, are chosen on which we assume that the anomaly vanishes, and hence

$$f_{abf} = \frac{C_{obs\ rem}(t_2) - C_{obs\ rem}(t_1)}{\int_{t_1}^{t_2} F_{IND}(t)\, dt} \qquad (2.6)$$

In practice (see subsection 4.4, below) we have chosen dates near the beginnings and ends of the $CO_2$ records, avoiding times, however, when the seasonally adjusted concentration departs markedly from its long-term trend. Henceforth, we usually restrict the term "interannual variation" in $CO_2$ to refer to the anomalous $CO_2$ concentration variation, $C_{anom}(t)$.

TABLE 1. Seasonally Adjusted Concentration of Atmospheric $CO_2$ as a Function of Latitude, Trend Corrected to January 1, 1962

| Latitude Interval of Shipboard Data or Name of Fixed Station | Mean Latitude (deg.) | Concentration (ppm) | Standard Error (ppm) | Number of Observations |
|---|---|---|---|---|
| South Pole | 90.0S. | 317.77 | 0.025 | 13 |
| 63.0S. – 43.5S. | 52.2S. | 317.64 | 0.12 | 10 |
| 17.0S. – 12.5S. | 14.6S. | 318.69 | 0.07 | 10 |
| 11.3S. – 8.8S. | 10.3S. | 319.01 | 0.12 | 10 |
| 8.6S. – 5.0S. | 6.5S. | 319.27 | 0.10 | 10 |
| 4.9S. – 2.8S. | 3.6S. | 319.20 | 0.19 | 10 |
| 2.5S. – 0.2S. | 1.2S. | 319.33 | 0.16 | 10 |
| 0.0S. – 2.5N. | 0.8N. | 319.23 | 0.23 | 10 |
| 2.5N. – 5.0N. | 4.2N. | 319.38 | 0.17 | 10 |
| 5.1N. – 7.5N. | 5.9N. | 318.99 | 0.19 | 10 |
| 7.6N. – 10.0N. | 9.1N. | 318.73 | 0.17 | 10 |
| 10.0N. – 11.6N. | 10.7N. | 318.57 | 0.15 | 10 |
| 12.5N. – 14.2N. | 13.3N. | 318.11 | 0.06 | 10 |
| 15.0N. – 18.8N. | 16.7N. | 318.29 | 0.18 | 10 |
| Mauna Loa | 19.5N. | 318.26 | – | – |
| Hilo | 19.7N. | 318.62 | 0.16 | 43 |
| 19.9N. – 21.5N. | 20.8N. | 318.48 | 0.23 | 10 |
| 22.9N. – 24.3N. | 23.6N. | 318.27 | 0.07 | 10 |
| 24.4N. – 26.1N. | 25.0N. | 318.80 | 0.18 | 8 |
| 26.3N. – 27.2N. | 26.6N. | 318.10 | 0.14 | 8 |
| 27.6N. – 29.2N. | 28.6N. | 318.74 | 0.10 | 8 |
| Station N | 30.0N. | 318.58 | 0.19 | 22 |
| 30.0N. – 31.4N. | 30.8N. | 318.00 | 0.16 | 10 |
| Point Barrow | 71.3N. | 319.24 | 0.18 | 49 |
| Arlis | 82.0N. | 319.09 | 0.20 | 38 |

TABLE 2. Seasonally Adjusted Concentration of Atmospheric $CO_2$ as a Function of Latitude, Trend Corrected to January 1, 1968

| Latitude Interval of Shipboard Data or Name of Fixed Station | Mean Latitude (deg.) | Concentration (ppm) | Standard Error (ppm) | Number of Observations |
|---|---|---|---|---|
| South Pole | 90.0S. | 321.57 | 0.04 | 19 |
| 77.7S. – 70.0S. | 73.7S. | 321.35 | 0.06 | 10 |
| 68.4S. – 55.3S. | 62.8S. | 321.73 | 0.08 | 10 |
| 53.0S. – 49.1S. | 51.9S. | 321.61 | 0.06 | 10 |
| 46.7S. – 43.3S. | 44.0S. | 321.63 | 0.11 | 10 |
| 43.3S. – 43.2S. | 43.2S. | 322.05 | 0.05 | 10 |
| 43.2S. – 33.3S. | 36.8S. | 321.73 | 0.08 | 10 |
| 32.4S. – 28.4S. | 30.4S. | 321.45 | 0.10 | 10 |
| 28.4S. – 28.3S. | 28.3S. | 321.44 | 0.09 | 10 |
| 28.3S. – 28.1S. | 28.2S. | 321.49 | 0.07 | 10 |
| 28.1S. – 27.1S. | 27.6S. | 321.73 | 0.06 | 10 |
| 27.1S. – 26.4S. | 26.7S. | 321.69 | 0.04 | 10 |
| 26.0S. – 23.4S. | 24.5S. | 321.76 | 0.05 | 10 |
| 23.2S. – 21.7S. | 22.7S. | 321.98 | 0.05 | 10 |
| 20.2S. – 20.0S. | 20.0S. | 321.87 | 0.07 | 10 |
| 20.0S. – 18.0S. | 18.8S. | 322.07 | 0.13 | 10 |
| 18.0S. – 17.4S. | 17.7S. | 322.18 | 0.11 | 10 |
| 17.3S. – 15.7S. | 16.6S. | 322.11 | 0.07 | 10 |
| 15.7S. – 14.1S. | 14.9S. | 322.18 | 0.11 | 10 |
| 14.1S. – 13.6S. | 13.8S. | 322.04 | 0.08 | 10 |
| 13.6S. – 13.2S. | 13.4S. | 322.09 | 0.14 | 10 |
| 12.6S. – 11.4S. | 12.1S. | 322.18 | 0.15 | 10 |
| 11.4S. – 11.1S. | 11.2S. | 321.97 | 0.19 | 10 |
| 9.8S. – 8.6S. | 9.3S. | 322.32 | 0.22 | 10 |
| 8.6S. – 8.0S. | 8.3S. | 322.20 | 0.17 | 10 |
| 7.8S. – 6.3S. | 7.0S. | 322.70 | 0.13 | 10 |
| 5.4S. – 4.0S. | 5.0S. | 322.93 | 0.10 | 10 |
| 3.9S. – 2.3S. | 3.2S. | 323.03 | 0.09 | 10 |
| 2.1S. – 0.2S. | 0.8S. | 323.25 | 0.10 | 10 |
| 0.0S. – 0.8N. | 0.3N. | 323.22 | 0.12 | 10 |
| 1.1N. – 2.4N. | 1.7N. | 323.40 | 0.05 | 10 |
| 2.5N. – 3.9N. | 3.4N. | 323.20 | 0.13 | 10 |
| 3.9N. – 6.1N. | 5.1N. | 323.36 | 0.13 | 10 |
| 6.1N. – 7.9N. | 7.4N. | 323.00 | 0.18 | 10 |
| 8.6N. – 9.4N. | 9.2N. | 322.79 | 0.16 | 10 |
| 9.6N. – 10.5N. | 10.1N. | 323.12 | 0.12 | 10 |
| 10.5N. – 13.0N. | 11.6N. | 322.91 | 0.10 | 10 |
| 13.2N. – 14.4N. | 13.7N. | 322.63 | 0.09 | 10 |
| 14.6N. – 15.8N. | 15.2N. | 322.92 | 0.08 | 10 |
| 15.9N. – 16.5N. | 16.3N. | 322.91 | 0.17 | 10 |
| 16.9N. – 18.5N. | 17.9N. | 322.97 | 0.21 | 10 |
| 18.6N. – 19.9N. | 19.2N. | 323.33 | 0.22 | 10 |
| Mauna Loa | 19.5N. | 322.28 | – | – |
| 20.0N. – 21.2N. | 20.7N. | 323.01 | 0.25 | 10 |
| 21.4N. – 24.5N. | 23.1N. | 322.80 | 0.12 | 10 |
| 24.5N. – 26.7N. | 25.4N. | 323.01 | 0.19 | 10 |
| 27.3N. – 31.5N. | 29.0N. | 323.07 | 0.17 | 11 |
| 31.6N. – 34.1N. | 32.7N. | 322.66 | 0.25 | 11 |
| 34.2N. – 34.6N. | 34.4N. | 323.17 | 0.16 | 11 |
| Station P | 50.0N. | 323.02 | 0.15 | 35 |
| Point Barrow | 71.3N. | 324.15 | 0.15 | 53 |

### 2.3 *Seasonally Adjusted Data*

For our most detailed analysis of the global carbon cycle we have selected a 2-year portion of the SIO atmospheric $CO_2$ data record centered on the year 1980. This is a period when time series measurements of $CO_2$ concentration at our array of land stations were supplemented in the tropical Pacific Ocean area by a detailed series of measurements from air samples collected on ships.

For two other periods $CO_2$ concentration data from ships are also available to supplement land based measurements. We have therefore constructed similar seasonally adjusted data sets for periods centered on January 1, 1962 and 1968. Because the original samples for these two periods were collected at irregularly spaced intervals along the ships' tracks, and we wished to average the data to reduce scatter, we have grouped the observations, usually 10 at a time, and assigned a single location to the average of the measurements in each group.

The isotopic data, which are centered on January 1, 1980, provide inadequate coverage at high latitudes. We have therefore provided a fourth set of seasonally adjusted concentration data, centered on May 15, 1984, which are adequate to estimate the north-south isotopic distribution from pole to pole.

The concentration data for the four periods are listed in Tables 1 to 4. Tables 3 and 4 include isotopic data. The concentration data from land stations are derived from spline fits and expressed by the function $C_{obs\ rem}(t)$ of equation (2.2) for the specified dates. The concentration data from ships and ice floe station Arlis are derived by averaging individual measurements ($C_{obs}(t)$ of equation (2.4))

TABLE 3. Seasonally Adjusted Concentration and Isotopic Ratio, $^{13}\delta$, of Atmospheric $CO_2$ as a Function of Latitude, Trend Corrected to January 1, 1980

| Latitude Interval of Shipboard Data or Name of Fixed Station | Mean Latitude (deg.) | Concentration (ppm) | Standard Error (ppm) | Number of Observations | $^{13}\delta$ (‰) | Standard Error (‰) | Number of Observations |
|---|---|---|---|---|---|---|---|
| South Pole | 90.0S. | 335.84 | 0.042 | 18 | −7.539 | 0.010 | 11 |
| Baring Head | 41.4S. | 335.67 | 0.038 | 64 | – | – | – |
| FGGE, 14–17 S. | 15.6S. | 336.59 | 0.039 | 72 | −7.496 | 0.006 | 17 |
| FGGE, 8–12 S. | 9.6S. | 337.01 | 0.035 | 74 | −7.502 | 0.008 | 21 |
| FGGE, 2–6 S. | 4.0S. | 337.70 | 0.029 | 78 | −7.509 | 0.009 | 19 |
| FGGE, 1 N.–1 S. | 0.0 | 337.93 | 0.023 | 85 | −7.534 | 0.009 | 21 |
| FGGE, 2–4 N. | 3.0N. | 337.89 | 0.026 | 85 | −7.529 | 0.012 | 21 |
| Fanning/Christmas | 3.0N. | 338.07 | 0.089 | 24 | −7.594 | 0.012 | 20 |
| FGGE, 6–10 N. | 8.0N. | 337.71 | 0.031 | 77 | −7.542 | 0.008 | 19 |
| FGGE, 12–16 N. | 13.8N. | 337.84 | 0.033 | 91 | −7.581 | 0.009 | 23 |
| FGGE, 18–20 N. | 19.0N. | 337.89 | 0.074 | 39 | −7.542 | 0.028 | 10 |
| Mauna Loa | 19.5N. | 337.57* | 0.048 | 52 | – | – | – |
| La Jolla | 32.9N. | 339.16 | 0.264 | 9 | −7.720 | 0.052 | 2 |
| Station P | 50.0N. | 338.21 | 0.123 | 93 | – | – | – |
| Point Barrow | 71.3N. | 338.81 | 0.260 | 16 | – | – | – |

*Data not used in analysis.

TABLE 4. Seasonally Adjusted Concentration and Isotopic Ratio, $^{13}\delta$, of Atmospheric $CO_2$ as a Function of Latitude, Trend Corrected to May 15, 1984

| Name of Fixed Station | Mean Latitude (deg.) | Concentration (ppm) | Standard Error (ppm) | Number of Observations | $^{13}\delta$ (‰) | Standard Error (‰) | Number of Observations |
|---|---|---|---|---|---|---|---|
| South Pole | 90.0S. | 342.29 | 0.040 | 20 | −7.686 | 0.009 | 13 |
| Baring Head | 41.4S. | 342.15 | 0.040 | 59 | – | – | – |
| Raoul Is.* | 29.2S. | 342.30 | 0.088 | 10 | −7.640 | 0.010 | 7 |
| Cape Matatula | 14.2S. | 343.40 | 0.105 | 36 | −7.630 | 0.013 | 22 |
| Fanning/Christmas | 3.0N. | 344.38 | 0.085 | 26 | −7.665 | 0.010 | 26 |
| Cape Kumukahi | 19.5N. | 344.29 | 0.106 | 45 | −7.721 | 0.011 | 44 |
| Mauna Loa | 19.5N. | 344.18 | 0.050 | 48 | −7.734 | 0.013 | 38 |
| La Jolla | 32.9N. | 345.30 | 0.107 | 55 | −7.826 | 0.014 | 26 |
| Point Barrow | 71.3N. | 345.33 | 0.162 | 41 | −7.852 | 0.013 | 28 |

* Isotopic data are derived by averaging the original observations without a seasonal adjustment or spline fit owing to the short record. The average concentration of the 7 samples with isotopic control is 342.40 ppm, in close agreement with the spline fit to the time series of concentration as shown in the third column.

or by use of special functions. The isotopic data are derived by corresponding techniques. In Appendix A we discuss more specifically how we compiled the original concentration data. In Appendix B we discuss our treatment of the isotopic data. The analysis of the full set of data to derived these tables is explained in detail by Keeling et al. [1989]. Plots of the geographic distribution of sampling locations are included in Appendix A.

### 2.4 *Seasonal Variations*

At stations with short records, we set the gain factor, $\gamma$, to zero in equation (2.1) and computed a time invariant harmonic function. For the remaining stations, with records adequate to establish $\gamma$, we used the full expression (2.1). For the latter stations we then computed the seasonal cycle for January 1, 1980 in terms of the factors $(1+\gamma)a_k$ and $(1+\gamma)b_k$. The original values for the $a_k$, $b_k$, and for $\gamma$ are listed by Keeling et al. [1989].

To represent the change in amplitude of the seasonal cycle for other years, we have applied a single global adjustment based on $\gamma$ as computed from the record for Mauna Loa, a record which we consider to be the most representative of changes in the globally averaged seasonal cycle. For 1962 we reduce the cycle everywhere to 88.5 percent of the 1980 cycle, for 1968 we reduce the cycle to 92.3 percent, and for 1984 we raise it to 102.8 percent. We thus avoid the introduction of regional differences in the interannual variation in the cycle which would unnecessarily complicate the three-dimensional model predictions.

Harmonic coefficients of the seasonal cycle in the tropics, based on measurements from shipboard sampling during 1979 and 1980, have been previously derived by Heimann and Keeling [1986, Table 2] from an interpolating surface in space and time. This two-dimensional analysis in time and latitude reduces the error of estimate of the cycles at individual latitudes, because the analysis takes into account the correlation of the cycle at nearby locations represented in the data set. As described in Appendix A, we use the results of this analysis to represent the seasonal cycle between 16°N. and 14.5°S., where we lack adequate data from land stations. Plots of the seasonal cycles for 1980 at individual stations, and at 4°S. based on shipboard sampling, are shown by Heimann et al. [this volume].

### 2.5 *Distinction Between Provisional and Supplementary Data*

The atmospheric $CO_2$ measurements described here are derived from an observational program still in progress. When final modeling calculations for this article commenced, it became necessary to set aside a fixed data set which could be fully documented and cited. It is this body of data, available to us in June 1986, which is discussed above and presented *in toto* by Keeling et al. [1989]. We refer to these data as "provisional" in the literal sense that they were set aside beforehand. A few model parameters were derived from earlier sets of data, as noted elsewhere in this text. In no instance does this usage result in significant inconsistencies.

In the 3 years since our setting aside this "provisional" data set, additional data have been gathered which substantially extend and improve upon both our isotopic and concentration records. Therefore we use these "supplementary" data where appropriate. These data, where joined to earlier sets of provisional data, lead to minor revisions in those sets back to the beginnings of the records. None of the supplementary data are final, because they extend beyond the time of the most recent manometric calibration of our primary reference gas standards in 1985 [Keeling et al., 1986]. Final corrections, however, are anticipated from previous experience to be less than 0.20 parts per million, so that the supplementary data are not likely to cause significant errors in interpretation.

### 2.6 *Concluding Remarks*

Before we discuss our data generally, we explain some additional features of isotopic carbon in section 3 below. Then, in section 4, in preparation for modeling studies, we discuss selected qualitative features of the seasonal and interannual variations in $CO_2$ concentration and isotopic ratio. In section 5 we explain the construction of a compartment model, the results of which we use to reinterpret interannual variations in $CO_2$ in section 6.

## 3. Isotopic Carbon

Approximately 1 percent of stable natural carbon has an atomic weight of 13; the rest has a weight of 12. The ratio of abundances of carbon-13 to carbon-12, $^{13}C/^{12}C$, is calculated from mass spectrometric measurements in which the 45/44 mass ratio of $CO_2$ (mainly owing to $^{13}C^{16}O_2$ / $^{12}C^{16}O_2$) is corrected for a small contribution from $^{17}O$ [Mook and Grootes, 1973]. In practice, samples are alternated with standards which are attributable to a conventional carbonate standard, "PDB", assigned a nominal ratio of 0.0112372 [Craig, 1957; Mook and Grootes, 1973]. Ratios are expressed by the relative variation from this standard using the reduced ratio

$$^{13}\delta = r/r_s - 1 \tag{3.1}$$

where $r$ denotes the $^{13}C/^{12}C$ ratio of the sample, and $r_s$ = 0.0112372. Customarily the reduced ratios are multiplied by 1000, and thus are expressed in "per mil" (symbol, ‰). From extensive replicate isotopic measurements of atmospheric $CO_2$, we have established for the mass spectrometers of Groningen University, where our measurements were carried out, an individual measurement standard deviation of approximately 0.05‰. We have also shown that, under carefully controlled circumstances, we obtain time series of atmospheric data in which mean $^{13}\delta$ values vary in time and space to an imprecision approaching 0.01‰ [Keeling et al., 1984].

The product of $^{13}\delta$ and carbon mass is very nearly an additive function when $CO_2$ samples are mixed [Mook et al., 1983], e.g., if $^{13}\delta_1$ and $^{13}\delta_2$ denote the isotopic ratios of samples containing $N_1$ and $N_2$ moles of $CO_2$ respectively, then the mixture has very nearly the $^{13}\delta$ value

$$^{13}\delta_M = (N_1{}^{13}\delta_1 + N_2{}^{13}\delta_2)/(N_1 + N_2) \tag{3.2}$$

The $^{13}\delta$ of atmospheric $CO_2$ is close to −8‰; that of plant carbon is in the vicinity of −25‰. Thus when the $CO_2$ concentration is raised from a typical value of 340 ppm (parts per million of dry air by volume) by adding one ppm of biospheric $CO_2$, the rate of change in $^{13}\delta$ with respect to concentration C, is

$$\Delta^{13}\delta/\Delta C = \left[(340(-8‰) + 1(-25‰))/341\right] - 1\ (-8‰) \qquad (3.3)$$
$$\approx -0.050‰\text{ppm}^{-1}$$

In contrast, when the atmospheric $CO_2$ concentration is raised by adding oceanic $CO_2$, the corresponding rate of change owing to a kinetic fractionation of −1.8‰ [Siegenthaler and Münnich, 1981] is only about a tenth as great, i.e.,

$$\Delta^{13}\delta/\Delta C = \left[(340(-8‰) + 1(-9.8‰))/341\right] - 1\ (-8‰) \qquad (3.4)$$
$$\approx -0.0053‰\text{ppm}^{-1}$$

If we take into account a lag in the $^{13}\delta$ of ocean water with respect to the atmosphere in responding to industrial $CO_2$ emissions at the present time (the carbon-13 Suess effect), the effective contrast in $^{13}\delta$ between $CO_2$ in air and water is reduced from −1.8‰ to −1.2 ‰, as discussed by Heimann and Keeling [this volume, subsection 5.4, equation (5.57) and Table 8]. Thus $\Delta^{13}\delta/\Delta C$ is reduced to about –0.0035 ‰.nr 12 11 $\text{ppm}^{-1}$, and consequently, the shift in $^{13}\delta$ for $CO_2$ of oceanic origin is presently even less than calculated by equation (3.4).

An isotopic imprecision as low as 0.01‰, sometimes realized in the isotopic standard errors listed in Tables 3 and 4, is thus equivalent to specifying biospheric $CO_2$ within 0.2 ppm, i.e., close to the least imprecision which we typically attribute to atmospheric $CO_2$ concentration measurements (about 0.1 ppm). For variations in concentration even as small as 1 ppm, it is therefore possible to distinguish the biospheric and oceanic components under the most favorable circumstances to within 20 percent.

The first extensive measurements of the $^{13}C/^{12}C$ ratio of atmospheric $CO_2$ in non-urban air were made in 1955 and 1956 by Keeling [1958, 1961] using almost the same sampling and extraction techniques as used in the more recent measurements. When Keeling et al. [1979] compared these data with the recent data at approximately the same locations in midlatitudes of the northern hemisphere, they deduced that the mean $CO_2$ concentration in air rose between 1956 and 1978 from 314 ppm to 334 ppm, while the isotopic ratio had shifted from –6.69‰ to –7.24‰. The average rate of change of $^{13}\delta$ with respect to concentration over this period was thus 0.028 ‰ $\text{ppm}^{-1}$, a rate intermediate between those for biospheric and oceanic $CO_2$ exchange expressed by equation (3.3) and (3.4), respectively. As shown by Keeling et al. [1980] this intermediate rate is consistent with the addition to the air of approximately $46 \times 10^{12}$ kg of carbon as $CO_2$ from the combustion of fossil fuels, bearing in mind that the $^{13}\delta$ of the carbon from fuels is approximately the same as of carbon from land plants. (The intermediate rate, rather than the rate of land plants, results from the subsequent partial removal of the industrial $CO_2$ by exchange with the oceans.)

From more extensive measurements at five stations, Mook et al. [1983] established the broad outline of the regional variations and seasonal cycle of $^{13}\delta$. From still further measurements of air collected on ships in the tropical Pacific during the FGGE Shuttle Expedition, Keeling et al. [1984] determined the seasonal cycle and mean annual north-south gradient in $^{13}\delta$ for 1980 from 20°N. to 17°S. near 150°W.

Isotopic measurements have been continued for the five stations reported by Mook et al. [1983] and more recently have been supplemented by measurements for three additional stations. In the sections which follow we consider these new data as well as previously published data. We also make note of data obtained in the southern hemisphere and reported by Goodman and Francey [1988].

## 4. Preliminary Description of the Observational Data

### 4.1 *Summary of Data*

Concentration and isotopic data for atmospheric $CO_2$ obtained by the Scripps Institution of Oceanography from the beginning of 1969 through most of 1985, at the locations shown in Figure 1, are plotted in Figures 2 to 5. To reveal similarities between properties, the plotted isotopic data are inverted so that higher values on plots of both concentration and isotopic ratio reflect the addition of $CO_2$ from plant carbon or fossil fuels. As a further aid, the vertical axes are scaled in the proportion of –0.05‰ per ppm (see equation (3.3)). The seasonal cycles in atmospheric $CO_2$ at various locations are clearly seen in Figures 2 to 5. The same measurements, seasonally adjusted, are shown in Figures 6 to 9. These latter data reveal interannual variations and define the mean annual north-south gradient in concentration and isotopic ratio near 150°W., as discussed below.

There is much information revealed by these data, only a part of which can be reviewed here. We first discuss the seasonal cycle of concentration and isotopic ratio and afterwards the seasonally adjusted data.

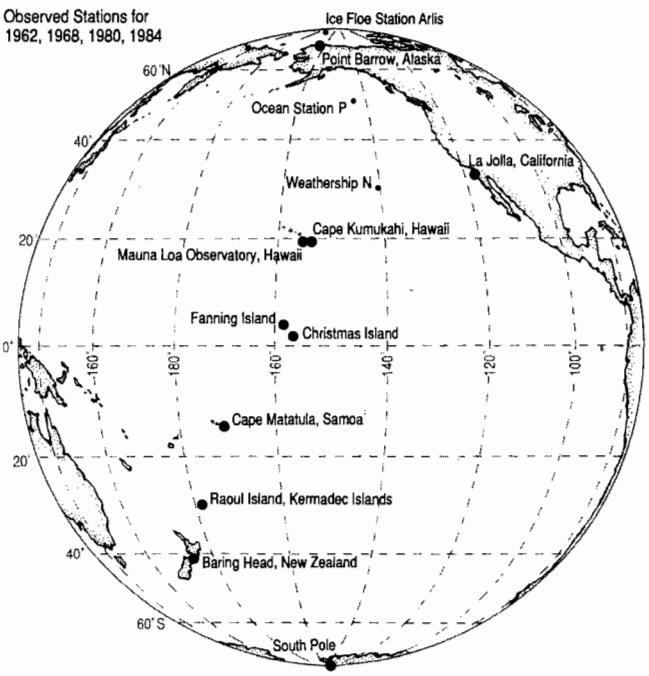


Fig. 1. Locations of air sampling stations on land and over water. Location of Ice Floe Station Arlis is approximate.

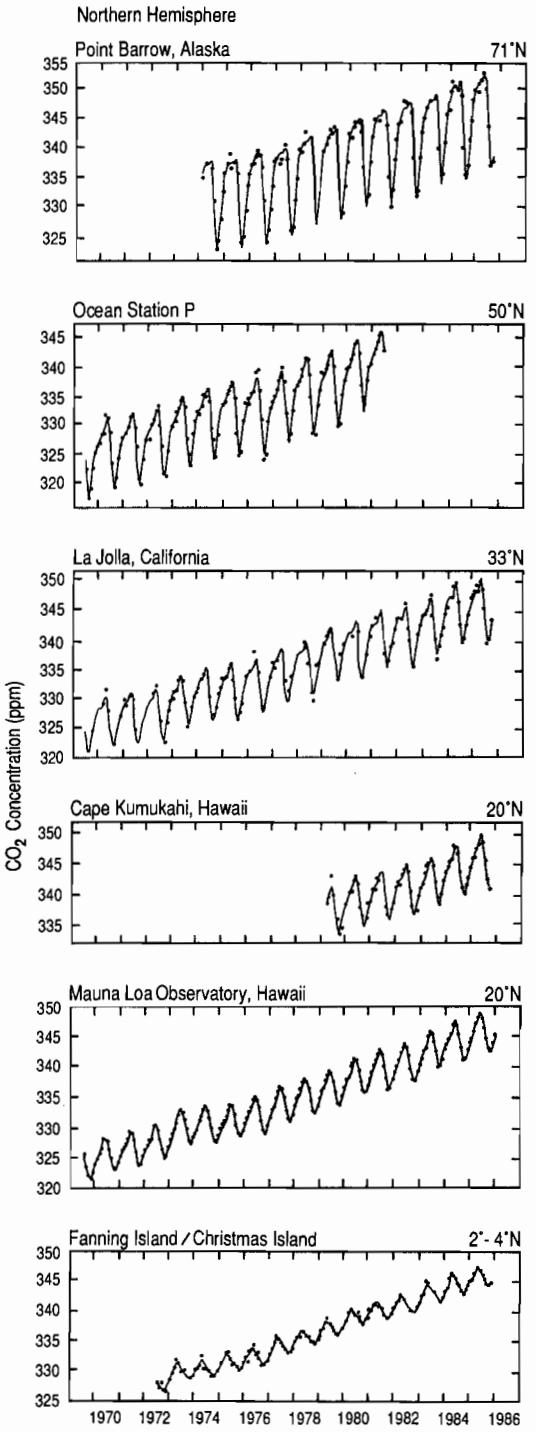


Fig. 2. Time trend of the concentration of atmospheric $CO_2$, in ppm, at northern hemisphere stations shown from north to south. The oscillating curves are fits of daily average concentration to a spline function combined with an exponential function and four harmonic terms ($C_{obs\ rem} + C_{obs\ seas}$ of equation (2.4)). The dots denote monthly mean concentrations ($C_{obs}$, of equation (2.3)).

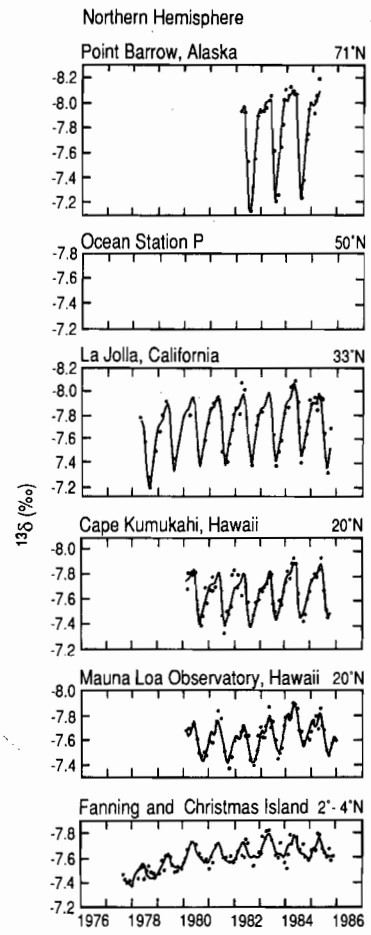


Fig. 3. Time trend of the reduced isotopic ratio, $^{13}\delta$, of atmospheric $CO_2$ in per mil from standard PDB, for the same stations as in Figure 2. The oscillating curves are fits similar to those in Figure 2. The dots denote monthly averages. (Ocean Station P lacks isotopic data.)

### *4.2 Seasonal Cycle*

At Point Barrow, Alaska, where the seasonal cycle of atmospheric $CO_2$ is well developed, the seasonal variation in $^{13}\delta$ is very similar to that of concentration, as can be seen by comparing the respective time plots (Figures 10 and 11). From the additivity of the product of $^{13}\delta$ and carbon mass (see equation 3.2), we deduce that the reduced isotopic ratio, $^{13}\delta_I$, of the $CO_2$ added to and removed from the air to produce the isotopic seasonal cycle is approximately −25‰, and thus is as expected from terrestrial plant activity [Degens, 1969].

Similar values of $^{13}\delta_I$ are computed for other stations, and are listed in Table 5. The range somewhat exceeds that expected statistically on the basis of the computed standard errors for the individual stations, and there is a tendency for less negative values to be found in the tropics and in the southern hemisphere. Less

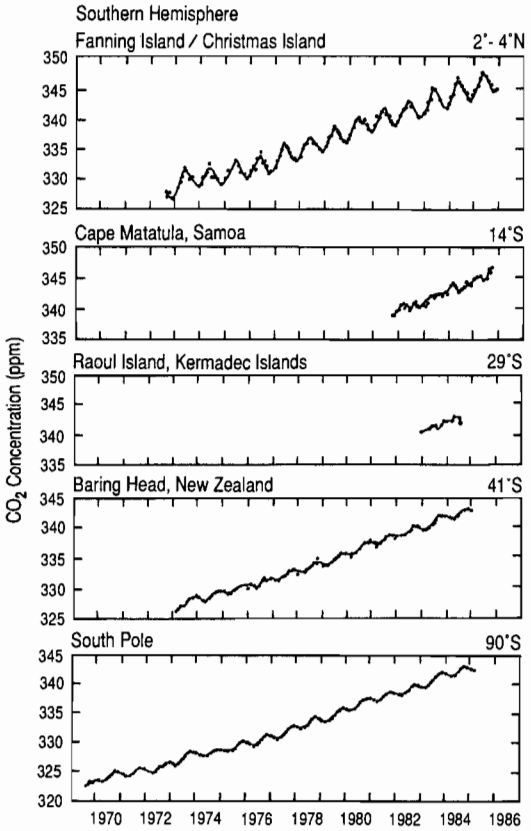


Fig. 4. Same as Figure 2 but for the southern hemisphere. Fanning and Christmas Islands are repeated from Figure 2 for comparison.

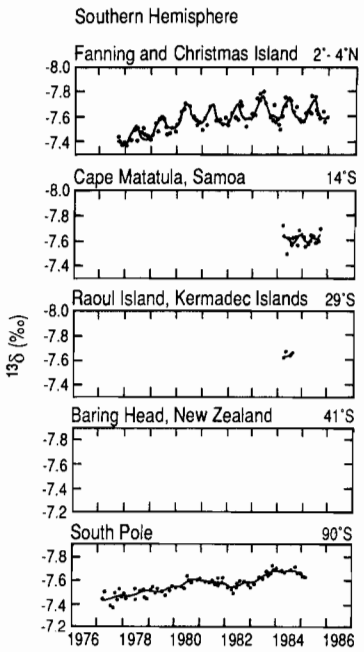


Fig. 5. Same as Figure 3 but for the southern hemisphere. Baring Head, New Zealand lacks isotopic data.

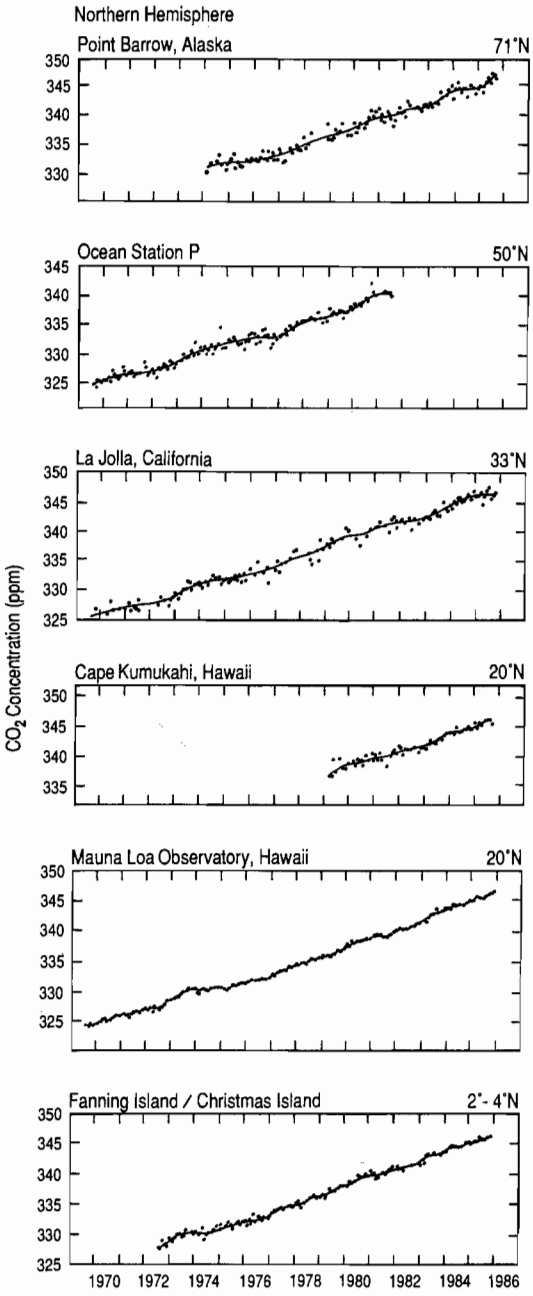


Fig. 6. Time trend of the seasonally adjusted concentration of atmospheric $CO_2$, in ppm, at northern hemisphere stations. The smooth curves are from the same fit as in Figure 2 but with the seasonal term $C_{obs\ seas}$ subtracted. (Thus they represent the function, $C_{obs\ rem}$.) Monthly average seasonally adjusted data ($C_{obs\ rem} + \varepsilon_{obs}$ of equation (2.3)) are shown by dots.

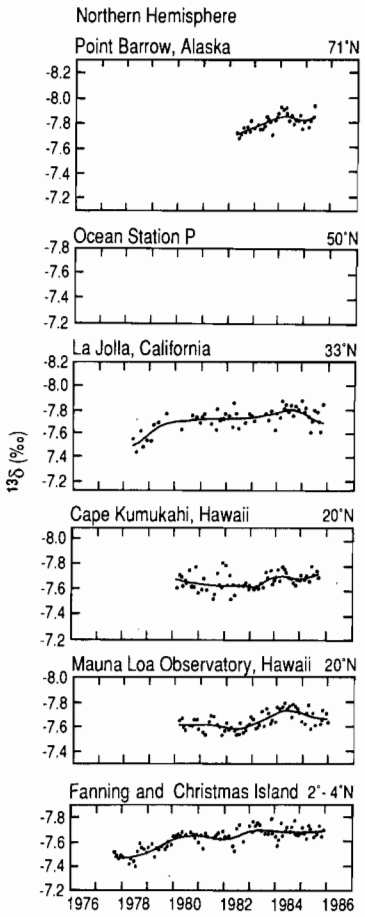


Fig. 7. Time trend of the seasonally adjusted isotopic ratio, $^{13}\delta$, for the same stations as in Figure 6. The smooth curves and dots are similar to those in Figure 6. Units are the same as for Figure 3.

negative $^{13}\delta_I$ values in the tropics might be attributed to the influence of certain kinds of land plants, growing in warmer climates, which incorporate and respire isotopically less negative carbon [O'Leary, 1981], but an additional reason for a spread in $^{13}\delta_I$ values, either more positive or more negative, is the likelihood that part of the seasonal cycle in atmospheric $CO_2$ is produced by oceanic processes which influence the concentration without significantly affecting the phase and amplitude of the seasonal cycle of $^{13}\delta$. Furthermore (see Figure 12), when $^{13}\delta$ is plotted against concentration for the same samples, the patterns deviate substantially from the nearly linear segments of hyperbolas expected for a single source or sink with constant $^{13}\delta_I$ [Keeling, 1958]. Similarly deviating patterns have been predicted and observed by Francey [1985].

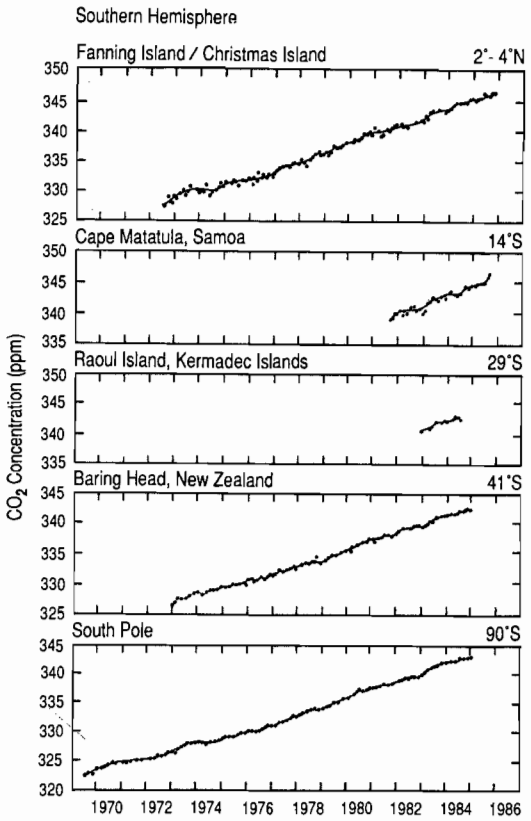


Fig. 8. Same as Figure 6 but for the southern hemisphere (with Fanning and Christmas Islands repeated).

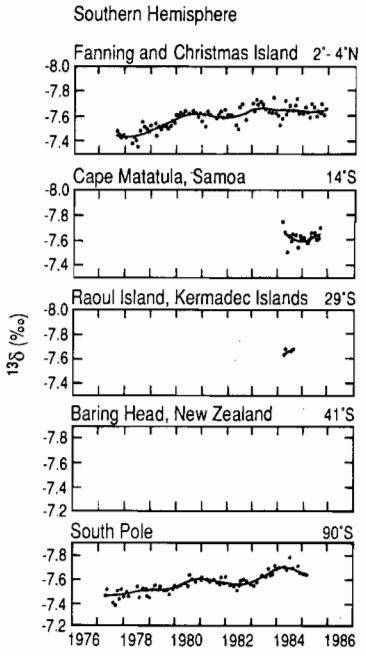


Fig. 9. Same as Figure 7 but for the southern hemisphere (with Fanning and Christmas Islands repeated).

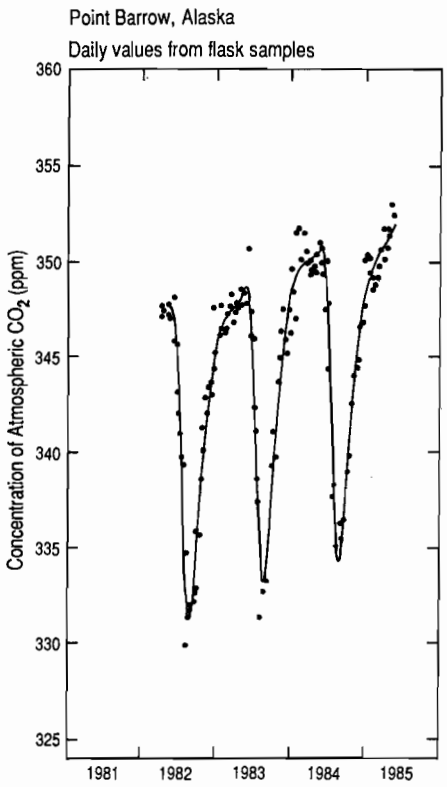


Fig. 10. Time trend of the concentration of atmospheric $CO_2$, in ppm, at Point Barrow, Alaska. The oscillating curve represents the function $C_{obs\ rem} + C_{obs\ seas}$, as in Figure 2. The dots denote daily values of the concentration obtained from flask samples.

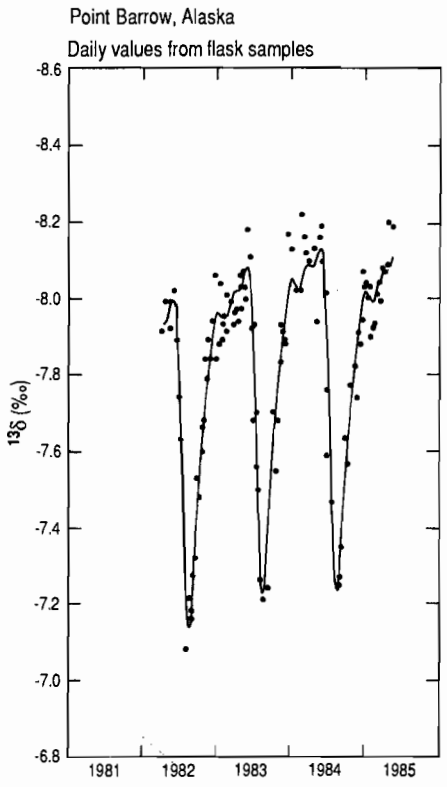


Fig. 11. Time trend of the reduced isotopic ratio, $^{13}\delta$, of atmospheric $CO_2$ in per mil difference from standard PDB, at Point Barrow, Alaska. The oscillating curve is the same curve as shown in Figure 3. The dots denote daily values, as in Figure 10.

We defer an analysis of these patterns pending analysis of our longer records which more precisely define the $^{13}\delta$ seasonal cycle. It is clear, however, that the isotopic data presented here generally support the view that the predominant component in the seasonal signal of $CO_2$ is owing to terrestrial plant activity.

As can be seen from the plots of Figures 2 and 4, the seasonal cycle in $CO_2$ concentration diminishes in amplitude from north to south as expected from the greater seasonality of plant activity at high latitudes, and the greater amount of land area in the northern hemisphere than in the south. The isotopic seasonal cycle diminishes southward in a similar manner, except that it is hardly discernible in the southern hemisphere. At two stations, Samoa and Kermadec Islands, this lack of definition may be a result of short records where the cycle is obscured by scatter, but even the considerably longer South Pole record shows only a weak cycle (Figure 5). Goodman and Francey [1988] show evidence of a $^{13}\delta$ oscillation for Cape Grim, Tasmania (at 40°41'S., 144°41'E.) with a peak to peak amplitude of approximately 0.05‰, as expected for a seasonal oscillation in concentration of about 1 ppm.

The isotopic oscillation is nearly in phase with that for concentration, with the most negative values in the austral spring, the same season as observed in the northern hemisphere. In our study

TABLE 5. Apparent Isotopic Ratio, $^{13}\delta_I$, of the $CO_2$ Added to or Removed from the Atmosphere at Various Stations

| Station Name | Approximate Latitude | Inclusive Dates of Observations | $^{13}\delta_I$ (‰) | Standard Error of $^{13}\delta_I$ (‰) |
|---|---|---|---|---|
| Point Barrow | 71°N. | April 8, 1982 – May 15, 1985 | −25.09 | 0.40 |
| La Jolla | 33°N. | April 1, 1978 – Oct. 7, 1985 | −28.28 | 0.64 |
| Mauna Loa | 19°N. | Feb. 15, 1980 – Dec. 13, 1985 | −23.70 | 0.91 |
| Cape Kumukahi | 19°N. | Feb. 4, 1980 – Sept. 23, 1985 | −26.62 | 0.64 |
| Fanning/Christmas | 3°N. | Aug. 2, 1977 – Nov. 30, 1985 | −23.85 | 1.76 |
| South Pole | 90°S. | March 15, 1977 – Feb. 1, 1985 | −23.25 | 3.50 |

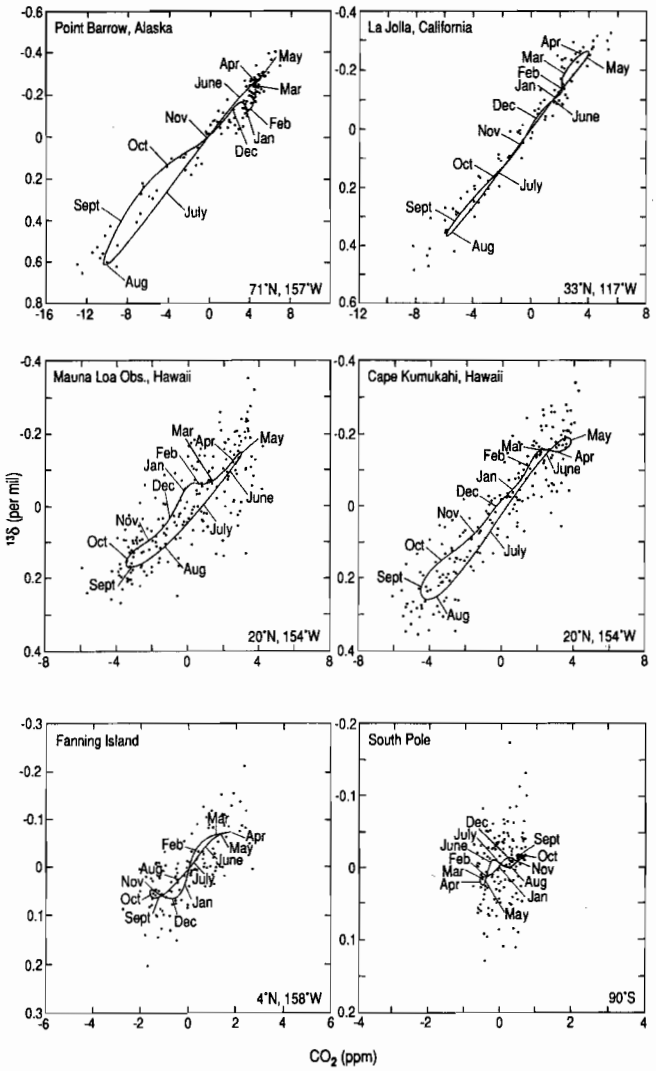


Fig. 12. The seasonal interrelationship between atmospheric $CO_2$ concentration, in ppm, and $^{13}\delta$, in per mil, at various stations. Dots denote daily averages of the departures of parameters from their respective seasonally adjusted values. The smooth curves are obtained by combining the harmonic functions for concentration and $^{13}\delta$. Positions on the curves representing the 15th day of each month are identified naming each month by its first three letters. The fifth panel displays the combined records of Fanning and Christmas Islands.

the harmonic fit to the isotopic data for the South Pole, especially the less scattered data after 1981, also suggests an oscillation of approximately this phase and amplitude.

At stations with long records there is evidence, as noted in subsection 2.4 above, that the seasonal cycle in concentration has changed in amplitude. Bacastow et al. [1985] show that for Mauna Loa Observatory from 1959 to 1982, the amplitude has

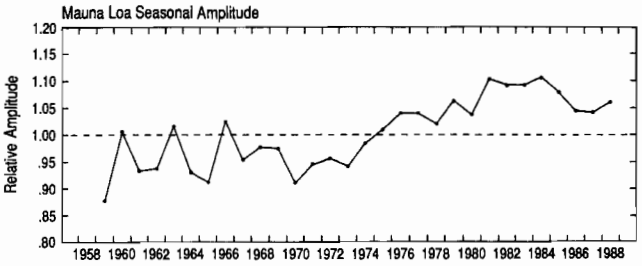


Fig. 13. Relative amplitudes of the seasonal cycle in atmospheric $CO_2$ concentration from year to year at Mauna Loa Observatory, Hawaii. The dots depict values of the gain factor, $\gamma$, obtained by separately fitting the function, $C_{obs\ seas}(t_m)$ of equation (2.1) to each year of daily-averaged data, where $t_m$ denotes the difference in time from the midpoint of the record. The dots are connected by line segments to show their trend. The amplitudes, as required by equation (2.1), assume constant phase.

been on average increasing by 0.7 percent per year. With the record extended through 1985, an even larger annual average rate of 0.84 percent is found [Keeling et al., 1989]. Most of the increase has occurred since the mid-1970's and, having remained high after 1982, has caused the average rate to increase. This can be seen in Figure 13, which includes supplementary data for 1986 through 1988. There is evidence, however, that the amplitude reached a maximum in the early 1980's and has since declined. We will return to this topic briefly in subsection 6.6 below.

### *4.3 Seasonally Adjusted Data*

North-south profiles of $CO_2$ concentration and $^{13}\delta$, seasonally adjusted, are plotted for the 1st of January of each year from 1978 through 1986 in Figures 14 and 15, respectively. The profiles for 1986 are derived from supplementary data (see subsection 2.5). As in Tables 1 to 4 for land stations we present values of $C_{obs\ rem}(t)$ and corresponding values for $^{13}\delta$. The individual data, as derived from revised fits of a spline plus exponential function that include supplementary data, are listed in Table 6. Data in the table for years before 1986 are slightly inconsistent with the data of Tables 3 and 4 and the smooth curves of Figures 6 to 9 because the fitting functions used to derive the data are affected throughout by the supplementary data.

These profiles show common features, especially the persistent piling up of $CO_2$ depleted in $^{13}C$ in the northern hemisphere. This accumulation we ascribe to the combustion of fossil fuels, most of which occurs north of 20°N.

The profiles also show striking dissimilarities. Firstly, although a peak in $CO_2$ concentration is seen near the equator every year from 1979 through 1986, it is weak or absent from the $^{13}\delta$ profile in 1980, as noted by Keeling et al. [1984], and is probably weak or absent in other years, except in 1983. This peak, as explained by Keeling et al. [1984], seems normally to be a result of the release of $CO_2$ from ocean water and is thus without a $^{13}\delta$ signature. There is evidently an additional source near January 1, 1983, which, from its isotopic expression at Christmas Island, suggests a release of $CO_2$ from the tropical terrestrial biosphere. Secondly,

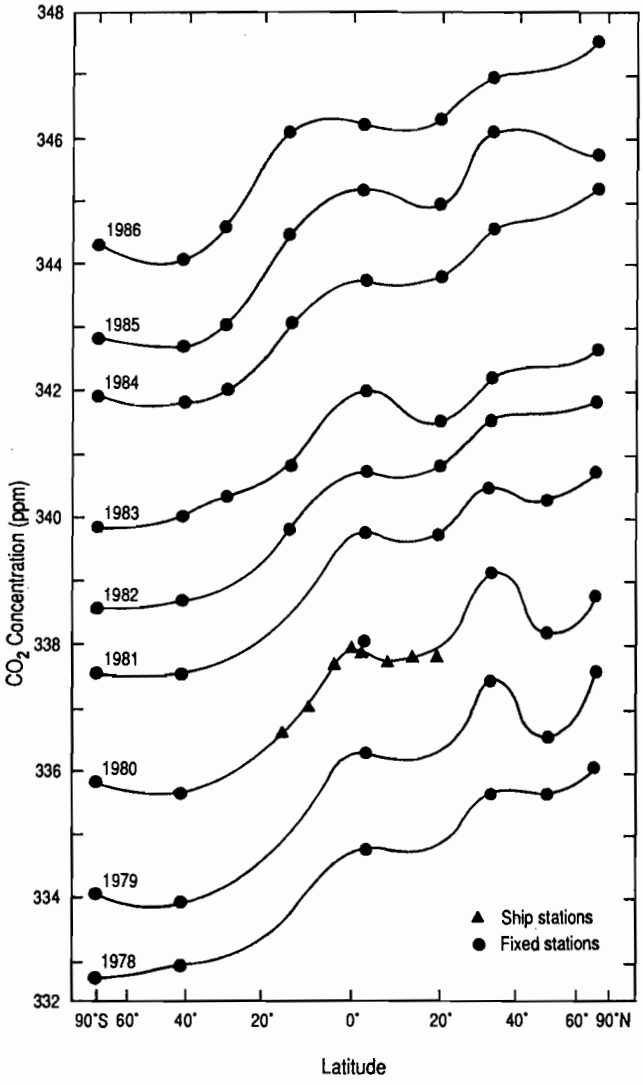


Fig. 14. Annual profiles for 1978 to 1986 of the seasonally adjusted concentration of atmospheric $CO_2$, in ppm, as a function of latitude based on the observations at fixed stations and from sampling at ship stations of the FGGE Shuttle Expedition of 1979/80. The profile for 1986 is based on supplementary data as explained in the text. The data plotted at 3°N are for Fanning and Christmas Islands combined (1978-1983) and at 2°N are for Christmas Island alone (1984-1986). The curves are drawn with a free hand by the first author.

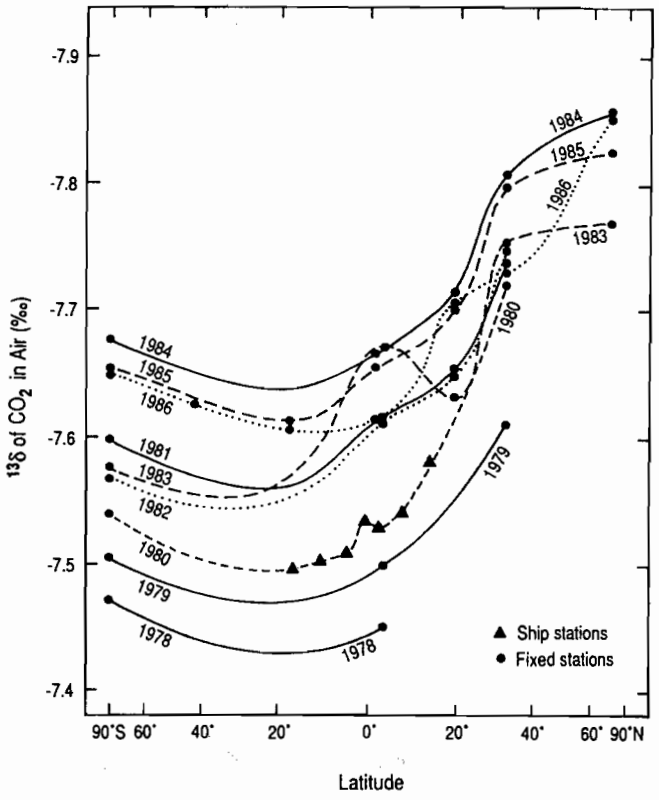


Fig. 15. Same as Figure 14, but for the reduced isotopic ratio, $^{13}\delta$, in per mil difference from standard PDB. The data plotted at 4°N are for Fanning Island alone (1978-1983) and at 2°N for Christmas Island alone (1984-1986).

the concentration profiles shift upward quite steadily at approximately 1.5 ppm per year. In contrast the $^{13}\delta$ profile, although generally trending toward more negative values, remains nearly stationary from 1981 to 1983, except near the equator, and again from 1984 to 1986. These irregularities are further discussed below.

Finally, the concentration profiles, except for the persistent peak near the equator and a second, variable, peak near 30°N. (reflecting the partially continental character of the La Jolla sampling site), decrease monotonically from north to south as expected from the release of $CO_2$ from fossil fuels, whereas the $^{13}\delta$ profiles reverse their trend when approaching the South Pole. This reversal is a result of the temperature dependence of the air-sea fractionation factor as discussed in the accompanying article of Keeling et al. [this volume].

### 4.4 *Interannual Variations*

The north-south profiles of Figures 14 and 15 suggest that a spectrum of interannual variations exist in both atmospheric $CO_2$ concentration and $^{13}C/^{12}C$ ratio in addition to the persistent rise attributed to industrial $CO_2$ emissions. The seasonally adjusted time plots, Figures 6 through 9, with their similar patterns for different stations, suggest a common cause for a substantial part of the variations.

Interannual variations in $CO_2$ concentration are too large to be a result of year to year variations in fossil fuel $CO_2$ emissions, which amount to only a few percent of the total release to the atmosphere. The variations in $CO_2$, however, have been shown [Bacastow, 1976; Bacastow et al., 1980; Thompson et al., 1986] to correlate

TABLE 6. Seasonally Adjusted Concentration and Isotopic Ratio of Atmospheric $CO_2$ for January 1 of the Specified Year

| Station Name | Lat. (°) | Long. (°) | Year 1978 | 1979 | 1980 | 1981 | 1982 | 1983 | 1984 | 1985 | 1986 |
|---|---|---|---|---|---|---|---|---|---|---|---|
| | | | Concentration (in ppm)[a] | | | | | | | | |
| Point Barrow | 71.3N. | 156.6W. | 336.09 | 337.63 | 338.81 | 340.78 | 341.85 | 342.66 | 345.19 | 345.67 | 347.61 |
| Station 'P' | 50.0N. | 145.0W. | 335.65 | 336.59 | 338.21 | 340.33 | – | – | – | – | – |
| La Jolla | 32.9N. | 117.3W. | 335.69 | 337.46 | 339.16 | 340.48 | 341.56 | 342.23 | 344.59 | 346.05 | 347.01 |
| Mauna Loa[b] | 19.5N. | 155.6W. | 334.50 | 335.83 | 337.57 | 339.04 | 340.05 | 341.52 | 343.75 | 345.00 | 346.24 |
| Cape Kumukahi | 19.5N. | 154.8W. | – | – | – | 339.76 | 340.84 | 341.54 | 343.82 | 344.96 | 346.30 |
| Line Islands[c] | | | 334.76 | 336.31 | 338.07 | 339.78 | 340.74 | 342.02 | 343.72 | 345.19 | 346.28 |
| Cape Matatula | 14.2S. | 170.6W. | – | – | – | – | 339.82 | 340.82 | 343.06 | 344.51 | 346.09 |
| Raoul Is. | 29.2S. | 177.9W. | – | – | – | – | – | 339.94 | 341.94 | 343.25 | 344.59 |
| Baring Head[d] | 41.4S. | 174.9E. | 332.96 | 333.93 | 335.67 | 337.58 | 338.71 | 340.02 | 341.82 | 342.59 | 344.07 |
| South Pole | 90.0S. | – | 332.77 | 334.06 | 335.84 | 337.58 | 338.58 | 339.83 | 341.91 | 342.84 | 344.49 |
| | | | Isotopic Ratio, $^{13}\delta$ (in ‰)[a] | | | | | | | | |
| Point Barrow | 71.3N. | 156.6W. | – | – | – | – | – | –7.768 | –7.856 | –7.825 | –7.853 |
| La Jolla | 32.9N. | 117.3W. | – | –7.611 | –7.720 | –7.737 | –7.746 | –7.753 | –7.807 | –7.797 | –7.728 |
| Mauna Loa | 19.5N. | 155.6W. | – | – | – | –7.605 | –7.580 | –7.612 | –7.712 | –7.698 | –7.660 |
| Cape Kumukahi | 19.5N. | 154.8W. | – | – | – | –7.653 | –7.649 | –7.631 | –7.714 | –7.700 | –7.704 |
| Line Islands[c] | | | –7.451 | –7.500 | –7.594 | –7.618 | –7.613 | –7.670 | –7.666 | –7.654 | –7.614 |
| Cape Matatula | 14.2S. | 170.6W. | – | – | – | – | – | – | – | –7.612 | –7.607 |
| Baring Head | 41.4S. | 174.9E. | – | – | – | – | – | – | – | – | –7.626 |
| South Pole | 90.0S. | – | –7.471 | –7.505 | –7.539 | –7.598 | –7.568 | –7.576 | –7.676 | –7.653 | –7.650 |

[a]Entries for 1980 and 1984 are slightly inconsistent with corresponding entries in Tables 3 and 4 because of the inclusion of supplementary data (see text).

[b]Data are from a continuous analyzer record.

[c]Records for Fanning Is. (3.9°N., 157.3°W.) and Christmas Is. (2.0°N., 159.3°W.) are combined.

[d]Data obtained by the New Zealand Institute of Nuclear Sciences, for 1978–1984 inclusive, are from a continuous gas analyzer record, for 1985 and 1986 by the Scripps Institution of Oceanography from flask analyses. Separate spline fits were obtained for the two records.

with the El Niño-Southern Oscillation phenomenon, a large scale climatic anomaly which recurs every few years with varying intensity and especially involves the trade winds and underlying ocean water of the low latitudes. In the strict sense, El Niño events are defined as extreme warming of surface ocean water along the west coast of South America near Ecuador and Peru. Maximum warming tends to occur in December when upwelling is weaker than normal [Rasmusson and Carpenter, 1982]. The events, which occur approximately every 4 years, are not confined to the eastern Pacific region but involve anomalous atmospheric and oceanic conditions over a wide area, even extending beyond the Pacific ocean basin [see, for example, Rasmusson and Wallace, 1983].

A rise in $CO_2$ concentration during the strong El Niño of 1972 is seen at four stations where our series of concentration data extend back to that period: La Jolla, Mauna Loa and the Line Islands in the northern hemisphere (see Figure 6) and the South Pole in the southern hemisphere (see Figure 8). These data show that, during late 1972 and early 1973, when the trade winds were weak, the concentration of $CO_2$ rose abnormally rapidly in both the northern and southern hemispheres. The rate of rise correlates closely with the Southern Oscillation Index (SOI) [Bacastow, 1976], a measure of the barometric pressure gradient across the Pacific Ocean, and also with tropical Pacific sea-surface water temperatures which respond to changing wind patterns [Newell et al., 1978]. Similar increases in $CO_2$ occurred at all of these same stations during the very strong El Niño event of 1982 and 1983 [Gill and Rasmusson, 1983].

Sea water, when warmed, tends to release $CO_2$ owing to the lower solubility of this gas at higher temperature. It might be supposed, therefore, that tropical surface ocean water was anomalously heated during the 1972/1973 and 1982/1983 El Niño events, and that $CO_2$ was driven off. This explanation is implausible, however, because during such events anomalously warm water spreads eastward and displaces normally cooler surface water of the eastern tropical Pacific ocean. This water in the east is higher in $CO_2$ partial pressure ($pCO_2$) than the warmer water from the west [Keeling, 1968] which displaces it. Thus one would expect a decrease in the rate of rise in $CO_2$ concentration, not an increase as observed.

The isotopic data suggest a possible explanation for a $CO_2$ rise in 1980 and 1983 unrelated to oceanic processes, and therefore not necessarily tied to the degree of warming of sea water in the eastern tropical Pacific ocean. As can be seen in Figures 7 and 9, the seasonally adjusted $^{13}\delta$ records show indistinct, but possibly

significant, peaks in negative $^{13}\delta$ in 1980 and 1983, alternating with troughs in 1979, 1982 and 1985. These oscillations suggest that $CO_2$ may have been released to the air during El Niño events by the terrestrial biosphere.

To examine these nearly simultaneous anomalies in concentration and $^{13}\delta$ more closely, we have carried out a further analysis of the atmospheric $CO_2$ records of Mauna Loa Observatory and the South Pole, our longest records of concentration, and nearly our longest isotopic records. We include supplementary concentration and isotopic data through 1988, as described in Appendices A and B. In deriving seasonal and interannual trends by the methods described in subsection 2.2 above, we have made minor adjustments affecting the analysis of the earlier data. Monthly averages of the Mauna Loa and South Pole concentration data are listed in Table A.4, corresponding seasonally adjusted data in Table A.5. Seasonal adjusted isotopic data are listed in Table B.1.

The $CO_2$ concentration record for Mauna Loa Observatory is shown in Figure 16. The same record, with the seasonal cycle subtracted, is shown in Figure 17. Interannual variations can be seen in this seasonally adjusted plot, but they are largely masked by the persistent rise in concentration associated with fossil fuel combustion. As discussed in subsection 2.2, above, we have removed this persistent rise from the record by subtracting a constant fraction of the cumulative input from industrial $CO_2$. As shown in Figure 18, this cumulative record, based on the data listed in the report of

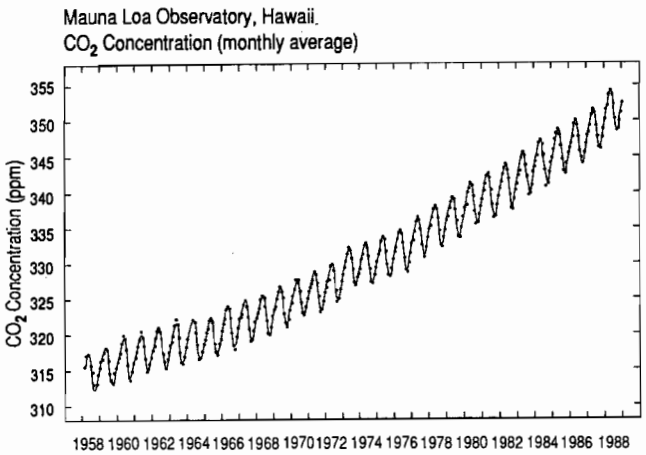


Fig. 16. Time trend of the concentration of atmospheric $CO_2$, in ppm, at Mauna Loa Observatory Hawaii, including supplementary data after December, 1985. The dots denote monthly mean concentrations obtained from a continuously recording gas analyzer. The oscillating curve is a fit of weekly average concentration to a spline function combined with an exponential function and four harmonic terms, as in Figures 2 and 4.

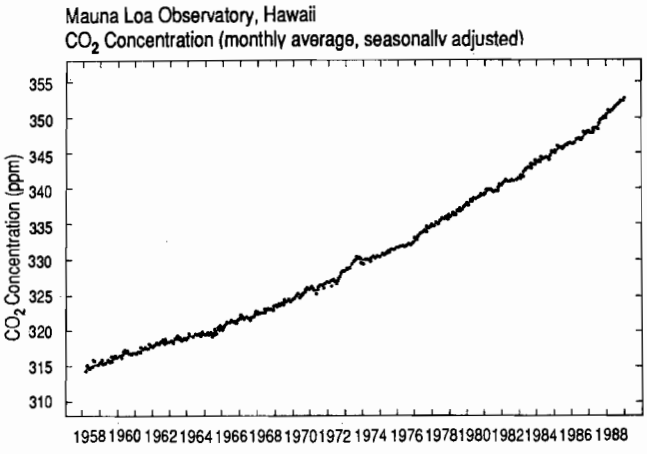


Fig. 17. The monthly averages of Figure 16 after seasonal adjustment. The smooth curve is from the same fit as in Figure 16 but with the seasonal term subtracted. The dots are seasonally adjusted monthly mean concentrations, as in Figures 6 and 8.

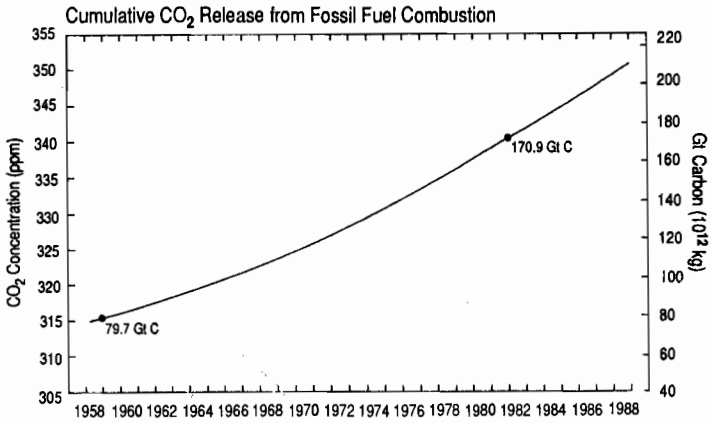


Fig. 18. Cumulative release of $CO_2$ from fossil fuel combustion and cement production during the period of the Mauna Loa $CO_2$ record. The scale, in units of $10^{12}$ kg of carbon, is shown on the right. On the left side is shown a scale for $CO_2$ concentration in the range of the data for Mauna Loa Observatory. The two scales are adjusted so that the cumulative productions of 1 January of 1959 and 1982 coincide with the seasonally adjusted concentrations of $CO_2$ at Mauna Loa on these dates. The cumulative productions are indicated for these dates (1 Gt = $10^{12}$ kg).

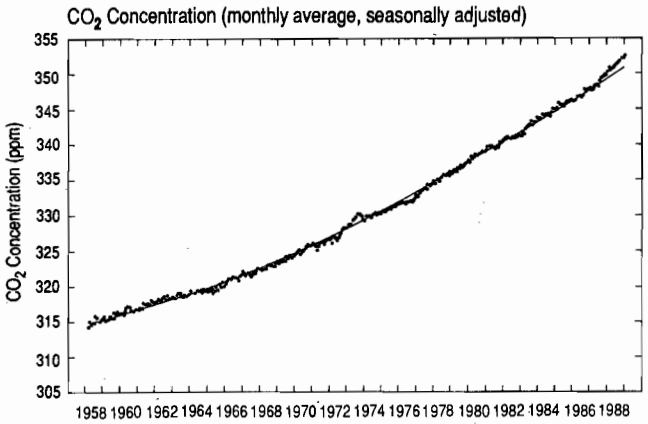


Fig. 19. Same as Figure 18, except that the monthly means of the seasonally adjusted concentration of $CO_2$ at Mauna Loa Observatory are also shown, plotted as in Figure 17.

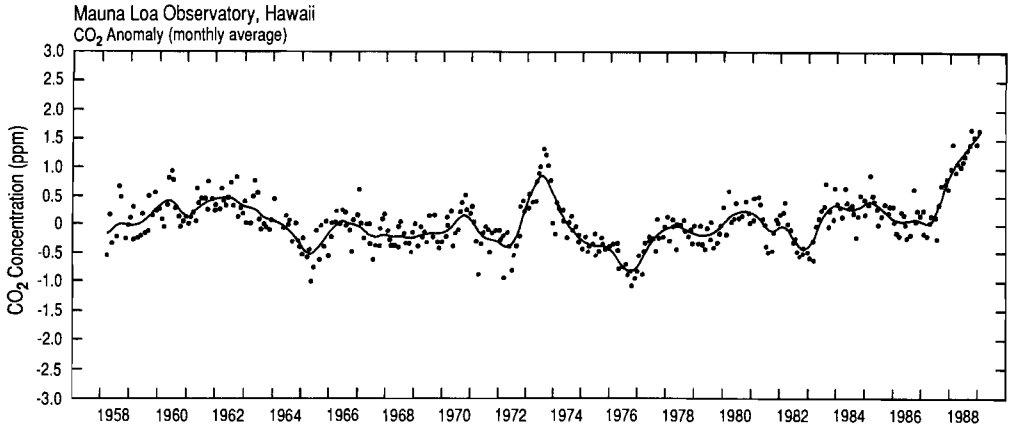


Fig. 20. Anomaly in the concentration of atmospheric $CO_2$, in ppm, at Mauna Loa Observatory, based on the same data as Figures 16 and 17. The dots depict monthly averaged concentrations after seasonal adjustment, and after subtraction of a constant fraction of the increase in $CO_2$ which would have occurred if all of the industrial $CO_2$ release to the air had remained airborne (see text). The smooth curve is derived from the same fitting function employed for Figure 17, with a standard error, $\sigma$, of 0.3441 ppm.

Keeling et al. [1989], shows a similar rising trend. Indeed, if the two records are overlaid, as in Figure 19, with the two trends forced to agree on January 1, 1959 and 1982 ($t_1$ and $t_2$, respectively, of equation (2.6)), the curves are strikingly similar. Nevertheless there is evidence of atmospheric $CO_2$ fluctuations not reflected in the industrial emissions. Upon subtracting the industrial $CO_2$ curve from the Mauna Loa curve, these interannual variations (term, $C_{anom}(t)$ of equation (2.5)) are clearly seen (Figure 20). A similar anomaly plot for the South Pole (Figure 21) shows that more or less simultaneous fluctuations occur in both hemispheres.

The South Pole $CO_2$ record corresponds slightly less well than that for Mauna Loa to a constant fraction of industrial $CO_2$ emissions. The anomaly near the middle of the record is lower, in general, than the Mauna Loa anomaly, because the South Pole is cut off from the main source of industrial emissions in the northern hemisphere by an equatorial barrier to interhemispheric mixing of air, as discussed a few paragraphs below.

Apart from this feature the two anomaly records show such similar interannual fluctuations, as do records for other stations (discernible in Figures 6 and 8), that it is reasonable to regard these fluctuations as essentially global in extent. We have therefore averaged the Mauna Loa and South Pole records so as to approximate a global time series, shown in Figure 22. Because the increases in $CO_2$ between the reference dates of 1959 and 1982 are different for the two records, the airborne fraction of industrial $CO_2$ required to create each anomaly plot is different. For the combined anomaly the fraction is 56.55 percent, which is the mean of that for Mauna Loa (58.25 percent) and the South Pole (54.85 percent).

Also indicated in Figure 22 are the times of occurrence of recent El Niño events, with strengths expressed according to the classification of Rasmusson [1984, p. 7], and times of occurrence of weak summer monsoons in southeast Asia as tabulated from data for India by Meehl [1987]. Except for the El Niño event of

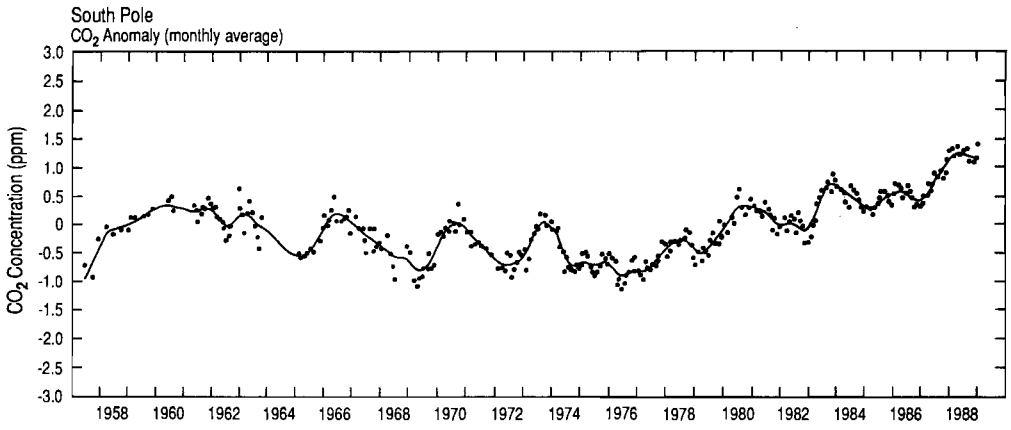


Fig. 21. Same as Figure 20, except for the South Pole. Data after February, 1985 are supplementary (see text). The standard error, $\sigma$, of the spline is 0.1628 ppm.

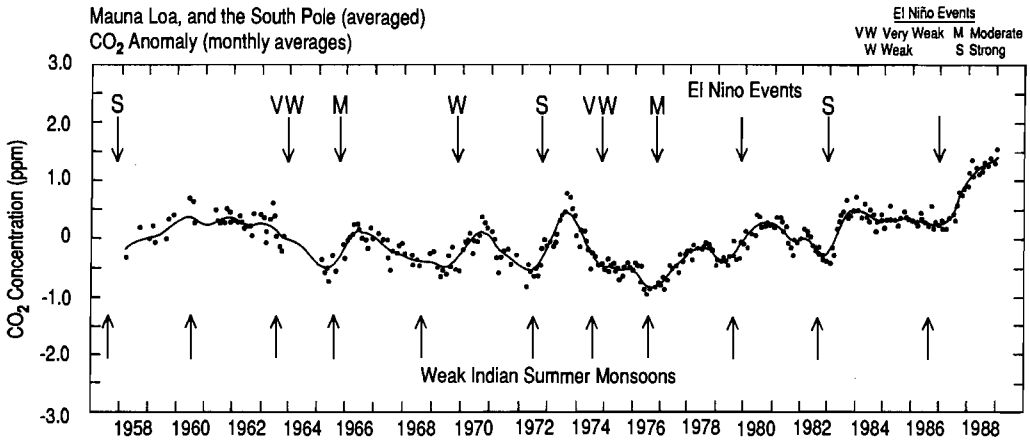


Fig. 22. Same as Figure 20, but for Mauna Loa Observatory and the South Pole records combined by averaging both the functions and individual data points of Figures 20 and 21. The upper arrows denote the times of El Niño events, each shown for December of the year of onset. The strengths are indicated as ranging from strong to very weak. The event in 1979 is doubtful [Donguy et al. 1982] and not ranked; that in 1986 occurred subsequent to the ranking by Rasmusson [1984]. The lower arrows denote weak summer monsoons in India according to [Meehl, 1987], shown for July of the year of occurrence.

1963, for which atmospheric $CO_2$ data are lacking, there is evidence that the $CO_2$ rose anomalously, either during the onset year or soon after, for each El Niño since 1957. Even the most recent event of 1986–1987 [Wagner, 1987], not classified by Rasmusson, is represented. According to Rasmusson, there was no event in 1979. Nevertheless, some of the characteristics of El Niño occurred that year and continued into the next year [Donguy et al., 1982]. With one exception (1969), weak monsoons occurred during the same years as El Niño events, regarding 1979 as an El Niño year. Thus rises in $CO_2$ also correlate with weak monsoon conditions in southeast Asia.

Interannual variations are further evident in plots of the reduced isotopic ratio $^{13}\delta$ plotted for Mauna Loa Observatory and the South Pole in Figures 23 and 24, respectively. Because the long-term trend in $^{13}\delta$ is nearly stationary relative to short-term interannual variations, these plots are practically equivalent to the anomaly plots for concentration. The data for 1977 at the South Pole and 1978 at Mauna Loa Observatory have been omitted from consideration because they are less reliable than subsequent data. A plot of the records of $^{13}\delta$ for the two stations, averaged and seasonally adjusted, is shown in Figure 25.

If isotopic $CO_2$ data had been obtained for the entire record period since 1958, it would be possible to estimate the extent to which the terrestrial biosphere and the oceans separately contributed to each of the anomalous oscillations in concentration seen

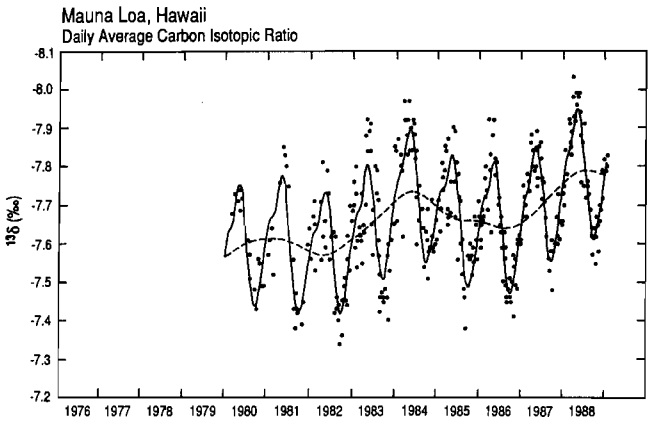


Fig. 23. The reduced isotopic ratio, $^{13}\delta$, of atmospheric $CO_2$ in per mil difference from standard PDB, at Mauna Loa Observatory, Hawaii. The solid curve is a fit of daily average values to a spline function combined with an exponential function and four harmonic terms, as in Figures 3 and 5. The dashed curve denotes the same fit as the solid curve, but with the harmonic terms subtracted to show the long-term trend, as in Figures 7 and 9. The dots denote daily values. A few data in 1978 are not shown, although they were used to prepare the curves. The standard error, $\sigma$, of the spline is 0.068‰.

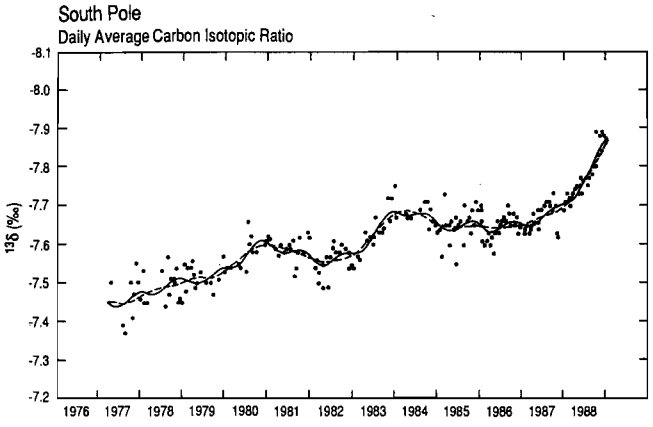


Fig. 24. Same as Figure 23 but for the South Pole. The solid curve is fit to two harmonic terms instead of four. The standard error, $\sigma$, of the spline is 0.032‰.

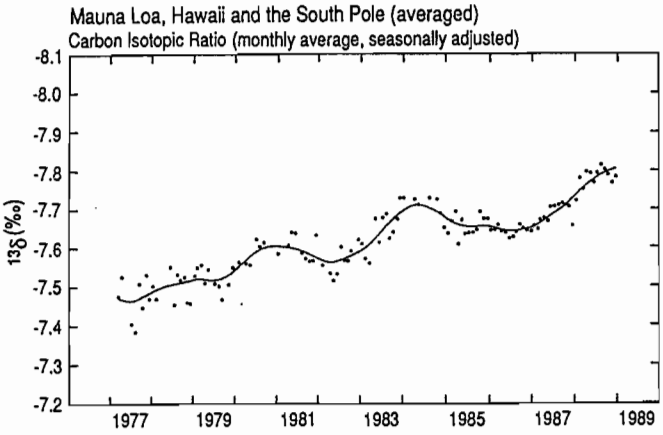


Fig. 25. Seasonally adjusted record of $^{13}\delta$, in per mil, obtained by averaging the data for Mauna Loa Observatory and the South Pole. The curve defines the average of the dashed curves of Figures 23 and 24. The dots denote combined monthly averages of the data shown in these two previous figures.

in Figure 22. Since the combined Mauna Loa-South Pole isotopic record, shown in Figure 25, begins only in 1978, we can address only the three most recent El Niño events in the light of isotopic data. As can be seen in this figure, anomalous peaks in negative $^{13}\delta$ occurred late in 1980, 1983, and probably in 1988. These are nearly coincident with rises in $CO_2$ concentration, shown in Figure 22.

The concentration and isotopic data, combined for Mauna Loa and the South Pole, are thus consistent with a release of $CO_2$ by the terrestrial biosphere during the year of onset of El Niño events and of a weak summer monsoon in southeast Asia. The respective amplitudes in 1983, however, are not consistent with an exclusively biospheric source. The isotopic shift, peak to trough, is approximately 0.10‰, equivalent to a concentration shift of 2.0 ppm (see equation 3.3), and thus nearly three times as large as the observed 0.7 ppm rise in concentration (Figure 22).

This discrepancy suggests that during the 1983 event, while the $CO_2$ was rising in response to a short-term biospheric source, a substantial amount of $CO_2$ was being simultaneously withdrawn from the air by the oceans. Such a conclusion is consistent with our understanding, discussed above, that El Niño events should be accompanied by a reduction of $CO_2$ partial pressure in the tropical Pacific Ocean, and is also consistent with observations of low $pCO_2$ in the eastern Pacific Ocean in 1983 as compared to more normal years [Keeling and Revelle, 1985; Feely et al., 1987]. Furthermore, the tendency for the $CO_2$ concentration to rise anomalously during the year of a weak summer monsoon in southeast Asia, suggests that, if the source is biospheric it may be related to wide-spread drought conditions. We will return in section 6 to a discussion of the relative importance of the oceans and biosphere in producing a $CO_2$ response to El Niño events and weak monsoons.

The Mauna Loa and South Pole atmospheric $CO_2$ records indicate that the $CO_2$ concentration gradient between the northern and southern hemisphere increased from 1958 to 1989, as seen when the seasonally adjusted trends for both stations are plotted together (Figure 26). In addition to a persistent rise in both records, and nearly simultaneous wiggles associated with El Niño events, there is a gradual separation of the trends, indicating that the $CO_2$ concentration at Mauna Loa has generally risen more rapidly than at the South Pole. This tendency is seen more clearly in Figure 27,

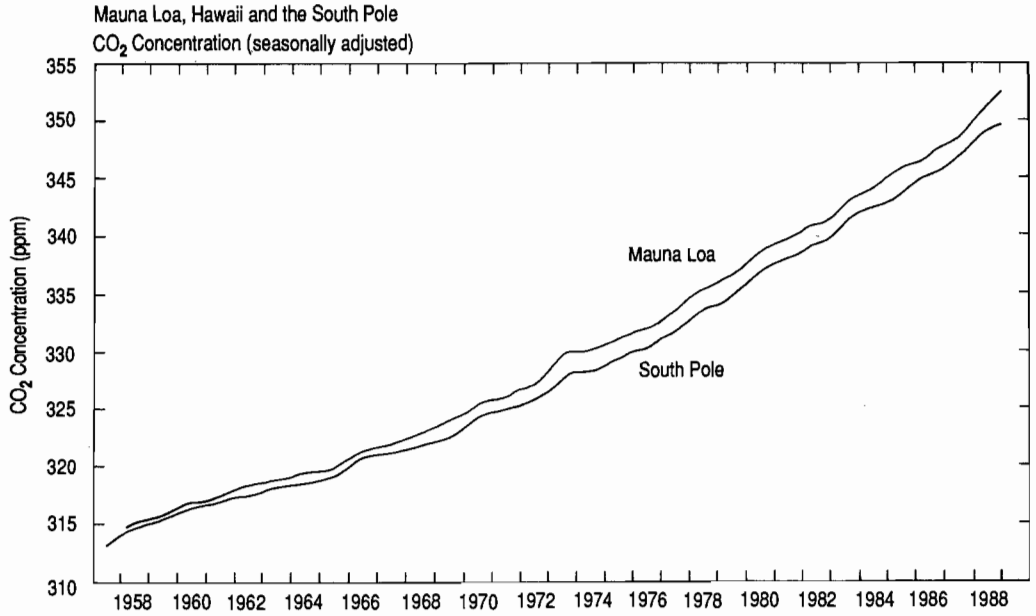


Fig. 26. Comparison of the seasonally adjusted time trends of atmospheric $CO_2$, in ppm, at Mauna Loa and the South Pole. The upper curve is identical to the smooth curve in Figure 17. The lower curve is a similar function for the South Pole.

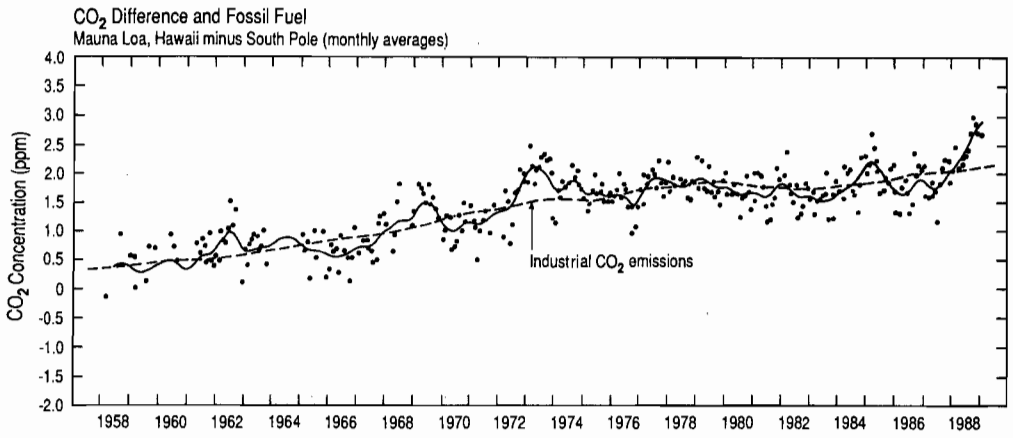


Fig. 27. Difference in concentration of atmospheric $CO_2$, in ppm, between Mauna Loa and the South Pole versus time. Positive values indicate that the concentration at Mauna Loa is higher. The solid curve is the difference between the two curves of Figure 26. The dashed line is a plot of the pattern of industrial $CO_2$ emissions (see text). The dots denote monthly average differences.

where the differences between the records are plotted after seasonal adjustment.

The more rapid increase in the difference early in the records is similar to a more rapid increase which occurred in the rate of industrial $CO_2$ emissions, shown by a dashed line, scaled so that the plot of emission rate roughly coincides with the plot of $CO_2$ differences near the beginning and end of the later record. After the oil crisis of 1974, industrial $CO_2$ emissions increased only very slowly, and the $CO_2$ difference, likewise. A close relationship of the interhemispheric gradient in $CO_2$ to the rate of industrial $CO_2$ emissions occurs, because most of these emissions (95 percent according to Marland et al. [1985]) are produced in the northern hemisphere and because a barrier to interhemispheric mixing exists near the equator. Industrial $CO_2$ tends to pile up in the northern hemisphere in proportion to its rate of production. It follows that the airborne fraction must be higher in the northern hemisphere whenever the rate of emissions is accelerating. Indeed, Bacastow and Keeling [1981], computed an interhemispheric mixing time of 1.1 yr from the observed difference in airborne fractions between Mauna Loa and the South Pole from 1959 to 1978, which is in reasonable agreement with meteorological estimates.

This barrier to mixing also explains why the South Pole anomaly of Figure 21 is lower in the middle of the record than the anomaly for Mauna Loa in Figure 20. Consistent with the difference plot of Figure 27, the $CO_2$ concentration at Mauna Loa rises more rapidly than at the South Pole until 1974, and thereafter at nearly the same rate as at the South Pole. Since the Mauna Loa $CO_2$ record has a pattern which agrees near its middle with the pattern for industrial $CO_2$ emission when the two patterns are forced to coincide in 1959 and 1982, the pattern for the South Pole record, similarly forced to coincide with the industrial $CO_2$ record, must show a dip near the middle of the record.

The $CO_2$ differences between Mauna Loa and the South Pole are not directly proportional to industrial $CO_2$ emissions, however. If the scaling factor for fuel emissions which produces the dashed line in Figure 27 (0.508 ppm/$10^{12}$ kgC) is applied to estimate the concentration difference at zero fuel emission rate, the concentration of $CO_2$ at the South Pole before the industrial era is found to be higher than in the northern hemisphere by 0.82 ppm.

The possibility of such an imbalance between the hemispheres has been previously noted by Pearman and Hyson [1980, p. 4461], who proposed that it arises from differences in the seasonal cycle

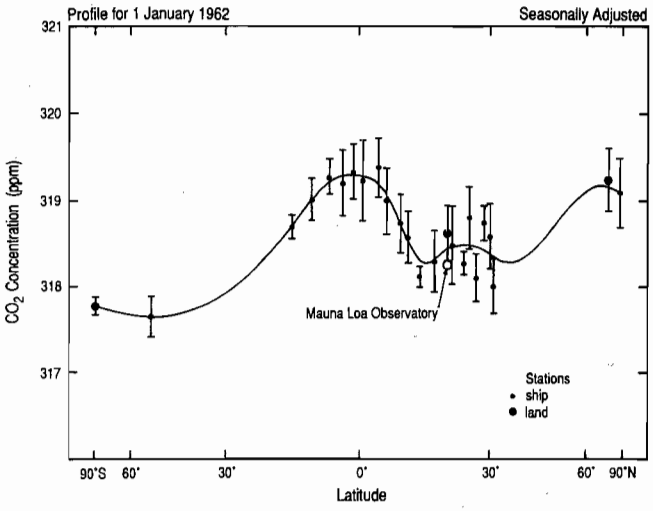


Fig. 28. Seasonally adjusted concentration of atmospheric $CO_2$ near the earth's surface, in ppm, as a function of the sine of latitude on 1 January, 1962, as listed in Table 1. Large dots denote values of $C_{obs\ rem}$ at fixed stations. Small dots denote sampling on board ships. Bars indicate twice the standard error of individual data points (see text). The solid curve is a weighted fit to the data, using a cubic spline function [Reinsch, 1987] forced to agree with data for the South Pole and Ice Floe Station Arlis. The concentration at Mauna Loa Observatory is indicated by an open circle, and is not included in the spline fit, owing to the high elevation of the station.

of the terrestrial biosphere in the two hemispheres. The three-dimensional model computations of Keeling et al. [this volume] confirms that this mechanism contributes to an imbalance, but indicate that an imbalance in air-sea exchange of $CO_2$ is more likely the major contributor.

Further evidence of changing interhemispheric $CO_2$ gradients is seen in the seasonally adjusted data, which we assembled for special periods having additional sampling from ships. These data, from Tables 1 to 4, are plotted in Figures 28 through 31, with smooth curves drawn to display the north-south trends. In Figure 32 the first two plots and the last plot are compared in terms of concentration differences from that of the South Pole. Throughout the northern hemisphere a progressive piling up of $CO_2$ between 1962 and 1984 is seen, consistent with our deduction, discussed above, based only on the Mauna Loa and South Pole records.

We return in a later section to a discussion of interannual variations in atmospheric $CO_2$, enlarging the time span of interest to include the entire industrial era. However, before doing so, we explain in the next section the use of a compartment model to simulate global scale exchanges of carbon between reservoirs of the carbon cycle. This model is then used to assess both El Niño events and long-term variations in atmospheric $CO_2$.

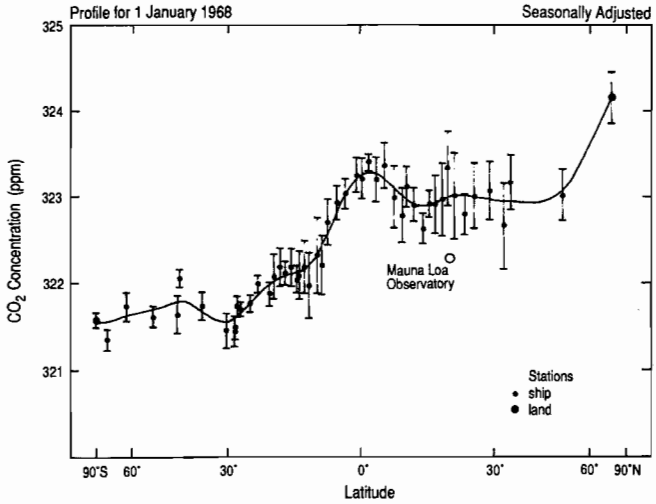


Fig. 29. Same as Figure 28, but for 1968. Data are listed in Table 2.

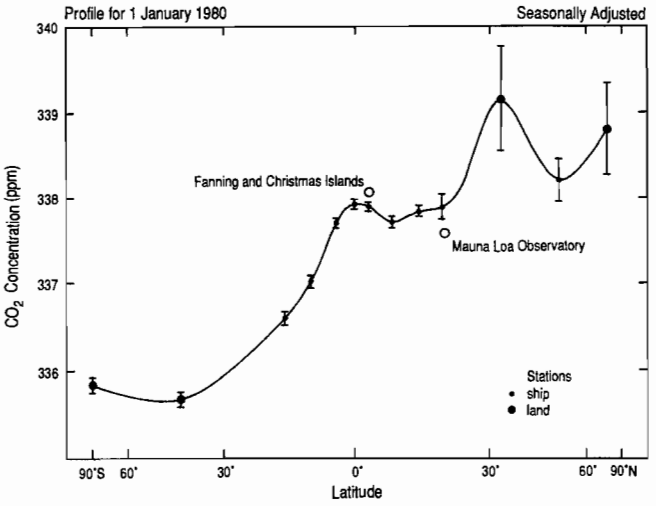


Fig. 30. Same as Figure 28, but for 1980. The solid curve is an interpolating taut spline [Cline, 1974] (which passes exactly through the fitted points). The point for La Jolla, at 33°N, although included in the fit, is not reliable owing to too few measurements in 1979 and 1980. Open circles denote data for Fanning and Christmas Islands combined and for Mauna Loa Observatory (left and right, respectively). Both data were omitted from the spline fit. All data are listed in Table 3.

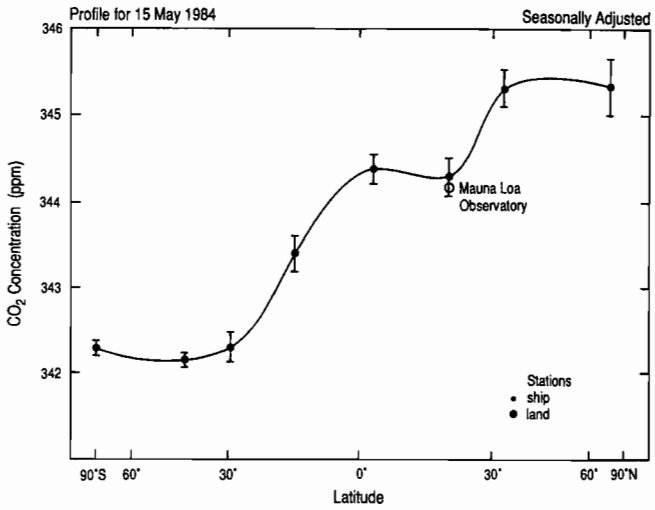


Fig. 31. Same as Figure 30, but for 15 May, 1984. The open circle denotes the datum for Mauna Loa Observatory, omitted from the spline fit. All data are listed in Table 4.

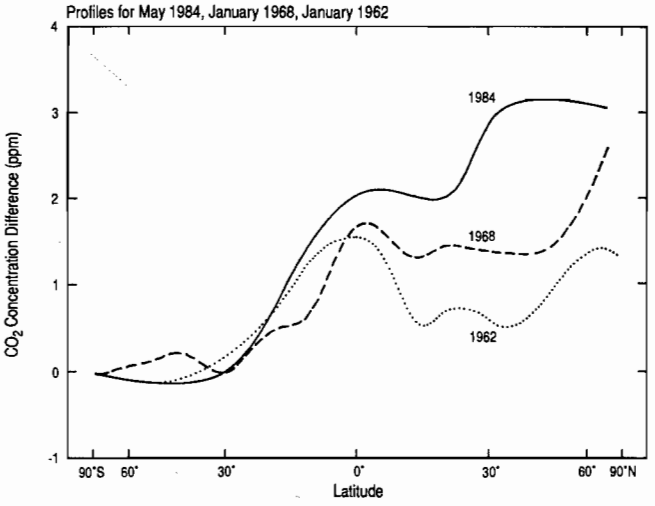


Fig. 32. The north-south profiles of Figures 28, 29 and 31 plotted as differences from the atmospheric $CO_2$ concentration at the South Pole. The curve for 1980 (Figure 30) is similar to that for 1984 and not shown.

### 4.5 *Concluding Remarks*

This qualitative survey indicated that atmospheric $CO_2$ is perceptibly perturbed by all three of the rapidly interacting reservoirs of the carbon cycle. The imprint of the lithospheric reservoir from which fossil fuel is derived is seen in the accumulation of industrial $CO_2$ in the northern hemisphere, in the similarity of the pattern of atmospheric $CO_2$ rise at Mauna Loa Observatory with the cumulative rate of industrial $CO_2$ emissions, and in the $CO_2$ concentration difference between the hemispheres, which increased rapidly during the period of sustained growth in fuel consumption in the 1950's and 1960's, but became nearly stationary after emission rates leveled off in the mid–1970's. The terrestrial biosphere impacts atmospheric $CO_2$ by way of seasonal and interannual variations seen not only in the $CO_2$ concentration but also in the reduced isotopic ratio, $^{13}\delta$. The intensity of the seasonal cycle varies spatially, as expected from the distribution of plant activity on land and the increasing seasonality in plant growth with distance from the equator, and probably varies temporally as well, as seen in the increasing amplitude of the seasonal cycle with time. Interannual variations in $^{13}\delta$, reflecting longer term variations in plant growth or decay, are less well established but appear to be approximately of the same amplitude wherever they have been observed.

The oceanic reservoir produces the least obvious impacts on atmospheric $CO_2$. Its response to rising atmospheric $CO_2$ concentrations is not readily apparent when examining either time series or the spatial distribution of $CO_2$. Oceanic influences on the seasonal cycle of $CO_2$ are largely masked by the activity of land plants, while oceanic influences on the mean annual spatial distribution are obscured by the emission of fossil fuels. Nevertheless, oceanic processes appear to influence the relationship of $CO_2$ concentration to $^{13}\delta$. A peak in concentration near the equator, not mirrored by $^{13}\delta$, suggests a release of $CO_2$ by the tropical oceans. The seasonal interrelationships of concentration and $^{13}\delta$, shown for various stations in Figure 12 as significant departures from a smooth monotonic line pattern, are suggestive of a seasonal oceanic signal out of phase with the terrestrial biospheric signal.

If the $CO_2$ concentration in preindustrial times was higher in the southern hemisphere than in the northern, as our analysis of the $CO_2$ gradient between Mauna Loa and the South Pole suggests, then the oceans are likely to have been responsible. Wind-driven ocean currents and thermohaline circulation of deep water can transport tracers great distances, whereas the terrestrial biosphere can displace carbon spatially only by means of subtle, regional imbalances and relatively minor interactions between the seasonal cycles of $CO_2$ exchange and air transport.

The causes of the observed atmospheric $CO_2$ variations deserve a more quantitative analysis than afforded by this survey. In the next section we begin such an analysis by examining the carbon cycle in the context of a compartment model which predicts carbon transfers between global scale reservoirs as they vary over decadal time scales. With this model we address secular changes in the carbon cycle in broad quantitative terms over the entire industrial era. Then in the following section, with the model modified to address finer temporal details of the carbon cycle, we investigate the causes of interannual variations in atmospheric $CO_2$ associated with El Niño and the Southern Oscillation, and longer term variations not accounted for in our original formulation of the model. Afterwards, in three accompanying articles, the quantitative results of the original formulation are made the basis for explaining the seasonal cycle and spatial distribution of $CO_2$ taking into account the three-dimensional transport of $CO_2$.

## 5. Compartment Model of the Long-Term Variations in Atmospheric $CO_2$

In our three-dimensional modeling of the atmospheric carbon cycle, discussed in the accompanying articles, we take notice of interannual variations only with respect to carbon fluxes which vary so slowly that their influence on atmospheric $CO_2$ is predictable assuming the atmosphere to be spatially uniform. These fluxes include perturbations arising from the combustion of fossil fuels and from human disturbances to the terrestrial biosphere. We have also accepted the premise, still controversial, that plant growth on land has been stimulated by the rise in atmospheric $CO_2$ concentration. The biospheric fluxes are specified to vary only on time scales long with respect to the time of mixing of atmospheric $CO_2$, which, as shown by Heimann and Keeling [this volume], is approximately 1 year. Thus, with respect to the distribution of atmospheric $CO_2$ at any given moment, they appear as steady fluxes which produce the same change in $CO_2$ concentration throughout the atmosphere. Fossil fuel emissions, specified from annually reported data, vary by only a few percent from year to year so that they also may be regarded as steady for the same reason. Oceanic fluxes are specified only in so far as they are responses to these perturbations.

For computing these slowly varying $CO_2$ exchanges we have selected the box diffusion model of Oeschger et al. [1975], which has been widely used and several times revised. This model has been evaluated extensively and contrasted with other one-dimensional models, especially by Enting and his collaborators [Enting and Pearman, 1982, 1983, 1986, 1987; Thompson et al., 1986; Enting and Mansbridge, 1987]. We have chosen the version of Keeling et al. [1980] which incorporates stable isotopic carbon in the formulation, but we have assigned the principal model parameters to conform as closely as possible with the recent carefully calibrated version of Siegenthaler [1983]. Our analysis was completed before the appearance of a further revision by Siegenthaler and Oeschger [1987].

We have incorporated the results of this compartment model calculation into a series of quasi-stationary computations of the mean annual three-dimensional field of atmospheric $CO_2$ for 1962, 1968, 1980, and 1984 on the above assumption that the slowly varying sources and sinks of atmospheric $CO_2$ are approximately steady during any given year. In the three-dimensional model the oceanic fluxes derived from the compartment model are distributed uniformly over the ocean surface, while those involving the terrestrial biosphere are assumed to vary spatially in proportion to the local rate of net primary productivity, and the fossil fuel flux is distributed realistically.

In the box diffusion model the response of the oceans to a disturbance at the air-sea boundary is approximated by postulating that a mixed layer of 75 m depth overlies a deep oceanic reservoir which is vertically mixed by eddy diffusion. The assumption of a constant eddy diffusion coefficient is not realistic, but the model mimics responses of the oceans to changes in atmospheric $CO_2$ when calibrated to predict the distribution of radiocarbon. For responses on time scales from decades to a few hundred years Siegenthaler [1983] calibrated the model to predict the distribution of radiocar-

bon produced since the 1950's by nuclear bomb testing. For responses over considerably longer time periods, he carried out a separate calibration using a smaller diffusion coefficient based on the pre-bomb, preindustrial radiocarbon distribution, presumed time to be stationary. We have made computations using both of his model calibrations.

The terrestrial biosphere, for modeling purposes, was divided by Keeling [1973a] into two compartments to represent carbon stored for shorter and longer times. In the present model we have reduced the biosphere to a single compartment by omitting the compartment with the shorter storage time. This simplification, first made by Oeschger et al. [1975], has little effect on the box diffusion model predictions of perturbations in the carbon cycle owing to the small amount of carbon associated with short storage times, but it results in a considerably reduced exchange of $CO_2$ between the atmosphere and the biosphere compared to the total based on net primary productivity: approximately $25 \times 10^{12}$ kgC $yr^{-1}$ in preindustrial times instead of about $60 \times 10^{12}$ kgC $yr^{-1}$ [Keeling, loc. cit., p. 308, Table 7]. The full flux is used in the three-dimensional model, as discussed by Heimann and Keeling [this volume], by adding back the remaining flux of about $35 \times 10^{12}$ kgC $yr^{-1}$. The assumption is made in the three-dimensional model that this latter flux is unaffected by perturbations in the carbon cycle, and hence is constant, whereas the former flux, associated with longer storage times, is subject to perturbations as discussed below.

We prescribe all of the invariant oceanic parameters of the model at the outset of our computations, but we adjust a parameter representing the response of the terrestrial biosphere to rising $CO_2$ so as to produce exact agreement between the model prediction and direct measurements of the seasonally adjusted concentration of atmospheric $CO_2$ for reference dates near the beginning and end of the records at Mauna Loa Observatory and the South Pole. As direct measurements we used averages for these two stations of $C_{obs\ rem}(t)$ (see subsection 2.2) based on the provisional data sets (see subsection 2.5), which extend to 1985. As reference dates we chose January 1, 1959 and 1982, the same dates used in the preparation of Figures 20 and 21, thus avoiding times when the $CO_2$ records appear to be strongly influenced by El Niño events (see subsection 4.4).

To obtain realistic predictions of atmospheric $CO_2$ in the 19th century and earlier, we further postulate a biospheric source of atmospheric $CO_2$ owing to changes in land use and deforestation. The amount of this release near 1980 is fixed in this model according to an estimate by ecologists, as discussed below, but the total amount and the timing of the release is left initially adjustable.

Atmospheric $CO_2$ data obtained prior to 1950 are of questionable accuracy. Several attempts have been made to deduce $CO_2$ variations during the earlier stages of the industrial era from proxy records such as isotopic ratios of tree rings [Pearman, 1984], but the most convincing evidence for changes in atmospheric concentration in recent centuries prior to the Mauna Loa record is embodied in measurements of air reclaimed from ice cores collected in Antarctica.

These data [Neftel et al., 1985; Friedli et al., 1986; Siegenthaler and Oeschger, 1987], shown in Figures 33 and 34 for concentration and $^{13}\delta$, respectively, are without large scatter versus time and, in the most recent samples analyzed, agree closely with the Mauna Loa record. We have relied on them to estimate the total amount and the timing of the $CO_2$ released by the terrestrial biosphere since the middle of the 18th century.

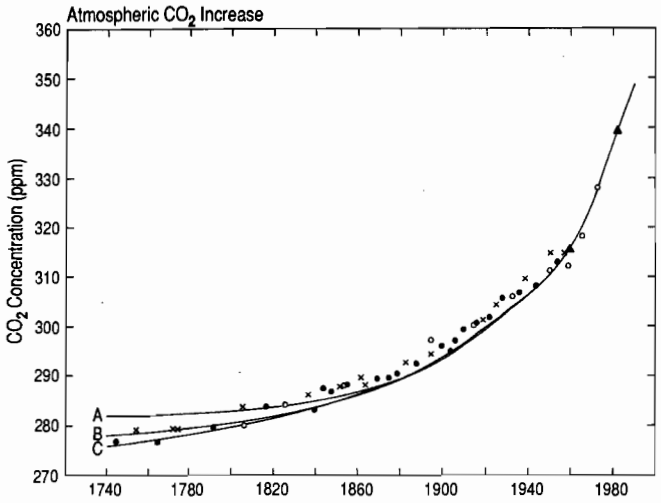


Fig. 33. Time trend of the concentration of $CO_2$ in air, in ppm, extracted from Antarctic ice compared with predictions by the box diffusion model, labeled A, B, and C which assume different Gaussian widths of 150 years, 125 years and 100 years respectively (see equation (5.1)). Open circles denote data tabulated by Neftel et al. [1985]. Dots denote data tabulated by Friedli et al. [1986]. Crosses denote additional data digitized from a graph by Siegenthaler and Oeschger [1987, p. 141] and include two data points, near 1755 and 1770, evidently from Neftel et al. [1985] but plotted for later dates. Solid triangles indicate the observed $CO_2$ concentration after seasonal adjustment for 1 January 1959 and 1982. The model is forced to predict the observed $CO_2$ concentration on these dates.

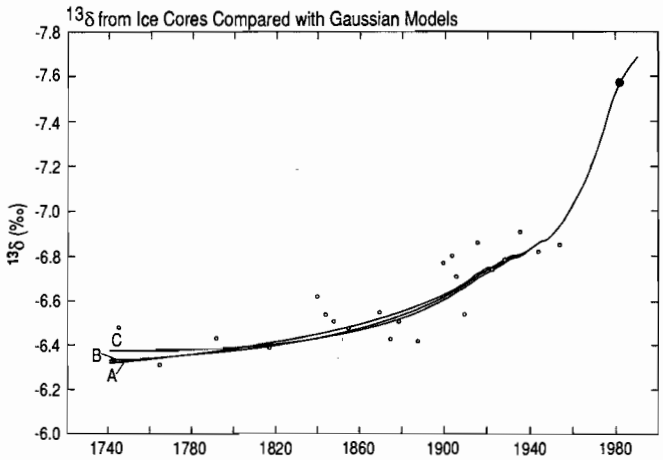


Fig. 34. Three model predictions of the time trend of the reduced isotopic ratio, $^{13}\delta$, of atmospheric $CO_2$ in per mil difference from standard PDB, compared with the ice core samples tabulated by Friedli et al. [1986]. Curves labeled A, B, and C, correspond to respective curves of Figure 33. The solid circle indicates the observed $^{13}\delta$ value for 1 January 1982. The model is forced to predict this value.

To a fair approximation the release of industrial $CO_2$ from fossil fuel combustion and cement manufacture since 1860 has been an exponential function of time, producing a situation in which the fraction of $CO_2$ accumulating in each major carbon reservoir is expected to be nearly a fixed fraction of this $CO_2$ release [Bacastow and Keeling, 1979, Appendix B]. If an assumption of a fixed fraction remaining airborne is made (as in equation (2.5)), a backward extrapolation of the $CO_2$ record at Mauna Loa, using annual records of fossil fuel production, indicates that the preindustrial $CO_2$ concentration was about 296 ppm. The ice core data indicate a $CO_2$ concentration in 1740 of about 277 ppm. This value, being substantially lower than found by extrapolation, suggests an additional source of $CO_2$ to the air since 1740. We have adopted the widely accepted hypothesis that this disparity primarily reflects a post–1740 release of $CO_2$ from the terrestrial biosphere related mainly to forestry and agricultural practices, but possibly influenced by natural biospheric variations as well.

Siegenthaler and Oeschger [1987] have employed the box diffusion model to infer the globally averaged exchange of $CO_2$ between the atmosphere and the terrestrial biosphere, using a mathematical deconvolution technique. They prescribed the release of industrial $CO_2$ and then adjusted the net exchange with the terrestrial biosphere to reproduce the ice core $CO_2$ data. Alternatively, we have chosen here a simple mathematical representation of biospheric $CO_2$ exchange to accomplish an approximate fit of a compartment model prediction to the ice core data, also taking industrial $CO_2$ into account. Afterwards, however, in section 6 we compare our results to a deconvolution carried out in the manner of Siegenthaler and Oeschger [1987].

Firstly, we prescribed the release of industrial $CO_2$ from annual statistical data. For the period 1860 through 1949 we used the data of Keeling [1973b], and for 1950 through 1984 those of Rotty [1987]. Prior to 1860, where only fragmentary production data are available, we assumed exponential growth in production at the same rate of acceleration as for 1860 to 1900 [see Keeling 1973b, p. 192]. For 1985 we assume a 1.0 percent annual increase. Secondly, we prescribed the $^{13}C/^{12}C$ ratio of the released $CO_2$ using the annual average ratios of Tans [1981] for the period 1850 through 1978. Prior to 1850 we assumed the 1850 value of −24.00‰ versus standard PDB, and after 1978 the 1978 value of −27.28‰ versus PDB. Both sets of data are summarized in Table 7.

TABLE 7. Annual Production and Isotopic Ratio, $^{13}\delta$, of $CO_2$ from Fossil Fuel Combustion and Cement Manufacture
[Updated annual production and isotopic ration data, as employed in section 6, differ slightly and extend the data listed here.]

| | Year of Decade: | | | | | | | | | |
|---|---|---|---|---|---|---|---|---|---|---|
| Decade | (0) | (1) | (2) | (3) | (4) | (5) | (6) | (7) | (8) | (9) |
| | Carbon Production (in kgC × $10^9$)[a] | | | | | | | | | |
| 1860 | 93.30 | 98.70 | 98.40 | 105.90 | 115.10 | 121.90 | 128.70 | 137.90 | 136.80 | 141.90 |
| 1870 | 145.10 | 162.00 | 176.00 | 188.60 | 183.90 | 189.30 | 191.70 | 196.20 | 196.70 | 207.80 |
| 1880 | 227.40 | 244.70 | 262.80 | 280.30 | 282.40 | 276.70 | 279.10 | 298.10 | 322.50 | 329.00 |
| 1890 | 350.40 | 366.00 | 369.40 | 362.50 | 377.90 | 399.50 | 412.60 | 432.50 | 455.70 | 498.30 |
| 1900 | 526.20 | 541.70 | 554.40 | 608.00 | 615.30 | 648.40 | 697.90 | 773.40 | 739.00 | 771.50 |
| 1910 | 807.40 | 824.70 | 869.20 | 932.60 | 842.00 | 834.50 | 898.80 | 949.70 | 936.50 | 833.90 |
| 1920 | 965.00 | 834.50 | 897.90 | 1013.70 | 1007.00 | 1015.40 | 1015.40 | 1108.00 | 1102.10 | 1184.40 |
| 1930 | 1089.90 | 980.60 | 886.10 | 932.20 | 1010.80 | 1047.20 | 1163.10 | 1245.00 | 1180.30 | 1253.00 |
| 1940 | 1321.40 | 1358.20 | 1355.50 | 1387.00 | 1377.50 | 1230.80 | 1300.10 | 1453.90 | 1553.50 | 1504.30 |
| 1950 | 1639.00 | 1776.00 | 1803.00 | 1848.00 | 1872.00 | 2050.00 | 2185.00 | 2278.00 | 2339.00 | 2470.00 |
| 1960 | 2586.00 | 2602.00 | 2709.00 | 2855.00 | 3016.00 | 3154.00 | 3313.00 | 3420.00 | 3595.00 | 3808.00 |
| 1970 | 4116.00 | 4267.00 | 4435.00 | 4678.00 | 4684.00 | 4660.00 | 4924.00 | 5065.00 | 5108.00 | 5345.00 |
| 1980 | 5255.00 | 5115.00 | 5082.00 | 5054.00 | 5330.00 | 5383.30[b] | | | | |
| | $^{13}\delta$ (in ‰)[a] | | | | | | | | | |
| 1860 | −24.00 | −24.00 | −24.00 | −24.00 | −24.00 | −24.00 | −24.00 | −24.00 | −24.00 | −24.00 |
| 1870 | −24.00 | −24.00 | −24.00 | −24.01 | −24.02 | −24.01 | −24.02 | −24.02 | −24.02 | −24.03 |
| 1880 | −24.05 | −24.06 | −24.09 | −24.06 | −24.08 | −24.10 | −24.12 | −24.13 | −24.15 | −24.16 |
| 1890 | −24.18 | −24.18 | −24.18 | −24.20 | −24.20 | −24.20 | −24.22 | −24.22 | −24.22 | −24.21 |
| 1900 | −24.22 | −24.24 | −24.25 | −24.25 | −24.27 | −24.27 | −24.26 | −24.26 | −24.32 | −24.31 |
| 1910 | −24.31 | −24.32 | −24.32 | −24.32 | −24.37 | −24.39 | −24.41 | −24.42 | −24.40 | −24.46 |
| 1920 | −24.47 | −24.49 | −24.52 | −24.59 | −24.62 | −24.66 | −24.71 | −24.74 | −24.79 | −24.81 |
| 1930 | −24.84 | −24.90 | −24.92 | −24.90 | −24.93 | −24.93 | −24.95 | −24.99 | −25.00 | −25.00 |
| 1940 | −24.98 | −24.93 | −24.99 | −25.06 | −25.17 | −25.42 | −25.42 | −25.41 | −25.50 | −25.57 |
| 1950 | −25.62 | −25.71 | −25.79 | −25.85 | −25.85 | −25.90 | −25.91 | −25.95 | −25.99 | −26.05 |
| 1960 | −26.13 | −26.32 | −26.38 | −26.45 | −26.52 | −26.61 | −26.70 | −26.87 | −26.94 | −27.05 |
| 1970 | −27.17 | −27.28 | −27.26 | −27.29 | −27.28 | −27.21 | −27.26 | −27.29 | −27.28 | −27.28[c] |
| 1980 | −27.28 | −27.28 | −27.28 | −27.28 | −27.28 | −27.28 | | | | |

[a] Updated data, employed in section 6, differ slightly and extend the data listed here.

[b] Assumed to be 1 percent higher than in 1984.

[c] Assumed constant after 1978.

Following the approach of Keeling et al. [1980], we assume that the biospheric release of $CO_2$ obeys the Gaussian function

$$F_{DES} = \frac{\int_{-\infty}^{\infty} F_{DES}\,dt}{(2\pi)^{1/2}\,\sigma_b} \exp\left\{-\frac{(t-t_b)^2}{2\sigma_b{}^2}\right\} \qquad (5.1)$$

where $F_{DES}$ denotes the annual rate of release of $CO_2$ from the terrestrial biosphere by changes in land use and deforestation, $\sigma_b$ is a curve width parameter, $t$ denotes the time, and $t_b$ is the date on which the curve is centered. We will refer to this release as "biosphere destruction" (hence the subscript "DES").

The model, sketched in Figure 35, has non-isotopic parameters set to agree with those of Siegenthaler [1983]. For most of these, the values are as recommended by the La Jolla modeling conference of 1979 [Bolin, 1981]. For isotopic carbon we generally use parametric values of Keeling et al. [1980]. Input data are listed in Table 8, where the original literature references and the basis of our choices are explained in footnotes. The model is adjusted to produce a $^{13}\delta$ value for atmospheric $CO_2$ of −7.574 on January 1, 1982, approximately in accord with our observational data. No other isotopic adjustment is made. (The value of −7.574‰ represents the isotopic ratio for the South Pole according to a computation carried out before final isotopic corrections were available. It differs slightly from the corresponding value listed in Table 6).

The box diffusion model, as adapted for our use, calculates separately the transport of total stable carbon, i.e., ($^{12}C + {}^{13}C$), and of $^{13}C$. This is convenient because it corresponds to our measurements, and because the equations are thereby simplier than when isotopic ratios are employed. Accordingly, the model needs fractionation factors for $^{13}C$ relative to ($^{12}C + {}^{13}C$) rather than to $^{12}C$. Fractionation factors are expressed in Table 8 relative to both kinds of ratios. The conversions between the two kinds are explained by Keeling et al. [1980, Appendix A].

By trial, we found values of $t_b$ and $\sigma_b$ in equation (5.1) that yield a nearly optimal fit to the ice core data for the chosen function,

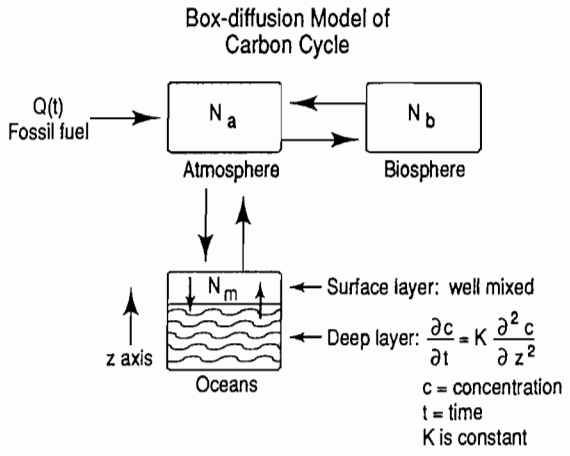


Fig. 35. Reservoir model of the global carbon cycle. Carbon exchanges are assumed to be functions of the total amounts of carbon, $N_i$, in each reservoir, except for the deep ocean layer which transports carbon by vertical diffusion.

under the constraint that the biospheric release gradually levels out after 1950 in accordance with the estimate of Houghton et al. [1987]. We required that the predicted $CO_2$ concentration agree with the average of observational data for Mauna Loa and the South Pole on January 1, 1959 and 1982, as noted above, and that the biospheric release for the average of 1979 and 1980 agree exactly with the estimate of Houghton et al. [1987] of $1.7910 \times 10^{12}$ kg of carbon per year. The model consequently predicts that the fraction of industrial $CO_2$ remaining airborne between these dates was 56.55‰, consistent with the anomaly plot in Figure 22.

We selected the values

$$t_b = 2020 \text{ A.D.}$$

$$\sigma_b = 125 \text{ years}$$

$$\int_{-\infty}^{\infty} F_{DES}\,dt = 590.7358 \times 10^{12} \text{ kg C}$$

We also made computations with $\sigma_b$ = 100 and 150 years as a sensitivity experiment. The annual releases of $CO_2$ according to equation (5.1) are plotted in Figure 36 for these three values of $\sigma_b$. We carried out further sensitivity experiments varying the center date, $t_b$. When we optimally adjusted $\sigma_b$ each time that we varied $t_b$, we found only a slight change in prediction for central dates between 2000 and 2050. For earlier dates the flux $F_{DES}$ leveled out too soon, and for longer times too late to simulate the pattern of Houghton et al. [1987].

We do not pretend that any of these model curves agree closely with the history of $CO_2$ releases estimated by Houghton et al. [1983] and shown in the figure as open circles. The curves are, however, forced to agree with their estimate for 1980, and agree quite well for all times after 1950.

Consistent with the models of both Keeling et al. [1980] and Siegenthaler [1983], we also assumed that the terrestrial biosphere not only lost carbon because of agriculture and forestry, but took up carbon at a rate proportional to the increase in $CO_2$ concentration through stimulation of plant growth induced by elevated $CO_2$ levels. Plant stimulation, which we will call "$CO_2$ fertilization", is modeled by assuming that the perturbation in the flux of $CO_2$ from the atmosphere to the terrestrial biosphere is given by the expression

$$F_{ab} = F_{bo}\,[\beta_a\,(N_a - N_{ao})/N_{ao} + \beta'_b\,(N_b - N_{bo})/N_{bo}] \qquad (5.2)$$

and the return flux by

$$F_{ba} = F_{bo}\,[\beta_b\,(N_b - N_{bo})/N_{bo}] \qquad (5.3)$$

where, respectively, $F_{bo}$, $N_{ao}$, and $N_{bo}$ denote the unperturbed biospheric flux and the unperturbed atmospheric and long-lived biospheric carbon inventories; $N_a$ and $N_b$ denote the corresponding inventories during the perturbation; and $\beta_a$, $\beta_b$ and $\beta'_b$ are first order perturbation factors. These quantities all refer to total stable carbon ($^{12}C + {}^{13}C$).

The fertilization factor, $\beta_a$, expresses the degree to which the perturbation in the atmospheric $CO_2$ concentration (proportional to $N_a - N_{ao}$) influences plant uptake of $CO_2$. For example, the value of 0.41 which we found in our preferred fit to the ice core data ($\sigma_b$ = 125 years) implies that the increase in uptake by the long-lived biosphere, per unit mass, has been 41 percent of the fractional

TABLE 8. Quantities and Parameters Used in the Box Diffusion Model

| Symbol | Definition | Value | Notes |
|---|---|---|---|
| $N_{a\ ref}$ | Carbon in atmosphere as $CO_2$, corresponding to a mixing ratio of 290 ppm relative to dry air and to a $CO_2$ partial pressure at sea level of $289.04 \times 10^{-6}$ atm | $615.6 \times 10^{12}$ kg | 1 |
| $N_{bo}$ | Carbon in preindustrial terrestrial biosphere | $2.4\ N_{a\ ref}$ | 2 |
| $F_{ba}$ | Preindustrial flux of carbon (as $CO_2$) from terrestrial biosphere | $0.04\ N_{a\ ref}$ yr$^{-1}$ | 3 |
| $A_{oc}$ | Area of ocean surface | $3.62 \times 10^{14}$ m$^2$ | 4 |
| $h_m$ | Depth of oceanic well-mixed surface layer | 75 m | 5 |
| $h_a$ | Thickness of oceanic layer containing as much carbon as an atmosphere with 290 ppm of $CO_2$ | 69.06 m | 6 |
| $h_s$ | Mean depth of the ocean adjusted to a constant concentration of dissolved inorganic carbon equal to surface concentration | 4199 m | 7 |
| $k_{am}$ | Transfer (exchange) coefficient for $CO_2$ from air to sea surface for model calibrated with preindustrial $^{14}C$ | 1/7.87293 y | 8 |
| | Same except calibrated with bomb $^{14}C$ | 1/6.87926 y | 9 |
| $K$ | Vertical eddy diffusion coefficient below surface oceanic layer for model calibrated with preindustrial $^{14}C$ | 4005 m$^2$ y$^{-1}$ | 10 |
| | Same except calibrated with bomb $^{14}C$ | 7685 m$^2$ y$^{-1}$ | 10 |
| $\xi$ | $CO_2$ evasion factor for surface oceanic layer (preindustrial value: 8.876) | variable | 11 |
| $\alpha_{ab}$ | $^{13}C/^{12}C$ fractionation factor for $CO_2$ uptake by the terrestrial biosphere | 0.9818731 | 12 |
| $\alpha_{ab}'$ | Corresponding $^{13}C/(^{13}C + ^{12}C)$ ratio | 0.9820696 | 12 |
| $\alpha_{ba}$ | $^{13}C/^{12}C$ fractionation factor for $CO_2$ release by the terrestrial biosphere | 1.000 | 13 |
| $\alpha_{ba}'$ | Corresponding $^{13}C/(^{13}C + ^{12}C)$ ratio | 1.000 | 13 |
| $\alpha_{am}$ | $^{13}C/^{12}C$ fractionation factor for $CO_2$ uptake by surface ocean | 0.9982000 | 14 |
| $\alpha_{am}'$ | Corresponding $^{13}C/(^{13}C + ^{12}C)$ ratio | 0.9982198 | 14 |
| $\alpha_{ma}$ | $^{13}C/^{12}C$ fractionation factor for $CO_2$ evasion from the surface ocean | 0.9896604 | 15 |
| $\alpha_{ma}'$ | Corresponding $^{13}C/(^{13}C + ^{12}C)$ ratio | 0.9897743 | 15 |
| $\lambda$ | Radiocarbon decay constant | 1/8267 yr | 16 |

Notes

(1) From Keeling [1973a, p. 301] based on an estimate of the mass of dry air in the atmosphere of $5.119 \times 10^{18}$ kg [Verniani, 1966]. The corresponding mixing ratio with respect to moist air is 289.04 ppm assuming, as did Verniani, that the average content of water vapor in the atmosphere is 0.33 percent. Hence the corresponding $CO_2$ partial pressure existed at sea level is $289.04 \times 10^{-6}$ atmospheres.

(2) From SCEP [1970, p. 162]. A ratio of 2.433 (based on $1498 \times 10^{12}$ kgC for long-lived organic carbon) was rounded to 2.4 as was done by Siegenthaler and Oeschger [1978, p. 390]. Short-lived organic carbon amounting to $82 \times 10^{12}$ kgC according to SCEP, p. 162, has been disregarded.

(3) SCEP [1970 p. 162] quotes 62 years for the mean residence time of long-lived organic carbon. This value, rounded to 60 years as was done by Siegenthaler [1983, p. 3600], yields a flux of $N_{bo}/60=0.04\ N_{ao}$. A flux associated with short-lived organic carbon (with a pool size of $82 \times 10^{12}$ kgC, a residence time of 2.3 y and a flux of $36 \times 10^{12}$ kgC yr$^{-1}$ according to SCEP [1970, p. 162]) has been disregarded.

(4) From Menard and Smith [1966, p. 4315], including Arctic and "adjacent" (i.e., mediterranean type) seas. Original value has been rounded.

(5) Bathen [1972] is cited by Bolin et al. [1981, p. 15] and Bacastow and Björkström [1981, p. 37] who offer further arguments for this estimate.

(6) From Bacastow and Björkström [1981, p. 37], based on an average concentration of dissolved inorganic carbon of 2002 $\mu$m kg$^{-1}$ in the upper 50 m of the world oceans [Takahashi et al., 1981, p. 282] and an assumed density of 1025 kg m$^{-3}$, corresponding to a salinity of 34.78‰.

(7) From Bacastow and Björkström [1981, p. 37], based on an ocean volume of $1.349929 \times 10^{18}$ m$^3$ Menard and Smith [1966, p. 4315], on the value of $A_{oc}$ listed in Table 1, and on a concentration ratio for dissolved inorganic carbon of subsurface relative to near surface ocean water of 2254 $\mu$M kg$^{-1}$/2002 $\mu$M kg$^{-1}$. The latter ratio is from Takahashi et al. [1981, p. 282]. The compressibility of seawater was not taken into account.

(8) Computed as the ratio of the presumed preindustrial amount of $CO_2$ in the atmosphere, $N_{ao}$, to the preindustrial steady state

Notes to Table 8 -- continued

exchange flux between the atmosphere and the oceans as determined by Siegenthaler [1983], based on the uptake of natural ("preindustrial") radiocarbon by the oceans. The preindustrial amount of $CO_2$ is equal to $N_{a\,ref}$ (see note 1), the value used by Siegenthaler [1983, Table 1], and we compute the exchange flux as the product of $k_{ex}$, the average $CO_2$ exchange flux between the atmosphere and the surface ocean, and the area of the world oceans, $A_{oc}$ (see note 4). We set $k_{ex}$ (Siegenthaler's symbol $F_{as}$) equal to 18.0 moles $m^{-2}$ $yr^{-1}$ (Siegenthaler's value of 17.99 moles $m^{-2}$ $yr^{-1}$ [loc. cit., Table 2], rounded to three figures. We convert $k_{ex}$ to g $m^{-2}$ $yr^{-1}$ assuming 12.00 as the molecular weight of carbon.

(9) Same as reference (8) but based on 20.6 moles $m^{-2}$ $yr^{-1}$, the exchange flux based on the uptake of bomb radiocarbon by the oceans, as determined by Siegenthaler [1983, Table 2], rounded from 20.63 moles $m^{-2}$ $yr^{-1}$.

(10) From Siegenthaler [1983, p. 3604].

(11) Calculated from the temperature, total dissolved inorganic carbon (DIC), titration alkalinity, and salinity according to the algorithm of Bacastow [1981] using equilibrium constants of dissociation of carbonic acid, $K_1$ and $K_2$, from an analyses of data of Hansson and Mehrbach carried out by Dickson and Millero [1987] and the carbon dioxide solubility of Weiss [1974].

(12) Based on $^{13}\delta C$ of –7‰ for atmospheric $CO_2$ and –25‰ for carbon in living matter on land, as reported by Degens [1969, p. 322].

To compute $\alpha_{ab}$, we write for the $^{13}C/^{12}C$ ratio of atmospheric $CO_2$:

$$r_a = (1 - 0.007)r_s = 0.993r_s$$

where $r_s$ (= 0.0112372) denotes the $^{13}C/^{12}C$ ratio of the reference standard PDB [Mook and Grootes 1973, p. 296]. Similarly for living matter

$$r_b = (1 - 0.025)r_s = 0.975r_s$$

The fractionation factor is defined by

$$\alpha_{ab} = r_b/r_a$$

The same fractionation is expressed in terms of $^{13}C/(^{13}C + ^{12}C)$ ratios by the formula

$$\alpha_{ab}' = (r_b/(1+r_b))/(r_a/(1+r_a))$$

(The $\alpha$ factors are quoted as an aid to literature citation; $\alpha'$ factors are used in the compartment model computations.)

(13) Zero fractionation is assumed, consistent with versions of the box diffusion model of Keeling et al. [1980] and Siegenthaler [1983].

(14) From Siegenthaler and Münnich [1981, p. 255] (their symbol $\alpha_{as}$) based on the surface renewal gas exchange model of Danckwerts [1970]. Their estimate of 0.2‰ for the contribution to $\alpha_{ab}$ from the reaction of $CO_2$ with hydroxide ion is included, but fractionation related to the hydration of $CO_2$ is not included.

The same fractionation is expressed in terms of $^{13}C/(^{13}C + ^{12}C)$ ratios by the formula

$$\alpha_{am}' = \alpha_{am}(1+r_a)/(1+\alpha_{am}r_a)$$

where $r_a$ is defined as in footnote (12).

(15) Computed from the equilibrium fractionation factor for $CO_2$ gas in exchange with bicarbonate solution (where $\alpha_{eq} = \alpha_{ma}/\alpha_{am}$) and from the factor $\alpha_{am}$ as quoted above. The equilibrium factor, $\alpha_{eq}$, is computed from a three dimensional tracer transport model by Heimann and Keeling [this volume] using an equation [loc. cit., eq. 5.40] equivalent to the equation of Mook et al. [1974, p. 175, Table 4, (with T = 273.15°)] to specify the temperature dependence of the per mil difference, at equilibrium, between gaseous $CO_2$ and an aqueous bicarbonate solution (Mook et al.'s symbol $\varepsilon_b(g)$), assumed to fractionate to the same extent as ocean water. The three dimensional model predicts a global average per mil depletion of carbon-13 in the gaseous phase ($\varepsilon_b(g)$) of –8.555‰ which corresponds to a mean ocean water temperature for dynamic isotopic equilibrium of 19.129°C. The small influences of aqueous $CO_2$ and carbonate ions on the isotopic equilibrium are neglected. Hence

$$\alpha_{eq} = 1 + \varepsilon_b(g) = 0.991445$$

and the fractionation for $CO_2$ evasion is computed by the formula

$$\alpha_{ma} = \alpha_{am}\alpha_{eq}$$

The same fractionation is expressed in terms of $^{13}C/(^{13}C + ^{12}C)$ ratios by the formula

$$\alpha_{ma}' = \alpha_{ma}(1 + \alpha_{am}r_a/\alpha_{ma})/(1 + \alpha_{am}r_a)$$

where $r_a$ is defined as in footnote (12).

(16) From Siegenthaler [1983, p. 3600], as adopted by the Twelfth Nobel Symposium [Olsson, 1970].

---

increase in $CO_2$ concentration. The other two factors, $\beta_b$ and $\beta_b'$, we set equal to unity. This is equivalent to our assuming that both biospheric uptake and release of $CO_2$ are proportional to the size of the long-lived biospheric carbon pool, whether perturbed or not. The resultant net fertilization flux, $F_{FER}$, is thus given by the expression

$$F_{FER} = F_{ba} - F_{ab} \qquad (5.4)$$
$$= -(F_{bo}/N_{ao})\beta_a (N_a - N_{ao})$$

where, to be consistent with the terminology of Heimann and Keeling [this volume], $F_{FER}$ is defined to be positive for transfer to the atmosphere. Plots of $F_{FER}$ for the Gaussian width parameter, $\sigma_b$ equal to 100, 125, and 150 years are shown in Figure 37. Also plotted, for the same values of $\sigma_b$, is the net biospheric flux, $F_b$, representing the sum of destruction and fertilization, during the recent past, i.e.,

$$F_b = F_{DES} + F_{FER} \qquad (5.5)$$

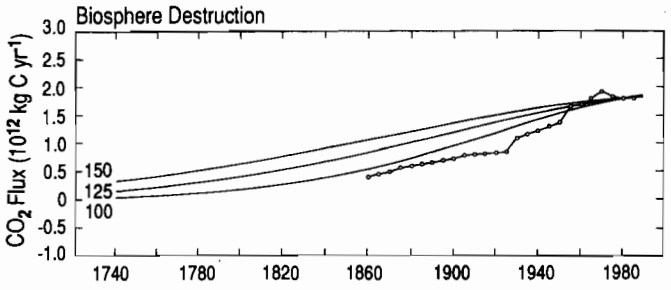


Fig. 36. Three versions of the history of the release of $CO_2$ from the terrestrial biosphere, $F_{DES}$, shown as solid curves, in units of $10^{12}$ kgC $yr^{-1}$, brought about by deforestation and changing land use by man ("biospheric destruction"). Also shown for comparison is an estimate from direct observations (shown as connected open circles) according to a plot by Houghton and Woodwell [1989, p. 39]. Solid curves corresponding to the curves labeled A, B, and C in Figure 33, depict the Gaussian function of equation (5.1) with the width parameter, $\sigma_b$, set equal to 150 years, 125 years, and 100 years, respectively. The curve which best accords with the ice core data of Figure 33 is for $\sigma_b$ of 125 years.

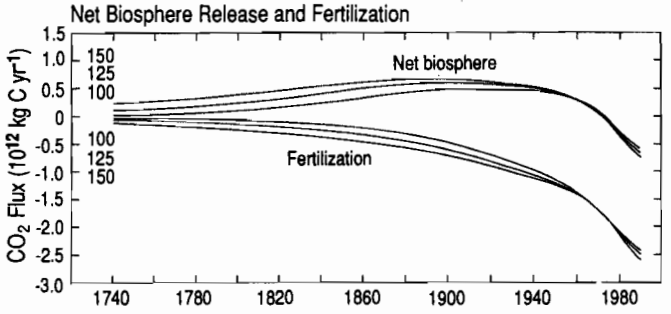


Fig. 37. Upper three curves: The net rate of release of $CO_2$ from the terrestrial biosphere, $F_b$, versus time, in units of $10^{12}$ kgC $yr^{-1}$, predicted by the reservoir model for width parameter, $\sigma_b$, of 150, 125, and 100 years, as in Figure 36. Lower curves: Rate of withdrawal of $CO_2$ from the atmosphere produced by $CO_2$ fertilization, $F_{FER}$, according to the same model and for the same three values of $\sigma_b$, as labeled. The difference between the net release and the withdrawal by fertilization, for each value of $\sigma_b$, is equal to biospheric destruction, $F_{DES}$, as plotted in Figure 36.

where, numerically, $F_{DES}$ is usually positive and $F_{FER}$ is always negative. (Subscripts in capital letters refer to fluxes that are utilized by Heimann and Keeling [this volume] in the three-dimensional model.)

Our representation of plant stimulation by $CO_2$ fertilization is a first order approximation, expected to be valid only for small perturbations. If the source of biospheric destruction were turned off, the predicted atmospheric $CO_2$ concentration would in time return unrealistically to exactly its initial value according to equation (5.4). We here address only the behavior of the carbon cycle during the past. According to our direct measurements, and the ice core data shown in Figure 33, atmospheric $CO_2$ increased in concentration by only about 25 percent during the past two and a half centuries. The rise has been relatively steady, suggesting a nearly linear response to slowly growing sources of $CO_2$ to the atmosphere. Future trends in the carbon cycle may involve much larger perturbations, and will inevitably be followed by a diminution and eventual cessation of fossil fuel combustion owing to exhaustion of the resource. To portray such processes is beyond the scope of our analysis here.

With our preferred choices of parameters, the box diffusion model predicts an increase in atmospheric $CO_2$ concentration from 278 ppm in 1740 to 342 ppm in 1984. The rate of rise agrees approximately with the ice core data (curve B in Figure 33), although between 1820 and 1900 these data indicate a somewhat higher rate, while from 1900 to 1960 they suggest a lower rate. As a consequence, the model prediction would be improved if more $CO_2$ were assumed to be released from the biosphere or oceans in the earlier part of the 19th century and less later on. This cannot be accomplished by a change in the width parameter, $\sigma_b$. For example, a change in $\sigma_b$ from 125 years to 100 or 150 years (curves A and C, respectively, in Figure 33) hardly changes the shape of the model prediction after 1850. The predictions for $^{13}\delta$ for the three choices of $\sigma_b$ are nearly the same and agree well with the ice core data as shown in Figure 34 for $\sigma_b$ equal to 125 years. (For the three choices of $\sigma_b$, in ascending order, the predicted value of $^{13}\delta$ shifts from –6.37, –6.33, and –6.32‰, respectively in 1740 to –7.60‰ in 1984.)

It is of interest to contrast the model representation of the terrestrial biospheric fluxes of $CO_2$ with direct estimates of the biospheric release of $CO_2$ by Houghton et al. [1983]. They computed the amount of organic carbon released by various regional ecosystems since 1860 owing to establishment and abandonment of croplands, to the harvest and regrowth of forests, and to the release $CO_2$ by oxidation of wood products. They based their computations on agricultural and forestry statistics, and, in a preferred calculation that produced a global release of $2.6 \times 10^{12}$ kgC in 1980 [loc. cit., p. 1083], they assumed the rate of agricultural expansion since 1950 in the tropical regions to be proportional to population growth. On the basis of alternative scenarios of agricultural expansion they estimated a range of global releases of $CO_2$ in 1980 from 1.8 to $4.7 \times 10^{12}$ kgC. With additional data, Houghton et al. [1987] have since computed a lower preferred release for 1980: $0.133 \times 10^{12}$ kgC from temperate and boreal regions [loc. cit., Table 1] and $1.659 \times 10^{12}$ kgC from the tropics [loc. cit., Table 4] for a total of $1.791 \times 10^{12}$ kgC.

We obtained the release curve shown in Figure 36 (connected open circles) on the basis of the newer estimate, while retaining the relative change with time of Houghton et al. [1983]. (This retention was recommended by Houghton by private communication in 1987 and agrees closely with a still newer estimate of the annual production of $CO_2$ from changes in land use by Houghton and Woodwell [1989, p.39].) The agricultural and forestry data of Houghton et al. [1983] indicate a more rapidly increasing release of $CO_2$ after 1920 than do our model curves of destruction, and thus would not produce a good prediction of the ice core data, if used as a source function in our model. Without plant stimulation, expressed in our model by equations (5.2) and (5.3), the Houghton et al. curve would fit the observations even less well.

Whether plant growth has been stimulated by the recent rise in atmospheric $CO_2$ concentration is, however, controversial. Hough-

ton et al. [1983, p. 250] find little ecological or physiological basis for expecting stimulation. They imply that the lack of direct evidence to support an increase in biomass or soil carbon argues against stimulation, and they support this view by pointing out that the increase in the average temperature of the earth during the 20th century probably promoted additional release of $CO_2$ and opposed $CO_2$-stimulated growth. Two of the authors of Houghton et al. [1983] have further shown that a lack of available nitrogen and phosphorus inhibits increased plant growth [Peterson and Melillo, 1985]. Nitrogen fixation might be stimulated simultaneously and reduce the lack of this nutrient, but additional phosphorus must be extracted from the soil itself and is not expected to be available in significant amounts.

Peterson and Melillo assert that stimulation of growth can lead to additional carbon storage on the scale which the box diffusion model requires only if there has been a widening of the carbon/nutrient ratios in the organic carbon pools, an unlikely possibility in their opinion. Increased nitrogen fixation may tend to compensate, but the authors also note that the impact of man appears to have moved terrestrial systems towards less available nutrients in recent years. The possibility of plant growth stimulation under natural conditions is rejected in the categorical statement of Goudriaan and Ajtay [1979, p. 248] that "on a global scale, $CO_2$ increase will not appreciably affect the net $CO_2$ assimilation [of plants]." Also, Strain and Armentano [1982, p. i] question any prediction of global carbon cycling which includes an increase in the storage of carbon proportional to an increase in atmospheric $CO_2$ by means of a "$\beta$ factor". In their opinion, "the $\beta$ factor concept is ill-conceived".

Since we force the box diffusion model to produce agreement with direct atmospheric $CO_2$ data in 1959 and 1982, the net biospheric exchange inferred from the model between these dates cannot be altered to fit the curve of Houghton et al. [1983] unless the oceanic formulation of the model is changed so significantly as to violate oceanic radiocarbon data. Our scaling of the curve of Houghton et al. [1983] downward using the 1980 release estimate of Houghton et al. [1987] makes the discrepancy smaller but does not remove the over-all incompatibility.

We admit that uncertainties attend the use of radiocarbon data to calibrate our oceanic model, but we also perceive that large uncertainties exist in the direct estimates of net biospheric $CO_2$ release. We regard the study of Houghton et al. [1987] as possibly the most reliable direct estimate of $CO_2$ releases presently available for the terrestrial biosphere, but the consistent evidence from oceanic models that this $CO_2$ cannot be absorbed by the oceans leads us to accept the hypothesis of plant stimulation. Two other studies making use of the ice core data of Friedli et al. [1986] suggest the need for plant stimulation in recent years to explain the trend in the data [Siegenthaler and Oeschger, 1987, p. 148; Enting and Mansbridge, 1987, p. 322]. Finally, the opinion of ecologists may be changing towards at least tentative acceptance of some degree of stimulation by $CO_2$. In the executive summary of an exhaustive report on the direct effects of increasing $CO_2$ on vegetation, Strain and Cure [1985, p. xxiv] state that, although the magnitude is unknown, "practically all information points to a $CO_2$ stimulation of the biosphere". Detwiler and Hall [1988, p. 46], after summarizing numerous opinions expressed by others, conclude that "the possibility that $CO_2$ fertilization occurs in undisturbed ecosystems cannot be dismissed". We further discuss this issue in section 6, below.

The degree of stimulation of the terrestrial biosphere by $CO_2$ fertilization, expressed by the growth factor $\beta_a$, is insensitive to which radiocarbon calibration of Siegenthaler [1983] is used in the box diffusion model. For $\sigma_b$ equal to 125 years, the greatest differ-

TABLE 9. Parameters of the Box Diffusion Carbon Cycle Model

[Forced to predict atmospheric $CO_2$ concentration of 315.33 ppm and 339.31 ppm on January 1, 1959 and 1982, respectively, and $^{13}\delta$ of atmospheric $CO_2$ of −7.574‰ on January 1, 1982]

| | Stationary $^{14}C$ | Bomb-Produced $^{14}C$ | | | |
|---|---|---|---|---|---|
| *Adjustable Model Parameters* | | | | | |
| Central year of Gaussian function | 2020 | 2020 | 2020 | 2020 | (*) |
| Gaussian width parameter (yr) | 125 | 100 | 125 | 150 | (*) |
| Rate of biospheric $CO_2$ release on Jan. 1, 1980 ($10^{12}$ kgC $yr^{-1}$) | 1.791 | 1.791 | 1.791 | 1.791 | 0 |
| Reciprocal of air-sea exchange coefficient, $k_{am}^{-1}$ (yr) | 7.87293 | 6.87926 | 6.87926 | 6.87926 | 6.87926 |
| Oceanic vertical diffusion coefficient, $K$ ($m^2 yr^{-1}$) | 4005 | 7685 | 7685 | 7685 | 7685 |
| *Diagnostic Parameters* | | | | | |
| Biological growth factor, $\beta_a$ | 0.5187 | 0.4601 | 0.4129 | 0.3801 | 0.1068 |
| Accumulated biospheric $CO_2$ release to 1980 ($10^{12}$ kgC) | 220.90 | 167.52 | 220.90 | 273.68 | – |
| Accumulated industrial $CO_2$ release to 1980 ($10^{12}$ kgC) | 160.52 | 160.52 | 160.52 | 160.52 | 160.52 |
| Accumulated atmospheric $CO_2$ uptake to 1980 ($10^{12}$ kgC) | 126.85 | 117.20 | 127.56 | 136.37 | 86.58 |
| Accumulated biospheric $CO_2$ uptake to 1980 ($10^{12}$ kgC) | 158.67 | 104.83 | 126.88 | 150.26 | −11.34 |
| Accumulated oceanic $CO_2$ uptake to 1980 ($10^{12}$ kgC) | 95.90 | 106.00 | 126.98 | 147.57 | 62.60 |
| Preindustrial atmospheric $CO_2$ concentration, $N_{ao}$ (ppm) | 277.12 | 281.69 | 276.79 | 272.62 | 295.95 |
| Atmospheric $CO_2$ concentration in 1750 (ppm) | 278.70 | 282.03 | 278.36 | 276.40 | 295.96 |
| Atmospheric $CO_2$ concentration in 1980 (ppm) | 336.88 | 336.90 | 336.88 | 336.86 | 336.74 |
| $^{14}C$ Suess Effect in 1954 (%) | −2.625 | −2.303 | −2.370 | −2.428 | −2.105 |
| Increase in dissolved inorganic carbon at ocean surface in 1980 ($\mu$m/kg) | 38.57 | 31.92 | 38.19 | 40.84 | 25.55 |

*Case with no biospheric release.

ence in predicted $CO_2$ concentration from the observed concentration occurs close to the year 1785, when the model calibrated by preindustrial (or, as we call it, "stationary") radiocarbon predicts a concentration only 0.35 ppm higher than when calibrated by bomb radiocarbon. The growth factor, $\beta_a$, varies from 0.52 for the stationary radiocarbon case to 0.41 for the bomb radiocarbon case, also a relatively small difference.

In Tables 9 to 11 we summarize the results of the box diffusion model using the bomb-produced radiocarbon calibration with $\sigma_b$ equal to 100, 125, and 150 years and the stationary radiocarbon calibration with $\sigma_b$ equal to 125 years. Variable parameters are listed for January 1 of the specified year. (The time resolution of the model is too course to justify distinguishing January 1 and May 15 of 1984 in preparing model results for comparison with our observations). The rate of release of industrial $CO_2$ is computed as the average of the annual release for the specified year and the preceding year. Exchange fluxes are computed as half of the $CO_2$ transferred between January 1 of the previous and following years. It can be seen that the timing of the biospheric release (controlled by the value of $\sigma_b$), as well as the choice of radiocarbon calibration, is not critical. This circumstance is largely owing to the model being constrained to predict exactly the rise in $CO_2$ concentration between 1959 and 1982. In Table 12 we list the changes in carbon storage, $CO_2$ fluxes, and $^{13}\delta$ values for the 4 years in which Heimann and Keeling [this volume], Heimann et al. [this volume] and Keeling et al. [this volume] employ these data.

TABLE 10. Exchange Fluxes Predicted by the Box Diffusion Carbon Cycle Model (in $10^{12}$ kgC $yr^{-1}$) for January 1, 1980
[Computed as one half of the difference in accumulated carbon in reservoir between January 1, 1979 and 1981]

| | Stationary $^{14}C$ | Bomb-Produced $^{14}C$ | | | |
|---|---|---|---|---|---|
| *Adjustable Model Parameters* | | | | | |
| Central year of Gaussian function: | 2020 | 2020 | 2020 | 2020 | (a) |
| Gaussian width parameter (yr): | 125 | 100 | 125 | 150 | (a) |
| *Exchange Fluxes* | | | | | |
| Industrial $CO_2$ release[b] | 5.3000 | 5.3000 | 5.3000 | 5.3000 | 5.3000 |
| Atmospheric $CO_2$ accumulation | 2.7692 | 2.7447 | 2.7636 | 2.7797 | 2.9010 |
| Surface oceanic $CO_2$ uptake[c] | 0.2531 | 0.2511 | 0.2487 | 0.2487 | 0.2720 |
| Deep oceanic $CO_2$ uptake[d] | 1.4406 | 1.9415 | 1.9750 | 1.9942 | 1.7579 |
| Terrestrial biospheric $CO_2$ release | 1.7910 | 1.7910 | 1.7910 | 1.7910 | 0 |
| Terrestrial biospheric $CO_2$ stimulated uptake | 2.6281 | 2.1538 | 2.1038 | 2.0705 | 0.3692 |
| Total oceanic $CO_2$ uptake[e] | 1.69 | 2.19 | 2.22 | 2.24 | 2.03 |
| Net biospheric $CO_2$ uptake[f] | 0.84 | 0.36 | 0.31 | 0.28 | 0.37 |

[a]Case with no biospheric release.
[b]As in Table 12 below.
[c]Uptake in well-mixed surface layer of depth, $h_m$, (see Table 8).
[d]Uptake in ocean below the surface layer of depth, $h_m$.
[e]Sum of surface oceanic and deep oceanic $CO_2$ uptake.
[f]Terrestrial biospheric $CO_2$ stimulated uptake minus release.

TABLE 11. Isotopic Ratios Predicted by the Box Diffusion Carbon Cycle Model (in ‰)

| | Stationary $^{14}C$ | Bomb-Produced $^{14}C$ | | | |
|---|---|---|---|---|---|
| Central year of Gaussian Function: | 2020 | 2020 | 2020 | 2020 | (*) |
| Gaussian width parameter (yr): | 125 | 100 | 125 | 150 | (*) |
| Preindustrial atmospheric $CO_2$, $^{13}\delta_{ao}$ | −6.2799 | −6.3639 | −6.3040 | −6.2546 | −6.5384 |
| Atmospheric $CO_2$ in A.D. 1980, $^{13}\delta_a$ | −7.5356 | −7.5384 | −7.5379 | −7.5375 | −7.5313 |
| $^{13}\delta_a - {}^{13}\delta_{ao}$ | −1.2557 | −1.1745 | −1.2339 | −1.2829 | −0.9929 |
| Preindustrial surface ocean, $^{13}\delta_{mo}$ | 2.2948 | 2.2100 | 2.2704 | 2.3203 | 2.0340 |
| Surface ocean in A.D. 1980, $^{13}\delta_m$ | 1.6180 | 1.6202 | 1.6373 | 1.6511 | 1.5816 |
| $^{13}\delta_m - {}^{13}\delta_{mo}$ | −0.6768 | −0.5898 | −0.6331 | −0.6692 | −0.4524 |
| Preindustrial terrestrial biosphere, $^{13}\delta_{bo}$ | −24.2930 | −24.3755 | −24.3167 | −24.2682 | −24.5468 |
| Terrestrial Biosphere in A.D. 1980, $^{13}\delta_b$ | −24.8961 | −24.9123 | −24.9296 | −24.9493 | −24.8920 |
| $^{13}\delta_b - {}^{13}\delta_{bo}$ | −0.6031 | −0.5368 | −0.6129 | −0.6811 | −0.3452 |

*Case with no biospheric release.

TABLE 12. Predictions of the Box Diffusion Carbon Cycle Model for Various Years
[Computed for January 1 of each year for model calibrated with bomb-produced $^{14}C$ and Gaussian width parameter of 125 yr]

| | 1962 | 1968 | 1980 | 1984 |
|---|---|---|---|---|
| Atmospheric $CO_2$ concentration (ppm) | 317.46 | 322.51 | 336.88 | 341.54 |
| Accumulated terrestrial biospheric $CO_2$ release ($10^{12}$ kgC) | 189.50 | 199.77 | 220.90 | 228.10 |
| Accumulated terrestrial biospheric $CO_2$ uptake ($10^{12}$ kgC) | 95.72 | 104.78 | 126.88 | 135.63 |
| Accumulated oceanic $CO_2$ uptake ($10^{12}$ kgC) | 94.80 | 103.76 | 126.98 | 136.05 |
| Industrial $CO_2$ release rate ($10^{12}$ kgC $yr^{-1}$)*up** | 2.6555 | 3.5075 | 5.3000 | 5.1920 |
| Atmospheric $CO_2$ uptake rate ($10^{12}$ kgC $yr^{-1}$) | 1.5382 | 2.0168 | 2.7636 | 2.4348 |
| Surface oceanic $CO_2$ uptake rate ($10^{12}$ kgC $yr^{-1}$) | 0.1429 | 0.1796 | 0.2487 | 0.2249 |
| Deep oceanic $CO_2$ uptake rate ($10^{12}$ kgC $yr^{-1}$) | 1.2422 | 1.4383 | 1.9750 | 2.0721 |
| Terrestrial biospheric $CO_2$ release rate ($10^{12}$ kgC $yr^{-1}$) | 1.6927 | 1.7288 | 1.7910 | 1.8086 |
| Terrestrial biospheric $CO_2$ stimulated uptake rate ($10^{12}$ kgC $yr^{-1}$) | 1.4250 | 1.6018 | 2.1038 | 2.2688 |
| $^{13}C/^{12}C$ ratio of atmospheric $CO_2$, $^{13}\delta_a$, (‰) | −7.0717 | −7.1977 | −7.5379 | −7.5974 |
| $^{13}C/^{12}C$ ratio of biospheric carbon, $^{13}\delta_b$, (‰) | −24.7437 | −24.7914 | −24.9296 | −24.9864 |
| $^{13}C/^{12}C$ ratio of dissolved inorganic carbon at ocean surface, $^{13}\delta_m$, (‰) | 1.8507 | 1.7968 | 1.6373 | 1.5824 |

*up**Computed as the averages of the annual data of Table 7 for the 2-year period beginning on January 1 of the previous year.

## 6. Global Scale Interannual Variations in Atmospheric $CO_2$

### 6.1 *Introduction*

The above described observational data were analyzed and model computations were carried out primarily to prepare input data for the three-dimensional tracer transport model which is the main subject of this series of articles. In the 3 years that have elapsed since most of this effort took place, our longest isotopic records have been extended to over 10 years, and the world has experienced another El Niño event, better documented than any previous one with respect to atmospheric $CO_2$. We have added this section to take advantage of this new information, to explain better the interannual variations in atmospheric $CO_2$, and to put in clearer perspective the limitations of our box diffusion model computations. A reader mainly concerned with our three-dimensional model study need not read this section.

### 6.2 *Challenging the Box Diffusion Model Predictions*

In the previous section variations in atmospheric $CO_2$ associated with human activities were investigated by means of the box diffusion model. The focus was on time scales of 10 years or more. The box diffusion model is, however, also capable of simulating more rapidly occurring variations and can portray natural as well as anthropogenic perturbations. Using this model, we will now examine shorter duration variations in atmospheric $CO_2$, some of which are caused by natural processes. We will also reconsider longer time scales based on a more detailed analysis of the $CO_2$ record over the whole industrial era.

The box diffusion model is restricted to simulating variations in atmospheric $CO_2$ that are essentially global. This restriction is not serious, however, because these variations, even on a 2-year time scale, are observed to be similar from the arctic to the antarctic. Thus, to the extent that the box diffusion model is able to provide realistic global scale simulations of oceanic and biospheric fluxes, virtually all interannual variations in atmospheric $CO_2$ can be studied by the model.

By way of introduction we will first examine how well the model reproduces observed variations in $CO_2$ on the decadal scale. The model, as described in section 5, was forced to predict the $CO_2$ concentration at Mauna Loa Observatory and the South Pole, averaged, for two specified dates 23 years apart, near the beginning and end of the combined record. These data, expressed as an anomaly (function $C_{anom}(t)$ of equation (2.5)), are compared with their prediction by the box diffusion model, in Figure 38. The anomaly, previously plotted in Figure 22, is defined to be zero for the same two dates on which the model predictions are forced to agree with the observations, and hence the cumulative airborne fraction predicted between these dates is 56.55% in agreement with the observations. Prominent year to year variations in $CO_2$ which correlate with El Niño events are present in the observations, but are not reproduced by the model. The only short-term variations predicted by the model arise from fossil fuel combustion which is prescribed on an annual basis (see Table 7). They are scarcely discernible because, from year-to-year, they amount to only a few percent of the total $CO_2$ release from combustion.

Even on a decadal scale, however, the observed $CO_2$ anomaly is not closely reproduced by the model. In contrast to the observed, slightly bowed shape after 1960, the model predicts an opposite pattern. If a biospheric release of $CO_2$ to the atmosphere by biospheric destruction is eliminated from the model and $CO_2$ fertilization appropriately reduced, so that the model predicts the same airborne fraction between January 1, 1959 and 1982 as before, the predicted pattern, shown in Figure 39, is still distinctly different from that observed. In the absence of a biospheric release, the model curve deviates from a zero anomaly almost exclusively because of variable acceleration in industrial $CO_2$ emissions. These emissions increased nearly exponentially at about 4 percent per year until 1973, but since then have increased more slowly. The model predicts that the sharply reduced acceleration in emission rate in the decade after 1973 should have resulted in a gradu-

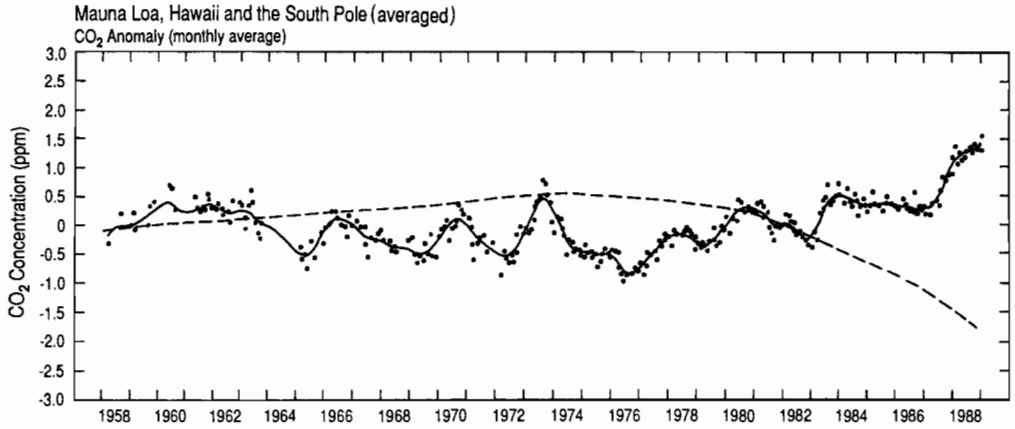


Fig. 38. Anomaly in the concentration of atmospheric $CO_2$, in ppm, based on the combined records of Mauna Loa Observatory and the South Pole, as in Figure 22. Also shown is a dashed curve which depicts a prediction based on the box diffusion model, in which the model terrestrial biosphere releases $CO_2$ according to curve for $\sigma_b$ of 125 years in Figure 36. The anomaly, as in Figures 20-22, is defined to be zero on 1 January 1959 and 1982.

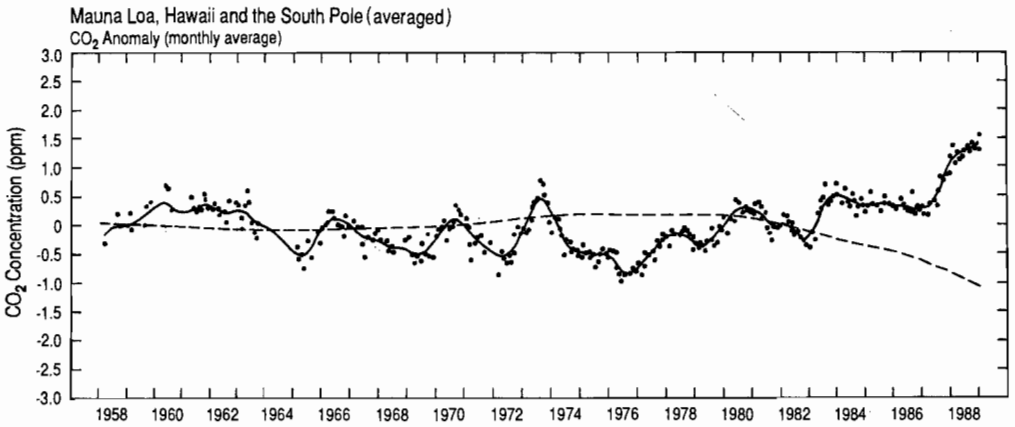


Fig. 39. Same as Figure 38 except that the model prediction assumes no release of $CO_2$ from the terrestrial biosphere owing to agriculture, grazing, harvest of forests, and decay of wood.

ally diminishing airborne fraction, expressed by a downward bending of both model predictions (Figures 38 and 39) beginning in the mid–1970's. The model, with or without an explicit biospheric release, thus assumes too much $CO_2$ to be entering the atmosphere before 1974 and too little afterwards.

The poorness of the prediction, when a biospheric release is included in the specification of the model, suggests that our representation of this release is an underestimate after the mid–1970's. The Gaussian function that we have used (see curve for $\sigma_b$ equal to 125 years in Figure 36), prescribes only a slight increase in the rate of release since the mid–1970's, as does the estimate of biospheric release by Houghton and Woodwell [1989] with which it is in close agreement after 1950. This function, and hence these direct estimates, are evidently unrealistic, unless the poorness of the model prediction of atmospheric $CO_2$ concentration results from our neglecting to consider some as yet unidentified oceanic perturbation that strongly affects the air-sea exchange of $CO_2$ during recent decades.

### *6.3 Deconvolution of Concentration and Isotopic Data*

To help establish the causes of the anomalous variations in atmospheric $CO_2$ just described, we have carried out an additional study to identify the relative importance of the terrestrial biosphere and the oceans in producing these variations, especially the recent anomalous increase in atmospheric $CO_2$. We have inverted the box diffusion model computations, in the manner employed by Siegenthaler and Oeschger [1987], to establish the anomalous net $CO_2$ exchange required for the model predictions to agree exactly with the seasonally adjusted atmospheric $CO_2$ observations after prescribing air-sea exchange and industrial $CO_2$ emissions as described in section 5, above. Since the determination of sources and sinks from the atmospheric $CO_2$ data with use of a model is equivalent to the inversion of an integral convolution equation, this inverse solution is commonly referred to as a "deconvolution". Enting and Pearman [1986] have carried out a similar inversion using a different model of the oceanic carbon cycle, and Enting

and Mansbridge [1987] have employed a linear programming method toward similar ends.

Subsequently we have also forced the model to agree with our isotopic data after 1978 by assuming that the anomalous net $CO_2$ exchange is made up of an oceanic component as well as a biotic component. We call this procedure a "double deconvolution".

In both the single deconvolution of the atmospheric $CO_2$ concentration record and the double deconvolution of the atmospheric $CO_2$ concentration and isotopic records together, the full set of equations for the box diffusion model were employed. The atmospheric $CO_2$ balance equation

$$\frac{dN_a}{dt} = F_{IND} + F_{ex} + F_{rem} \tag{6.1}$$

was solved for $F_{rem}$, a "remaining" net $CO_2$ flux, where $dN_a/dt$ denotes the time rate of change of the atmospheric $CO_2$ abundance of stable carbon, $N_a$, determined from the smoothed, seasonally adjusted observations expressed by the function $C_{obs\ rem}$, as defined by equation (2.2). The flux, $F_{IND}$, denotes the known rate of release of industrial carbon, while $F_{ex}$ denotes the rate of transfer of carbon from the oceans to the atmosphere as determined by the box diffusion model. These two fluxes, as well as the abundance $N_a$, and the residual flux, $F_{rem}$, are all functions of time, $t$. These fluxes are all defined as positive when sources to the atmosphere. The oceanic flux, $F_{ex}$, is always negative because it invariably involves a net transfer from the atmosphere to the oceans; it is computed to be directly proportional to the gas transfer coefficient, $k_{am}$, to the area of the oceans, $A_{oc}$ (see Table 8), and to the extent of disequilibrium at the air-sea interface. Concentrations and fluxes refer to total stable carbon, i.e., the sum $^{12}C + {}^{13}C$.

Fossil fuel $CO_2$ emissions, $F_{IND}$, were derived from a report by Marland [1989] that updates the annual production data of Table 7. In addition to small revisions before 1984, the updated fuel production for 1984 ($5238 \times 10^9$ kgC) is considerably less than as listed in Table 7. Projecting from new values for 1985 and 1986 (5338 and $5555 \times 10^9$ kgC, respectively), we assumed in these calculations a 3.5% annual increase in production for 1987 and 1988. A recent estimate [Marland, private communication] indicates a lesser increase of only 1.6% for 1987. A projection of 1.6% increase for 1987 and 1988 results in $0.3 \times 10^{12}$ kgC less release for 1987 and 1988 combined than our projection of 3.5% per year. This lesser amount is too small to affect significantly any of our conclusions.

The industrial $^{13}CO_2$ flux which is required in the double deconvolution, was determined from $^{13}\delta$ values as listed in Table 7, except that after 1949 we made revisions based on the updated production data of Marland [1989] for each fuel and for cement and on the corresponding $^{13}\delta$ values determined by Tans [1981]. For example, the $^{13}\delta$ of industrial $CO_2$ for 1986 is computed to be -27.11‰, compared to -27.28‰ as listed in Table 7. This revised ratio is assumed for 1987 and 1988.

The residual flux, $F_{rem}$, which remains after the known industrial $CO_2$ release and model computed oceanic uptake are subtracted from the observed atmospheric $CO_2$ increase, may reflect either biospheric or oceanic $CO_2$ exchange with the atmosphere. Let us therefore assume that it includes both a biospheric term, $F_b$, previously defined by equation (5.5), and an oceanic term, $F_{oc}$, i.e.,

$$\begin{aligned} F_{rem} &= F_b + F_{oc} \\ &= F_{DES} + F_{FER} + F_{oc} \end{aligned} \tag{6.2}$$

The oceanic flux, $F_{oc}$, is that part of the air-sea $CO_2$ exchange not accounted for by $F_{ex}$. If we choose model parameters such that $F_{ex}$ closely approximates the true uptake of $CO_2$ by the oceans, $F_b$ accounts for most of $F_{rem}$, except for short-term oscillatory perturbations, such as are caused by El Niño events. In the context of the present model, such oscillatory exchanges cannot be accounted for by $F_{ex}$ because the rates of gas exchange and oceanic vertical diffusion in the box diffusion model are defined to be time-invariant. Consequently, $F_{oc}$ changes sign frequently, whereas $F_b$ is typically positive.

The double deconvolution that we employ to separate $F_{rem}$ into $F_b$ and $F_{oc}$ requires that the fertilization factor, $\beta_a$, first be specified so that $F_{FER}$ is determined. However, it turns out that the magnitude $F_b$, as found by double deconvolution, is insensitive to its division into components $F_{FER}$ and $F_{DES}$. This double deconvolution is described in more detail in Appendix C.

It would have been possible to carry out a double deconvolution over the entire period since 1740 using $^{13}C/^{12}C$ data from ice cores. A recent challenge of these isotopic data by Craig et al. [1988], however, casts doubt on their validity. Also their lower precision reduces the value of such a calculation. We therefore first carried out a single deconvolution of the concentration data to establish $F_{rem}$, and then separately computed $F_b$ and $F_{oc}$ by a double deconvolution only for the period of direct isotopic data, beginning in 1978. Afterwards, however, as a check, we compared the isotopic ice core data with the model prediction of the $^{13}C/^{12}C$ ratio, based on a single deconvolution.

While running the deconvolution of the concentration data, we computed the isotopic ratios of all compartments by the method used for direct computations (see section 5, above). To set the initial value for $^{13}\delta$ of atmospheric $CO_2$ we first used an estimate such that the model predicted a value on 1 January, 1978 close to the observed value. We afterwards shifted by a constant all reduced isotopic ratios predicted by the model in order to produce exact agreement for atmospheric $^{13}\delta$ on this date. (The resulting $^{13}\delta$ of atmospheric $CO_2$ on 1 January, 1982, –7.601‰, differs slightly from the value used in the direct computations of the observation.)

To establish the global average concentration of atmospheric $CO_2$ as a continuous function of time, we combined the analyses of air from ice cores with direct observations for Mauna Loa Observatory and the South Pole. For the period 1955 to 1957 we employed proxy data of Keeling [1978] to effect a transition between the ice core data and the direct observations cited above. The assembled data, listed in Table A.6 of Appendix A, were fit by a spline function as shown in Figure 40. To establish the global average isotopic ratio of atmospheric $CO_2$ as a continuous function of time we used the average of the spline fits of the observations of $^{13}\delta$ for Mauna Loa Observatory and the South Pole, plotted in Figure 25 and listed in Table B.1 of Appendix B.

A comparison of this curve with the cumulative release of industrial $CO_2$, shown in Figure 41, allows us to anticipate the general features of the residual flux, $F_{rem}$, which is to be determined by deconvolution. Prior to 1900, the rise in atmospheric $CO_2$ exceeded the accumulated release of industrial $CO_2$ by a proportionally large amount, suggestive of a substantial release of $CO_2$ to the air unrelated to fossil fuel combustion, especially since part of the inferred release should have been absorbed by the oceans in response to the attending rise in atmospheric $CO_2$. Unless the oceans discharged substantial amounts of $CO_2$ to the air in the 19th

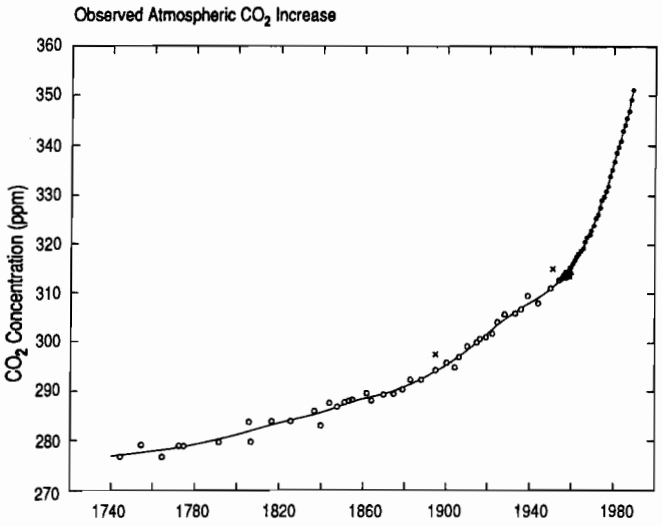


Fig. 40. Time trend of the concentration of $CO_2$, in ppm, in air extracted from an Antarctic ice core combined with the trend based on direct atmospheric measurements. The ice core data, shown as open circles, are as plotted in Figure 33. Crosses indicate two points rejected as outliers. Also rejected are ice core data after 1955 which overlap direct measurements. Dots depict annual values selected from a spline fit to direct monthly data for Mauna Loa Observatory and the South Pole combined. Triangles denote similarly derived proxy data for 1955 to 1958, as described in Appendix A. The curve is a spline function which combines separate fits to the direct data, the proxy data, and the ice core data; it was used to define the $CO_2$ concentration in the deconvolution computations described in the text.

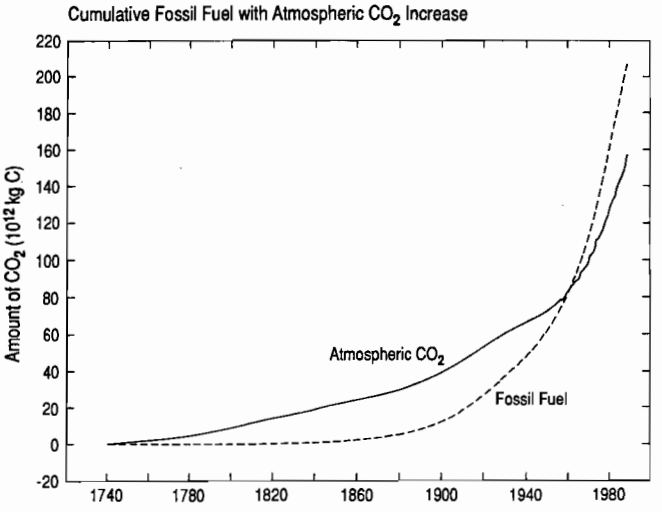


Fig. 41. The cumulative production of industrial $CO_2$ from fossil fuel and cement, versus time, in units of $10^{12}$ kgC, compared to the observed increase in atmospheric $CO_2$ in the same units. The latter curve is the spline curve shown in Figure 40.

century by some mechanism, yet unknown, this release must have come primarily from the terrestrial biosphere. After 1900 the cumulative release of industrial $CO_2$ grew more and more rapidly, and after 1960 exceeded the increase in atmospheric $CO_2$. The residual release therefore seems to become progressively less and less critical to determining the atmospheric $CO_2$ budget. This last surmise, however, needs to be tested quantitatively by carrying out the deconvolution.

With the oceanic parameters of the box diffusion model set to be consistent with bomb-produced radiocarbon, the cumulative residual flux,

$$N_{rem} = \int_{t_o}^{t} F_{rem}\, dt \tag{6.3}$$

as computed by deconvolution, is found to grow steadily in the 19th century, as shown in the time plot of Figure 42 with $t_o$ set to the year 1740. It continued to grow, but more and more slowly, until about 1940, after which it has remained more or less stationary. Thus since 1940, its rate of change, $F_{rem}$, has been close to zero, except for oscillations associated with El Niño events, which appear as small undulations on the plot after 1955, and a subtle upturn after 1974 reminiscent of the bow shaped $CO_2$ anomaly of Figure 22. If the 19th century and early 20th century releases were caused by man-made disturbances to the biosphere, the leveling off of the release after 1940 is perplexing, because we believe biospheric disturbances by man to have increased markedly in the 20th century, especially since 1950.

A closer view of the recent trend in $N_{rem}$, is displayed in Figure 43 with $t_o$ of equation (6.3) reset to 1957. The vertical axis is expressed both in mass units ($10^{12}$ kgC) and converted by the factor 290 ppm/615.6 × $10^{12}$ kgC (see Table 8) to the equivalent change in global atmospheric $CO_2$ concentration, in ppm. The function is shown both as a solid curve, derived by deconvolution from a spline fit to the observations, and as dots, derived directly from monthly concentration data, in the manner of the anomaly plots of Figures 38 and 39. The trend in the function on a decadal scale is shown by a dashed line. The bowed shape of the $CO_2$ anomaly plot of Figure 22 is also seen in this plot. Evidently $N_{rem}$ diminishes from about 1962 until approximately 1978 and then increases. The rise is quite considerable towards the end of the record.

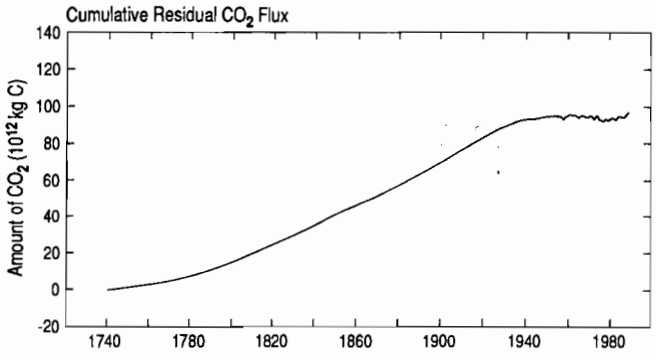


Fig. 42. That part of the cumulative release of $CO_2$ to the atmosphere, $N_{rem}$, not accounted for explicitly by the resultant oceanic uptake flux, $F_{ex}$. Time integration begins in 1740.

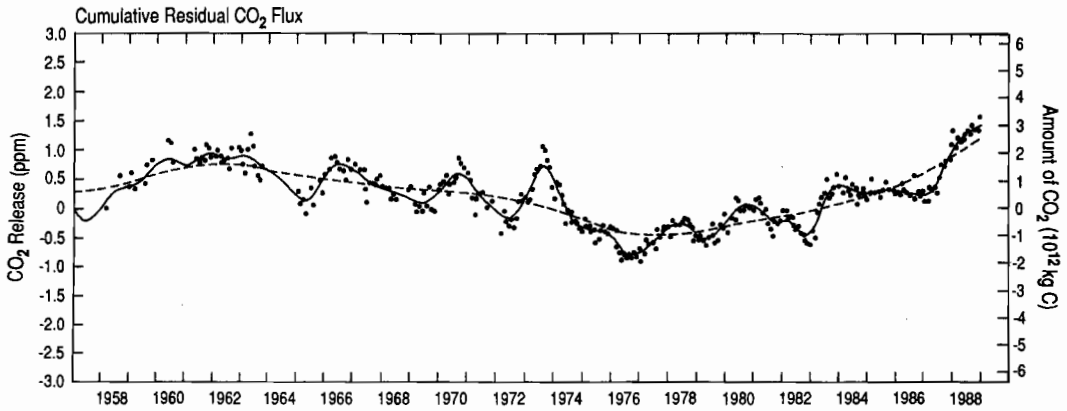


Fig. 43. Same as Figure 42 but showing in more detail the cumulative release, $N_{rem}$, since 1957, plotted in units of $10^{12}$ kgC (right vertical scale) and also as the global increase in atmospheric $CO_2$, in ppm, produced by the release (left scale). Time integration begins on 1 January 1957 when the cumulative release, shown in Figure 42, is 93.74 x $10^{12}$ kgC. Dots denote monthly averages of $N_{rem}$, consistent with individual unsmoothed monthly averages of $CO_2$ concentration. The solid curve shows $N_{rem}$ computed by deconvolution of the observed atmospheric $CO_2$ concentration as expressed by the spline curve of Figure 40. The dashed curve depicts a spline fit to $N_{rem}$, starting in 1953, to reveal its long-term trend. The spline has a standard error, $\sigma$, of 0.45 x $10^{12}$ kgC.

The flux $F_{rem}$, equal to $dN_{rem}/dt$, is plotted in the perspective of the entire industrial era in Figure 44. From the beginning of the record period in 1740 until about 1920, $F_{rem}$ gradually rises. Then it diminishes in an irregular manner until its trend is obscured by large oscillations associated with El Niño events. Similar events presumably affected atmospheric $CO_2$ in earlier years but are not reflected in the ice core record because of mixing of the trapped air before complete enclosure in solid ice [Neftel et al., 1985]. Irregularities appearing before 1955 are inverse reflections of small, but relatively abrupt variations in industrial $CO_2$ emissions compared to the smoothly varying ice core data. These irregularities do not appear to be significant when viewed on plots of cumulative fluxes or their equivalent (e.g., Figures 38, 39, and 42), but become prominent here, where the flux is plotted directly. Before 1920, even the industrial $CO_2$ record, and hence $F_{rem}$, is smooth as a result of less precise statistical data.

If the function $N_{rem}$ is first smoothed after 1955 in the manner defined by the dashed curve of Figure 43, the resulting smooth trend in its time derivative, $F_{rem}$, as seen in Figure 45, shows a general decline until the mid–1970's and then an abrupt rise. Thus after 1920 the curve for $F_{rem}$ scarcely resembles the global biospheric release as directly estimated by Houghton and associates and shown in Figure 36 as open circles. This poor resemblance indicates either that the box diffusion model poorly predicts the long-term trend in uptake of $CO_2$ by the oceans, or that the bios-

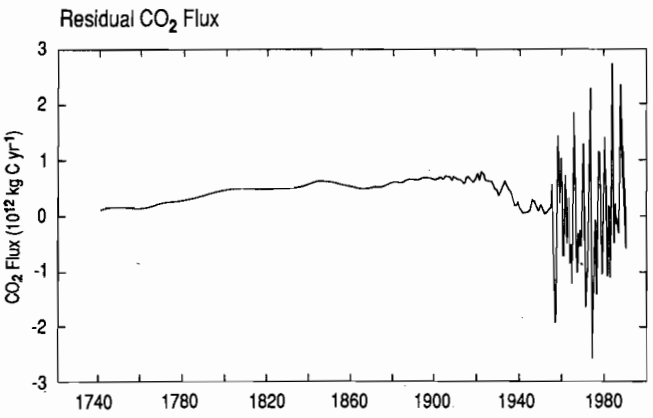


Fig. 44. Time trend in $F_{rem}$, the rate of $CO_2$ release, in units of $10^{12}$ kgC $yr^{-1}$, not accounted for explicitly by the resultant oceanic uptake flux, $F_{ex}$. The trend in $F_{rem}$ is consistent with its time integral, $N_{rem}$, shown in Figure 42.

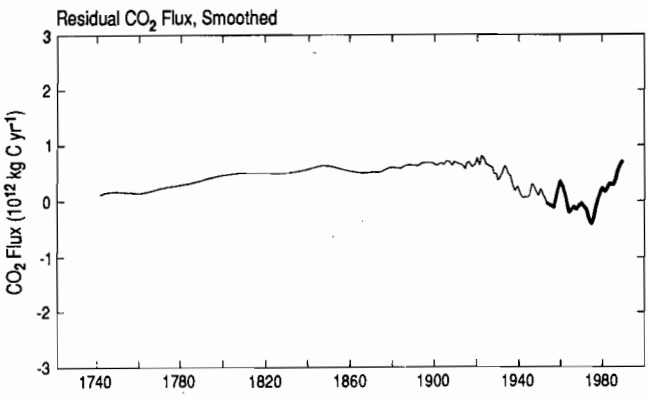


Fig. 45. Time trend in $F_{rem}$, same as Figure 44 except that after 1955 it has been smoothed, consistent with the dashed curve in Figure 43, to suppress short-term oscillations attributed to El Niño events. The bold curve after 1955 denotes the period of direct observations of atmospheric $CO_2$. The temperature of the oceans is assumed to be constant.

pheric release as estimated by Houghton and associates is a poor representation of the long-term variation in the biospheric flux, $F_b$.

Admittedly the box diffusion model highly simplifies oceanic circulation. It cannot simultaneously predict the steady state distribution of radiocarbon before the industrial era and also the transient uptake of bomb carbon. Siegenthaler [1983], to portray the stationary distribution of radiocarbon, was obliged to employ a vertical diffusion coefficient of 4005 $m^2$ $yr^{-1}$, about half that required to predict the distribution of bomb radiocarbon. As a test of the realism of the box diffusion model in portraying the long-term trend in atmospheric $CO_2$, we have carried out a deconvolution using the 27,000 grid point three-dimensional oceanic tracer transport model of Maier-Reimer and Hasselmann [1987], described in Appendix D. This model does not require a tuned parameter to represent vertical transport in the oceans. As shown in Figure 46, this physically more realistic model predicts a trend in $F_{rem}$ which is intermediate between predictions of the box diffusion model calibrated using stationary and bomb radiocarbon, and thus resembles the global release estimated by Houghton and his associates even less well than the upper curve, previously plotted in Figure 45, and discussed above.

Isotopic data are a means to help establish the extent to which the residual flux, $F_{rem}$, is a result of anomalous oceanic exchange, but they accompany our direct measurements only since 1978 (excluding a few preliminary data in 1977). Thus they are useful to assess oceanic influences only in the recent period of increasing residual flux, $F_{rem}$. We now consider these data. Afterwards we also make limited use of the isotopic data from ice cores to assess the oceanic contribution to $F_{rem}$ over the entire industrial era.

Retaining the parameters used in the deconvolution of the concentration record, and setting the initial values of reduced isotopic ratio, $^{13}\delta$, in the model so that the predicted atmospheric value on January 1 1978 agrees with the spline fit of the observations on that date (-7.487‰), we obtain by isotopic deconvolution the time plot of the cumulative biospheric flux shown in Figure 47. This function, the time integral of $F_b$, is shown both as discrete monthly values and as a smooth curve, expressed in $CO_2$ concentration units as in Figure 43. The discrete values are consistent with monthly averages of the isotopic data; the curve is consistent with

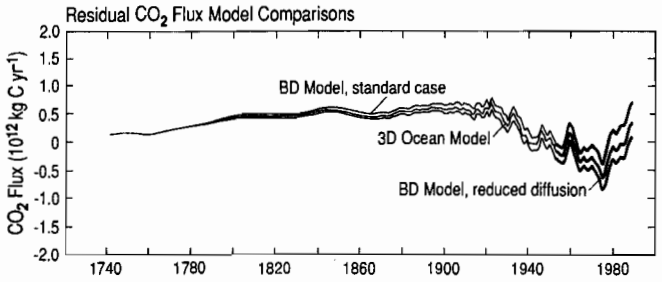


Fig. 46. Time trend in $F_{rem}$, plotted as in Figure 45 in units of $10^{12}$ kgC $yr^{-1}$, for a deconvolution based on a three-dimensional (3D) tracer transport model of the oceanic carbon cycle. For comparison the same function is shown as computed by the box diffusion (BD) model with a vertical diffusion coefficient of 7685 $m^2$ $yr^{-1}$ (upper curve, standard case), corresponding to calibration with bomb $^{14}C$, and 4005 $m^2$ $yr^{-1}$ (lower curve, reduced diffusion case), corresponding to calibration with preindustrial $^{14}C$.

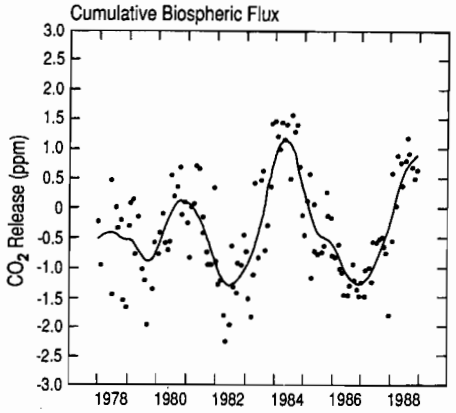


Fig. 47. Cumulative release of $CO_2$ from the terrestrial biosphere to the atmosphere versus time as given by the time integral of $F_b$ with the integration beginning on 1 January 1978. The release is expressed as the resultant global increase in atmospheric $CO_2$, in ppm, as in Figure 43. The smooth curve shows the time integral as a continuous function determined by double deconvolution. The dots denote unsmoothed monthly averages of the integral consistent with the monthly averages of $^{13}\delta$ plotted in Figure 25. The time integration begins in 1978.

the spline fit to these data shown as a solid curve in Figure 25. The large oscillations, approximately in phase with the oscillations in concentration, are evidently associated with El Niño events. They obscure any longer term trend. Nevertheless, when the cumulative function $N_{rem}$ and the integral of $F_b$ are plotted together, as in Figure 48, there is a suggestion that $N_{rem}$ oscillates about a long-term trend that is steeper than the trend in $F_b$, as though there were also an oceanic release of $CO_2$ to the atmosphere not accounted for by the explicitly calculated flux term, $F_{ex}$, of equation (6.1).

The time integral of the oceanic anomaly flux, $F_{oc}$, expressed in $CO_2$ concentration units, is shown in Figure 49. The plot is dominated by large oscillations similar, but nearly opposite in phase, to those of $F_b$; but, as with $N_{rem}$, there is a suggestion of a net release of $CO_2$ by the oceans over the 11 years of record, seen as a slight rising tendency in the plot. The most obvious explanation for such a release of $CO_2$ by the oceans is a response to recent warming of surface waters, not accounted for by the box diffusion model computations of the oceanic uptake, $F_{ex}$.

To explore this possibility quantitatively by deconvolution, we carried out an additional model computation including a provision that surface ocean water has warmed and cooled to the extent indicated by the global air temperature record shown in Figure 50, based on the data of Hansen and Lebedeff [1988, and private communication]. We chose to use air temperature data as a proxy for ocean water data because of uncertainties in the calibration of the latter and the expected close correspondence of air and sea data on interannual time scales [Jones et al., 1986a]. This air temperature record has been smoothed, with a spline function also shown in the figure. Short-term oscillations are largely suppressed by this smoothing, but variations on a decadal scale are retained. The predicted influence of this temperature record on ocean chemistry was modeled by adjusting the thermodynamic constraints on the carbonic acid system, including those on isotopic fractionation. As shown in Figure 51 the resulting curve for the time integral of the

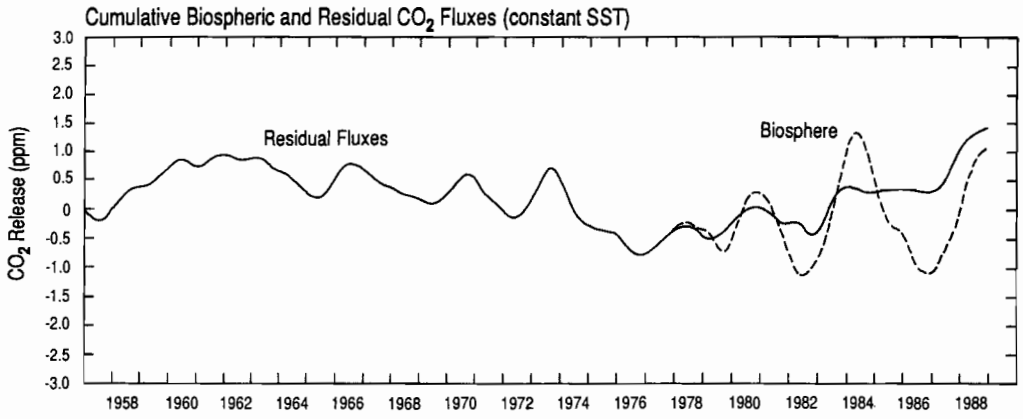


Fig. 48. Cumulative residual flux, $N_{rem}$, converted to ppm as in Figure 43, shown as a solid curve, compared with the time integral of $F_b$, shown as a dashed curve, in the same units. Surface ocean water temperature is assumed constant. The latter integral is assumed to coincide with $N_{rem}$ in 1978.

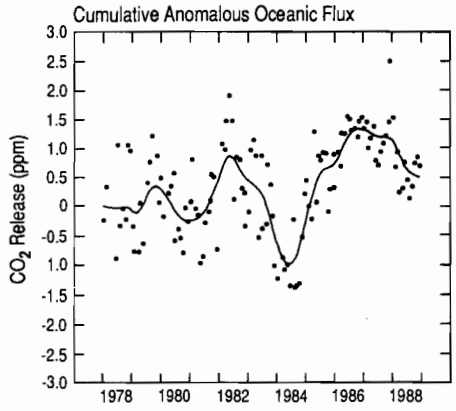


biospheric flux, $F_b$, in $CO_2$ concentration units, is changed only slightly, but compared to the plot in Figure 48 the curve for $N_{rem}$ has an appreciably lesser average slope after the mid–1970's because ocean warming is explicitly accounted for by the oceanic flux term, $F_{ex}$.

The best agreement of the decadal trends in the two fluxes would evidently be obtained by an intermediate prediction of $N_{rem}$ which

Fig. 49. Cumulative release of $CO_2$ to the atmosphere by anomalous air-sea exchange, versus time, in ppm, as given by the time integral of $F_{oc}$, with the integration beginning in 1978. The smooth curve and dots represent continuous and unsmoothed values, respectively, as in Figure 47.

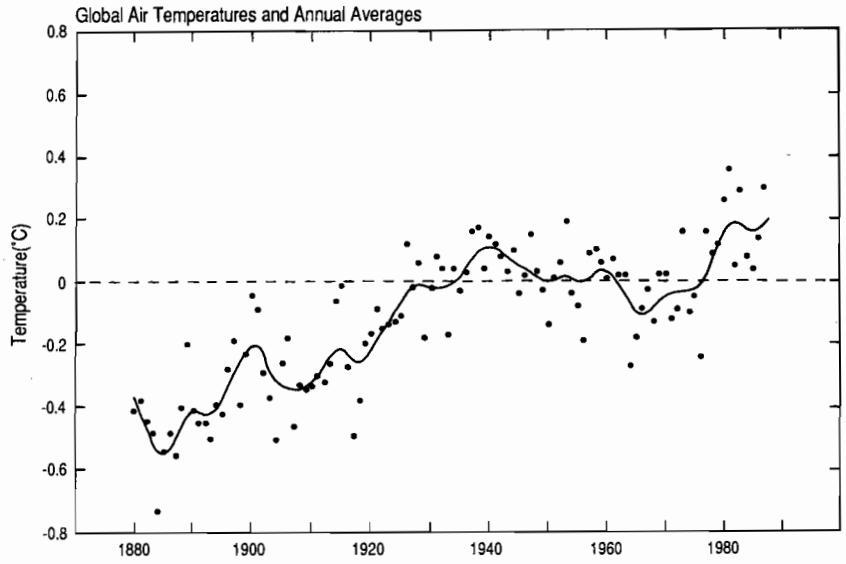


Fig. 50. Time trend of the global surface air temperature in °C based on monthly temperature anomalies as described in the text from 1880 through 1987. The smooth curve is a spline fit to monthly values, with a standard error, $\sigma$, of 0.195°C. Dots denote annual averages.

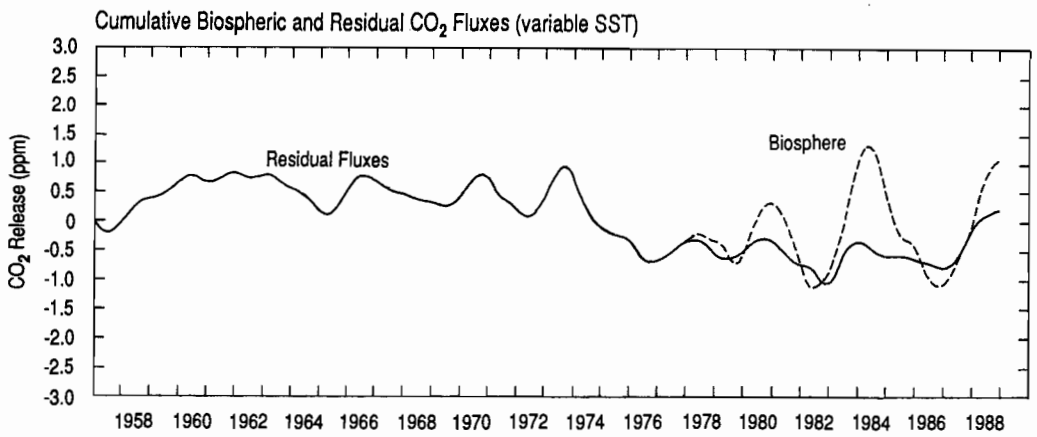


Fig. 51. Comparison of the cumulative residual flux, $N_{rem}$, and the time integral of $F_b$, as in Figure 48 except that surface ocean water temperature is assumed to vary after 1879 according to the smooth curve in Figure 50.

would result from assuming a somewhat lesser response to temperature in the model. However, as shown in Figure 52, even if the oceanic response to temperature is as large as assumed in our computations, an abrupt rise is still seen in the flux, $F_{rem}$, representing the time rate of change of $N_{rem}$. Analysis of combined isotopic and concentration data thus suggests that an accelerated release of $CO_2$ by the terrestrial biosphere is mainly responsible for the upturn in $F_{rem}$ since 1978.

Furthermore, the isotopic data from ice cores suggest that the function $F_{rem}$ mainly reflects a release of $CO_2$ from the terrestrial biospheric before 1978. Although we chose not to include the ice core data in our isotopic deconvolution because of uncertainties in their validity, it is worthwhile to compare these data with the model predictions of $^{13}\delta$ of atmospheric $CO_2$ obtained by deconvolution of the $CO_2$ concentration, to see if, within the uncertainty posed by possible gravitational separation of isotopes within the ice, one can distinguish biospheric and oceanic sources and sinks of $CO_2$.

As shown in Figure 53, predictions of the $^{13}\delta$ of atmospheric $CO_2$ by deconvolution of $CO_2$ concentration using the box diffu-

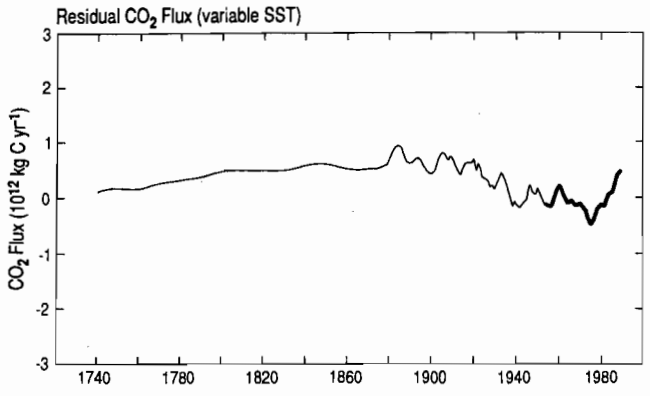


Fig. 52. Time trend of $F_{rem}$, as in Figure 45, except that surface ocean water temperature is assumed to vary after 1879 as in Figure 51.

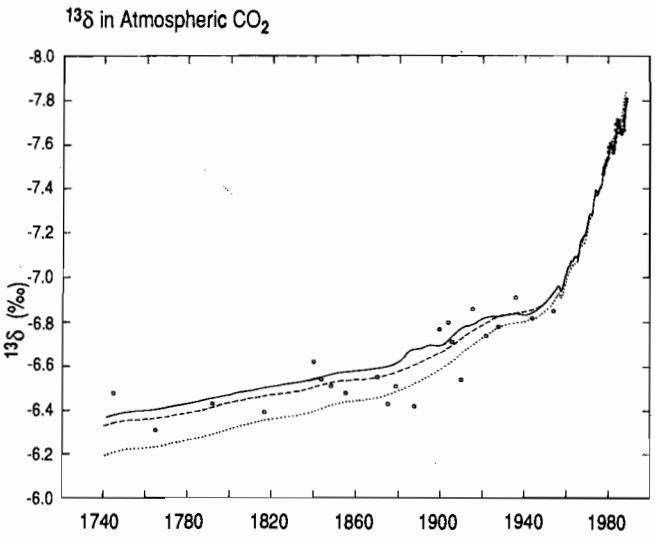


Fig. 53. Time trend of the reduced isotopic ratio, $^{13}\delta$, of atmospheric $CO_2$ in per mil from standard PDB, from ice core samples, shown as open circles, and from recent direct air measurements (data from Mauna Loa Observatory and the South Pole averaged) shown as dots. The ice core observations are as plotted in Figure 40. Also shown are three predictions of the time trend in $^{13}\delta$ based on single deconvolutions using the box diffusion model. The upper solid curve is a prediction assuming an oceanic vertical diffusion coefficient of 7685 $m^2$ $yr^{-1}$ and variable sea surface temperature (SST) after 1879 according to the global air temperature plot of Figure 50. The middle, dashed, curve is a prediction with the same diffusion coefficient but assuming constant surface ocean water temperature. The lowest, dotted, curve is a prediction with a vertical diffusion coefficient of 46110 $m^2$ $yr^{-1}$ assuming constant temperature. In all predictions the atmosphere-ocean $CO_2$ exchange time is held constant at 6.87 years. Isotopic ratios were subsequently computed assuming that the residual flux, $F_{rem}$, is exclusively biospheric. The $^{13}\delta$ for each model prediction was adjusted to the same value in 1978.

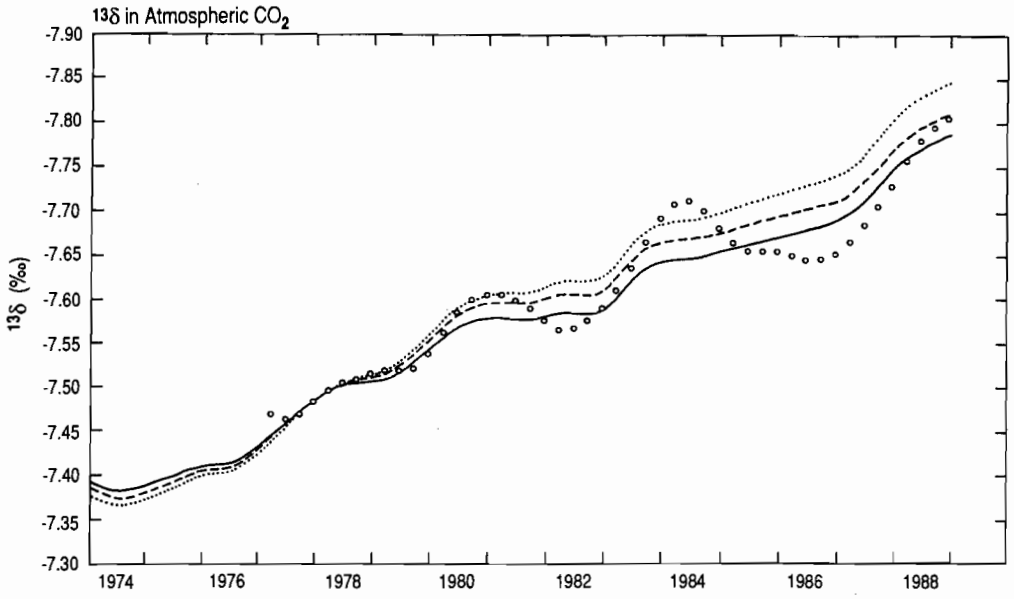


Fig. 54. Observed and predicted time trend of $^{13}\delta$, in per mil, showing details of the plot in Figure 53 for the recent period. Direct measurements of air, from Mauna Loa Observatory and the South Pole, have been averaged and smoothed to give tri-monthly averages and are shown as open circles.

sion model, agree with ice core data within scatter, if variable temperature is assumed for surface ocean water. The agreement is equally satisfactory if constant temperature is assumed. If gravitational separation in the ice has caused an overestimate of the variation in $^{13}\delta$, perhaps by as much as 0.35‰, as suggested by Craig et al. [1988], then this agreement is fortuitous. However, as seen by the lower dotted curve in the figure, a higher vertical diffusion rate, implying a larger net biospheric $CO_2$ release, $F_b$, produces a larger shift in $^{13}\delta$, and is in poor agreement with the $^{13}\delta$ data from ice cores, especially before 1860. Furthermore, the predicted trend in $^{13}\delta$ since 1978, assuming greater vertical diffusion, agrees poorly with our direct observations as demonstrated in Figure 54. We must be cautious in attempting to validate the box diffusion model using isotopic data from ice core samples, but these data, if correct, support a hypothesis that the flux, $F_{rem}$, determined by deconvolution of the $CO_2$ concentration data, is mainly biospheric.

### 6.4 *Analysis of El Niño Oscillations*

Before we investigate the consequences of assuming that the residual flux, $F_{rem}$, is mainly biospheric, we examine in greater detail the oscillations in the biospheric and oceanic fluxes which appear to be responses to El Niño events. For each event we determine the mass transfers of carbon between reservoirs, and whether these amounts accord with other knowledge of the carbon cycle. We also examine whether the phasing of the oscillations seems reasonable in terms of the timing of these events.

We focus on model results which are based on a constant-temperature ocean. The corresponding results, from the deconvolutions of concentrations and isotopic ratio assuming variable temperature, are practically the same with respect to these short-term oscillations, as we show below.

To carry out this examination we decompose the biospheric flux, $F_b$, and the oceanic flux $F_{oc}$, into short-term components, $\Delta F_b$ and $\Delta F_{oc}$, on the time scale of El Niño events, and long-term trends $\langle F_b \rangle$ and $\langle F_{oc} \rangle$, on scales of a decade or longer. Specifically, we define the sums

$$F_{oc} = \Delta F_{oc} + \langle F_{oc} \rangle \tag{6.4}$$

$$F_b = \Delta F_b + \langle F_b \rangle \tag{6.5}$$

where all terms are functions of time. Consistent with equation (6.2), we also define short-term and long-term components of the residual flux, $F_{rem}$, such that

$$\langle F_{rem} \rangle = \langle F_{oc} \rangle + \langle F_b \rangle \tag{6.6}$$

and

$$\Delta F_{rem} = \Delta F_{oc} + \Delta F_b \tag{6.7}$$

Since our isotopic records extend over only 11 years, the longest term trends seen in these data are, in fact, just barely on the decadal scale. There is no direct means to establish a decadal trend for $F_{oc}$, given the large oscillations in its time integral (see Figure 49). We have therefore set $\langle F_{oc} \rangle$ equal to the average of $F_{oc}$ over the full isotopic record after 1978 ($0.07 \times 10^{12}$ kgC $yr^{-1}$). Because short-term oscillations in $F_{rem}$ are smaller than those in $F_{oc}$ and $F_b$, and the function, derived from concentration data, has been computed over a longer time interval, the long-term trend, $\langle F_{rem} \rangle$, is more readily estimated than $\langle F_{oc} \rangle$ or $\langle F_b \rangle$. Therefore we have computed $\langle F_b \rangle$ from $\langle F_{rem} \rangle$ and $\langle F_{oc} \rangle$ via equation (6.6) with $\langle F_{oc} \rangle$ set to the constant value already adopted. We accepted the dashed line in Figure 43 as our best estimate of the time integral of $\langle F_{rem} \rangle$ from which we derived $\langle F_{rem} \rangle$ by differentiation.

Plots of $F_{oc}$ and $\langle F_{oc} \rangle$ are shown in Figure 55, and plots of $F_b$ and $\langle F_b \rangle$ in Figure 56. The long-term trend $\langle F_{oc} \rangle$ is seen to be invariant, as assumed, while $\langle F_b \rangle$, defined as equal to $\langle F_{rem} \rangle - \langle F_{oc} \rangle$, rises gradually.

Because El Niño events arise from physical interactions of the atmosphere and oceans, we expect the oscillating oceanic flux,

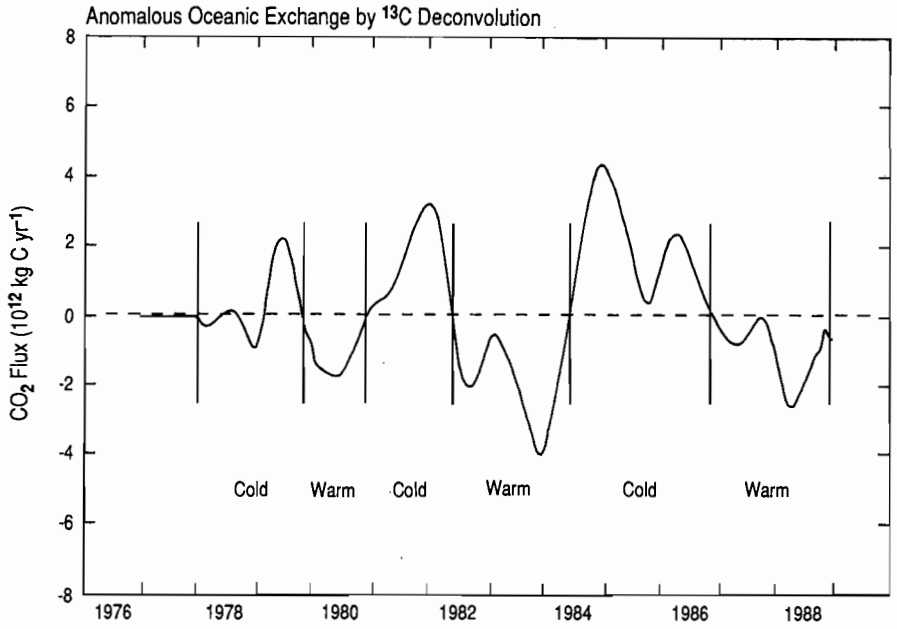


Fig. 55. Time trend of $F_{oc}$, the anomalous release of $CO_2$ by the oceans, shown as a solid curve, in units of $10^{12}$ kgC $yr^{-1}$. Vertical lines separate warm and cold events, as defined in the text. A dashed curve indicates the long-term trend, $<F_{oc}>$, evaluated as the mean of $F_{oc}$ over the isotopic record period (0.07 x $10^{12}$ kgC $yr^{-1}$). $\Delta F_{oc}$, the departure of $F_{oc}$ from $<F_{oc}>$ is nearly the same as $F_{oc}$ because $<F_{oc}>$ is close to zero. In 1977, prior to the start of the isotopic record, $F_{oc}$ is zero, as plotted.

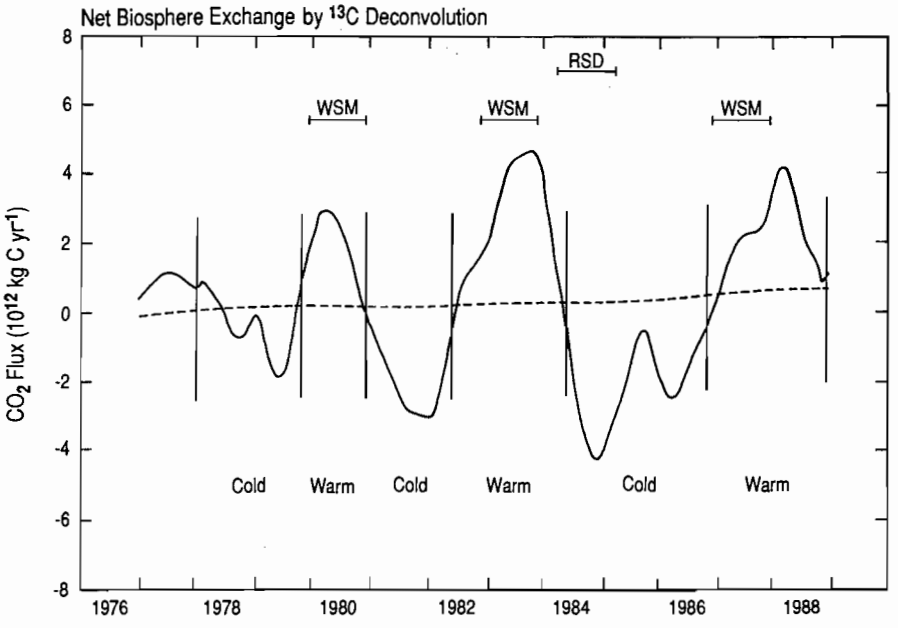


Fig. 56. Time trend of $F_b$, the net release of $CO_2$ by the biosphere, shown as a solid curve, in units of $10^{12}$ kgC $yr^{-1}$. The dashed curve indicates the long-term trend derived by differentiation of the smoothed curve of $N_{rem}$ shown as a dashed line in Figure 43. Horizontal line segments labeled 'WSM', indicate yearly intervals following the onset of "weak summer monsoons" in India. Another line segment, labeled 'RSD', indicates the period of "remote sensing data" from satellites used to establish global net primary productivity, as described in the text. Symbols are otherwise as in Figure 55. $\Delta F_b$ is given by the departure of $F_b$ from the dashed line, denoting $<F_b>$. In 1977, prior to the start of the isotopic deconvolution, $F_b$ is set equal to $F_{rem}$, as plotted in the next figure.

$\Delta F_{oc}$, *a priori* , to be more directly coupled to the El Niño phenomenon than the corresponding terrestrial biospheric flux, $\Delta F_b$. We have therefore defined the timing of the short-term interannual oscillations in the carbon cycle in terms of $\Delta F_{oc}$. As shown in Figure 55, the times since 1978 when this flux alternated between positive and negative values are easily identified. We assume, therefore, that these times mark the beginning and end of each event. Events associated with the mature phase of El Niño we will henceforth call "warm events", following Rasmusson and Carpenter [1982] and van Loon [1984]. Alternate periods, by the same terminology, we will call "cold events". As can be established by comparison with the times of El Niño events shown in Figure 22, periods of negative $\Delta F_{oc}$ are associated with warm periods, positive $\Delta F_{oc}$ with cold periods.

The times of alternation of the biospheric flux, $\Delta F_b$, as seen in Figure 56, generally agree with those of the oceanic flux, $\Delta F_{oc}$ within 2 months. In contrast, as shown in Figure 57, the times of alternation for the sum of these fluxes, $\Delta F_{rem}$, depart considerably from those of $\Delta F_{oc}$. The close timing of oscillations in $\Delta F_{oc}$ and $\Delta F_b$ is a direct consequence of the large amplitude of these oscillations relative to their sum, $\Delta F_{rem}$. We discuss this near synchroneity below.

Fortuitously, the first cold event recorded by the isotopic data appears to commence near the beginning of the isotopic record, and the last warm event terminates near the end of the record. Because $\Delta F_{oc}$ is close to zero at both ends of this record, we assume that these times identify actual reversals.

Computed time integrals of the oscillating fluxes for each defined warm and cold event are listed in Table 13. Because the record period comprises an equal number of warm and cold events, we have adjusted $\Delta F_b$ and $\Delta F_{rem}$ in this table to sum to zero. (The oscillatory flux, $\Delta F_{oc}$, automatically sums to zero because $<F_{oc}>$ is set equal to the average of $F_{oc}$ over the record period). In Table 13 we also list time integrals based on our assuming that the temperature of surface ocean water varied according to the plot in Figure 50. As can been seen, the latter integrals differ only slightly from those for constant temperature. This close agreement arises in part because of the relatively short intervals associated with each event. As noted earlier the time integral of $F_{oc}$ over the entire isotopic record (131 months) depends on whether constant or variable surface ocean water temperature is assumed. For variable temperature the integral is $-1.5 \times 10^{12}$ kgC; for constant temperature, it is $0.8 \times 10^{12}$ kgC. These integrals are influenced by the choice of start and end dates of the record, but their difference, $2.3 \times 10^{12}$ kgC, reflects the predicted cumulative influence of warming on $<F_{oc}>$, except for a difference of $0.6 \times 10^{12}$ kgC in the integral of $F_b$.

This latter difference exists because variations in $^{13}\delta$ of $CO_2$ do not uniquely indicate biospheric fluxes. There is not only a small isotopic dependency on oceanic fluxes (see equation 3.4) but an additional small dependency on the previous distribution of $^{13}\delta$ in all of the carbon cycle reservoirs, as predicted by the box diffusion model. This distribution is not independently known, and in the model it is slightly different depending on whether variable or constant temperature is assumed prior to 1978. Thus the predicted cumulative influence of oceanic warming associated with $<F_{oc}>$ is actually $2.9 \times 10^{12}$ kgC, integrated over the entire isotopic record, an average rate of release of $CO_2$ to the air of $0.3 \times 10^{12}$ kgC $yr^{-1}$.

The largest fluxes inferred from the isotopic record occur during the warm event associated with the El Niño of 1982–1983 and the ensuing cold event. During this warm event, defined by $\Delta F_{oc}$ to have occurred between June 1982 and June 1984, the oceans evi-

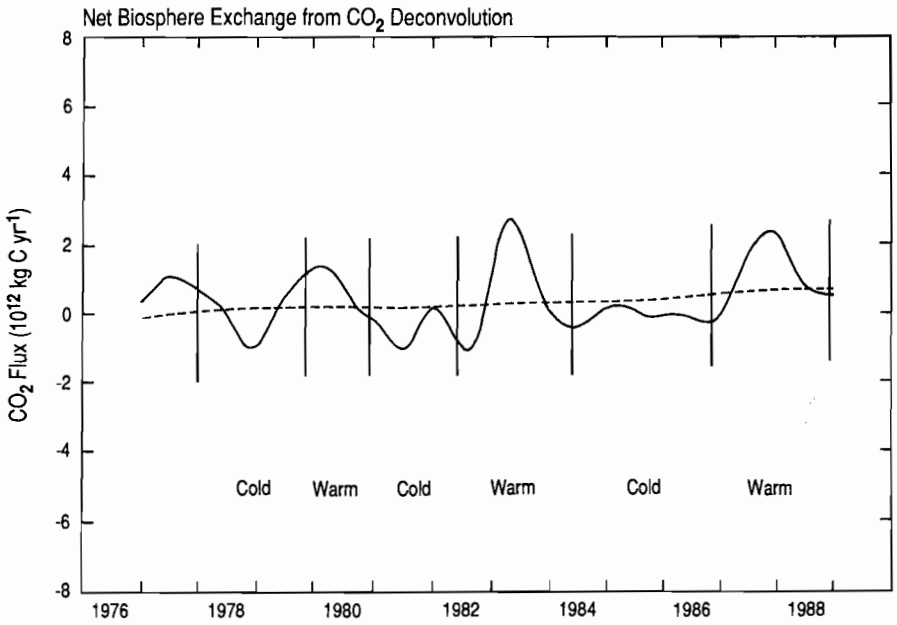


Fig. 57. Time trend of the function $F_{rem}$, representing the sum of the fluxes $F_{oc}$ and $F_b$, shown in Figures 55 and 56, respectively. Units and symbols are the same as in Figure 56. $\Delta F_{rem}$ is given by the departure of $F_{rem}$ from the dashed curve denoting $<F_{rem}>$.

TABLE 13. Cumulative Fluxes of $CO_2$ (in $10^{12}$ kgC) during Warm and Cold Events as Predicted by Deconvolution using the Box Diffusion Model

| Event | Inclusive Period | No. of months | Constant Temperature | | | Variable Temperature | | |
|---|---|---|---|---|---|---|---|---|
| | | | $\Delta F_{oc}$ | $\Delta F_b$ | $\Delta F_{rem}$ | $\Delta F_{oc}$ | $\Delta F_b$ | $\Delta F_{rem}$ |
| cold | Jan. 1978 – Oct. 1979 | 22 | 0.59 | –0.92 | –0.33 | 0.49 | –0.83 | –0.35 |
| warm | Nov. 1979 – Nov. 1980 | 13 | –1.32 | 1.95 | 0.62 | –1.46 | 2.04 | 0.58 |
| cold | Dec. 1980 – May 1982 | 18 | 2.27 | –3.27 | –1.00 | 2.18 | –3.21 | –1.04 |
| warm | June 1982 – May 1984 | 24 | –4.01 | 4.75 | 0.74 | –3.95 | 4.74 | 0.79 |
| cold | June 1984 – Oct. 1986 | 29 | 4.73 | –5.85 | –1.12 | 4.96 | –6.03 | –1.08 |
| warm | Nov. 1986 – Nov. 1988 | 25 | –2.26 | 3.35 | 1.09 | –2.21 | 3.30 | 1.09 |

dently absorbed $4.0 \times 10^{12}$ kgC while the terrestrial biosphere released $4.8 \times 10^{12}$ kgC. During the subsequent cold event, lasting 29 months, the oceans released $4.7 \times 10^{12}$ kgC and the biosphere absorbed $5.8 \times 10^{12}$ kgC. We now investigate whether these computed oscillatory fluxes are plausible in the context of the carbon cycle. We will first discuss the phasing of these oscillations and then their magnitudes.

The phasing of oscillations in the oceanic flux, $F_{oc}$, is more readily scrutinized because it can be compared with temperature data for the tropical oceans, where reduced upwelling and spreading of warm water during strong El Niño events is attended by marked increases in average sea surface temperature as well as changes in carbon distribution. We have compared $F_{oc}$ with sea-surface temperature data averaged by Abraham Oort [Oort and Pan, 1986 and private communication] over an extensive region that he calls the "Eastern Equatorial Pacific" (EEP). As seen in Figure 58 an inverted plot of $F_{oc}$ correlates well with EEP sea-surface temperature, with a lag of about 6 months. It thus seems likely that the short-term oscillations in $F_{oc}$ are largely produced by the processes which cause short-term interannual variations in EEP sea-surface temperature.

The lag in temperature with respect to $F_{oc}$ is similar to that found by Bacastow [1976] in the first derivative of the atmospheric $CO_2$ data with respect to the Southern Oscillation index. It may largely, if not entirely, reflect the time required for equatorial air to mix with air at the latitudes of the observation stations, especially the South Pole, but we have not carried out a detailed investigation of its cause, pending development of a three-dimensional tracer model which treats short-term interannual variations in the carbon cycle.

The phasing of oscillations in the biospheric flux, $F_b$, is less readily verified, because we lack a closely related ecological parameter with which to compare it, in the manner in which we compared $F_{oc}$ with ocean temperature. The beginning of $CO_2$

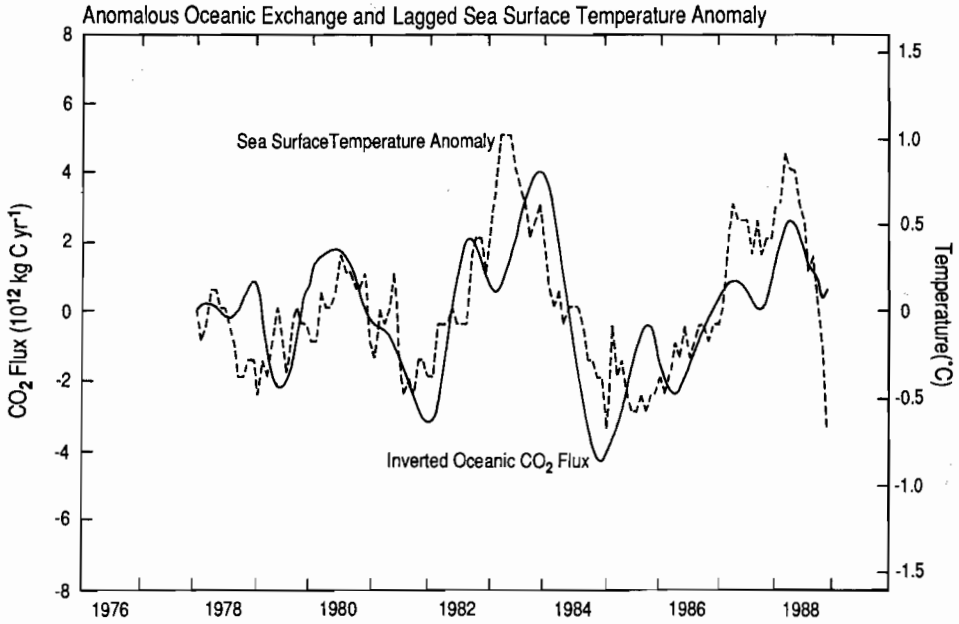


Fig. 58. Sea surface temperature (SST) anomaly in the eastern equatorial Pacific ocean, in °C, compared to the anomalous oceanic $CO_2$ release $F_{oc}$, in units of $10^{12}$ kgC $yr^{-1}$. The temperature anomaly [Oort and Pan, 1986] is defined as the monthly average departure from the long-term mean between 1950 and 1979, over the region from 180°W to 80°W and 20°N to 20°S. The plot of $F_{oc}$ (cf. Figure 55) is inverted to show a direct correlation with SST. The time scale of SST is lagged by 6 months. (Gigaton = $10^{12}$ kg).

releases by the biosphere associated with El Niño can be estimated from the time integral of $F_b$, plotted in Figure 47. This function starts to rise from a minimum value approximately when the southeast Asian monsoon failed to appear with its normal strength in the summers of 1979, 1982, and 1986. This near coincidence is expected if the lack of normal monsoonal rains causes an almost immediate reduction in net primary productivity large enough to be detected on a global scale. For a more quantitative assessment of the timing of $\Delta F_b$ , we have assumed a phase lag in $\Delta F_b$ of 6 months relative to NPP which is equal to the lag found in the oceanic flux component, $\Delta F_{oc}$, relative to equatorial sea-surface temperature. We have then assumed that the intervals of reduced growth caused by drought typically begin at the normal time of onset of the summer monsoon in India in June and last for 1 year. Lagging these periods by 6 months, we see, as shown in Figure 56, that they correspond approximately to the times of greatest release of $CO_2$ during the warm events in 1980 and 1983. The period occurs perhaps too early in 1987, but not if the biospheric $CO_2$ release was prolonged into the next year, in the manner that the warm anomaly in EEP temperature was prolonged, as seen in Figure 58. We may also expect some prolongation in all of these periods of drought because the southern hemisphere should contribute to the release of $CO_2$ 6 months after the northern hemisphere [Meehl, 1987].

Our success in correlating the computed oceanic flux component, $F_{oc}$, with sea-surface temperature strongly suggests that the phasing of interannual oscillations in our isotopic data reflect real variations in the carbon cycle. The relatively close timing of oscillations in the computed biospheric flux component, $F_b$, with failure of the southeast Asian monsoon suggests that the direct cause for these isotopic oscillations is variable plant growth and decay related to variations in monsoonal rainfall. Nevertheless, we need also to establish that the amplitudes of oscillations in $F_{oc}$ and $F_b$ are reasonable. As we now show, this is not readily accomplished, although we find no irrefutable evidence to reject the observations as incorrect.

With respect to oceanic $CO_2$ exchange, we expect the strongest perturbations to be in the tropics, especially in those equatorial waters where El Niño events originate. Under normal conditions, these waters upwell and release $CO_2$ to the extent that the equatorial zone of the oceans, on average, is a net source of $CO_2$. During 1983, direct oceanographic data reported by Keeling and Revelle [1985], Chavez and Barber [1985] and Feely et al. [1987] indicate that equatorial upwelling virtually ceased in the eastern Pacific ocean, the region which normally has the greatest intensity of upwelling. Chavez and Barber noted that during the mature stage of the El Niño event that year, which lasted for 210 days, the primary productivity of surface water was reduced by about $1 \times 10^{12}$ kgC $yr^{-1}$, and equatorial degassing by about half that amount.

An independent estimate of the $CO_2$ fluxes associated with equatorial upwelling is furnished by a model calculation. Using again the three-dimensional oceanic tracer transport model described in Appendix D, we have estimated that the oceans over the entire zone between 16°N. and 16°S. normally release $1.7 \times 10^{12}$ kgC $yr^{-1}$, an amount which agrees approximately with an independent estimate, derived from model calculations based on atmospheric $CO_2$ observations, that 1.5 to $2.2 \times 10^{12}$ kgC $yr^{-1}$ is typically released from this zone [Keeling et al., this volume, Table 1]. To explain a global net absorption of $4.0 \times 10^{12}$ kgC by the oceans in 2 years therefore requires that equatorial upwelling virtually ceased during the entire warm event of 1982–1984. According to the data of Chavez and Barber [1985], the period of extreme conditions was shorter, and therefore the computation of $F_{oc}$ from deconvolution seems to overstate the $CO_2$ uptake during the warm event. Similarly the release of $4.7 \times 10^{12}$ kgC by the oceans in 29 months during the subsequent cold event seems too large. Perhaps a lesser release or greater uptake of oceanic $CO_2$ than normal occurred outside of the equatorial zone during the warm event, for example as a result of cooling produced by abnormally strong westerly winds in midlatitudes and followed by a return to more normal conditions during the subsequent cold event [see, for example, Oort and Pan, 1986, p. 254; Namias et al., 1988, p. 699; Semazzi et al., 1988]. Without more direct evidence of these possibilities, however, the time integrals of $\Delta F_{oc}$, found for each event by deconvolution, cannot be substantiated, although they are not so large as to be ruled out.

According to the isotopic $CO_2$ record as interpreted by double deconvolution, even larger terrestrial biospheric fluxes are produced in association with the warm and cold events which accompany and follow the appearance of El Niño. To help decide whether these predicted fluxes are reasonable, we have estimated the normal annual $CO_2$ fluxes for the regions over land most likely to be perturbed by these warm and cold events and the expected timing of anomalous rates of $CO_2$ exchange. For this estimate we rely upon two facts: firstly, during the 31 years of direct $CO_2$ observations, El Niño events have almost always occurred during years in which the southeast Asian summer monsoon over India was weak, as noted in section 4, above, and shown in Figure 22. Secondly, rainfall in specified regions of the tropics correlates with the Southern Oscillation and thus with El Niño events [Stoeckenius, 1981]. This correlation is especially pronounced in the regions of the Asian monsoon, but is also found for parts of Australia, South America, and Africa.

The correlation for southeast Asia and Australia has been explained by Meehl [1987]. The same east-west circulation in the tropics which interacts with upwelling water in the eastern Pacific ocean under normal conditions, also produces strong vertical convection in the air masses of the western Pacific with attending heavy rainfall. When this circulation weakens during an El Niño event, rainfall is reduced in the west at almost the same time as oceanic upwelling is reduced in the east.

Thus reduced tropical rainfall appears primarily responsible for a release of $CO_2$ by the biosphere during an El Niño event, although warmer temperatures in the affected areas could also contribute because abnormally warm conditions typically accompany drought. During droughts, reductions occur in both net primary productivity [Lange et al. 1982, (see especially chapters 7, 9, and 10)] and in respiration including that of soils [Singh and Gupta, 1977]. Although the effects of water stress on plants have been studied extensively, investigations have mainly involved short-term, controlled experiments. These cannot readily be used to make quantitative predictions over an entire season or annual cycle, and in particular they do not explain whether net primary productivity (NPP) or respiration is more depressed by drought. Our data can be interpreted, however, only if NPP is reduced much more than respiration through the annual cycle. We have assumed, therefore, for purposes of estimate, that the biospheric fluxes inferred from the isotopic data mainly reflect oscillations about a

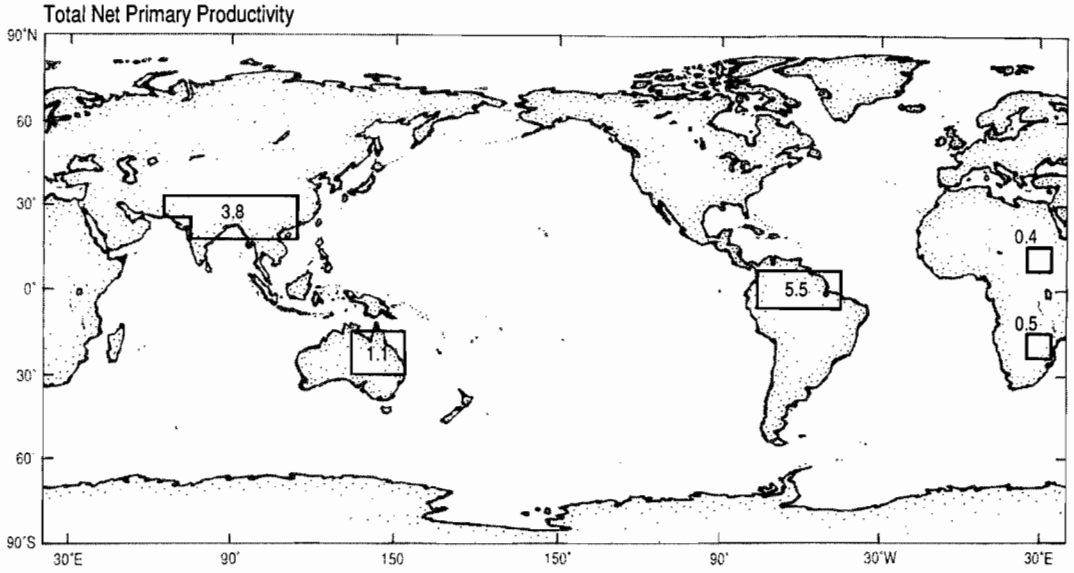


Fig. 59. Approximate locations of areas where an average normalized anomaly of rainfall negatively correlates with the Southern Oscillation Index, significant at the 90% level or greater, according to Stoeckenius [1981, p. 1242]. Also shown for each area is the annual net primary productivity of land plants in units of $10^{12}$ kgC $yr^{-1}$ as derived from the model study of Heimann and Keeling [*this volume*].

long-term average value for NPP, with respiration contributing to a considerably lesser extent.

Assuming the existence of oscillations about a long-term average, we have computed NPP on an annual basis in the regions which are likely to be affected by drought during El Niño events. We were guided by a chart by Stoeckenius [1981] which shows where rainfall in a statistical sense correlates significantly with the Southern Oscillation. As can be deduced from Figure 59, annual NPP over the regions identified by Stoeckenius amounts to approximately $11 \times 10^{12}$ kgC ($7 \times 10^{12}$ kgC in the northern hemisphere and $4 \times 10^{12}$ kgC in the southern) on the basis of computations by Heimann and Keeling [this volume]. The computations are for a one year period beginning in October 1983, thus immediately following the mature stage of the 1983 El Niño. The annual integral of $\Delta F_b$ over this period is found to be $-2.9 \times 10^{12}$ kgC, when the integral is evaluated from April 1984 to April 1985 to be consistent with the 6 month lag found in $\Delta F_{oc}$ with respect to ocean temperature. Evidently, in the absence of a warm or cold event, NPP in that year would have been approximately $8 \times 10^{12}$ kgC.

Given this estimate of NPP, we have calculated the average range of NPP over an annual growth period, defined as beginning when the summer monsoon typically arrives in India. We find NPP to have varied since 1978 between extremes of $5 \times 10^{12}$ kgC $yr^{-1}$ (from June 1983 to June 1984) and $11 \times 10^{12}$ kgC $yr^{-1}$ (from June 1985 to June 1986). This is a broad range. We note, however, that Stoeckenius identified only areas which showed a strong statistical correlation for all years from 1940 through to 1975. For example, Bradley et al. [1987] show in their Figure 6 a larger area of southeastern Asia and Indonesia having statistically significant rainfall fluctuations which are extreme during the extreme years of warm and cold events. It is quite possible that additional land areas suffered reduced rainfall during the unusually intense event of 1983–1984 and its aftermath. Furthermore, recently acquired data, not included in this article, indicate a biospheric contribution to the 1987-1988 event at high northern latitudes, seen in an unusually large anomalous increase in $CO_2$ at Point Barrow, Alaska, and at a new station on Ellesmere Island, Canada. If so, the range that we have computed should be with respect to a higher average NPP. Also, global warming during this event may have caused higher respiration in areas of normal or excessive rainfall, possibly accounting for part of the variability in $F_b$. Thus, as in the case of $\Delta F_{oc}$, the time integrals of $\Delta F_b$ for each event appear to be exaggerated, but not to the extent that they can be ruled out on the basis of existing information.

In conclusion, although the oscillations in $^{13}\delta$ of atmospheric $CO_2$ seem plausible when compared to ocean surface temperature data, to the timing of the weak monsoons, and to the model calculations of $CO_2$ fluxes influenced by El Niño, the evidence is not entirely conclusive. The isotopic signals to establish interannual oscillations are weak relative to scatter in the observations at individual observing stations and to expected errors in sampling and isotopic analysis. It is also possible that we have not applied isotopic fractionation properly in the model. Although the fractionation factor used to simulate photosynthetic uptake of $CO_2$ on a global scale cannot be in serious error because it is consistent with the seasonal oscillation in $^{13}\delta$ for Mauna Loa Observatory as seen in Figure 23, and similar data for all other stations, perhaps it should not be used directly to compute the biospheric flux, $F_b$. Conceivably, some areas where plants tend only weakly to fractionate carbon are stimulated by greater rainfall at the same time that drought affects plants having normal fractionation, thus producing a large isotopic signal relative to the signal in concentration. Finally, the

only other published isotopic record of high precision, for Cape Grim, Tasmania, shows no oscillatory behavior from 1982 to 1986 [Goodman and Francey, 1988]. Thus we are hesitant to state definite conclusions until longer isotopic records are obtained, and until we are sure that isotopic fractionation has been properly simulated in the model. Nevertheless, the isotopic data strongly suggest that El Niño events to some degree perturb the carbon cycle on land as well as in the oceans.

### 6.5 *Patterns of Biospheric $CO_2$ Exchange over the Industrial Era*

Returning to a discussion of the causes of long-term anomalies in atmospheric $CO_2$, we first note that the deconvolutions described in subsections 6.3 and 6.4, above, predict a difference of about $0.3 \times 10^{12}$ kgC yr$^{-1}$ in the net air-sea flux of $CO_2$ since 1978, depending on whether constant or variable temperature is assumed in surface ocean water. Either prediction gives near agreement with the observed $^{13}\delta$ of atmospheric $CO_2$, as seen in Figure 54 and either prediction, as seen in Figures 48 and 51, produces a decadal trend in the biospheric flux, $F_b$, approximately the same as that of the composite residual flux, $F_{rem}$. The best agreement of model simulated and observed $^{13}\delta$ would appear to result from assuming a somewhat lesser rate of warming of ocean water since 1978 than given by the calculations assuming variable temperature, but the presence of short-term interannual oscillations in the $^{13}\delta$ record evidently limits our establishing the oceanic flux to better than about $0.2 \times 10^{12}$ kgC yr$^{-1}$, so that we cannot decide precisely the influence of warming. However, within the range of error just stated the computed residual flux, $F_{rem}$, appears to reflect biospheric processes, and therefore to be approximately equal to $F_b$.

We now discuss some consequences of assuming this to be the case, not only during the recent period, interpretable using direct isotopic data, but also over the entire preceding industrial era. We are encouraged to do so because of some supporting evidence from isotopic ice core data and because of the relatively good agreement of the predictions of the box diffusion model calibrated by radiocarbon with a prediction by a three-dimensional oceanic tracer transport model (see Appendix D, especially Figures D.1 and D.2). Since it appears physically reasonable to do so, we will here assume variable ocean surface temperature, and for convenience we will continue to use the record of Figure 50 to specify this variation. We employ the version of the box diffusion model calibrated by bomb radiocarbon. We suppose that the biospheric flux, $F_b$, which we now set equal to $F_{rem}$, is the sum of terms representing destruction by human activities, $F_{DES}$, and $CO_2$ fertilization, $F_{FER}$, resulting from plant growth stimulated by higher ambient $CO_2$ levels, in accordance with equation (5.5). Afterwards, in the next subsection, we consider the possibility that $F_b$ is also influenced by climatic factors.

Short-term variations in $F_b$ such as those related to El Niño, represented in our previous discussion by the function $\Delta F_b$, probably occurred throughout the industrial era together with short-term variations in the oceanic flux $\Delta F_{oc}$. Whether or not either of these types of variations occurred, they cannot be seen in the ice core record, because, as noted earlier, air mixes as it is trapped in the ice over the span of decades. Therefore to simplify the discussion, we will now regard $F_b$ as synonymous with its long-term component $<F_b>$.

As we noted in section 5, our hypothesis that the terrestrial biosphere has sequestered carbon by $CO_2$ fertilization is at odds with the opinion of Woodwell et al. [1983] who estimated that the global release of $CO_2$ by the biosphere in 1980 was between 1.8 and $4.7 \times 10^{12}$ kgC without a compensating flux produced by stimulation of plant growth. As a consequence they could not balance the recent carbon cycle without postulating a larger uptake of $CO_2$ by the oceans than appears reasonable from an oceanographic perspective. Because no other sinks of atmospheric $CO_2$ have been positively identified that explain how so much carbon could be released by the biosphere and not show up in the atmosphere or be explained as normal oceanic uptake, there has been a reluctance by most investigators to accept the high estimates of biospheric destruction of Woodwell and his coworkers. More recent estimates of biospheric destruction have all been lower, that of Detwiler and Hall [1988], for example, being only $0.5 \times 10^{12}$ kgC yr$^{-1}$. Low estimates, such as this one, imply patterns for biospheric destruction that are essentially the same as the plot of $F_{rem}$, shown in Figure 52 and now equated with the biospheric flux, $F_b$. Yet this pattern is implausible when viewed over the entire industrial era, because it calls for biospheric destruction to decrease during most of this century, contrary to estimates of almost all investigators.

If, alternatively, we accept the hypothesis that the biospheric flux, $F_b$, reflects a combination of destruction, $F_{DES}$, and fertilization, $F_{FER}$, it becomes possible to predict a long-term pattern for destruction that resembles our expectations from direct evidence of deforestation and other land use changes. For example, as shown by the middle curve in Figure 60, the model by deconvolution of $CO_2$ concentration predicts that destruction remains roughly constant from 1920 to 1975 provided that we adopt a biospheric

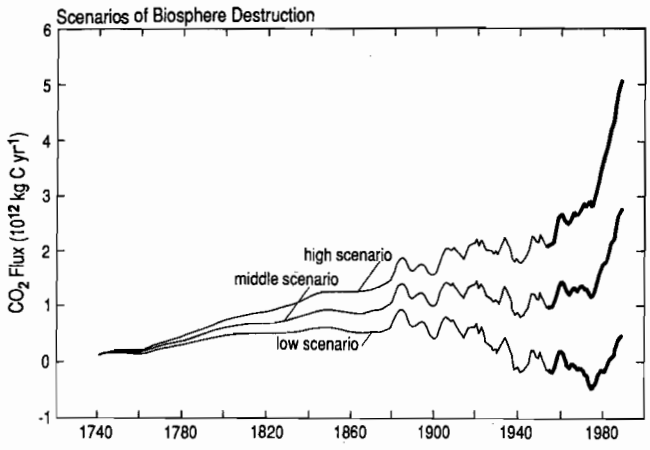


Fig. 60. Three alternative scenarios of the time trend of biospheric destruction (the estimated release of $CO_2$ from the biosphere by deforestation and changing land use by man) in units of $10^{12}$ kgC yr$^{-1}$. The lowest curve (low scenario) is the same as the curve in Figure 45 and assumes no counteracting sequestering of plant carbon caused by $CO_2$ fertilization of plant growth. The intermediate curve (middle scenario) assumes sequestering with a growth factor, $\beta_a$, of 0.37, the top curve (high scenario) a growth factor of 0.74. All three curves are based on computations of the box diffusion model assuming, as in Figure 52, a vertical diffusion coefficient of 7685 m$^2$ yr$^{-1}$ and variable sea surface temperature.

growth factor, $\beta_\alpha$, of about 0.4 to define the intensity of fertilization. A factor of this magnitude was shown in section 5 to result in a balanced carbon cycle with a $CO_2$ release by destruction of 1.791 $\times 10^{12}$ kgC in 1980. (With the data set extended by supplementary data through 1988 the equivalent factor, employed in preparing Figure 60, is 0.37 instead of 0.41).

Even this non-decreasing destructive flux would seem to be unrealistically low, however. To produce a significantly rising trend between 1920 and 1975, consistent with steadily increasing biospheric destruction, the growth factor in the model must be approximately doubled. In this "high scenario", shown in the top curve of Figure 60, the trend in destruction has a pattern that resembles that deduced by Woodwell et al. [1983] from tropical forest data of Norman Myers [loc. cit. Figure 4], although the rapid, recent rise is somewhat delayed in our scenario, as seen in Figure 61. Furthermore, the surge after 1974 is no longer so abrupt when attributed to an increase in destruction that was already increasing before the surge begins.

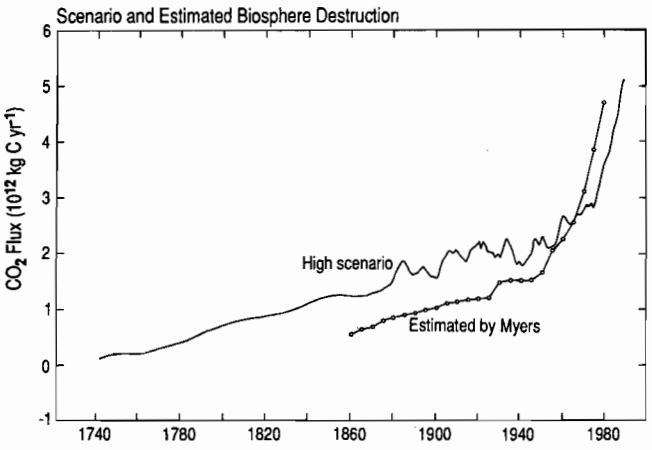


Fig. 61. High scenario of biospheric destruction from Figure 60 (solid curve), compared to an estimate of destruction by Woodwell et al. [1983] (connected open circles) based largely on observations of Myers for tropical moist forests.

To better understand this high scenario we have prepared Table 14, which summarizes the essential factors that contribute to the atmospheric $CO_2$ budget. The increase in atmospheric $CO_2$ for selected years near the beginning, middle, and end of the period of direct measurements are listed on the first line of the table. El Niño events are reflected in these rates, as seen in Figure 22. Alternatively, on the third line are listed atmospheric $CO_2$ increases with El Niño events effectively removed by smoothing in the manner discussed in the previous subsection. The removal of the effect of El Niño events is important because their impact, seen in the differences listed on the second line, is significant with respect to the inferred net biospheric releases, listed on the seventh line. The industrial $CO_2$ releases, listed on the sixth line, are known only to within about 10 percent [Marland and Rotty, 1984], but year to year differences should be known considerably more precisely. Thus changes in net biospheric release, obtained by comparing entries on the seventh line for different years, is probably nearly correct unless the estimated oceanic uptake rates are in error. However, given the constraints on modeling the oceanic uptake, as discussed above, such errors being of the order of $0.2 \times 10^{12}$ kgC yr$^{-1}$, are too small to produce a large relative error in the difference in net biospheric release from 1975 to 1988 ($0.92 \times 10^{12}$ kgC yr$^{-1}$). Thus a surge in biospheric $CO_2$ on the order of $10^{12}$ kgC yr$^{-1}$ since 1974 appears to be well determined.

TABLE 14. Atmospheric $CO_2$ Budget--High Scenario
[Atmospheric Increase and Fluxes in $10^{12}$ kgC yr$^{-1}$]

| $CO_2$ Flux | 1959 | 1975 | 1988 | Difference 1975–1988 |
|---|---|---|---|---|
| Atmospheric $CO_2$ increase[a] | 1.89 | 2.46 | 4.15 | 1.69 |
| El Niño release | 0.32 | 0.04 | 0.44 | 0.40 |
| Net atmospheric $CO_2$ increase[b] | 1.57 | 2.42 | 3.71 | 1.29 |
| Oceanic $CO_2$ uptake[c] | 1.09 | 1.74 | 2.69 | 0.95 |
| Total atmospheric loading[d] | 2.66 | 4.16 | 6.40 | 2.24 |
| Industrial $CO_2$ release[e] | 2.47 | 4.63 | 5.95 | 1.32 |
| Net biospheric release[f] | 0.19 | −0.47 | 0.45 | 0.92 |
| Biospheric fertilization[g] | −2.43 | −3.34 | −4.59 | −1.25 |
| Biospheric destruction[h] | 2.62 | 2.87 | 5.04 | 2.17 |

[a] Based on the spline fit of Figure 22.

[b] Consistent with the smoothed net flux $F_{rem}$ shown in Figure 52.

[c] Computed by the box diffusion model with a vertical diffusion coefficient of 7685 m$^2$ yr$^{-1}$ and assuming variable ocean surface temperature.

[d] Inferred as the sum of net atmospheric $CO_2$ increase and oceanic $CO_2$ uptake.

[e] From statistically data.

[f] Total atmospheric loading less industrial $CO_2$ release.

[g] Computed by equation (5.4).

[h] Inferred as the net biospheric release less the biospheric fertilization flux.

The causes of this surge are far less well established. The high scenario implies that biospheric destruction increased by about $2.2 \times 10^{12}$ kgC yr$^{-1}$ between 1975 and 1988, offset by an increase of $1.2 \times 10^{12}$ kgC yr$^{-1}$ in carbon sequestered by fertilization. The reader may replace this high scenario with any other by changing fertilization by a constant factor and then adjusting destruction each year to preserve the same net biospheric release. In all such scenarios fertilization grows at a nearly constant rate; by 37 percent from 1959 to 1975, and again by this factor from 1975 to 1988. In contrast destruction in our high scenario increased by only 9 percent during the first interval, but by 76 percent in the second. To produce more equal rates of destruction in the two intervals, even higher rates of fertilization in the model are required.

The predicted rate of destruction in 1980, according to our high scenario, is $3.7 \times 10^{12}$ kgC yr$^{-1}$, an estimate approaching the value computed by Woodwell et al. [loc.cit] from Myers' data, and well above all more recent estimates. By 1988, in this scenario, destruction had increased to $5.0 \times 10^{12}$ kgC yr$^{-1}$, a flux rate that has not been detected, to our knowledge, according to any reported studies of deforestation or land use changes. Nevertheless, in our

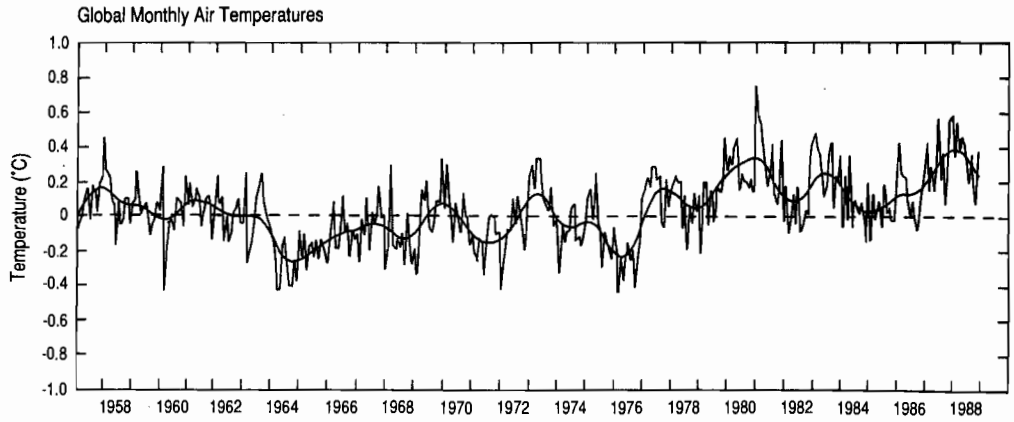


Fig. 62. Time trend of the global surface air temperature shown as departures in °C from the mean for 1951-1970. Monthly means are connected by straight line segments to show their trend. A smooth curve, generated by a spline function fit to the monthly data with a standard error, $\sigma$, of 0.125°C, is also plotted to show the interannual variability. The data, as in Figure 50, are from Hansen and Lebedeff [1988], updated by private communication through 1988.

analysis of the atmospheric $CO_2$ budget and our appraisal of biological data, we find no compelling reasons to rule out the possibility that this high scenario may be nearly correct. We conclude that the present rates of fertilization and destruction may each be of the order of $5 \times 10^{12}$ kgC $yr^{-1}$.

This deduction is reached, however, by assuming that the trend in $F_b$ does not reflect any processes other than fertilization and destruction. Perhaps the recent surge in biological $CO_2$ release, which we sense has occurred, was in part induced by global warming or other climatic changes without a compensating increase in net primary productivity. If so, we should amend equation (5.5) to read

$$F_b = F_{DES} + F_{FER} + F_{cli} \tag{6.8}$$

where $F_{cli}$ denotes biospheric releases related to changing "climatic" conditions. Our investigation of El Niño events already suggests a measurable impact of changing climatic factors on the biospheric $CO_2$ exchange on short time scales. In the next section we address the possibility of climatic impacts on the scale of decades and longer.

### 6.6 *Association of Atmospheric $CO_2$ Variations with Temperature and Their Causes*

There can be little doubt that variations in temperature to some extent influence the carbon budget. To assess this influence we now consider the correlation of atmospheric $CO_2$ concentration with global air temperature and inferences that may be drawn from this correlation with respect to both the oceans and the terrestrial biosphere.

The global mean temperature of the air near the ground, as shown in Figure 62, decreased from 1958 until the mid–1960's, remained relatively constant until the mid–1970's, and since has

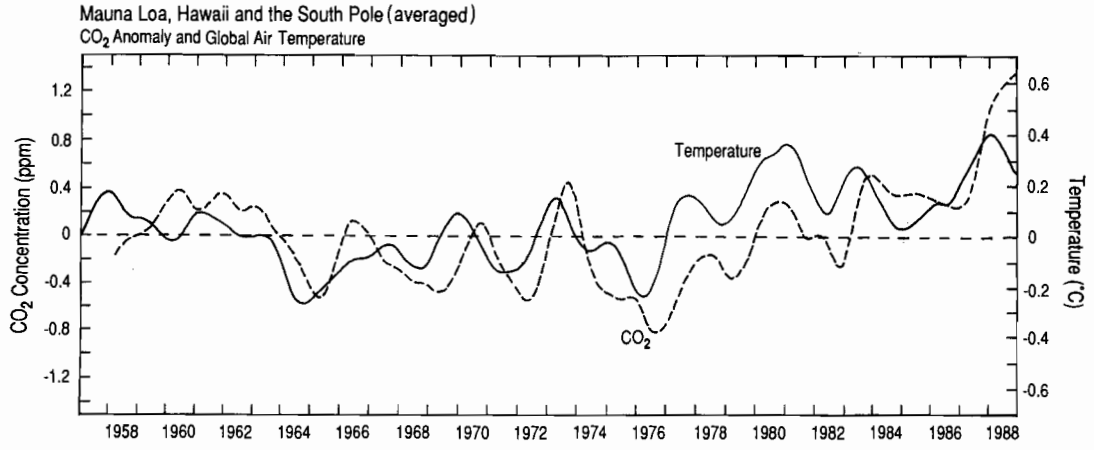


Fig. 63. Comparison of interannual variability in anomalies of surface air temperature (solid line) and atmospheric $CO_2$ (dashed line). The $CO_2$ curve is the same as that shown by a solid line in Figure 22. The temperature curve is the same as the smooth solid line in Figure 62.

risen by about 0.3°C. [Jones et al., 1986a; Jones et al. 1988; Hansen and Lebedeff, 1988]. In Figure 63 the $CO_2$ concentration anomaly of Figure 22 is superimposed on this temperature record, after smoothing the latter with a spline function. The two records show a striking correlation on the time scale of El Niño events, with the $CO_2$ anomaly lagging by about 6 to 12 months. On a decadal time scale, too, the temperature anomaly correlates with $CO_2$. Both anomalies have a bowed shape since the early 1960's. The pervasive influence of the El Niño phenomenon makes it difficult to be sure of the causal relationship of air temperature and $CO_2$ on short-term scales. The connection appears to be indirect (see subsection 6.4), arising through mutual correlations between temperature, equatorial oceanic upwelling, tropical rainfall, and the Southern Oscillation. On a decadal time scale, however, the causal relationship may be less complex. We will in any case focus our further analysis on possible direct relationships of $CO_2$ exchange with temperature.

To begin this analysis we note three points. Firstly, even if the relationships between the carbon cycle and temperature vary locally or regionally, their impact on atmospheric $CO_2$ will be global, because of the long time scales relative to the time of atmospheric mixing. Secondly, we need not distinguish between trends in air temperature over land or over the oceans, because global marine temperature anomalies closely follow global surface air temperature anomalies [Jones et al., 1986a,b]. Thirdly, as discussed in subsection 6.3, our isotopic records support an hypothesis that the temperature dependence of oceanic $CO_2$ exchange to a first approximation is adequately formulated by the box diffusion model.

To define broadly the spectral character of the trend in $CO_2$ anomaly for time scales longer than El Niño events, monthly data were fit by two additional spline functions, the first being the looser spline, yet still almost free of oscillations at the frequency of El Niño events, the second being stiffer so that only the longer term bowed shape is represented. These two splines are plotted together in Figure 64 with the previous still looser spline of Figure 22 which oscillates in association with El Niño events. The spline of intermediate stiffness (solid line) shows regular oscillations suggesting a repeat period of approximately 11 years. In Figure 65 are shown similar splines fit to the monthly air temperature anomaly. Again the spline of intermediate stiffness shows approximately 11 year oscillations. As shown in Figure 66, these oscillations appear to be correlated with each other and even possibly with the solar sunspot numbers, at least for the two most recent cycles.

We have not attempted to seek out a more precise filter to detect these oscillations, since loss of information at ends of the filtered record becomes an important factor with only 3 cycles represented. By comparing the spline for the truncated record of temperature, shown in Figure 66, with that for the longer temperature record, shown in Figure 50, it is seen that the peak near 1960 is advanced by about two years in the truncated record relative to that of the longer record. The latter shows a better correlation with the sunspot peak in 1958 than the shorter record. It is possible that the $CO_2$ record, had it begun earlier, might also have correlated better with this peak.

The almost direct correlation with temperature of the $CO_2$ concentration rather than of its time derivative suggests that the cause is oceanic rather than biospheric. A change in temperature of surface ocean water produces a transient response which dies out relatively quickly because of the low storage capacity of the surface ocean layer for $CO_2$ [Siegenthaler, 1983], whereas the terrestrial biosphere should respond to elevated or depressed temperatures for several years or more [Esser, 1987]. Consequently, the $CO_2$ response of the oceans to temperature should be nearly in phase, whereas the $CO_2$ response of the biosphere to temperature should lag by about $\pi/2$ radians, i.e., about 2.8 years, because the time derivative of the response should be proportional to temperature, whether the response is direct or inverse.

The ratio of amplitudes of the $CO_2$ and temperature oscillations is approximately 2.0 ppm per °C. (judged from the third oscillation, which shows in Figure 66 the best correlation of $CO_2$ and temperature). The phase lag of $CO_2$ with respect to temperature is about 1 year (again with respect to the third oscillation). We have computed the expected amplitude ratio and phase lag using the box diffusion model, solved analytically in the manner of Bacastow [1979, see equation A.12]. With the same parameters and abun-

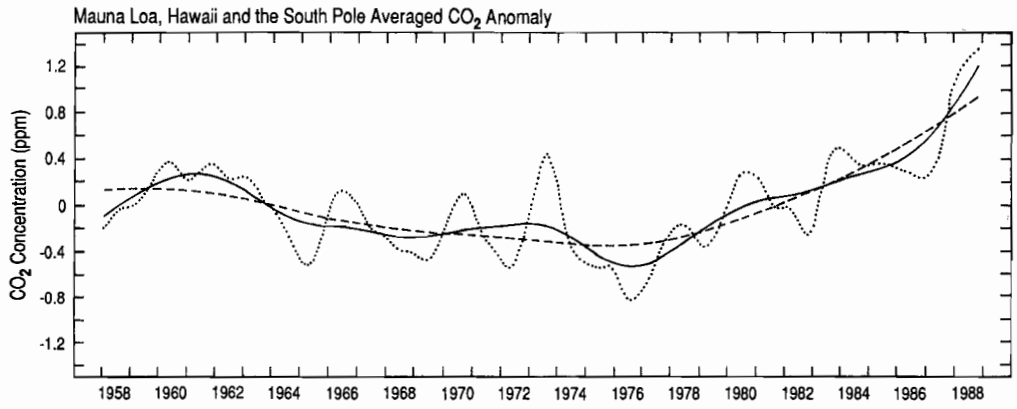


Fig. 64. Interannual variability of atmospheric $CO_2$ concentration, in ppm, smoothed to varying extents. The solid line is a spline fit to monthly data shown in Figure 22 with a standard error, $\sigma$, of 0.190 ppm. The dashed curve is a stiffer spline with $\sigma$ equal to 0.240 ppm. The dotted curve is the same as shown by a solid line in Figure 22 and is based on the average of splines for the Mauna Loa Observatory and the South Pole data.

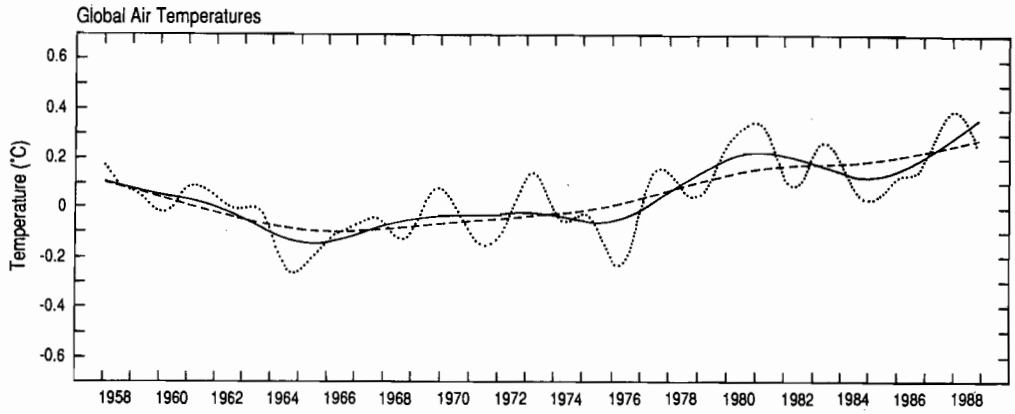


Fig. 65. Interannual variability in the global air temperature in °C. The solid line is a spline fit to monthly data (shown in Figure 62) with a standard error, $\sigma$, of 0.75°C. The dashed curve is a stiffer spline with $\sigma$ equal to 0.95°C. The dotted curve is the same as shown as a solid line in Figure 62.

dances as in the deconvolutions described above, the model predicts a ratio of 1.5 ppm per °C. and a phase lag of 1.5 years. A higher vertical diffusion coefficient or the greater mixed layer depth would produce a better agreement with the spline curves. Since the predicted phase lag is slightly greater than observed, the addition of a biospheric component, directly correlated with temperature and lagged by 2.8 years, would increase the lag and result in a poorer prediction. An inverse correlation would shorten the predicted lag but require a larger oceanic response, and thus also result in a poorer prediction. Therefore we conclude that warming and cooling of ocean water is probably mainly responsible for the correlation.

A correlation with sunspot numbers of the time derivative of the first 16 years of the $CO_2$ record at Mauna Loa Observatory was found by Rust et al. [1979]. This result is not confirmed by the more recent data, although it can be seen in Figure 66 by the greater lag in the first cycle with respect to sunspots. The validity of the 11 year oscillation in $CO_2$ is critically dependent on the

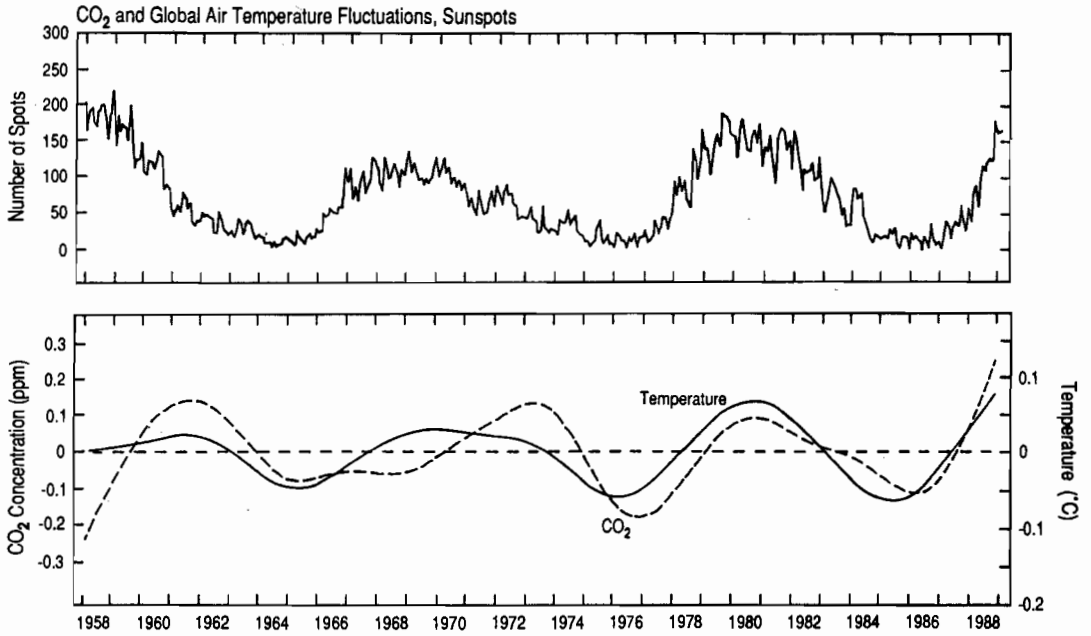


Fig. 66. Lower Panel: Comparison of an approximately 11 year oscillation of atmospheric $CO_2$ concentration and global air temperature. The solid line denotes the temperature oscillation, in °C; the dashed line the $CO_2$ oscillation, in ppm. Both oscillating curves are calculated as the differences between the intermediate and stiff splines of Figures 64 and 65, respectively. Also shown, in the upper panel, is a plot of monthly averaged sunspot numbers [U.S. Department of Commerce, 1987].

long-term calibration of the data, because the peak to peak amplitude of the oscillation is only about 0.25 ppm. The early data are the least well calibrated. Furthermore, in 1968 and 1969 errors in the calibration of the $CO_2$ data, as noted in Appendix A and by Keeling et al. [1982, p. 383], may have contributed to depressing the concentration in 1968 and raising it in 1969, such that the first derivative agrees better than it should with sunspot numbers. The long-term calibration of the $CO_2$ data improved after the creation of semi-permanent primary standards in 1970 [Keeling et al. 1986]. The data after 1970 agree more closely than earlier data with the temperature anomaly and with sunspot numbers. Therefore the agreement found by Rust et al. [1979] seems to be fortuitous.

A correlation of temperature with sunspots has been repeatedly suggested but never conclusively established. Reid [1987] found a fair correspondence of 11 year means of sunspot number with global sea surface temperature, while Newell et al. [1989] found evidence of a correlation of the 22-year oscillation. According to Newell et al. [loc. cit.] every second interval of high sunspot numbers correlates with high temperature, including the sunspot peaks near 1958 close to the beginning of the $CO_2$ record and near 1980. Thus their study suggests that the bow shaped temperature anomaly after 1957 may partially reflect the 22-year cycle. Oceanic $CO_2$ exchange should respond directly to temperature on all time scales longer than decadal, so that the bowed shape of the $CO_2$ record may also reflect temperature changes correlated with solar irradiance. On the other hand, their study does not support our finding of an 11-year oscillation.

Most evidence of solar influence on global temperature has been based on statistical correlations typified by the studies of Schönwiese [1984] and Schönwiese and Malcher [1987]. Recently, however, direct measurements of solar irradiance have been obtained from the Nimbus 7 satellite. These data suggest that the solar cycle since 1978 has been accompanied by a variation of about 0.12 percent in the irradiance reaching the upper atmosphere of the earth [Seitz et al. 1989], thus about 0.29 watts $m^{-2}$ at the earth's surface (assuming an albedo of 0.7 [Mitchell, 1989] and the same fractional change at the earth's surface). In comparison, the global temperature variation associated with the same solar cycle was 0.13°C., according to our analysis.

A change of 0.13 °C. for a change of 0.29 watts $m^{-2}$ is comparable to, albeit somewhat larger than, the rate of change predicted by the models of the warming of the atmosphere by greenhouse gases [Mitchell, 1989]. Therefore hypothesizing that variations in the energy reaching the earth from the sun cause the observed, approximately 11 year oscillations in temperature, which in turn modulate air-sea exchange of $CO_2$, may be explainable from the point of view of physical principles.

Without reaching any clear conclusions regarding a response of the carbon cycle to the solar cycle, we now turn to a discussion of biospheric fluxes. We argued in subsection 6.5 that $F_{rem}$ is probably mainly biospheric. If this hypothesis is accepted, the question arises as to whether this flux results mainly from deforestation and other human activities, or also reflects biospheric responses to changing climatic factors. We now briefly consider the latter possibility with respect to temperature as a climatic factor. Rainfall variations may also be important to the biospheric carbon budget, but the pronounced regional variability in rainfall, seen for example in the time series of Bradley et al. [1987] suggests the need for a comprehensive investigation which is beyond the scope of this article.

The respiration of plants rises with increasing temperature. For a rise of 10°C. the rate under controlled laboratory conditions typically increases by a factor, "$Q_{10}$", of 2 or 3 [Woodwell, 1984, p. 6]. A recent detailed review of the subject by Prentice [1986], summarized by Fung et al. [1987] suggests somewhat lower $Q_{10}$ values than Woodwell, in the range 1.4 to 2.6 [loc. cit.]. Heimann and Keeling [this volume] estimate a still lower global average $Q_{10}$ of 1.3, by means of a biospheric model that predicts optimally the seasonal oscillation of atmospheric $CO_2$, if 69 percent of seasonal respiration has a $Q_{10}$ of 1.5 while the remaining respiration is constant.

For a small increase in temperature, $\Delta T$, in the temperature range, $T$, of growing plants, the exponential response implied by a constant value for $Q_{10}$ can be approximated by the expression

$$\frac{F_{RES}(T+\Delta T)}{F_{RES}(T)} = (Q_{10})^{\Delta T/10} \qquad (6.9)$$

where $F_{RES}$ denotes the rate of release of $CO_2$ by plant respiration per unit area. Thus, for the global average increase in air temperature of 0.3°C. observed since the mid–1970's, the annual average of respiration is predicted to increase by approximately 1 to 3 percent. Because the global integral of the annual net primary productivity of plants, and hence of respiration, is the order of 50 to $60 \times 10^{12}$ kgC [Fung et al., 1983; Heimann and Keeling, this volume] we anticipate an increase in respiration in the range 0.5 to $1.8 \times 10^{12}$ kgC $yr^{-1}$. Unlike surface ocean water which responds to incremental warming with a short-lived release of $CO_2$, the corresponding biospheric release of $CO_2$ may continue undiminished for several years, perhaps even longer. If we assume an undiminishing release of $CO_2$ based on equation (6.9), a linear rate of rise in temperature, amounting to 0.3°C. in the 14 years since 1975, would produce a cumulative release between 3.5 and $13 \times 10^{12}$ kgC. The higher value considerably exceeds the increase of $3.3 \times 10^{12}$ kgC predicted by the box diffusion model for warming of surface sea water during the same period (compared to $2.9 \times 10^{12}$ kgC predicted for the 11-year interval of the isotopic data, as noted above in subsection 6.4). Cooling might produce similar reductions in respiration.

Temperature, in general, does not seem to be a major factor controlling net primary productivity, although some positive response to temperature is to be expected [Goudriaan and Ajtay, 1979, p. 243]. An estimate of a $CO_2$ rise based solely on a temperature response of respiration on a decadal time scale is therefore likely to be too high, but probably by only a small factor.

Over decades, or longer time periods, various biospheric factors might contribute to a reduced response to prolonged changes in temperature. For example, the exhaustion of plant detritus sensitive to oxidation during prolonged warming perhaps could slow down the excess release of $CO_2$ or even bring it to a halt. Similarly, a diminution of nutrients might slow down an increase in NPP. With respect to changes over a century, Esser [1987] estimated, by means of a detailed regional biospheric model which included impacts from human activities as well as climatic changes, that NPP would increase more than respiration, but the amount of carbon transferred to the biosphere as a consequence of a large, hypothetical 2°C. rise in temperature globally since 1860 would be a relatively insignificant $11 \times 10^{12}$ kgC.

The increase in amplitude of the seasonal cycle of atmospheric $CO_2$ observed at Mauna Loa Observatory may be largely in response to a stimulation of photosynthesis brought about by

increasing atmospheric $CO_2$, but the accelerated increase since the mid-1970's (see Figure 13) cannot be explained in this way; it may be a result of an enhanced response of the biosphere to rising air temperature, as noted by Kohlmaier et al. [1989]. An increase in NPP associated with warming, is likely to be the cause, although respiration from warming may also have contributed, if the enhancement occurred mainly during the winter or early spring seasons so as to produce an increase in amplitude of the associated seasonal cycle. Thus, from diverse observations and model results, we find evidence that global warming or cooling affects the carbon balance of the terrestrial biosphere, but good quantitative measures of the extent of these temperature effects are lacking.

As a final look at the possible sensitivity of biospheric fluxes to the impact of global temperature change, we now compare the patterns of temperature and inferred biospheric flux, $F_b$, by the technique of multiple regression analysis, similar to the study of Schönwiese and Malcher [1987], applied, however, to $CO_2$ rather than temperature.

The correlation of global temperature and atmospheric $CO_2$ is negligible when based on monthly or yearly averaged data, because of uncorrelated, short-term variations in both properties, but if the data are smoothed, for example by a running mean over several years, a greater degree of correlation results, part of which may be significant in spite of the tendency to produce autocorrelation. To establish a correlation coefficient, $a_{\Delta T}$, of the $CO_2$ flux, $F_{cli}$, with the temperature anomaly, $\Delta T$, we carried out a multiple regression analysis in which we assumed that

$$F_{cli} = a_{\Delta T}\Delta T \tag{6.10}$$

while the flux $F_{FER}$ arising from fertilization was assumed to be proportional to the increase in $CO_2$ concentration since preindustrial times according to equation (5.4) with the proportionality expressed by the growth factor, $\beta_a$. In the regression only the minimum fertilization required to predict the function $F_b$ is computed. Biospheric destruction, $F_{DES}$ is assumed to be uncorrelated with either $CO_2$ or temperature, and is therefore predicted as a residual not accounted for by the regression. Any additional destruction which might actually be taking place is assumed to be offset by additional fertilization, as in the calculations leading to the three curves in Figure 60. We assumed that $F_b$ is represented by the flux $F_{rem}$ computed by deconvolution as in Figure 52, where the influence of temperature variations on the oceanic $CO_2$ exchange has been already accounted for. We implemented the regression analysis, as described by Draper and Smith [1981, p. 193 ff.], using the subroutine RLMUL (in [IMSL, 1985]).

With all three variables prescribed by spline curves: $\Delta T$ as in Figure 50, the $CO_2$ concentration as in Figure 22, $F_b$ as in Figure 52, a multiple regression with annual values of the variables yields $a_{\Delta T}$ equal to $2.54 \times 10^{12}$ kgC per °C., and $\beta_a$ equal to 0.21. The result is not unique; using smoother representations of the variables, we found a greater correlation. The value of $a_{\Delta T}$ that we computed is equivalent to a $Q_{10}$ of 1.6, assuming temperature variations of the order of one degree and a global respiration rate of $56 \times 10^{12}$ kgC $yr^{-1}$, as adopted by Heimann and Keeling [this volume]. This value already substantially exceeds the $Q_{10}$ of about 1.3 for seasonal respiration found by Heimann and Keeling [loc. cit.], suggesting a relatively strong impact of temperature on the biospheric flux.

In Figure 67 the prediction of the biospheric flux, $F_b$, given by the above described regression analysis, is compared with the residual flux, $F_{rem}$, assumed equal to $F_b$ and shown previously in Figure 52. The prediction of $F_b$ by regression shows a bowed shape roughly similar to that of the residual flux $F_{rem}$, but only about half of the surge in $F_{rem}$ after 1975 is accounted for. This result could be anticipated, because the timing of the surge is only approximately synchronous with the temperature increase. We conclude that part of the surge could be a result of global warming, but that biospheric destruction by human activities, or a response to regional climatic change not well represented by global temperature, probably contribute as well. Given the uncertainty of any conclusions based mainly on regression analysis, biospheric destruction may be the principal cause.

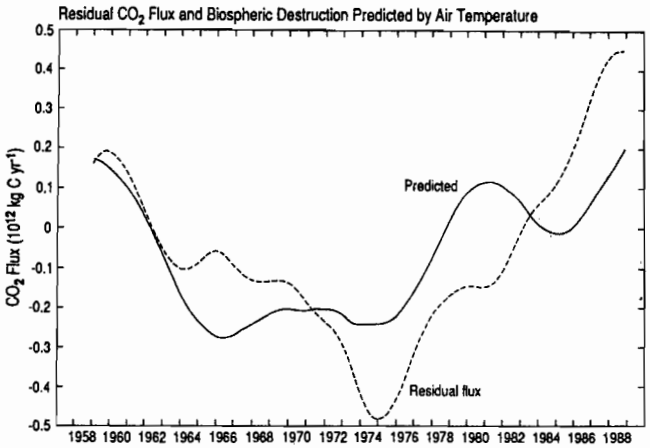


Fig. 67. Comparison of the residual flux, $F_{rem}$, (dashed curve) in units of $10^{12}$ kgC $yr^{-1}$ with a prediction of the biospheric flux, $F_b$, (solid curve) from variations in air temperature assuming a $Q_{10}$ of 1.6 for biospheric release of $CO_2$ and a growth factor, $\beta_a$, of 0.21 for fertilization.

In summary, a comparison of anomalies of atmospheric $CO_2$ concentration with global air temperature suggest that the oceans may respond to small variations in temperature on the time scale of decades approximately in phase with the sunspot cycle. Although the variations are small, they are approximately as expected from changes in solar irradiance measured from the Nimbus 7 satellite since 1978 and with the expected thermodynamic response of surface ocean water to warming and cooling according to the box diffusion model.

On the basis of general knowledge of how plants grow and decay, one expects a response of land vegetation to temperature as well, but this response is difficult to establish. Most likely, biospheric destruction, fertilization, and climatic change have all contributed to perturbing the terrestrial biosphere. Specific factors include inadvertent releases resulting from global warming, especially since the mid–1970's; a decrease in the effective global growth factor of plants because of limitations in nutrients or stimulation of organisms consuming newly sequestered carbon; and, as is widely suspected for tropical rain forests in South America and elsewhere, a substantial increase in biospheric destruction. Finally, it is likely that, regardless of which process is most important at present, all will contribute in the future, because $CO_2$ concentrations will continue to rise, deforestation will continue as long as old growth forests are available for exploitation, and some degree of global warming will continue as a result of industrial gas emissions.

*6.7 Comparison of the Box Diffusion Model Predictions by Deconvolution and by Direct Computation*

In the following three articles the distribution of $CO_2$ in the atmosphere is simulated by a three-dimensional tracer transport model in which the carbon cycle is assumed to be in a quasi-steady state. Slow global imbalances are represented by 2-year averages of the carbon fluxes predicted by direct use of the box diffusion model, assuming that the terrestrial biosphere releases $CO_2$ according to a Gaussian function and absorbs $CO_2$ by stimulated growth of plants in proportion to the rise in atmospheric $CO_2$. Both fluxes are therefore without short-term variations. Also, the flux of industrial $CO_2$ and the response of the oceans to rising $CO_2$ are nearly free of short-term variations. Thus the approximation that all of these fluxes are constants does not seriously violate the assumption of a quasi-steady state.

These predictions, based on the direct use of the box diffusion model with a Gaussian function, are not likely to be as realistic, however, as those produced by deconvolution of $CO_2$ concentration (single deconvolution) or both the $CO_2$ concentration and its $^{13}C/^{12}C$ isotopic ratio (double deconvolution), neither of which require *a priori* a specification of biospheric $CO_2$ releases. We now compare the three sets of predictions.

In Table 15 we list these for January 1, 1980, the central date of the principal model simulations discussed by Heimann et al. and Keeling et al. [this volume]. Fluxes represent averages from January 1, 1979 to January 1, 1981. For comparison, some quantities are also listed for 1740, the starting date for the deconvolution computations. Because only the net $CO_2$ exchange of the biosphere is determined by deconvolution, the factor $\beta_a$ is a free parameter in these computations. For purposes of preparing Table 15, $\beta_a$ in the deconvolutions was set to predict exactly the uptake of $CO_2$ predicted by the direct model for 1980. Thus in the table, the $CO_2$ release by destruction is the only biospheric flux which varies for the different models.

In comparing the results by deconvolution with those using the direct model, we find only small differences in accumulated uptakes and releases up to the year 1980. The Gaussian function in the direct model prescribes almost the same total release of $CO_2$ as that demanded by deconvolution of the ice core and direct atmospheric $CO_2$ data.

TABLE 15. Comparison of Box Diffusion Carbon Cycle Model Predictions on January 1, 1740 and 1980 by Direct Computation and by Deconvolutions of the Observed Atmospheric $CO_2$ Concentration and $^{13}C/^{12}C$ ratio

| | Year | Direct Model[a] | Deconvolutions[b] Single | Deconvolutions[b] Double |
|---|---|---|---|---|
| Atmospheric $CO_2$ concentration (ppm) | 1740 | 278.1 | 276.9 | unch. |
| Atmospheric $CO_2$ concentration (ppm) | 1980 | 336.9 | 336.7 | unch. |
| Accumulated Atmospheric $CO_2$ uptake ($10^{12}$ kgC) | 1980 | 127.6 | 127.0 | unch. |
| Accumulated terrestrial biospheric $CO_2$ release ($10^{12}$ kgC) | 1980 | 222.9 | 212.2 | 211.6 |
| Accumulated terrestrial biospheric $CO_2$ uptake ($10^{12}$ kgC) | 1980 | 126.9 | 119.0 | unch. |
| Net terrestrial biospheric $CO_2$ release ($10^{12}$ kgC) | 1980 | 94.0 | 93.2 | 92.6 |
| Accumulated oceanic $CO_2$ uptake ($10^{12}$ kgC) | 1980 | 127.0 | 126.5 | 125.9 |
| Industrial $CO_2$ release rate ($10^{12}$ kgC $yr^{-1}$) | 1980 | 5.300 | 5.292 | unch. |
| Atmospheric $CO_2$ uptake rate ($10^{12}$ kgC $yr^{-1}$) | 1980 | 2.764 | 3.606 | unch. |
| Surface oceanic $CO_2$ uptake rate ($10^{12}$ kgC $yr^{-1}$) | 1980 | 0.249 | 0.284 | 0.368 |
| Deep oceanic $CO_2$ uptake rate ($10^{12}$ kgC $yr^{-1}$) | 1980 | 1.975 | 1.919 | 1.998 |
| Terrestrial biospheric $CO_2$ release rate ($10^{12}$ kgC $yr^{-1}$) | 1980 | 1.791 | 2.621 | 2.784 |
| Terrestrial biospheric $CO_2$ stimulated uptake rate ($10^{12}$ kgC $yr^{-1}$)[c] | 1980 | 2.104 | unch. | unch. |
| $^{13}C/^{12}C$ ratio of atmospheric $CO_2$, $^{13}\delta_a$, (‰) | 1740 | −6.332 | −6.329 | unch. |
| $^{13}C/^{12}C$ ratio of biospheric carbon, $^{13}\delta_b$, (‰) | 1740 | −24.329 | −24.341 | unch. |
| $^{13}C/^{12}C$ ratio of dissolved inorganic carbon at ocean surface, $^{13}\delta_m$, (‰) | 1740 | 2.256 | 2.341 | unch. |
| $^{13}C/^{12}C$ ratio of atmospheric $CO_2$, $^{13}\delta_a$, (‰)[d] | 1980 | −7.538 | −7.556 | −7.542 |
| $^{13}C/^{12}C$ ratio of biospheric carbon, $^{13}\delta_b$, (‰) | 1980 | −24.930 | −24.945 | −24.945 |
| $^{13}C/^{12}C$ ratio of dissolved inorganic carbon at ocean surface, $^{13}\delta_m$, (‰) | 1980 | 1.637 | 1.725 | 1.730 |

[a] Employs a Gaussian function as in Table 12.

[b] Single deconvolution is of atmospheric $CO_2$ concentration; double deconvolution also involves the $^{13}C/^{12}C$ ratio of atmospheric $CO_2$. (unch. = unchanged from single deconvolution). Constant ocean surface temperature is assumed.

[c] Deconvolution values assume the biospheric growth factor, $\beta_a$, to be 0.4149, in order that the flux be the same as for the direct model.

[d] Values for the direct model differ from those for single deconvolution because of different assigned values on prescribed dates as discussed in the text, subsection 6.2.

A more important comparison, however, is of the rates of uptake and release of $CO_2$, because these drive the simulations of the three-dimensional model. Even with a 2-year averaging period for these fluxes, which suppresses short-term interannual variations, there are significant differences between results of the direct model and by deconvolution. By the direct model the atmospheric $CO_2$ increase is predicted to be $2.8 \times 10^{12}$ kgC $yr^{-1}$; the actual increase used in both the single and double deconvolution is $3.6 \times 10^{12}$ kgC $yr^{-1}$. This substantially larger increase reflects the warm event of 1979–1980 which the direct model does not take into account. Also, as a consequence of this event, the terrestrial biosphere by the more realistic double deconvolution releases $2.8 \times 10^{12}$ kgC $yr^{-1}$ instead of $1.8 \times 10^{12}$ kgC $yr^{-1}$, as predicted using the Gaussian function. The oceanic fluxes are larger by double deconvolution, but only by small amounts.

The $^{13}\delta$ of biospheric and oceanic carbon ($^{13}\delta_b$ and $^{13}\delta_m$, respectively) predicted by single and double deconvolution differ only slightly from each other because the computations by double deconvolution begin only 2 years before the date of the comparison, a time too short to bring about significant shifts in isotopic ratio in these reservoirs. The differences in $^{13}\delta$ of atmospheric $CO_2$ ($^{13}\delta_a$) between direct computation and deconvolution are a result of forcing the model with different values on specified dates. Additional differences for the other reservoirs are essentially negligible.

### 6.8 *Summary Remarks on Interannual Variations*

Records of the concentration and reduced isotopic ratio, $^{13}\delta$, of atmospheric $CO_2$ at Mauna Loa Observatory and the South Pole, extended through 1988, have been employed in computations in which the box diffusion model, by double deconvolution, is forced to be consistent with both the concentration and $^{13}\delta$ data. For the period of the isotopic data, 1978–1988, the model computations indicate that the terrestrial biosphere has released up to $5 \times 10^{12}$ kgC during "warm" El Niño events, and has reabsorbed this carbon during subsequent "cold" events. During the same events, only slightly smaller amounts of $CO_2$ are withdrawn by the oceans and then released, so that the sum of the biospheric and oceanic $CO_2$ exchanges, seen in the concentration data, is only about $1 \times 10^{12}$ kgC per event. The close synchroneity of the two exchanges is likely to reflect a common cause: the Southern Oscillation, which effects both variations in rainfall over land and changes in oceanic upwelling.

Given that during these short-term events the exchanges for each reservoir approach the magnitude of the annual fossil fuel $CO_2$ emissions, we are not surprised to find evidence for other, longer-term, anomalous $CO_2$ fluxes that are not directly linked to human activities. The double deconvolution computation suggests that the oceans have released, on net, approximately $3 \times 10^{12}$ kgC since 1978 as a result of an overall increase in surface temperature. Part of the atmospheric $CO_2$ anomaly, an oscillation with a period of about 11 years, may reflect changes in solar irradiance that produce changes in the heating rate at the earth's surface and thereby affect air-sea exchange of $CO_2$.

Biospheric exchange of $CO_2$ with the atmosphere is difficult to characterize because several poorly documented or understood processes contribute. To better understand these processes in the perspective of the entire industrial era, we have included data derived from ice core samples of air dating to 1740 in the deconvolution of $CO_2$ concentration. We argue that the residual flux to the atmosphere not accounted for by industrial $CO_2$ emissions or oceanic $CO_2$ exchange since 1740 is probably due not only to deforestation and land use changes, but also to an uptake of $CO_2$ by the biosphere fertilized by higher $CO_2$ concentrations in the ambient air. As evidence we show that the residual flux diminished after 1920 when biospheric destruction by human activities was almost surely increasing. We postulate that for some time after 1920 the $CO_2$ record reflected a near balance of fertilization and destruction, both of which were increasing at nearly the same rate. Since the mid–1970's , however, destruction appears to have overtaken fertilization and contributed to a surge of $CO_2$ from the biosphere to the air.

This surge may be partly a response to changing climate, but, finding only a modest correlation of $CO_2$ concentration with temperature at the longest time scales of the 30 year record of $CO_2$ concentration, we surmise that global trends in temperature are probably not the main cause for the surge. We cannot decide whether regional variations in climatic factors may have contributed to the surge because our study is limited to global scales.

In the three accompanying articles, it is not possible to address adequately the short-term interannual variations just discussed, because in the formulation of our three-dimensional atmospheric tracer transport model, which lacks realistic sub-models of either the oceans or the terrestrial biosphere, it is assumed that the carbon cycle is in a quasi-steady state. It is some consolation that the fluxes computed by deconvolution and by the direct model are in close enough agreement that no serious errors are introduced into the three-dimensional model by our substituting fluxes from the direct model for more realistic estimates by deconvolution. Nevertheless, we recognize the importance of explaining correctly the impacts on the carbon cycle of climatically important events such as El Niños and recent global warming. The interactions of physical processes with the major biological and chemical cycles of the earth, as seen in atmospheric $CO_2$ data, deserve further, careful attention as the world enters an era of possibly unprecedented alterations in the global environment.

## 7. Concluding Remarks

In this, the first of four articles dealing with the global carbon cycle, our principal objective has been to describe the preparation of data sets of the observed concentration and $^{13}C/^{12}C$ isotopic ratio of atmospheric $CO_2$ to be used in connection with a three-dimensional atmospheric $CO_2$ tracer model described in the accompanying articles. This model characterizes the global carbon cycle in terms of sources and sinks at the earth's surface, adjusted so that the predictions of the model agree closely with atmospheric observations. In order that the observational data for the model be as free as possible from systematic biases arising from differing techniques of sampling and calibration, we have made use principally of the results of a program conducted by the Scripps Institution of Oceanography, in which we have applied internally consistent procedures to edit over thirty years of atmospheric observations for use in modeling.

We have decomposed the data for each location into an harmonic oscillation, having a fundamental period of 1 year, superimposed on a mean concentration representing an average over

approximately 2 years. These data, as processed, thus furnish a view of the carbon cycle as though it were quasi-stationary, so that the three-dimensional model predicts the distribution of atmospheric $CO_2$ without reference to changing capacities of the oceans and terrestrial biosphere to store carbon and to respond to changes in atmospheric $CO_2$.

It is, however, important that a quasi-stationary characterization of the carbon cycle not be seriously in error owing to interannual variability of the carbon cycle. As a second objective we have examined the records of atmospheric $CO_2$ to assess whether interannual variability may interfere with quasi-stationary model predictions.

We have shown that the seasonally adjusted atmospheric $CO_2$ data tend to vary in association with El Niño events recurring approximately every 4 years. The variations are similar from near the North Pole to the South Pole, as though the original disturbances of the $CO_2$ concentration, irrespective of origin, become almost uniformly dispersed within the atmosphere by the time they are detected at the $CO_2$ observing stations. This uniformity is consistent with our knowledge that the air mixes from pole to pole with a characteristic time shorter than the typical time of recurrence of El Niño events. There are exceptions to this uniformity, however. For example, Christmas Island appears to be so near to the source of disturbances from El Niño that the $CO_2$ responds there slightly sooner than at our other observing stations.

Since El Niño events appear to be mainly an oscillatory phenomenon, they probably do not produce long-term imbalances in the carbon cycle. We have, however, looked for evidence in the $CO_2$ data of any such imbalances which may have been present during the past 30 years of $CO_2$ records, in addition to the conspicuous imbalance owing to fossil fuel combustion. The concentration of $CO_2$ is rising in close proportionality to the increase expected from industrial $CO_2$ production, but there are subtle departures from strict proportionality. The $CO_2$ concentrations recorded at Mauna Loa Observatory and at the South Pole both rise relative to industrial $CO_2$ emissions more rapidly in the latter part of the records than in the earlier part. This is contrary to our expectation that the global average rise relative to emissions should have declined after the oil crisis of 1974, when the acceleration in the fuel combustion decreased sharply.

To put this surmise into quantitative terms we have calculated the redistribution of industrial $CO_2$ emissions between the atmosphere, terrestrial biosphere, and the oceans using a compartment model that portrays the slowly varying responses of the carbon reservoirs not only to these emissions but to additional human disturbances brought about by deforestation and changing land use. Responses to all of these human interactions with the carbon cycle are modeled essentially as first order perturbations to an assumed, preindustrial, steady state. The model simulates the release of $CO_2$ by deforestation and changes in land use by a Gaussian function, with a peak flux predicted to occur in the year 2020. The model portrays plants as stimulated by rising concentrations of $CO_2$ since the beginning of the industrial era. Given these assumptions, the model predicts that the fraction of industrial $CO_2$ remaining airborne should have diminished after 1974. As a tentative explanation of the contrary behavior of the real system we conjecture that human activities may have caused the terrestrial biosphere recently to release additional $CO_2$ not accounted for by the Gaussian function, and that both the biosphere and the oceans may have released stored carbon in response to natural climatic factors, especially higher air and water temperatures.

To explore this conjecture we carried out an additional model computation in which the box diffusion model was forced by deconvolution to predict the observed concentration $CO_2$ since 1740 and the reduced isotopic ratio, $^{13}\delta$, since 1978. This computation, which we call a "double deconvolution", provides a tentative confirmation that the surge in atmospheric $CO_2$ after 1974 is largely a result of accelerated deforestation and land use changes, although it probably includes a contribution from ocean warming and may also reflect a release of $CO_2$ by the terrestrial biosphere in response to rising temperature. The computation also indicates that short-term interannual variations in $CO_2$ associated with El Niño are not caused simply by $CO_2$ released from the oceans during these warm events followed by uptake during ensuing cold events, in which these exchanges are governed by the temperature dependent solubility of $CO_2$ in sea water. Rather, the short-term variations evidently reflect a residual of two, large, opposing oscillations produced jointly by the terrestrial biosphere in response to intermittent drought, and by the oceans in response to variable equatorial upwelling. These opposing oscillations are synchronized by the action of the tropical atmospheric circulation as part of the Southern Oscillation phenomenon.

In a separate analysis of the correlation of $CO_2$ concentration with global air temperature, we found evidence for an 11-year oscillation in $CO_2$ which, by its amplitude and phase lag with respect to a similar oscillation in temperature, appears to reflect changes in air-sea exchange driven by temperature changes in the surface water. The underlying cause of these oscillations may be changes in solar irradiance as detected in satellite data for the most recent sunspot cycle.

Evidence that sources and sinks of atmospheric $CO_2$ have changed in strength is provided by the obvious spatial differences in $CO_2$ for different years. North-south profiles in the 1960's show lesser interhemispheric gradients in $CO_2$ concentration than do profiles in the 1980's. This is as expected from increased industrial $CO_2$ emissions in the northern hemisphere during the intervening decade, but the observed interhemispheric differences, from decade to decade, are not closely proportional to these industrial $CO_2$ emissions, and we therefore surmise that other stationary or slowly varying sources and sinks have influenced north-south gradients of $CO_2$. We point out that decadal changes that produce spatial variations in $CO_2$ can be incorporated into predictions made by the quasi-stationary, three-dimensional transport model provided that the sources and sinks prescribed in the model are adjusted to portray the carbon cycle averaged over different time intervals.

In conclusion we note that the atmospheric $CO_2$ data provide a rich assortment of information on how the carbon cycle functions. By modeling the carbon cycle in the light of this information we may learn more about the rates at which the oceans and terrestrial biosphere redistribute carbon on average and how these rates have changed during recent decades of the industrial era.

## Appendices

### *Appendix A. Sampling Procedures and Data Processing: Atmospheric $CO_2$ Data*

Our most detailed record of atmospheric $CO_2$ concentration is that of Mauna Loa Observatory, Hawaii. Sampling has been carried out almost continuously since March 1958 with assistance of personnel of the National Oceanic and Atmospheric Administration (NOAA) and its predecessor agencies. Diaphragm pumps suck air from multiple intakes selected at any given time to be upwind of the observatory building. The air streams, after cryogenic removal of water vapor at −78°C., are successively passed through the cell of a nondispersive infrared (NDIR) gas analyzer where their absorption of radiation near 4 micrometers is compared with that of a suite of reference gas mixtures, which in turn are calibrated against manometric primary standards maintained at the Scripps laboratory [Keeling et al., 1976a; Keeling et al., 1982; Bacastow et al., 1985]. Ten minutes daily, weekly, and monthly averages of $CO_2$ concentration are computed from the original voltage signal of the analyzer. Here, we have used only monthly averaged data.

We also have used a second, almost continuous, record of $CO_2$ obtained at Baring Head, New Zealand, as a cooperative program with the Institute of Nuclear Sciences (INS) of the New Zealand Division of Science and Industrial Research (DSIR). Procedures used there are similar to those in use at Mauna Loa Observatory [Lowe et al., 1979]. These New Zealand data are closely calibrated against Scripps primary standards [Manning and Pohl, 1986]. They have been made available to us by M. Manning of INS (private communication).

We have compiled additional $CO_2$ data obtained from air samples taken with glass flasks having a capacity of 5 liters. These flasks, equipped with greased stopcocks and evacuated at our laboratory prior to use, were distributed to remote stations where they were exposed to air in pairs or triplets. Samples were taken in Alaska, Hawaii, Samoa, and the South Pole by NOAA personnel. Samples were taken elsewhere by a variety of agencies and individuals too numerous to cite here. Returned to the Scripps laboratory, the flasks were analyzed for their $CO_2$ concentration with an NDIR gas analyzer of the same design as that installed at Mauna Loa Observatory. Calibrations were performed with reference gases comparable to those used at Mauna Loa Observatory [Keeling et al., 1968; Keeling et al., 1986]. For the South Pole station, continuous data, obtained from 1960 to 1963 [Keeling et al., 1976b] have been combined with flask data from 1957 to 1989. For Point Barrow, Alaska, continuous data of Kelley [1969] obtained from 1960 to 1967 have been combined with flask data from 1974 to 1986 obtained by our laboratory.

We have also made use of data from sampling on oceanographic research vessels. Both flasks and in situ continuous analyzers were used.

It is obvious from examination of the more extensive $CO_2$ records that some samples were contaminated, probably by blunders. With respect to flask sampling, since most blunders should differently affect samples collected successively on the same day, we generally retained for further consideration only data from replicate samples in which the $CO_2$ concentrations agree within 0.4 ppm. If more than two samples were collected, we retained samples which agree within 0.4 ppm of the lowest value. In the absence of such agreement all analyses were discarded for that day. For some data of the 1960's we relaxed these criteria as specifically noted, below. Our rejection scheme eliminates approximately 20 percent of the data for each land station and for each oceanic expedition.

The data for both Mauna Loa Observatory and the South Pole pose problems in 1968 and at the South Pole also in 1969. At Mauna Loa Observatory a detector of the NDIR analyzer leaked its filling of gas from 1965 to 1969, resulting in a progressively more uncertain carrier gas effect [Keeling et al., 1982, p. 383], especially uncertain in 1968. The detector was replaced in January, 1969. With respect to the South Pole, the field effort in 1968 involved an unusually large number of unsuccessful flask samples, rendering uncertain the average $CO_2$ concentration, as well as the seasonal cycle, for that year. In 1969 the analysis of the flask samples was carried out at INS in New Zealand on a different NDIR analyzer [Keeling et al., 1976b, p. 553], for which the carrier gas effect could not be properly established afterwards. Therefore we cannot be certain of the change in annual average concentration between 1968 and 1969 at either station.

With respect to continuous sampling, the influence of local contamination was reduced or eliminated by accepting only those data which show steady concentrations for several hours or more. Selection procedures for Mauna Loa Observatory are described by Keeling et al. [1976a]. Similar procedures were used for Baring Head station (M. Manning, private communication), and for the South Pole and Point Barrow. For shipboard sampling, there was rarely evidence of local variability, but the analyzer data did not always agree closely with data for samples collected in glass flasks. We retained flask data and rejected continuous analysis data in cases of disagreement, on the assumption that the flask data were more nearly correct, having all been analyzed with the same laboratory instrument under closely controlled conditions. We usually rejected all continuous data on a given leg of an expedition when there was evidence of disagreement. With respect to Monsoon expedition [Keeling et al., 1965], we distrusted both the flask and analyzer data collected south of New Zealand. We retained only the continuous data for a few days in the far south which appear consistent and in reasonable agreement with contemporary data from the South Pole.

Evacuated flasks were used extensively to sample atmospheric $CO_2$ over the oceans and on an arctic ice floe. Results from sampling between 1959 to 1963 are summarized by Bolin and Keeling [1963]. Results for the FGGE shuttle expedition of 1979 and 1980 are described in part by Keeling et al. [1984]. The remaining data are hitherto unpublished.

The original measurements of the 1960's, including previously unpublished data from the Eastropac and Nova expeditions of 1967 and 1968 (noted by Keeling, [1968], Table 1) have all been reexamined. Consistent calibrational criteria have been applied [Keeling, 1989] to reduce systematic errors of analysis for data gathered over a span of 21 years. These oceanographic data and the data from land stations, and arctic Ice Floe Station Arlis, are all expressed using the Scripps calibrating scale of 1985 [Keeling et al., 1986]. All data are listed in a report by Keeling et al. [1989], available on microfiche.

From these data we have determined seasonally adjusted atmospheric $CO_2$ concentrations for January 1, 1960, 1968 and 1980,

and 15 May, 1984. These values are listed in Tables 1 to 4, respectively. The locations of the sampling sites are shown in Figures A.1 to A.4, respectively, and the tabulated data are shown plotted versus latitude in Figures 28 to 31, respectively. The treatment of the data to establish these north-south profiles is similar to that described by Heimann and Keeling [1986]. Seasonally adjusted data for January 1, 1978 through 1986 are listed in Table 6. The data for 1986 are based on an analysis which includes the most recent provisional data for each station. We have summarized our procedures below. The discussion of isotopic carbon data in Tables 3 and 4 is deferred to Appendix B.

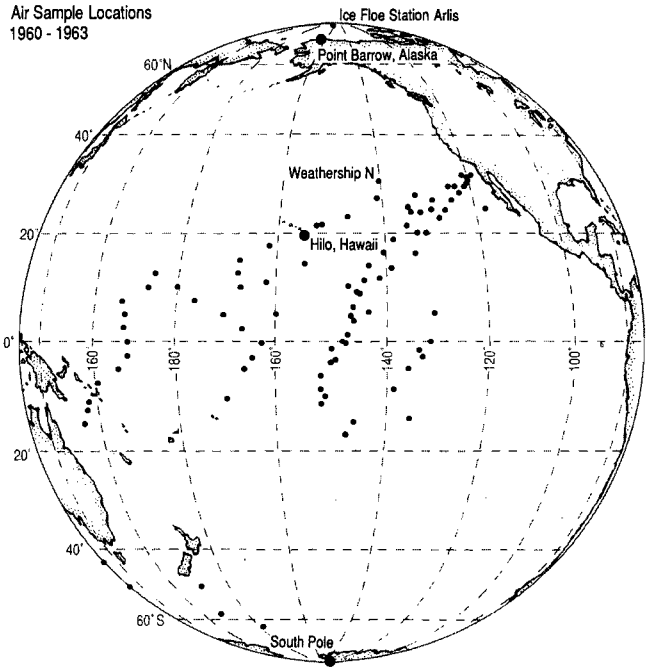


Fig. A.1. Location of air sampling for data shown in Table 1 for 1961-1962. Large dots: land stations; small dots: collections over water or, in the case of Ice Floe Station Arlis, over sea ice.

For each land station record, the data were first combined into daily averages. Usually two or three flask samples were taken, although in some cases as many as 12 samples, and the results were averaged. At all stations with continuous analyzer records, except Baring Head, the daily averages were further combined into longer term averages. For Point Barrow, La Jolla, and Mauna Loa, averages were computed over successive seven day intervals beginning with the first day of record, irrespective of any days with missing data. For the South Pole, daily averages were averaged over two intervals per month, each interval containing approximately the same number of days with data, as set forth in a data report by Keeling et al. [1976c].

In order to produce smooth representations of the seasonal and interannual variations in atmospheric $CO_2$, the daily or longer term averages of each entire station record were fit to a series of functions which separately expressed the seasonal and interannual variations. First, the daily or period averages were fit to a cubic power series in time combined with the harmonic function

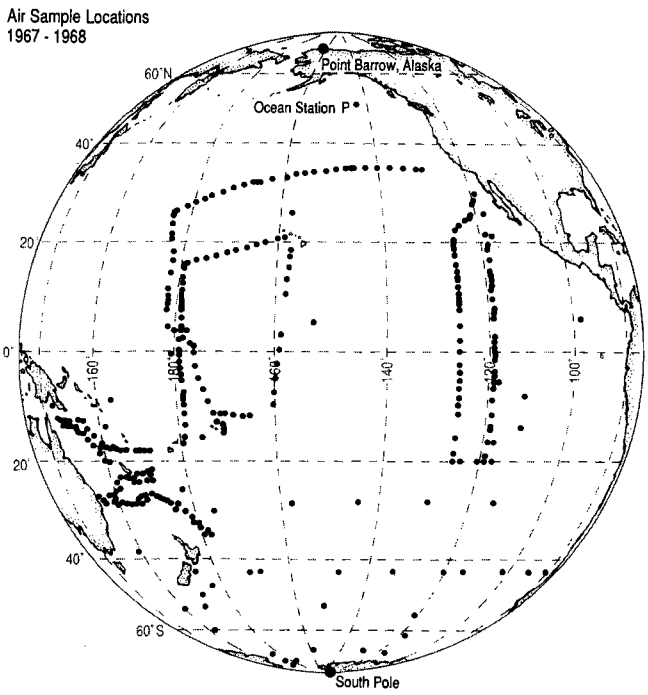


Fig. A.2. Location of air sampling for data shown in Table 2 for 1967-1968. Symbols are as in Figure A.1.

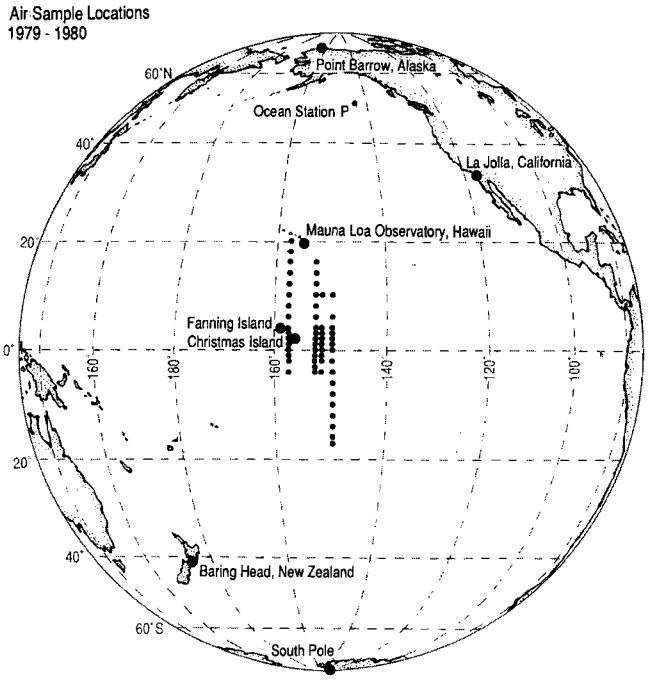


Fig. A.3. Location of air sampling for data shown in Table 3 for 1979-1980. Symbols are as in Figure A.1.

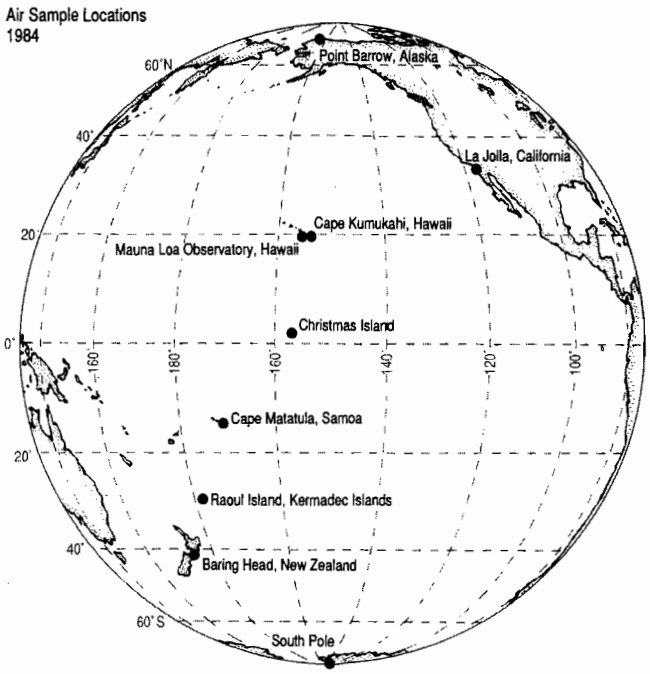


Fig. A.4. Location of air sampling for data shown in Table 4 for 1983-1984. Symbols are as in Figure A.1.

$$S = \sum_{k=1}^{m} [a_k \sin(2k\pi t) + b_k \cos(2k\pi t)] \qquad (A.1)$$

where $m = 4$, $t$ denotes time in years since an arbitrary date shortly before the beginning of the record, and the $a_k$ and $b_k$ are constants. A linear fitting procedure was used which did not require prior estimates of the coefficients.

The interannual trend was next represented by an exponential function

$$E = C_1 + C_2 \exp(C_3 t) \qquad (A.2)$$

where $C_1$, $C_2$, and $C_3$ are constants. A fit to this function added to the harmonic function, $S$, was then made via a nonlinear fitting procedure which used initial estimates of the harmonic coefficients provided by the first fit. The function, $E$, was then subtracted from the data set, and the interannual variations were fit to a cubic spline function, $R$ [Reinsch, 1967], while the seasonal cycle was allowed to vary in amplitude by a gain factor, $\gamma$, incorporated in the harmonic fit.

The monthly atmospheric $CO_2$ data were thus finally represented by the expression

$$P = E + (1 + \gamma t)S + R \qquad (A.3)$$

where $P$ is equivalent to the sum of $C_{obs\ rem}(t)$ and $C_{obs\ seas}(t)$ of equation (2.3). The curve fitting procedures, involving iteration, are described in detail by Bacastow et al. [1985]. The data of Tables 1 to 4 for fixed stations are derived from the sum $E + R$ (identical to $C_{obs\ rem}(t)$) of the final fit to the data of each station as listed in the report of Keeling et al. [1989]. This report also lists the Fortran computer program used to produce the fit.

The FGGE shuttle expedition of 1979 to 1980 produced a set of $CO_2$ data at 23 latitudes which were uniformly sampled during most or all of 16 north-south transects between 20°N. and 17°S. We fitted these data to an interpolating surface in latitude and time as described by Heimann and Keeling [1986]. The surface is expressed as a truncated double series of Chebycheff polynomials in space and annual and semi-annual harmonic functions in time. An interannual trend, independent of latitude and linear in time, was included in the fitting procedure.

Data from ships obtained during the 1960's are too scattered to justify a similar seasonal analysis, although such an analysis was carried out by Bolin and Keeling [1963] when only these earlier data were available. For latitudes between 16.0°N. and 14.5°S. we assumed that the seasonal variation deduced from the data of the FGGE expedition is valid, except that the amplitudes of the harmonic functions should take into account the long-term increase in the seasonal cycle found for Mauna Loa, Hawaii by Bacastow et al. [1985]. For the data used to produce a $CO_2$ distribution for 1962 the amplitudes were therefore everywhere reduced to 88.5 percent of the FGGE amplitudes, and for 1968 to 92.3 percent of these amplitudes.

The seasonal representation was extended to the North and South Poles by fitting splines with fixed knots [de Boor, 1978, p. 235] through time dependent harmonic coefficients of annual and semi-annual components derived from land station data at Point Barrow Alaska, Ocean Station P, Baring Head, New Zealand, and the South Pole. Phases and amplitudes of this fit for 1980, derived from the coefficients $a_k$ and $b_k$, defined by equation A.1, are listed in Table A.1. For 1962 and 1968 the amplitudes were again reduced, consistent with the reductions at low latitudes noted in the previous paragraph.

The seasonally adjusted data of the 1960's from ships were further adjusted to remove the influence of interannual variations. This adjustment made use of trend functions for Mauna Loa Observatory, Hawaii at 19°N. and the South Pole, each expressed by the sum, $E + R$, of equation (A.3). These monthly values, listed in the report of Keeling et al. [1989], differ slightly from those of the provisional data of the main study, because they are based on earlier data sets. By linear interpolation of the two functions versus the sine of latitude, the interannual trend for any latitude between 19.5°N. and 90°S. was estimated for the date of each observation. The ship data, after seasonal adjustment, were further adjusted to a reference date of January 1, 1962 or 1968 by subtracting the difference in interannual trend from the date of observation to the reference date. For all data north of 19.5°N. the Mauna Loa trend was employed.

The data of the 1960's, with the influence of the long-term and seasonal variations thus essentially removed, were ordered from south to north and then grouped. Usually 10 observations were included in each group, but the number was varied slightly to produce nearly equal-sized groups of data from pole to pole. All data obtained from sampling on a weather ship at 30°N. during 1962 and 1963 were combined into a single group of 35 observations. The original observations, expressed on the 1985 calibration scale, and grouped as just indicated, are listed by Keeling et al. [1989], together with the trend value for the date of observation and the trend value for the reference date, the seasonal adjustment, and the resulting adjusted concentration.

TABLE A.1. Seasonal Variation of the Atmospheric $CO_2$ Concentration in 1980

| Latitude | $A_1$ (ppm) | $\phi_1$ (°) | $A_2$ (ppm) | $\phi_2$ (°) |
|---|---|---|---|---|
| 90 S | 0.60 | 80.0 | 0.04 | 88.0 |
| 85 | 0.60 | 80.0 | 0.04 | 88.0 |
| 80 | 0.60 | 80.1 | 0.04 | 88.2 |
| 75 | 0.60 | 80.3 | 0.04 | 89.1 |
| 70 | 0.60 | 80.9 | 0.04 | 91.5 |
| 65 | 0.59 | 82.0 | 0.03 | 97.0 |
| 60 | 0.59 | 83.7 | 0.03 | 109.7 |
| 55 | 0.58 | 86.3 | 0.02 | 137.4 |
| 50 | 0.56 | 89.7 | 0.02 | 176.2 |
| 45 | 0.52 | 93.8 | 0.04 | −160.1 |
| 40 | 0.47 | 98.9 | 0.05 | −149.9 |
| 35 | 0.39 | 105.2 | 0.06 | −146.4 |
| 30 | 0.26 | 115.1 | 0.06 | −148.2 |
| 25 | 0.10 | 154.5 | 0.04 | −161.8 |
| 20 | 0.23 | −94.6 | 0.03 | 124.7 |
| 15 | 0.10 | −85.1 | 0.17 | −55.1 |
| 10 | 0.37 | −129.6 | 0.35 | −81.3 |
| 5 | 0.90 | −119.2 | 0.20 | −50.5 |
| 0 | 1.03 | −122.6 | 0.04 | 31.5 |
| 5 N | 1.49 | −117.0 | 0.28 | 52.0 |
| 10 | 2.66 | −112.4 | 0.89 | 33.5 |
| 15 | 3.28 | −111.5 | 0.93 | 28.0 |
| 20 | 3.39 | −95.6 | 0.82 | 51.3 |
| 25 | 3.61 | −79.7 | 1.15 | 78.2 |
| 30 | 3.91 | −74.1 | 1.54 | 84.8 |
| 35 | 4.17 | −73.5 | 1.87 | 84.9 |
| 40 | 4.44 | −74.4 | 2.15 | 82.7 |
| 45 | 4.73 | −75.0 | 2.37 | 79.9 |
| 50 | 5.08 | −74.3 | 2.56 | 77.1 |
| 55 | 5.47 | −72.3 | 2.70 | 74.7 |
| 60 | 5.82 | −70.3 | 2.81 | 72.9 |
| 65 | 6.10 | −68.6 | 2.88 | 71.7 |
| 70 | 6.28 | −67.6 | 2.93 | 70.9 |
| 75 | 6.38 | −67.0 | 2.95 | 70.5 |
| 80 | 6.42 | −66.8 | 2.96 | 70.3 |
| 85 | 6.43 | −66.7 | 2.96 | 70.3 |
| 90 | 6.43 | −66.7 | 2.96 | 70.3 |

*Values shown represent amplitude and phase of the first and second harmonic as defined through

$$C(t) = A_1 \cos(2\pi t + \phi_1) + A_2 \cos(4\pi t + \phi_2)$$

where t is in years. The data for 16°N. to 14.5°S. are derived from the FGGE expedition, elsewhere from land station data.

For the 1979–1980 period, the report of Keeling et al. [1989] lists only the original data, but expressed on several calibration scales. This is done as an aid to interpreting previously published versions of the data of the FGGE shuttle expedition. A portion of the concentration data were published by Keeling et al. [1984] using a 1981 calibration scale. The seasonal analysis of these data by Heimann and Keeling [1986] used an earlier 1974 scale (erroneously quoted by these authors [loc. cit., p. 7768] as being on a 1980 scale). Keeling and Heimann [1986] determined a seasonally adjusted north-south trend in the FGGE data (their Table 2) using a 1983 calibration scale. This latter scale differs by a constant offset of 0.01 ppm below the 1985 scale used in the present article. In Table 3 we express the seasonally adjusted data based on the same interpolating surface used by Keeling and Heimann [1986], but with the values thus raised by 0.01 ppm.

The continuous analyzer data of Monsoon Expedition of 1961 were accepted from Table 2 of Keeling et al. [1965] where they are expressed as averages over 2.5° latitude intervals. Each of these averages, converted from the published values to mole fractions on the 1985 calibration scale, was assumed to be equivalent to a pair of flask analyses of $CO_2$, and was merged with the flask data so as to contribute to the group averages of Table 1. The unpublished continuous data of Eastropac and Nova Expeditions were combined into 12-hour averages, each assumed to be equivalent to a single flask analysis, and merged with the flask data after adjustment to the mole fraction calibration scale of 1985. Averages were computed for each group of data. They were assumed to apply to the average latitude and longitude of each group.

For fixed land stations we used the procedures of Bacastow et al. [1985], as described above, to derive seasonally and trend adjusted data expressed by the function, $E + R$, of Equation (A.3). The data for Ice Floe Arlis were treated as though Arlis were a fixed station. For Point Barrow the record of the 1960's terminates on September 13, 1967, while at Ocean Station P the record begins only on May 24, 1969. Estimates of concentration for January 1, 1968 at each station were obtained by extrapolation on the basis of the interannual trend given by the function, $E + R$, of Mauna Loa, Hawaii, as listed in the report of Keeling et al. [1989]. For Point Barrow, seasonally adjusted data for the last 12 months of the record, obtained from the fit to the full record, 1961 to 1985, were in this way detrended. The first 12 months of the record for Station P were similarly treated. Afterwards, averages were computed from the adjusted 12-month sets of data. The records for Fanning Island at 4°N. and Christmas Island at 2°N. were combined into a single record.

Standard errors of the seasonally adjusted concentrations listed in Tables 1 to 4 were derived different ways, depending on the method of averaging or smoothing of the original observational data. Standard errors for the FGGE Shuttle Expedition data, as listed in Table 3, were obtained from the interpolating surface in latitude and time of Heimann and Keeling [1986] using estimates computed for the nearest whole number latitude. Standard errors for the data from ships in the 1960's, as listed in Tables 1 and 2, were computed as the standard deviation of the means of each data group. Standard errors for the land stations, in all tables, were as derived from the spline fitting procedure. For Ice Floe Station Arlis and Hilo, Hawaii, the standard error of an individual data point, relative to the curve fit at that station, was divided by the square root of the total number of data points included in the fit to obtain an estimate of the standard error. For the other stations, with longer records, the individual standard errors were divided by the number of data points included in one year of record beginning on July 1 of the year, preceding either 1962 or 1968. For Point Barrow and Station P in 1968, standard deviations of the mean of the 12-month sets of adjusted data were used.

TABLE A.2. Atmospheric $CO_2$ Data from Fixed Stations and Arctic Ice Floe Station Arlis
[Data are from samples of air collected in glass flasks unless otherwise indicated by footnotes]

| Station | Code Name | Lat. (deg.) | Long. (deg.) | Elevation (m) | Inclusive Dates of Fit | Standard Error of Fit (ppm) | Seasonally Adjusted Concentration (ppm) for January 1[a] | | |
|---|---|---|---|---|---|---|---|---|---|
| | | | | | | | 1962 | 1968 | 1980 |
| Ice Floe Station Arlis | ARL | 77 to 89N | In Arctic Ocean | 2 | Sept. 18, 1961 to May 16, 1964 | 1.2513 | 319.09 | – | – |
| Point Barrow, Alaska[b] | | 71.3N | 156.6W | 11 | July 12, 1961 to Sept. 11, 1985 | 1.2450 | 319.24 | – | – |
| Point Barrow, Alaska[c] | | 71.3N | 156.6W | 11 | Sept. 14, 1966 to Sept. 13, 1967 | 1.1093 | – | 324.15 | – |
| Point Barrow, Alaska | PTB | 71.3N | 156.6W | 11 | Jan. 3, 1974 to Sept. 11, 1985 | 1.0382 | – | – | 338.81 |
| Ocean Weather Station P[c] | | 50.0N | 145.0W | 10 | May 24, 1969 to May 31, 1970 | 0.8761 | – | 323.02 | – |
| Ocean Weather Station P | STP | 50.0N | 145.0W | 10 | May 24, 1969 to June 21, 1981 | 1.1881 | – | – | 338.21 |
| La Jolla, California | LJO | 32.9N | 117.3W | 10 | Feb. 18, 1969 to Oct. 7, 1985 | 0.7916 | – | – | 339.16 |
| Weather Ship 'N'[d] | | 30.0N | 140.0W | 10 | Aug. 10, 1962 to Oct. 15, 1963 | 0.9023 | 318.58 | – | – |
| Hilo, Hawaii | | 19.7N | 155.1W | 2 | March 30, 1960 to Nov. 4, 1963 | 1.0234 | 318.62 | – | – |
| Mauna Loa, Hawaii[e] | MLO | 19.5N | 155.6W | 3397 | March 29, 1958 to Dec. 14, 1985 | 0.3452 | 318.26 | 322.28 | 337.57 |
| Cape Kumukahi, Hawaii | KUM | 19.5N | 154.8W | 3 | March 27, 1979 to Sept. 23, 1985 | 0.7089 | – | – | |
| Fanning Is./Christmas Is.[f] (combined) | FAN/ CHR | 3.9N/ 2.0N | 159.3W/ 157.3W | 2/2 | July 21, 1972 to Nov. 30, 1985 | 0.4356 | – | – | 338.07 |
| Cape Matutula, Tutuila Is. American Samoa | SAM | 14.2S | 170.6W | 30 | Sept. 4, 1981 to Sept. 12, 1985 | 0.6317 | – | – | – |
| Raoul Is., Kermadec Islands | KER | 29.2S | 177.9W | 2 | Dec. 8, 1982 to July 4, 1984 | 0.2788 | – | – | – |
| Baring Head, New Zealand[e] | NZD | 41.4S | 174.9E | 85 | Jan. 6, 1972 to Dec. 30, 1984 | 0.3062 | – | – | 335.67 |
| South Pole | SPO | 90.0S | – | 2810 | June 17, 1957 to Feb. 1, 1985 | 0.1775 | 317.77 | 321.57 | 335.84 |

[a]Function $C_{obs\ rem}\ (t)$ of equation (2.2).

[b]An exponential function in time was used to represent the long-term trend instead of a spline function, owing to gap in data set from 1968 through 1973. Data in the 1960's are from a continuous analyzer record of Kelley [1969]. Seven day averages were used in the fit and to derive the standard error of fit.

[c]Concentration determined as an average of detrended data. For Point Barrow, 53 seasonally adjusted daily averages from September 14, 1966 to September 13, 1967 were detrended to January 1, 1968 where the long-term trend was represented by the function (E + R) of Mauna Loa, Hawaii as discussed in the text. For Ocean Weather Station P, 35 daily averages from May 24, 1969 to May 31, 1970 were similarly adjusted, detrended, and averaged.

[d]Concentration determined by adjustments to the individual data points as described in the text for data from ships.

[e]Data from a continuous non-dispersive infrared gas analyzer.

[f]Republic of Kiribati.

TABLE A.3. Sources of Atmospheric $CO_2$ Data from Ship Sampling

| Code Name | Expedition Name | Vessel | Latitude Zone (deg.) | Period of Sampling | Data |
|---|---|---|---|---|---|
| ELT | – | Eltanin | 35N. to 78S. | July 12, 1962 to March 14, 1972 | Flasks |
| EST | Eastropac | Argo | 28N. to 20S. | Jan. 26, 1967 to March 28, 1968 | Continuous and Flasks |
| FGE | FGGE Shuttle Expedition | Various | 21N. to 17S. | Feb. 6, 1979 to June 14, 1980 | 627 Flasks |
| HIX | Hilo | Hugh M. Smith/ Stranger | 30N. to 21N. | March 24, 1962 to May 6, 1962 | Flasks |
| LUH | Luciad | Horizon | 20N. to 16S. | Jan. 6, 1963 to Feb. 3, 1963 | Flasks |
| MON | Monsoon | Argo | 34N. to 63S. | Aug. 27, 1960 to April 17, 1962 | Continuous and Flasks |
| NOV | Nova | Argo | 34N. to 34S. | April 23, 1967 to Sept. 10, 1967 | Continuous and Flasks |
| PRO | Proa | Spencer F. Baird | 18N. to 10S. | Aug. 7, 1962 to Aug. 29, 1962 | Flasks |
| RIS | Risepac | Spencer F. Baird | 31N. to 17S. | Oct. 29, 1961 to Feb. 4, 1962 | Flasks |
| STN | Weather Ship 'N' | Various | 30N. | Sept. 7, 1962 to Sept. 7, 1964 | Flasks |
| TET | Tethys | Spencer F. Baird | 30N. to 5S. | June 17, 1960 to Aug. 18, 1960 | Flasks |

The atmospheric $CO_2$ data and related information for the land stations and Ice Floe Station Arlis are listed in Table A.2. The data from ships are listed in Table A.3. We list in Table A.4 monthly mean concentrations ($\overline{C_{obs}}$ of equation 2.3) for Mauna Loa Observatory and the South Pole, updated from the report of Keeling et al. [1989, pp. 330–331 and 406–407, respectively]. Corresponding data, seasonally adjusted ($C_{obs\ rem} + \varepsilon_{obs}$ of equation 2.3), are listed in Table A.5. To approximate the global average concentration of atmospheric $CO_2$, seasonally adjusted data for these two stations were averaged, after expressing the data for each station by the

TABLE A.4. Concentration of Atmospheric $CO_2$ at Mauna Loa Observatory, Hawaii and the South Pole
[Entries express averages of daily values (in ppm) adjusted to the 15th of each month]

| MONTH | YEAR | | | | | | | | | | | | | | | | |
|---|---|---|---|---|---|---|---|---|---|---|---|---|---|---|---|---|---|
| | 1957 | 1958 | 1959 | 1960 | 1961 | 1962 | 1963 | 1964 | 1965 | 1966 | 1967 | 1968 | 1969 | 1970 | 1971 | 1972 | 1973 |
| Mauna Loa Observatory | | | | | | | | | | | | | | | | | |
| Jan. | | | 315.42 | 316.27 | 316.73 | 317.78 | 318.58 | 319.41 | 319.27 | 320.45 | 322.17 | 322.40 | 323.52 | 324.33 | 326.00 | 326.60 | 328.37 |
| Feb. | | | 316.31 | 316.81 | 317.54 | 318.40 | 318.93 | | 320.28 | 321.43 | 322.34 | 322.99 | 323.89 | 325.30 | 326.51 | 327.47 | 329.40 |
| March | | 315.55 | 316.50 | 317.42 | 318.38 | 319.53 | 319.70 | | 320.73 | 322.23 | 322.88 | 323.73 | 325.04 | 326.29 | 327.01 | 327.58 | 330.14 |
| April | | 317.29 | 317.56 | 318.87 | 319.31 | 320.41 | 321.22 | | 321.97 | 323.54 | 324.25 | 324.86 | 326.01 | 327.54 | 327.62 | 329.56 | 331.33 |
| May | | 317.34 | 318.13 | 319.87 | 320.42 | 320.85 | 322.08 | 322.05 | 322.00 | 323.91 | 324.83 | 325.41 | 326.67 | 327.54 | 328.76 | 329.90 | 332.31 |
| June | | | 318.00 | 319.43 | 319.61 | 320.45 | 321.31 | 321.73 | 321.71 | 323.59 | 323.93 | 325.19 | 325.97 | 327.21 | 328.40 | 328.92 | 331.90 |
| July | | 315.68 | 316.39 | 318.01 | 318.42 | 319.44 | 319.58 | 320.27 | 321.05 | 322.25 | 322.38 | 323.97 | 325.13 | 325.98 | 327.20 | 327.88 | 330.70 |
| Aug. | | 314.78 | 314.66 | 315.75 | 316.64 | 317.25 | 317.61 | 318.54 | 318.71 | 320.21 | 320.76 | 321.92 | 322.90 | 324.42 | 325.27 | 326.17 | 329.15 |
| Sept. | | 313.03 | 313.68 | 314.00 | 314.84 | 316.12 | 316.06 | 316.54 | 317.66 | 318.48 | 319.11 | 320.10 | 321.61 | 322.91 | 323.20 | 324.68 | 327.35 |
| Oct. | | | 313.18 | 313.68 | 315.16 | 315.27 | 315.83 | 316.71 | 317.14 | 317.94 | 319.24 | 319.96 | 321.01 | 322.90 | 323.40 | 325.04 | 327.02 |
| Nov. | | 313.18 | 314.66 | 314.84 | 315.94 | 316.53 | 316.91 | 317.53 | 318.70 | 319.63 | 320.56 | 320.97 | 322.08 | 323.85 | 324.64 | 326.34 | 327.99 |
| Dec. | | 314.50 | 315.43 | 316.04 | 316.85 | 317.53 | 318.20 | 318.55 | 319.25 | 320.87 | 321.80 | 322.49 | 323.37 | 324.97 | 325.85 | 327.39 | 328.48 |
| AVE. | | | 315.83 | 316.75 | 317.49 | 318.30 | 318.83 | | 319.87 | 321.21 | 322.02 | 322.83 | 323.93 | 325.27 | 326.16 | 327.29 | 329.51 |

TABLE A.4. Concentration of Atmospheric $CO_2$ at Mauna Loa Observatory, Hawaii and the South Pole -- continued

| MONTH | YEAR | | | | | | | | | | | | | | | | |
|---|---|---|---|---|---|---|---|---|---|---|---|---|---|---|---|---|---|
| | 1974 | 1975 | 1976 | 1977 | 1978 | 1979 | 1980 | 1981 | 1982 | 1983 | 1984 | 1985 | 1986 | 1987 | 1988 | 1989 | |
| Jan. | 329.18 | 330.23 | 331.58 | 332.75 | 334.80 | 336.05 | 337.84 | 339.06 | 340.57 | 341.20 | 343.52 | 344.79 | 346.11 | 347.83 | 350.15 | 352.45 | |
| Feb. | 330.55 | 331.25 | 332.39 | 333.24 | 335.22 | 336.59 | 338.20 | 340.30 | 341.44 | 342.35 | 344.33 | 345.83 | 346.79 | 348.30 | 351.45 | | |
| March | 331.32 | 331.87 | 333.33 | 334.53 | 336.47 | 337.79 | 339.91 | 341.21 | 342.53 | 342.93 | 345.11 | 347.25 | 347.69 | 349.23 | 351.96 | | |
| April | 332.48 | 333.14 | 334.41 | 335.90 | 337.59 | 338.71 | 340.60 | 342.33 | 343.39 | 344.77 | 346.88 | 348.17 | 349.38 | 350.74 | 353.41 | | |
| May | 332.92 | 333.80 | 334.71 | 336.57 | 337.84 | 339.30 | 341.29 | 342.74 | 343.96 | 345.58 | 347.25 | 348.75 | 350.02 | 351.54 | 354.03 | | |
| June | 332.08 | 333.42 | 334.17 | 336.10 | 337.72 | 339.12 | 341.00 | 342.07 | 343.18 | 345.14 | 346.62 | 348.07 | 349.28 | 350.95 | 353.53 | | |
| July | 331.01 | 331.73 | 332.88 | 334.76 | 336.37 | 337.56 | 339.38 | 340.32 | 341.88 | 343.81 | 345.22 | 346.38 | 347.65 | 349.18 | 352.21 | | |
| Aug. | 329.23 | 329.90 | 330.77 | 332.59 | 334.52 | 335.92 | 337.43 | 338.27 | 339.65 | 342.22 | 343.11 | 344.52 | 345.69 | 347.75 | 350.29 | | |
| Sept. | 327.28 | 328.40 | 329.14 | 331.42 | 332.60 | 333.75 | 335.72 | 336.52 | 337.80 | 339.69 | 340.90 | 342.93 | 344.67 | 346.27 | 348.56 | | |
| Oct. | 327.21 | 328.17 | 328.77 | 330.98 | 332.37 | 333.70 | 335.84 | 336.68 | 337.69 | 339.82 | 341.17 | 342.63 | 343.98 | 346.17 | 348.73 | | |
| Nov. | 328.29 | 329.32 | 330.14 | 332.24 | 333.75 | 335.12 | 336.93 | 338.19 | 339.09 | 340.98 | 342.80 | 344.06 | 345.48 | 347.60 | 349.92 | | |
| Dec. | 329.41 | 330.59 | 331.52 | 333.68 | 334.79 | 336.56 | 338.05 | 339.44 | 340.32 | 342.82 | 344.04 | 345.39 | 346.73 | 348.78 | 351.19 | | |
| AVE. | 330.08 | 330.99 | 331.98 | 333.73 | 335.34 | 336.68 | 338.52 | 339.76 | 340.96 | 342.61 | 344.25 | 345.73 | 346.96 | 348.70 | 351.29 | | |

| | 1957 | 1958 | 1959 | 1960 | 1961 | 1962 | 1963 | 1964 | 1965 | 1966 | 1967 | 1968 | 1969 | 1970 | 1971 | 1972 | 1973 |
|---|---|---|---|---|---|---|---|---|---|---|---|---|---|---|---|---|---|
| South Pole | | | | | | | | | | | | | | | | | |
| Jan. | | | 314.93 | | | 317.29 | 317.97 | | | 320.19 | | 321.36 | 322.24 | 323.54 | 324.63 | | 326.58 |
| Feb. | | | 314.97 | | | 317.10 | 317.71 | | 318.52 | 319.84 | 320.84 | | | 323.38 | 324.44 | | 326.01 |
| March | | 314.12 | 314.92 | | | 316.90 | 317.31 | | 318.40 | 319.88 | | | 321.50 | 323.27 | 324.15 | 324.88 | 326.20 |
| April | | | | | | 316.95 | 317.74 | | 318.52 | 320.15 | 320.70 | 321.45 | 321.51 | 323.51 | 324.31 | 325.00 | 326.66 |
| May | | | | | 316.64 | 317.02 | 318.10 | | 318.72 | 320.52 | 320.84 | 321.31 | 321.83 | 323.62 | 324.51 | 325.14 | 326.94 |
| June | 313.21 | 314.37 | | 316.21 | 316.70 | 317.09 | 318.06 | | | 320.28 | 320.79 | 321.28 | 322.04 | 324.02 | 324.74 | 325.65 | 327.26 |
| July | | | | 316.51 | 316.78 | 317.11 | 318.10 | | 319.23 | | 320.89 | 321.34 | 322.48 | 324.30 | 324.99 | 325.96 | 327.57 |
| Aug. | | | 315.81 | 316.58 | 317.19 | 317.48 | 318.21 | | 319.51 | 320.91 | 321.67 | | 322.83 | 324.55 | | 325.95 | 328.24 |
| Sept. | 313.71 | 315.15 | 316.06 | | 317.52 | 317.91 | 318.24 | | | 321.19 | 321.92 | | 323.37 | 325.27 | 325.61 | 326.38 | 328.54 |
| Oct. | | | | | 317.57 | | 318.85 | | | 321.30 | 321.64 | | 323.20 | 325.03 | | 326.62 | 328.46 |
| Nov. | | | 316.16 | | 317.71 | | | | 320.01 | 321.40 | 321.66 | | 323.22 | 325.07 | 325.58 | 326.78 | 328.43 |
| Dec. | 314.31 | | | | 317.51 | 318.47 | | | 320.12 | 320.91 | 321.62 | 322.49 | | | | 326.65 | 328.43 |
| AVE. | | | | | | | | | | | | | | | | | 327.44 |

| | 1974 | 1975 | 1976 | 1977 | 1978 | 1979 | 1980 | 1981 | 1982 | 1983 | 1984 | 1985 | 1986 | 1987 | 1988 | 1989 |
|---|---|---|---|---|---|---|---|---|---|---|---|---|---|---|---|---|
| Jan. | 328.13 | 328.72 | 330.11 | 331.09 | 332.67 | 333.84 | 335.89 | 337.59 | | 339.68 | 341.87 | 342.83 | 344.48 | 345.75 | 348.15 | 349.81 |
| Feb. | 327.91 | 328.72 | 329.83 | 330.82 | 332.54 | 333.86 | 335.56 | 337.29 | 338.47 | 339.66 | | 342.63 | 344.43 | 345.65 | 347.94 | |
| March | 327.91 | 328.68 | 329.74 | 330.68 | 332.66 | 333.65 | | 337.26 | 338.21 | 339.69 | 341.54 | 342.56 | 344.36 | 345.61 | 347.78 | |
| April | 327.73 | 328.77 | 329.47 | 331.16 | 332.81 | 334.01 | 335.92 | 337.36 | 338.53 | 340.14 | 341.66 | 342.60 | 344.48 | 345.98 | 348.11 | |
| May | 327.84 | 328.76 | 329.76 | 331.23 | | 334.17 | 336.04 | 337.50 | 338.82 | 340.45 | 341.69 | 342.95 | 344.54 | 346.08 | 348.24 | |
| June | 327.71 | 328.90 | 329.81 | 331.45 | 333.21 | 334.37 | 336.73 | 337.98 | 339.01 | 340.83 | 341.85 | 343.29 | 344.87 | 346.48 | 348.49 | |
| July | 328.29 | 329.18 | 330.29 | 331.88 | 333.65 | 334.98 | 337.28 | 338.24 | 339.16 | 341.23 | 342.62 | 343.77 | 345.39 | 347.07 | 348.98 | |
| Aug. | 328.52 | 329.66 | 330.85 | 332.29 | 334.11 | 335.55 | 337.37 | 338.59 | 339.94 | 341.72 | 343.02 | 344.36 | 345.79 | 347.50 | 349.50 | |
| Sept. | 328.79 | 330.07 | 331.23 | 332.71 | 334.57 | 335.71 | 337.71 | 338.65 | 340.14 | 342.15 | 343.28 | 344.71 | 346.05 | 347.94 | 349.66 | |
| Oct. | 328.88 | 330.39 | 331.54 | 332.93 | 334.66 | 335.84 | 337.73 | 338.98 | 340.17 | 342.11 | 343.32 | 344.78 | 346.00 | 347.97 | 349.80 | |
| Nov. | 328.96 | 330.28 | 331.57 | 333.14 | 334.41 | 336.20 | 337.80 | 338.69 | 339.87 | 342.37 | 343.14 | 344.62 | 346.01 | 348.05 | 349.77 | |
| Dec. | 328.83 | 330.11 | 331.26 | 333.02 | 334.13 | 335.87 | 337.87 | 338.73 | 339.79 | 342.18 | 342.97 | 344.48 | 345.89 | 348.18 | 349.74 | |
| AVE. | 328.29 | 329.35 | 330.46 | 331.87 | | 334.84 | | 338.07 | | 341.02 | | 343.63 | 345.19 | 346.85 | 348.85 | |

function $E + R$ of equation A.3 ($C_{obs\ rem}$ of equation 2.3). Values for the 15th of each month are listed in Table A.6. Also listed are values for the middle of each year from 1740 to 1955, based on a spline fit to ice core data of Neftel et al. [1985] and Friedli et al. [1986]. From mid–1955 to mid–1957 monthly values are derived from proxy data of Keeling [1978], and henceforth to the beginning of the Mauna Loa record, from data of the South Pole after their adjustment so as to approximate the average concentration of the two stations. The procedures to obtain these smoothed data are further described in the report of Keeling et al. [1989].

TABLE A.5. Seasonally Adjusted Concentration of Atmospheric $CO_2$ at Mauna Loa Observatory, Hawaii and the South Pole
[Entries express averages of daily values (in ppm) for the 15th of each month.]

| MONTH | YEAR | | | | | | | | | | | | | | | | |
|---|---|---|---|---|---|---|---|---|---|---|---|---|---|---|---|---|---|
| | 1957 | 1958 | 1959 | 1960 | 1961 | 1962 | 1963 | 1964 | 1965 | 1966 | 1967 | 1968 | 1969 | 1970 | 1971 | 1972 | 1973 |
| Mauna Loa Observatory | | | | | | | | | | | | | | | | | |
| Jan. | | | 315.52 | 316.37 | 316.83 | 317.88 | 318.68 | 319.51 | 319.38 | 320.56 | 322.27 | 322.51 | 323.62 | 324.44 | 326.11 | 326.71 | 328.48 |
| Feb. | | | 315.78 | 316.28 | 317.01 | 317.86 | 318.38 | | 319.73 | 320.88 | 321.78 | 322.43 | 323.32 | 324.73 | 325.94 | 326.90 | 328.82 |
| March | | 314.34 | 315.28 | 316.17 | 317.15 | 318.28 | 318.45 | | 319.46 | 320.95 | 321.60 | 322.42 | 323.74 | 324.99 | 325.70 | 326.24 | 328.81 |
| April | | 315.10 | 315.35 | 316.63 | 317.08 | 318.17 | 318.96 | | 319.68 | 321.23 | 321.93 | 322.50 | 323.66 | 325.18 | 325.24 | 327.15 | 328.93 |
| May | | 314.67 | 315.44 | 317.16 | 317.69 | 318.11 | 319.32 | 319.28 | 319.21 | 321.10 | 322.00 | 322.56 | 323.81 | 324.66 | 325.86 | 326.99 | 329.38 |
| June | | | 315.90 | 317.34 | 317.49 | 318.31 | 319.16 | 319.59 | 319.53 | 321.40 | 321.73 | 323.00 | 323.74 | 324.97 | 326.14 | 326.67 | 329.62 |
| July | | 314.90 | 315.60 | 317.24 | 317.62 | 318.64 | 318.77 | 319.48 | 320.22 | 321.43 | 321.55 | 323.16 | 324.29 | 325.13 | 326.35 | 327.05 | 329.84 |
| Aug. | | 315.81 | 315.70 | 316.82 | 317.69 | 318.31 | 318.68 | 319.63 | 319.79 | 321.29 | 321.85 | 323.04 | 324.01 | 325.53 | 326.39 | 327.31 | 330.28 |
| Sept. | | 315.70 | 316.37 | 316.71 | 317.56 | 318.86 | 318.81 | 319.32 | 320.45 | 321.29 | 321.93 | 322.95 | 324.47 | 325.79 | 326.09 | 327.60 | 330.27 |
| Oct. | | | 316.10 | 316.61 | 318.11 | 318.24 | 318.82 | 319.72 | 320.17 | 320.98 | 322.30 | 323.03 | 324.10 | 326.02 | 326.54 | 328.19 | 330.19 |
| Nov. | | 315.06 | 316.55 | 316.74 | 317.86 | 318.45 | 318.85 | 319.47 | 320.67 | 321.60 | 322.55 | 322.97 | 324.09 | 325.87 | 326.67 | 328.38 | 330.05 |
| Dec. | | 315.35 | 316.28 | 316.90 | 317.72 | 318.40 | 319.08 | 319.43 | 320.14 | 321.77 | 322.70 | 323.39 | 324.28 | 325.88 | 326.77 | 328.32 | 329.41 |
| AVE. | | | 315.82 | 316.75 | 317.48 | 318.29 | 318.83 | | 319.87 | 321.21 | 322.02 | 322.83 | 323.93 | 325.27 | 326.15 | 327.29 | 329.51 |

| | 1974 | 1975 | 1976 | 1977 | 1978 | 1979 | 1980 | 1981 | 1982 | 1983 | 1984 | 1985 | 1986 | 1987 | 1988 | 1989 |
|---|---|---|---|---|---|---|---|---|---|---|---|---|---|---|---|---|
| Jan. | 329.29 | 330.34 | 331.69 | 332.87 | 334.91 | 336.17 | 337.96 | 339.17 | 340.69 | 341.31 | 343.64 | 344.91 | 346.23 | 347.95 | 350.27 | 352.57 |
| Feb. | 329.97 | 330.66 | 331.81 | 332.65 | 334.63 | 335.99 | 337.60 | 339.70 | 340.84 | 341.74 | 343.72 | 345.21 | 346.17 | 347.68 | 350.83 | |
| March | 329.98 | 330.53 | 331.95 | 333.17 | 335.11 | 336.42 | 338.50 | 339.82 | 341.13 | 341.52 | 343.67 | 345.83 | 346.26 | 347.80 | 350.48 | |
| April | 330.06 | 330.71 | 331.94 | 333.44 | 335.11 | 336.23 | 338.07 | 339.82 | 340.86 | 342.22 | 344.30 | 345.59 | 346.79 | 348.14 | 350.77 | |
| May | 329.97 | 330.83 | 331.73 | 333.58 | 334.82 | 336.27 | 338.24 | 339.67 | 340.88 | 342.48 | 344.14 | 345.61 | 346.87 | 348.37 | 350.84 | |
| June | 329.79 | 331.11 | 331.87 | 333.76 | 335.37 | 336.75 | 338.64 | 339.68 | 340.77 | 342.72 | 344.21 | 345.63 | 346.82 | 348.48 | 351.07 | |
| July | 330.15 | 330.86 | 332.03 | 333.88 | 335.48 | 336.67 | 338.52 | 339.42 | 340.98 | 342.90 | 344.33 | 345.46 | 346.72 | 348.25 | 351.31 | |
| Aug. | 330.37 | 331.04 | 331.95 | 333.75 | 335.68 | 337.09 | 338.64 | 339.45 | 340.84 | 343.41 | 344.34 | 345.73 | 346.91 | 348.97 | 351.55 | |
| Sept. | 330.22 | 331.36 | 332.13 | 334.41 | 335.62 | 336.77 | 338.78 | 339.59 | 340.88 | 342.79 | 344.02 | 346.06 | 347.82 | 349.44 | 351.76 | |
| Oct. | 330.40 | 331.38 | 332.00 | 334.22 | 335.64 | 336.98 | 339.14 | 340.00 | 341.03 | 343.17 | 344.55 | 346.03 | 347.40 | 349.60 | 352.18 | |
| Nov. | 330.36 | 331.40 | 332.23 | 334.34 | 335.87 | 337.25 | 339.07 | 340.34 | 341.26 | 343.16 | 344.99 | 346.27 | 347.70 | 349.82 | 352.15 | |
| Dec. | 330.35 | 331.54 | 332.47 | 334.63 | 335.74 | 337.53 | 339.01 | 340.42 | 341.30 | 343.81 | 345.03 | 346.38 | 347.73 | 349.79 | 352.20 | |
| AVE. | 330.08 | 330.98 | 331.98 | 333.73 | 335.33 | 336.68 | 338.51 | 339.76 | 340.95 | 342.60 | 344.24 | 345.72 | 346.95 | 348.69 | 351.28 | |

| | 1957 | 1958 | 1959 | 1960 | 1961 | 1962 | 1963 | 1964 | 1965 | 1966 | 1967 | 1968 | 1969 | 1970 | 1971 | 1972 | 1973 |
|---|---|---|---|---|---|---|---|---|---|---|---|---|---|---|---|---|---|
| South Pole | | | | | | | | | | | | | | | | | |
| Jan. | | | 314.97 | | | 317.33 | 318.02 | | | 320.23 | | 321.41 | 322.28 | 323.59 | 324.68 | | 326.63 |
| Feb. | | | 315.24 | | | 317.39 | 318.00 | | 318.82 | 320.14 | 321.15 | | | 323.70 | 324.77 | | 326.36 |
| March | | 314.49 | 315.29 | | | 317.29 | 317.72 | | 318.83 | 320.31 | | | 321.95 | 323.73 | 324.62 | 325.35 | 326.68 |
| April | | | | | | 317.32 | 318.12 | | 318.91 | 320.55 | 321.10 | 321.86 | 321.93 | 323.94 | 324.75 | 325.44 | 327.11 |
| May | | | | | 316.93 | 317.32 | 318.41 | | 319.04 | 320.84 | 321.17 | 321.64 | 322.17 | 323.97 | 324.86 | 325.49 | 327.31 |
| June | 313.39 | 314.55 | | 316.40 | 316.89 | 317.29 | 318.26 | | | 320.50 | 321.01 | 321.50 | 322.26 | 324.24 | 324.97 | 325.89 | 327.50 |
| July | | | | 316.51 | 316.78 | 317.12 | 318.10 | | 319.23 | | 320.90 | 321.34 | 322.49 | 324.31 | 324.99 | 325.96 | 327.57 |
| Aug. | | | 315.58 | 316.34 | 316.95 | 317.23 | 317.96 | | 319.25 | 320.64 | 321.40 | | 322.55 | 324.27 | | 325.65 | 327.94 |
| Sept. | 313.33 | 314.77 | 315.66 | | 317.11 | 317.50 | 317.82 | | | 320.75 | 321.47 | | 322.91 | 324.79 | 325.13 | 325.89 | 328.04 |
| Oct. | | | | | 317.15 | | 318.41 | | | 320.85 | 321.18 | | 322.72 | 324.54 | | 326.12 | 327.95 |
| Nov. | | | 315.86 | | 317.39 | | | | 319.67 | 321.05 | 321.31 | | 322.86 | 324.70 | 325.20 | 326.40 | 328.04 |
| Dec. | 314.15 | | | | 317.34 | 318.30 | | | 319.93 | 320.72 | 321.43 | 322.30 | | | | 326.45 | 328.22 |
| AVE. | | | | | | | | | | | | | | | | | 327.44 |

TABLE A.5. Seasonally Adjusted Concentration of Atmospheric $CO_2$ at Mauna Loa Observatory, Hawaii and the South Pole - continued

| MONTH | YEAR | | | | | | | | | | | | | | | |
|---|---|---|---|---|---|---|---|---|---|---|---|---|---|---|---|---|
| | 1974 | 1975 | 1976 | 1977 | 1978 | 1979 | 1980 | 1981 | 1982 | 1983 | 1984 | 1985 | 1986 | 1987 | 1988 | 1989 |
| Jan. | 328.18 | 328.77 | 330.16 | 331.14 | 332.72 | 333.89 | 335.94 | 337.64 | | 339.73 | 341.93 | 342.88 | 344.53 | 345.81 | 348.21 | 349.87 |
| Feb. | 328.26 | 329.08 | 330.19 | 331.19 | 332.90 | 334.23 | 335.94 | 337.68 | 338.86 | 340.06 | | 343.04 | 344.84 | 346.06 | 348.36 | |
| March | 328.40 | 329.18 | 330.24 | 331.19 | 333.17 | 334.18 | | 337.80 | 338.76 | 340.24 | 342.10 | 343.13 | 344.94 | 346.20 | 348.37 | |
| April | 328.18 | 329.23 | 329.94 | 331.63 | 333.29 | 334.49 | 336.41 | 337.86 | 339.04 | 340.65 | 342.18 | 343.13 | 345.01 | 346.52 | 348.66 | |
| May | 328.21 | 329.13 | 330.14 | 331.61 | | 334.56 | 336.44 | 337.90 | 339.23 | 340.87 | 342.11 | 343.38 | 344.97 | 346.51 | 348.68 | |
| June | 327.95 | 329.14 | 330.06 | 331.70 | 333.46 | 334.62 | 336.99 | 338.25 | 339.28 | 341.10 | 342.12 | 343.57 | 345.16 | 346.76 | 348.78 | |
| July | 328.29 | 329.18 | 330.29 | 331.88 | 333.65 | 334.98 | 337.28 | 338.24 | 339.17 | 341.23 | 342.62 | 343.77 | 345.40 | 347.07 | 348.98 | |
| Aug. | 328.22 | 329.35 | 330.54 | 331.98 | 333.80 | 335.23 | 337.04 | 338.26 | 339.61 | 341.37 | 342.67 | 344.01 | 345.44 | 347.14 | 349.13 | |
| Sept. | 328.28 | 329.55 | 330.71 | 332.18 | 334.04 | 335.17 | 337.15 | 338.09 | 339.58 | 341.58 | 342.70 | 344.13 | 345.45 | 347.34 | 349.04 | |
| Oct. | 328.36 | 329.87 | 331.01 | 332.38 | 334.10 | 335.28 | 337.16 | 338.41 | 339.59 | 341.52 | 342.72 | 344.18 | 345.39 | 347.35 | 349.17 | |
| Nov. | 328.56 | 329.88 | 331.17 | 332.73 | 333.99 | 335.78 | 337.37 | 338.26 | 339.43 | 341.93 | 342.69 | 344.16 | 345.55 | 347.59 | 349.30 | |
| Dec. | 328.62 | 329.89 | 331.04 | 332.79 | 333.91 | 335.64 | 337.64 | 338.50 | 339.55 | 341.94 | 342.73 | 344.23 | 345.64 | 347.93 | 349.49 | |
| AVE. | 328.29 | 329.36 | 330.46 | 331.87 | | 334.84 | | 338.07 | | 341.02 | | 343.63 | 345.19 | 346.86 | 348.85 | |

TABLE A.6. Global Average Concentration of Atmospheric $CO_2$ (in ppm) since 1740

| Year of Decade: Decade | (0) | (1) | (2) | (3) | (4) | (5) | (6) | (7) | (8) | (9) |
|---|---|---|---|---|---|---|---|---|---|---|
| | Annual Values Based on Air Collected in Ice Cores[a] | | | | | | | | | |
| 1740 | 276.92 | 276.98 | 277.03 | 277.09 | 277.15 | 277.20 | 277.26 | 277.32 | 277.38 | 277.43 |
| 1750 | 277.48 | 277.54 | 277.59 | 277.64 | 277.68 | 277.72 | 277.77 | 277.80 | 277.84 | 277.88 |
| 1760 | 277.92 | 277.96 | 278.00 | 278.04 | 278.09 | 278.14 | 278.19 | 278.25 | 278.31 | 278.37 |
| 1770 | 278.44 | 278.50 | 278.57 | 278.64 | 278.71 | 278.78 | 278.86 | 278.93 | 279.01 | 279.08 |
| 1780 | 279.16 | 279.24 | 279.32 | 279.41 | 279.49 | 279.58 | 279.67 | 279.76 | 279.85 | 279.95 |
| 1790 | 280.05 | 280.15 | 280.26 | 280.36 | 280.47 | 280.58 | 280.70 | 280.81 | 280.93 | 281.05 |
| 1800 | 281.17 | 281.29 | 281.41 | 281.53 | 281.65 | 281.77 | 281.88 | 282.00 | 282.12 | 282.24 |
| 1810 | 282.36 | 282.48 | 282.60 | 282.72 | 282.83 | 282.95 | 283.06 | 283.18 | 283.28 | 283.39 |
| 1820 | 283.50 | 283.61 | 283.71 | 283.82 | 283.92 | 284.03 | 284.14 | 284.24 | 284.35 | 284.46 |
| 1830 | 284.57 | 284.68 | 284.79 | 284.90 | 285.02 | 285.14 | 285.26 | 285.38 | 285.51 | 285.64 |
| 1840 | 285.78 | 285.92 | 286.06 | 286.20 | 286.35 | 286.49 | 286.63 | 286.78 | 286.92 | 287.06 |
| 1850 | 287.20 | 287.33 | 287.46 | 287.59 | 287.72 | 287.84 | 287.96 | 288.08 | 288.19 | 288.30 |
| 1860 | 288.41 | 288.52 | 288.62 | 288.73 | 288.83 | 288.94 | 289.05 | 289.16 | 289.28 | 289.39 |
| 1870 | 289.52 | 289.64 | 289.77 | 289.90 | 290.04 | 290.19 | 290.34 | 290.50 | 290.66 | 290.83 |
| 1880 | 291.00 | 291.18 | 291.36 | 291.54 | 291.74 | 291.93 | 292.13 | 292.33 | 292.54 | 292.75 |
| 1890 | 292.96 | 293.18 | 293.41 | 293.64 | 293.87 | 294.10 | 294.34 | 294.58 | 294.83 | 295.09 |
| 1900 | 295.34 | 295.61 | 295.88 | 296.17 | 296.47 | 296.78 | 297.10 | 297.44 | 297.77 | 298.11 |
| 1910 | 298.46 | 298.80 | 299.14 | 299.49 | 299.84 | 300.18 | 300.53 | 300.88 | 301.24 | 301.60 |
| 1920 | 301.96 | 302.32 | 302.69 | 303.06 | 303.43 | 303.79 | 304.14 | 304.48 | 304.81 | 305.13 |
| 1930 | 305.44 | 305.74 | 306.03 | 306.32 | 306.59 | 306.86 | 307.13 | 307.39 | 307.65 | 307.90 |
| 1940 | 308.14 | 308.38 | 308.62 | 308.88 | 309.14 | 309.42 | 309.71 | 310.01 | 310.34 | 310.68 |
| 1950 | 311.04 | 311.41 | 311.81 | 312.23 | 312.67 | 313.14 | | | | |

TABLE A.6. Global Average Concentration of Atmospheric $CO_2$ since 1740 -- continued

| MONTH | YEAR | | | | | | | | | | | |
|---|---|---|---|---|---|---|---|---|---|---|---|---|
| | 1955 | 1956 | 1957 | 1958 | 1959 | 1960 | 1961 | 1962 | 1963 | 1964 | 1965 | 1966 |
| | Monthly Values of Direct Measurements, Seasonally Adjusted[b] | | | | | | | | | | | |
| Jan. | | 313.75 | 313.66 | 314.33 | 315.25 | 316.22 | 316.81 | 317.64 | 318.26 | 318.75 | 319.12 | 320.38 |
| Feb. | | 313.78 | 313.65 | 314.43 | 315.31 | 316.30 | 316.87 | 317.68 | 318.32 | 318.79 | 319.17 | 320.52 |
| March | | 313.80 | 313.66 | 314.53 | 315.38 | 316.38 | 316.94 | 317.71 | 318.38 | 318.83 | 319.22 | 320.64 |
| April | | 313.81 | 313.67 | 314.63 | 315.45 | 316.46 | 317.01 | 317.75 | 318.42 | 318.87 | 319.29 | 320.75 |
| May | | 313.82 | 313.70 | 314.72 | 315.52 | 316.52 | 317.08 | 317.78 | 318.46 | 318.90 | 319.37 | 320.84 |
| June | 313.45 | 313.81 | 313.75 | 314.80 | 315.60 | 316.57 | 317.16 | 317.83 | 318.49 | 318.94 | 319.46 | 320.92 |
| July | 313.51 | 313.80 | 313.81 | 314.88 | 315.69 | 316.61 | 317.24 | 317.88 | 318.52 | 318.96 | 319.57 | 320.99 |
| Aug. | 313.56 | 313.78 | 313.88 | 314.95 | 315.77 | 316.64 | 317.32 | 317.93 | 318.55 | 318.99 | 319.69 | 321.05 |
| Sept. | 313.60 | 313.75 | 313.96 | 315.02 | 315.86 | 316.66 | 317.40 | 318.00 | 318.58 | 319.01 | 319.82 | 321.11 |
| Oct. | 313.64 | 313.73 | 314.04 | 315.08 | 315.95 | 316.69 | 317.47 | 318.06 | 318.62 | 319.04 | 319.96 | 321.16 |
| Nov. | 313.68 | 313.70 | 314.13 | 315.13 | 316.04 | 316.72 | 317.53 | 318.14 | 318.66 | 319.06 | 320.10 | 321.21 |
| Dec. | 313.72 | 313.68 | 314.23 | 315.19 | 316.13 | 316.76 | 317.59 | 318.20 | 318.70 | 319.09 | 320.24 | 321.26 |

| | 1967 | 1968 | 1969 | 1970 | 1971 | 1972 | 1973 | 1974 | 1975 | 1976 | 1977 | 1978 |
|---|---|---|---|---|---|---|---|---|---|---|---|---|
| Jan. | 321.31 | 321.94 | 322.76 | 323.98 | 325.29 | 325.96 | 327.56 | 329.04 | 329.64 | 330.79 | 331.94 | 333.79 |
| Feb. | 321.35 | 322.00 | 322.83 | 324.12 | 325.32 | 326.03 | 327.75 | 329.06 | 329.73 | 330.86 | 332.08 | 333.93 |
| March | 321.39 | 322.06 | 322.90 | 324.27 | 325.36 | 326.11 | 327.94 | 329.07 | 329.82 | 330.92 | 332.24 | 334.06 |
| April | 321.42 | 322.12 | 322.97 | 324.41 | 325.40 | 326.20 | 328.14 | 329.08 | 329.92 | 330.98 | 332.39 | 334.19 |
| May | 321.46 | 322.18 | 323.04 | 324.55 | 325.45 | 326.30 | 328.33 | 329.10 | 330.01 | 331.05 | 332.55 | 334.32 |
| June | 321.51 | 322.25 | 323.13 | 324.68 | 325.51 | 326.41 | 328.51 | 329.14 | 330.11 | 331.12 | 332.72 | 334.43 |
| July | 321.56 | 322.32 | 323.23 | 324.81 | 325.57 | 326.54 | 328.66 | 329.18 | 330.21 | 331.21 | 332.88 | 334.54 |
| Aug. | 321.62 | 322.40 | 323.34 | 324.93 | 325.64 | 326.68 | 328.79 | 329.23 | 330.31 | 331.31 | 333.04 | 334.64 |
| Sept. | 321.68 | 322.47 | 323.45 | 325.04 | 325.70 | 326.84 | 328.89 | 329.30 | 330.42 | 331.42 | 333.20 | 334.73 |
| Oct. | 321.75 | 322.54 | 323.58 | 325.12 | 325.77 | 327.01 | 328.96 | 329.37 | 330.52 | 331.54 | 333.35 | 334.82 |
| Nov. | 321.81 | 322.62 | 323.71 | 325.19 | 325.83 | 327.18 | 329.00 | 329.46 | 330.62 | 331.66 | 333.50 | 334.90 |
| Dec. | 321.88 | 322.69 | 323.84 | 325.25 | 325.90 | 327.37 | 329.03 | 329.55 | 330.71 | 331.80 | 333.65 | 334.98 |

| | 1979 | 1980 | 1981 | 1982 | 1983 | 1984 | 1985 | 1986 | 1987 | 1988 | 1989 |
|---|---|---|---|---|---|---|---|---|---|---|---|
| Jan. | 335.07 | 336.82 | 338.47 | 339.56 | 340.74 | 342.79 | 344.02 | 345.42 | 346.83 | 349.13 | 351.05 |
| Feb. | 335.16 | 336.99 | 338.56 | 339.68 | 340.93 | 342.89 | 344.14 | 345.54 | 346.97 | 349.32 | |
| March | 335.27 | 337.16 | 338.65 | 339.78 | 341.13 | 342.99 | 344.26 | 345.66 | 347.12 | 349.51 | |
| April | 335.39 | 337.33 | 338.73 | 339.88 | 341.34 | 343.08 | 344.38 | 345.77 | 347.29 | 349.68 | |
| May | 335.52 | 337.49 | 338.80 | 339.97 | 341.56 | 343.17 | 344.51 | 345.89 | 347.46 | 349.85 | |
| June | 335.66 | 337.64 | 338.87 | 340.04 | 341.76 | 343.27 | 344.63 | 346.01 | 347.65 | 350.00 | |
| July | 335.81 | 337.78 | 338.94 | 340.11 | 341.95 | 343.36 | 344.74 | 346.12 | 347.85 | 350.16 | |
| Aug. | 335.97 | 337.91 | 339.02 | 340.18 | 342.13 | 343.46 | 344.86 | 346.24 | 348.06 | 350.31 | |
| Sept. | 336.13 | 338.03 | 339.11 | 340.26 | 342.29 | 343.57 | 344.97 | 346.35 | 348.27 | 350.46 | |
| Oct. | 336.29 | 338.15 | 339.21 | 340.34 | 342.43 | 343.67 | 345.08 | 346.46 | 348.49 | 350.61 | |
| Nov. | 336.46 | 338.26 | 339.32 | 340.45 | 342.56 | 343.79 | 345.19 | 346.58 | 348.71 | 350.76 | |
| Dec. | 336.64 | 338.37 | 339.44 | 340.58 | 342.68 | 343.90 | 345.31 | 346.70 | 348.92 | 350.91 | |

[a]Data from Neftel et al. [1985] and Friedli et al. [1986] were fit to a spline with a standard error, $\sigma$, of 0.50. Entries, in ppm, are for the middle of each year; they are not seasonally adjusted.

[b]From January 1959 to January, 1989, entries, in ppm, are averages of values from spline fits to the measurements at Mauna Loa Observatory and the South Pole. The spline stiffnesses are as in Figures 20 and 21, respectively. For the period prior to 1959, special procedures were used to combine direct and proxy data, as described in the text.

*Appendix B. Sampling Procedures and Data Processing: Isotopic Measurements*

All isotopic data were obtained from samples of $CO_2$ extracted cryogenically from the 5-liter flasks that contained the air samples measured for $CO_2$ concentration by infrared analysis. The $^{13}C/^{12}C$ and $^{18}O/^{16}O$ ratios of the extracted $CO_2$ were determined using a VG Micromass 903 and a VG SIRA 9 spectrometer at the Groningen Isotopic Physics Laboratory. Procedures of analysis were as reported by Mook et al. [1983]. The extraction of the $CO_2$ gas quantitatively from the air removes $N_2O$ together with the $CO_2$. The mass ratios measured by the spectrometer therefore contain a contribution from $N_2O$, present in the original samples at a concentration of approximately 0.3 ppm [Weiss, 1981]. Mook and Van der Hoek [1983] and Mook and Jongsma [1987] have established that the presence of this amount of $N_2O$ produces a shift in $^{13}\delta$ of 0.23‰ towards more positive values relative to standard PDB. They found this shift by redetermining the mass ratios of samples after their passage over hot copper oxide to remove the $N_2O$, and also by measuring synthetic mixtures of $N_2O$ and $CO_2$. Because we are now confident in the magnitude of the $N_2O$ effect, all data are here reported with the influence of $N_2O$ on $^{13}\delta$ removed.

The $N_2O$ correction of 0.23‰ has meanwhile been shown to be applicable for several types of mass spectrometers (U. Siegenthaler, R. Francey, personal communications). In contrast, the correction for contemporary air, computed from theory by assuming equal ionization efficiency and ion yield for $CO_2$ and $N_2O$ with respect to masses 44 and 45, is 0.31‰ [Keeling et al. 1979].

Recently a reappraisal of the isotopic data was carried out by Roeloffzen (thesis, in preparation) resulting in adjustments up to 0.15‰ in some of the earlier data. We have applied these corrections to the data reported here. Previously published data of Mook et al. [1983] and Keeling et al. [1984], as revised, are listed in the report of Keeling et al. [1989]. These data and previously unpublished data will be listed *in toto* by Roeloffzen (thesis in preparation).

At the beginning of the study, in May, 1978, extracted samples for isotopic $CO_2$ measurement were stored in tubes equipped with stopcocks lubricated with Apiezon grease. In May 1979 we began storing samples in tubes equipped with O-ring stopcocks. In June 1982 we began storing samples in glass tubes sealed by a flame. By overlapping the use of each kind of storage tube we established that the samples stored in O-ring equipped tubes are not entirely stable, but show a systematic shift to less negative $^{13}\delta$ values between the time of extraction and analysis. If samples with unusually long storage times are excluded, the average offset is 0.06‰. Tubes with greased stopcocks were found to agree within the precision of measurement with the flamed-off tubes. Data reported by Mook et al. [1983] and Keeling et al. [1984] for samples stored in tubes with greased stopcocks or in flamed-off tubes were corrected to agree with those in O-ring equipped tubes, which at the time were regarded as the most reliable containers. It is now evident from the agreement of the flamed-off tubes with the tubes containing greased stopcocks, and from the evidence of drift in $^{13}\delta$ for samples in O-ring equipped tubes stored for long times, that the latter tubes are the major source of the discrepancies. We have therefore corrected data from these tubes by subtracting 0.06‰ from the $^{13}\delta$ values. This correction is in addition to adding 0.23‰ to $^{13}\delta$ of all samples to remove the influence of $N_2O$.

Isotopic samples analyzed in 1980 after an almost 6-month shutdown of the mass spectrometer, as noted by Keeling et al. [1984, p. 4618] showed an abrupt positive effect in isotopic ratio that only gradually went away. After applying the adjustments of Roeloffzen, noted above, this abrupt shift in ratio is seen to be smaller than before. Accordingly, we have reduced the corrections originally applied to compensate for this shift [see Mook et al. 1983, p. 10921] by 0.05‰, thus to –0.10‰ for isotopic group numbers 18 and 19, to –0.05‰ for group numbers 20–22, and to 0 for group number 23.

The seasonal and interannual variations in $^{13}\delta$ at fixed stations were determined by a function equivalent to equation (A.3) of Appendix A, as used for the concentration data, but with the gain, $\gamma$, set equal to zero because the records are not long enough to establish a change in amplitude to the isotopic seasonal cycle if

TABLE B.1. Globally Averaged Isotopic Ratio, $^{13}\delta$, of Atmospheric $CO_2$ since 1978, Seasonally Adjusted

[Entries (in ‰) are averages of values from spline fits to the measurements at Mauna Loa Observatory and the South Pole. The spline stiffnesses are as in Figures 23 and 24.]

| | YEAR | | | | | | | | | | |
|---|---|---|---|---|---|---|---|---|---|---|---|
| MONTH | 1978 | 1979 | 1980 | 1981 | 1982 | 1983 | 1984 | 1985 | 1986 | 1987 | 1988 |
| Jan. | –7.489 | –7.517 | –7.546 | –7.606 | –7.572 | –7.596 | –7.699 | –7.674 | –7.654 | –7.656 | –7.738 |
| Feb. | –7.493 | –7.519 | –7.555 | –7.606 | –7.569 | –7.602 | –7.705 | –7.668 | –7.652 | –7.661 | –7.748 |
| March | –7.497 | –7.520 | –7.563 | –7.605 | –7.566 | –7.610 | –7.709 | –7.663 | –7.650 | –7.666 | –7.757 |
| April | –7.500 | –7.520 | –7.570 | –7.604 | –7.564 | –7.618 | –7.711 | –7.659 | –7.648 | –7.672 | –7.766 |
| May | –7.503 | –7.519 | –7.578 | –7.602 | –7.565 | –7.627 | –7.711 | –7.656 | –7.646 | –7.679 | –7.774 |
| June | –7.506 | –7.519 | –7.585 | –7.599 | –7.566 | –7.637 | –7.710 | –7.654 | –7.645 | –7.685 | –7.781 |
| July | –7.508 | –7.519 | –7.591 | –7.596 | –7.569 | –7.646 | –7.708 | –7.654 | –7.644 | –7.692 | –7.786 |
| Aug. | –7.509 | –7.520 | –7.596 | –7.592 | –7.572 | –7.656 | –7.704 | –7.654 | –7.645 | –7.699 | –7.791 |
| Sept. | –7.510 | –7.522 | –7.600 | –7.588 | –7.576 | –7.665 | –7.700 | –7.655 | –7.646 | –7.706 | –7.796 |
| Oct. | –7.511 | –7.526 | –7.603 | –7.584 | –7.580 | –7.675 | –7.694 | –7.656 | –7.647 | –7.713 | –7.799 |
| Nov. | –7.512 | –7.532 | –7.605 | –7.580 | –7.585 | –7.684 | –7.687 | –7.656 | –7.649 | –7.720 | –7.803 |
| Dec. | –7.515 | –7.539 | –7.606 | –7.576 | –7.590 | –7.692 | –7.680 | –7.656 | –7.652 | –7.729 | –7.807 |

one is present in the record. The seasonally adjusted data for January 1, 1980 and May 15, 1984 are summarized in Tables 3 and 4. Standard errors of these averaged or smoothed data were determined in the same manner as for the concentration data: i.e., the error attributed to an individual data point, as derived from the spline fits, was divided by the square root of the number of isotopic data points included in one year of record beginning 6 months before the date of the data point. In the case of Raoul Island (one of the Kermadec Islands), however, the record was too short to use this procedure. The isotopic data there exhibit an essentially negligible seasonal variation. Therefore the individual $^{13}\delta$ values were averaged without seasonal adjustment, and the standard deviation in the mean was adopted as the standard error. The records for Fanning and Christmas Islands were combined into a single time series, but the two records are distinguished with respect to the latitudes when the data are plotted versus latitude in Figure 15 since the Fanning isotopic record terminates in 1983 when the Christmas Island isotopic record begins. Seasonally adjusted data for January 1 of 1978 through 1986 are listed in Table 6. The data for 1986 are based on an analysis which includes the most recent provisional data for each station.

The analysis of isotopic data for the FGGE shuttle expedition, originally carried out by Keeling et al. [1984], has been updated to reflect the revised concentration and isotopic data. The originally published tables [loc.cit.] with corrections, have been reproduced in the report of Keeling et al. [1989].

In addition to the isotopic data already discussed, we have considered provisional data for Mauna Loa Observatory and the South Pole through 1988. Seasonally adjusted daily averages, determined in the same manner as in the preparation of Tables 3, 4, and 6, (corresponding to the function $C_{obs\ rem}$ of equation 2.3) were averaged for the two stations to establish approximately global averages. The data, which refer to the 15th of each month, are listed in Table B.1.

## *Appendix C. Methodology of Double Deconvolution*

Deconvolution, in the present context, refers to the solution of the carbon balance equation (6.1) by means of the box-diffusion model for an anomalous net $CO_2$ flux, $F_{rem}$, defined as that part of the observed atmospheric $CO_2$ increase, $dN_a/dt$, not accounted for by either the known industrial $CO_2$ input, $F_{IND}$, or the $CO_2$ uptake by the oceans, $F_{ex}$, as computed by the model. We have further decomposed $F_{rem}$ into biospheric and oceanic parts (see equation (6.2)) by means of isotopic data, employing a model computation which we term "double deconvolution".

Because the $^{13}C$ content of a stable carbon flux in the carbon cycle depends on the direction of flow, it is necessary in this double deconvolution initially to specify the factor $\beta_a$ of equation (5.4) so that the biospheric perturbation fluxes $F_{ab}$ and $F_{ba}$ of equations (5.2) and (5.3) and their difference, $F_{FER}$, are determined before the balance equation is solved. The decomposition is then actually between the oceanic contribution to $F_{rem}$ which we denote as $F_{oc}$, and $F_{DES}$, a $CO_2$ source to the atmosphere from biospheric destruction. We have found, however, that the computed sum

$$F_b = F_{FER} + F_{DES} \tag{C.1}$$

(see equation (5.5)) depends only very weakly on the division between its two components. Therefore, to a good approximation, we may regard the decomposition as being between $F_b$ and $F_{oc}$.

Both the single and double deconvolutions employ the full set of equations for the box-diffusion model as listed in Appendix B of Keeling et al. [1980], a document obtainable on microfiche from the American Geophysical Union, Washington D.C. These equations include an expression for biospheric fertilization, equivalent to equations (5.2) and (5.3), and a biospheric destruction term, $\gamma_b$, identical to $F_{DES}$. For the double deconvolution, the equations were modified by adding the oceanic source term, $F_{oc}$, to the atmospheric stable carbon balance equation and subtracting it from the corresponding surface ocean equation, and similarly for the associated $^{13}C$ flux, which we denote here by the symbol $^*F_{oc}$.

This flux, and the $^{13}C$ flux $^*F_{DES}$ corresponding to $F_{DES}$, have different expressions in the model depending on whether their associated fluxes, $F_{oc}$, and $F_{DES}$, respectively, are positive or negative. If at a given time step $F_{oc}$ is positive, the model computes

$$^*F_{oc} = \alpha_{ma}'\left(\frac{^*N_m}{N_m}\right)F_{oc} \tag{C.2}$$

where $^*N_m$ denotes the mass of $^{13}C$ in the surface ocean corresponding to $N_m$, defined as the mass of stable carbon ($^{12}C + ^{13}C$) in the surface ocean. Isotopic fractionation is provided for by the factor $\alpha_{ma}'$ (see Table 8). If $F_{oc}$ is negative the model computes

$$^*F_{oc} = \alpha_{am}'\left(\frac{^*N_a}{N_a}\right)F_{oc} \tag{C.3}$$

where $^*N_a$ denotes the mass of $^{13}C$ in the atmosphere corresponding to $N_a$, the mass of stable carbon in the atmosphere, and $\alpha_{am}'$ denotes the appropriate isotopic fractionation factor analogous to $\alpha_{ma}'$.

The equations for the flux $^*F_{DES}$ are similarly expressed. If $F_{DES}$ is positive

$$^*F_{DES} = \alpha_{ba}'\left(\frac{^*N_b}{N_b}\right)F_{DES} \tag{C.4}$$

whereas, if $F_{DES}$ is negative

$$^*F_{DES} = \alpha_{ab}'\left(\frac{^*N_a}{N_a}\right)F_{DES} \tag{C.5}$$

The equations of the model were integrated by taking time steps of ⅓ month, starting with an assumed pre-industrial steady state at the beginning of the year 1740. To evaluate $dN_a/dt$ we numerically differentiated a spline fit to seasonally adjusted $CO_2$ concentration data (Mauna Loa Observatory and South Pole records combined) after conversion to mass units by the factor $615.6 \times 10^{12}$ kgC/290 ppm (see Table 8). For the double deconvolution we additionally performed an iterative search by Newton's method [Acton, 1970] at the end of each time step to find the value of $F_{oc}$ that causes the predicted value of the reduced isotopic ratio, $^{13}\delta$, of atmospheric $CO_2$ (see equation 3.1) by the model to agree with a spline fit to the observed values of $^{13}\delta$ after seasonal adjustment.

The derivative required by Newton's method was calculated numerically.

During the double deconvolution, the computed changes in carbon content of the oceans resulting from the additional oceanic flux, $F_{oc}$, cause the model to compute successive values of $F_{ex}$ that differ from those by single deconvolution. To produce a decomposition of $F_{rem}$, consistent with equations (6.1) and (6.2) where $F_{rem}$ is established by single deconvolution, we calculated the total air-sea exchange by both single and double deconvolution, and then corrected $F_{oc}$ by the difference in total exchange as determined by the two deconvolutions. The values of $F_{oc}$ so obtained are almost, but not exactly, independent of the assigned parameters of the box-diffusion model for gas exchange and vertical diffusion.

The decomposition of $F_{rem}$ into biospheric and oceanic parts by our method of double deconvolution is almost unique as $\beta_a$ is varied, provided that the other physical parameters of the oceanic model are fully specified at the outset of the two deconvolutions. If, however, the ocean is allowed to exhibit time varying transport behavior, the proportions of biospheric and oceanic flux in $F_{rem}$ predicted by the model may be different from the results reported here. For example, we found that if the biospheric destruction flux, $F_{DES}$, is specified *a priori* by the curve of Houghton and Woodwell [1989], assuming no biospheric fertilization flux, and the deconvolution of $CO_2$ concentration is then carried out by varying the rate of oceanic $CO_2$ uptake, a considerably larger uptake is compatible with the isotopic data after 1978 than indicated by our double deconvolution. We have not further considered this deconvolution because the variations in rate of oceanic exchange necessary to satisfy it seem unrealistically large.

*Appendix D. Deconvolution with a Three-Dimensional Ocean-Circulation Model*

As a validation of the box diffusion model of the global carbon cycle, we have calculated by deconvolution the function $F_{rem}$ of equation (6.1) using a version of the three-dimensional ocean-circulation carbon cycle model of Maier-Reimer and Hasselmann [1987]. This model is based on an oceanic general circulation model that is driven by observationally derived winds, with temperature and salinity held close to observational values at the ocean surface. The model reproduces large-scale horizontal features of the ocean circulation, for example, the Gulf Stream and the mid-latitude gyres. The natural $^{14}C$ distribution is well represented on average, although the Atlantic Ocean is predicted to be a little too old (less $^{14}C$) and the Pacific too young (more $^{14}C$), because some of the convective deep water formation that should occur in the North Atlantic Ocean instead is simulated to occur in the southern oceans.

The model employs a 72×72 horizontal grid, thus a separation between grid points of about 555 km near the Equator. The equations of fluid dynamics were solved in a nearly geostrophic approximation so as to make possible a time step of one month. There are ten calculational levels where horizontal velocities are defined: at 75, 150, 250, 450, 700, 1000, 2000, 3000, 4000, and 5000 m below the surface. Vertical velocities are specified at levels half way between these calculational levels. Ocean coast lines and depth are realistic, within the limitations of the grid. Since many grid points are in continental areas or under shallow parts of the ocean, the ocean is effectively represented by 27,443 points. Each grid point is treated as the center of a well-mixed compartment which exchanges water and tracers with its neighbors.

Although the general circulation model is seasonal, the carbon cycle simulated by the model employs a yearly averaged oceanic circulation field. The field is as described by Bacastow and Maier-Reimer [submitted to Climate Dynamics] in an extension of the Maier-Reimer and Hasselmann model that includes the effect of the oceanic biota. Convective mixing, however, is parameterized by diffusion, as in the formulation of Maier-Reimer and Hasselmann [1987], whereas Bacastow and Maier-Reimer employ a direct convective mixing adjustment. The atmosphere and terrestrial biosphere are each represented by a single homogeneous reservoir. Integration of the chemical species in the model is by an implicit method in order that a relatively long, one year time step can be used for model initiation. The oceanic biota are modeled to include production of dissolved organic matter, which is advected with the current field, in addition to particulate matter, which falls vertically, as discussed by Bacastow and Maier-Reimer [1989].

The model of the terrestrial biosphere, the transfer coefficient for $CO_2$ from air to sea, (stationary radiocarbon case) and the $^{13}C/^{12}C$ fractionation coefficients are as given in Table 8. The surface

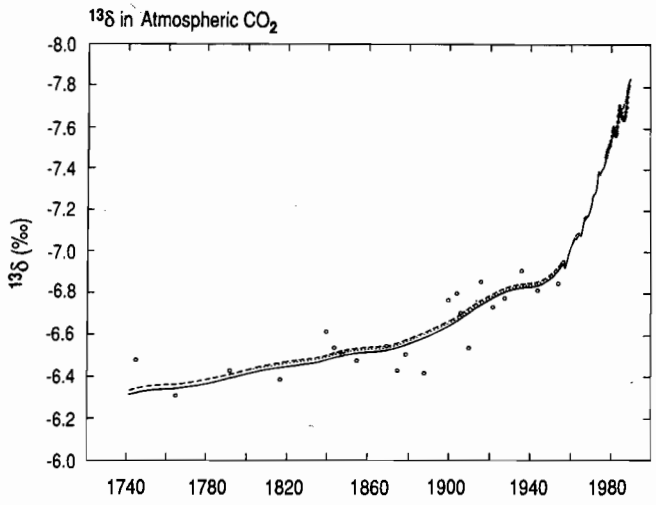


Fig. D.1. Observed and predicted time trend of $^{13}\delta$, in per mil. The data are as plotted in Figure 53. Observations from ice core samples are shown as open squares, and from recent direct measurements as plus marks. The $^{13}\delta$ for each model prediction has been adjusted to the same value in 1978. The prediction of the three-dimensional oceanic circulation model is indicated by the upper, dotted curve. The middle dashed curve shows, for comparison, a prediction of the box diffusion model calibrated by bomb radiocarbon (vertical diffusion coefficient of 7685 $m^2$ $yr^{-1}$ and atmosphere-ocean exchange time of 6.87 yr). This prediction was shown previously as the dashed curve in Figure 53. The solid, lower curve indicates an additional prediction of the box diffusion model calibrated by stationary radiocarbon (vertical diffusion coefficient of 4005 $m^2$ $yr^{-1}$ and atmosphere-ocean exchange time of 7.87 yr).

ocean reservoir depths, however, are 112.5 m rather than the 75 m used in the box diffusion model. The chemical concentrations in the model were initialized for 1200-model years at one step per year, starting with values obtained from an earlier run with slightly different parameters and with a version of the model that employed a direct convective mixing adjustment. The concentrations were then initialized for 100 more model years at 6 steps per year, during which time the atmospheric $CO_2$ concentration increased only 0.09 ppm, to 296.06 ppm. The resulting concentrations were assumed to represent steady state conditions for the year 1740, the starting time for the deconvolution. The difference between the initial atmospheric concentration of 296.06 ppm in the model and the observed concentration in 1740 of 276.93 ppm does not have much effect on either the deconvolved $F_{rem}$ or the change in $^{13}\delta$ of atmospheric $CO_2$. The deconvolution was run at 6 steps per year.

The deconvolution of the atmospheric $CO_2$ record with the ocean circulation carbon cycle model was carried out essentially as described for the box diffusion model. We did not attempt a double deconvolution because the $^{13}\delta$ predictions are almost indistinguishable from the predictions of the box diffusion model, calibrated either with bomb radiocarbon or stationary radiocarbon, as shown in Figures D.1 and D.2.

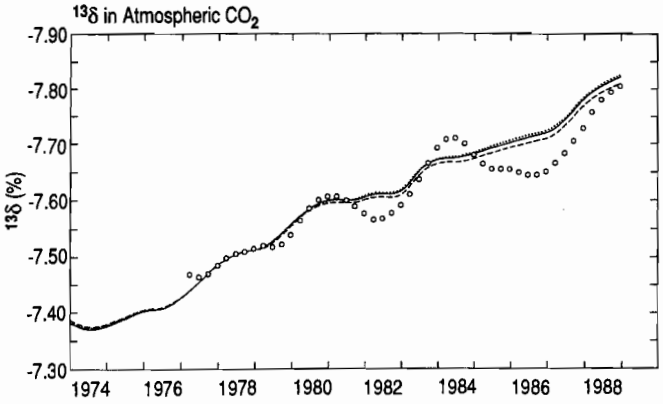


Fig. D.2. Observed and predicted time trend of $^{13}\delta$, in per mil, showing details of the plot of Figure D.1 for the recent period. Direct measurements are again shown as plus marks. The solid curve, upper curve after 1978, again shows a prediction of the box diffusion model calibrated by stationary radiocarbon. The predictions of the oceanic circulation model and the box diffusion model calibrated by bomb radiocarbon (shown below the curve for stationary radiocarbon) are indistinguishable.

*Acknowledgments.* The extensive study, discussed here and in the three companion articles, was made possible by the generous support of the Electric Power Research Institute (EPRI), and the encouragement of its vice president Duane Spencer. His advocacy of a long range rôle for the electric power industry in studying the environmental impacts of fossil fuel combustion provided the foundation for our study. Also, his personal participation, through discussions and meetings, and the initial substantial commitment of EPRI to fund this project for 3½ years, were vital factors in our ability to deal with the subject comprehensively. We were able at the outset to plan the use of our resources with a long-range view and without concern that the effort might be questioned before any clear-cut positive results could emerge. We also thank Alan Hansen, Glenn Hilst, Leonard Levin, and Ralph Perhac of EPRI who have guided our study and patiently granted us even more time to complete the reporting of our model results.

We are further indebted to William Nierenberg who, while director of the Scripps Institution of Oceanography, encouraged the study of atmospheric $CO_2$ as a result of his concern for improving the understanding of the earth's climate and its impact by man. He shared with us his personal inspiration, gave us useful advice, and made available, as part of the Scripps Climate Research Program, a new dedicated main-frame computer which turned out to be essential to the success of our modeling effort.

In this first article we have assembled data from observations extending for more than 30 years. In addition to the support of the Electric Power Research Institute with respect to costs of reassessing these data, we thank the U.S. government agencies which provided the funds to make these measurements in the first place. Foremost of these agencies is the National Science Foundation (NSF) which funded the majority of our studies of atmospheric $CO_2$ since 1956. We are also grateful for additional financial support in recent years from the Department of Energy and from the National Oceanic and Atmospheric Administration (NOAA). We are also indebted to the Antarctic Research Program of NSF and to NOAA and its antecedent agencies, the U.S. Weather Bureau and the Environmental Sciences Services Administration, for extensive logistic support and to Environment Canada, the Division of Scientific and Industrial Research of the Government of New Zealand, and NOAA for assistance in sampling and operation of field instruments.

We cannot adequately thank here all of the persons who contributed to the reported measurements. In addition to those mentioned in previous publications there are others, too numerous to cite, but all of whom deserve credit for their assistance. We specifically thank Robert Born and Lee Waterman for collecting air samples on Nova and Eastropac Expedition in 1967 and 1968, J. Tiaoni and John Bryden for collecting air samples at Fanning and Christmas Islands, respectively, and Peter Guenther and Frederick Vanwoy for help in collecting samples during the FGGE Shuttle Expedition in 1979 and 1980. We also thank Steve O'Neill of the Baring Head Light House, New Zealand, for his care and interest while assisting in the sampling program there for more than a decade, John Kelley of the University of Alaska for helping us in a reappraisal of the continuous measurements of atmospheric $CO_2$ which he had made at Point Barrow, Alaska, from 1961 to 1967, and Martin Manning of the Institute of Nuclear Studies in New Zealand for making available unpublished continuous data for Baring Head. We thank Neil Trivett of Atmospheric Environment Service of Canada for initiating and sustaining sampling for us at Alert Station on Ellesmere Island and for his sympathetic encouragement of our field program.

Deserving of special mention are the personnel of NOAA who arranged for and carried out a major part of the sampling reported here, and who have shared with us their experiences and expertise on all aspects of instrumentation and calibration. We are most indebted to James Peterson, director of the Geophysical Monitoring for Climatic Change (GMCC) program in Boulder, Colorado, for fostering a spirit of cooperation and promoting our joint participation in atmospheric $CO_2$ measurements far beyond the requirements of his office.

Of the staff at the Mauna Loa Observatory who assisted us in operating our continuous analyzer there, we are especially grateful

to John Chin who has carried out the major duties almost without interruption since 1964, a truly remarkable contribution since he has also operated a second, and sometimes a third, $CO_2$ analyzer for NOAA since 1969.

We thank James Hansen and Sergej Lebedeff of the Goddard Institute of Space Studies, Abraham Oort of the Geophysical Fluid Dynamic Laboratory, Princeton, and Richard Houghton and George Woodwell of the Woods Hole Research Center for supplying us with unpublished data and sharing with us their views of global change. We thank Gerald Meehl and Harry van Loon of the National Center for Atmospheric Research for enlightening discussions of El Niño and the Southern Oscillation. We are grateful to Eric Sundquist of the U.S. Geological Survey for a careful and highly constructive review of the entire article.

It is with great sadness that we are able to thank Ralph Rotty only posthumously for his assistance in documenting the rôle of fossil fuel combustion in the carbon cycle. His sustained effort to obtain the correct global releases of $CO_2$ continued until the last day in which he could work, as we can attest because on that day he sent to us his most recent updated data.

At the Scripps Institution of Oceanography we thank David Moss, our development engineer, for carrying out many aspects of the field logistics and for maintaining the complex equipment used in our study, Peter Guenther for additional field logistic assistance and general advice, and Justin Lancaster for his critical review of the text of this article. Alexander Adams, Alane Carter, Blanch Christman, Peter Guenther, and Tom Harris analyzed the flask samples at the La Jolla laboratory. The complicated preparation of the text of these four articles was carried out by Katy Piper and Suzie Conklin.

Finally, we are grateful to Dr. David Peterson, Dr. Jurate Landwehr, Jeanne DiLeo-Stevens, and Martha Nichols of the United States Geological Survey for facilitating the publication of these articles in the present monograph.

Computer time for three-dimensional ocean model runs was provided by the San Diego Supercomputer Center. Financial support was from the Electric Power Research Institute, via contracts RP2333–1 and RP8000–7; The National Science Foundation, grants ATM83–10667 and ATM85–16939; the Carbon Research Division of the U.S. Department of Energy, contracts DE–AT03–82ER60032 and DE–AC05–840R21400 and subcontracts 19X–89692C, 19X–SB004C, and 19X–43386C with the Martin Marietta Energy Systems Inc.; and the U.S. National Oceanic and Atmospheric Administration, contracts NA83RAC00034, NA84RAA03753 and NA84RAA05440. We acknowledge the support of the Max-Planck Institute for Meteorology in Hamburg for the employment of coauthor M. Heimann since 1985.

## References

Acton, F. S., Chapter 2 in *Numerical Methods That Work,* Harper and Row, New York, 1970.

Bacastow, R. B., Modulation of atmospheric carbon dioxide by the Southern Oscillation, *Nature,* v. 261, p. 116–118, 1976.

Bacastow, R., Dip in the atmospheric $CO_2$ level during the mid-1960's, *Journal of Geophysical Research,* v. 84, p. 3108–3114, 1979.

Bacastow, R. B., Numerical evaluation of the evasion factor, in *SCOPE 16: Carbon Cycle Modeling*, edited by B. Bolin, p. 95–101, John Wiley and Sons, Chichester, 1981.

Bacastow, R. B., and Björkström, A., Comparison of ocean models for the carbon cycle, in *SCOPE 16: Carbon Cycle Modelling,* edited by B. Bolin, p. 29–79, John Wiley and Sons, Chichester, 1981.

Bacastow, R. B., and Keeling, C. D., Models to predict future atmospheric $CO_2$ concentrations, *Workshop on the Global Effects of Carbon Dioxide from Fossil Fuels,* edited by W. P. Elliott and L. Machta, p. 72–90, U.S. Department of Energy, 1979.

Bacastow, R. B., and Keeling, C. D., Atmospheric carbon dioxide concentration and the observed airborne fraction, in *SCOPE 16: Carbon Cycle Modelling,* edited by B. Bolin, p. 103–112, John Wiley and Sons, Chichester, 1981.

Bacastow, R., and Maier-Reimer, E., Modeling oceanic new production, in *Interaction of the Global Carbon and Climate Systems,* edited by R. Keir, Electric Power Research Institute Report, in press, 1989.

Bacastow, R. B., Adams, J. A., Keeling, C. D., Moss, D. J., Whorf, T. P., and Wong, C. S., Atmospheric carbon dioxide, the Southern Oscillation, and the weak 1975 El Niño, *Science,* v. 210, p. 66–68, 1980.

Bacastow, R. B., Keeling, C. D., and Whorf, T. P., Seasonal amplitude increase in atmospheric $CO_2$ concentration at Mauna Loa, Hawaii, 1959–1982, *Journal of Geophyical Research,* v. 90, p. 10529–10540, 1985.

Bathen, K. H., On the seasonal changes in depth of the mixed layer in the North Pacific Ocean, *Journal of Geophysical Research,* v. 77, p. 7138–7150, 1972.

Beardsmore, D. J., and Pearman, G. I., Atmospheric carbon dioxide measurements in the Australian region: data from surface observatories, *Tellus,* v. 39B, p. 42–66, 1987.

Bolin B., editor, *SCOPE 16: Carbon Cycle Modelling,* 390 p., John Wiley and Sons, Chichester, 1981.

Bolin, B., and Keeling, C. D., Large-scale atmospheric mixing as deduced from the seasonal and meridional variations of carbon dioxide, *Journal of Geophysical Research,* v. 68, p. 3899–3920, 1963.

Bolin, B., Björkström, A., Keeling, C. D., Bacastow, R., and Siegenthaler, U., Carbon cycle modelling, in *SCOPE 16: Carbon Cycle Modelling,* edited by B. Bolin, p. 1–28, John Wiley and Sons, Chichester, 1981.

Bradley, R. S., Diaz, H. F., Eischeid, J. K., Jones, P. D., Kelly, P. M., and Goodess, C. M., Precipitation fluctuations over northern hemisphere land areas since the mid-19th century, *Science,* v. 237, p. 171–175, 1987.

Chavez, F. P., and Barber, R. T., Plankton production during El Niño, in *International Conference on the TOGA Scientific Programme,* World Climate Research Publications Series No. 4, p. 23–32, World Meteorological Organization, Geneva, 1985.

Cline, A. K., Scalar- and planar-valued curve fitting using splines under tension, *Commun. ACM 17,* p. 218–220, 1974.

Conway, T. J., Tans, P., Waterman, L. S., Thoning, K. W., Masarie, K. A., and Gammon, R. H., Atmospheric carbon dioxide measurements in the remote global troposphere, 1981–1984, *Tellus,* v. 40B, p. 81–115, 1988.

Craig, H., Isotopic standards for carbon and oxygen and correction factors for mass-spectrometric analysis of carbon dioxide, *Geochimica et Cosmochimica Acta,* v. 12, p. 133–149, 1957.

Craig, H., Horibe, Y., and Sowers, T., Gravitational separation of

gases and isotopes in polar ice caps, *Science*, v. 242, p. 1675–1678, 1988.

Danckwerts, P. V., *Gas-liquid reactions*, 276 p., McGraw-Hill, New York, 1970.

de Boor, C., *A Practical Guide to Splines*, 392 p., Springer-Verlag, New York, 1978.

Degens, E. T., Biogeochemistry of stable carbon isotopes, in *Organic Geochemistry, Methods and Results*, edited by G. Eglinton and M. T. J. Murphy, p. 304–439, Springer-Verlag, Berlin, 1969.

Detwiler, R. P., and Hall, C. A. S., Tropical forests and the global carbon cycle, *Science*, v. 239, p. 42–47, 1988.

Dickson, A. G., and Millero, F. J., A comparison of the equilibrium constants for the dissociation of carbonic acid in sea water media, *Deep Sea Research*, v. 34, p. 1733–1743, 1987.

Donguy, J. R., Henin, C., Morliere, A., and Rebert, J. P., Appearances in the Western Pacific of phenomena induced by El Niño in 1979–80, *Tropical Ocean-Atmosphere Newsletter*, no. 10, p. 1–2, 1982.

Draper, N. R., and Smith, H., *Applied Regression Analysis*, 709 p., John Wiley and Sons, New York, NY, 1981.

Enting, I. G., The interannual variation in the seasonal cycle of carbon dioxide concentration at Mauna Loa, *Journal of Geophysical Research*, v. 92, p. 5497–5504, 1987.

Enting, I. G., and Pearman, G. I., *Description of a one-dimensional global carbon cycle model*, CSIRO Division of Atmospheric Physics, Technical Paper, no. 42, 1982.

Enting, I. G., and Pearman, G. I., *Refinements to a one-dimensional carbon cycle model*, CSIRO Division of Atmospheric Research, Technical Paper, no. 3, 1983.

Enting, I. G., and Pearman, G. I., The use of observations in calibrating and validating carbon cycle models, in *The Changing Carbon Cycle: A Global Analysis, edited by J. R. Trabalka and D. E. Reichle, p. 425–458, Springer-Verlag, New York, 1986.*

Enting, I. G., and Mansbridge, J. V., The incompatibility of ice-core $CO_2$ data with reconstruction of biotic $CO_2$ sources, *Tellus*, v. 39B, p. 318–325, 1987.

Enting, I. G., and Pearman, G. I., Description of a one-dimensional carbon cycle model calibrated using techniques of constrained inversion, *Tellus*, v. 39B, p. 459–476, 1987.

Esser, G., Sensitivity of global carbon pools and fluxes to human and potential climatic impacts, *Tellus*, v. 39B, p. 245–260, 1987.

Feely, R. A., Gammon, R. H., Taft, B. A., Pullen, P. E., Waterman, L. S., Conway, T. J., Gendron, J. F., and Wisegarver, D. P., Distribution of chemical tracers in the eastern equatorial Pacific during and after the 1982–1983 El Niño/Southern Oscillation event, *Journal of Geophysical Research*, v. 92, p. 6545–6558, 1987.

Francey, R., Cape Grim carbon isotope measurements - a preliminary assessment, *Journal of atmospheric Chemistry*, v. 3, p. 247–260, 1985.

Fraser, P. J., Pearman, G. I., and Hyson, P., The global distribution of atmospheric carbon dioxide: 2. A review of provisional background observations, 1978–1980, *Journal of Geophysical Research*, v. 88, p. 3591–3598, 1983.

Friedli, H., Lötscher, H., Oeschger, H., Siegenthaler, U., and Stauffer, B., Ice core record of the $^{13}C/^{12}C$ ratio of atmospheric $CO_2$ in the past two centuries, *Nature*, v. 324, p. 237–238, 1986.

Fung, I., Prentice, K., Matthews, E., Lerner, J., and Russell, G., Three- dimensional tracer model study of atmospheric $CO_2$: Response to seasonal exchanges with the terrestrial biosphere, *Journal of Geophysical Research*, v. 88, p. 1281–1294, 1983.

Fung, I. Y., Tucker, C. J., and Prentice, K. C., Application of advanced very high resolution radiometer vegetation index to study atmosphere-biosphere exchange of $CO_2$, *Journal of Geophysical Research*, v. 92, p. 2999–3015, 1987.

Gill, A. E., and Rasmusson, E. M., The 1982–83 climate anomaly in the equatorial Pacific, *Nature*, v. 306, p. 229–234, 1983.

Goodman, H. S., and Francey, R. F., $^{13}C/^{12}C$ and $^{18}O/^{16}O$ in baseline $CO_2$, 1986, *Baseline Atmospheric Program (Australia)*, edited by B. W. Forgan and P. J. Fraser, Bureau of Meteorology, CSIRO, Canberra, Australia, p. 54–58, 1988.

Goudriaan, J., and Ajtay, G. L., The Possible Effects of Increased $CO_2$ on Photosynthesis, in *Scope 13: The Global Carbon Cycle*, edited by B. Bolin, E. T. Degens, S. Kempe, and P. Ketner, p. 237–249, John Wiley and Sons, New York, 1979.

Hansen, J., and Lebedeff, S., Global surface air temperatures: update through 1987, *Geophysical Research Letter*, no. 15, p. 323–326, 1988.

Heimann, M., and Keeling, C. D., Meridional eddy diffusion model of the transport of atmospheric carbon dioxide: 1. The seasonal carbon cycle over the tropical Pacific Ocean, *Journal of Geophysical Research*, v. 91, p. 7765–7781, 1986.

Heimann, M., and Keeling, C. D., A three-dimensional model of atmospheric $CO_2$ transport based on observed winds: 2. Model description and simulated tracer experiments, in *Aspects of Climate Variability in the Pacific and the Western Americas*, edited by D. H. Peterson, this volume, American Geophysical Union, Washington, DC, 1989.

Heimann, M., Keeling, C. D., and Tucker, C. J., A three-dimensional model of atmospheric $CO_2$ transport based on observed winds 3. Seasonal cycle and synoptic time scale variations, in *Aspects of Climate Variability in the Pacific and the Western Americas*, edited by D. H. Peterson, this volume, American Geophysical Union, Washington, DC, 1989.

Houghton, R. A., and Woodwell, G. M., Global climatic change, *Scientific American*, v. 260, no. 4, p. 36–44, 1989.

Houghton, R. A., Hobbie, J. E., Melillo, J. M., Moore, B., Peterson, B. J., Shaver, G. R., and Woodwell, G. M., Changes in the carbon content of terrestrial biota and soils between 1860 and 1980: A net release of $CO_2$ to the atmosphere, *Ecological Monograph*, no. 53, p. 235–262, 1983.

Houghton, R. A., Boone, R. D., Fruci, J. R., Hobbie, J. E., Melillo, J. M., Palm, C. A., Peterson, B. J., Shaver, G. R., Woodwell, G. M., Moore, B., Skole, D. L., and Myers, N., Geographic distribution of the biotic flux of carbon in 1980, *Tellus*, v. 39B, p. 122–139, 1987.

IMSL Library Reference Manual, ed. 9.2 (IMSL Inc., 7500 Bellair Blvd., Houston, TX 77036), Chapter R, 1985.

Jones, P. D., Wigley, T. M. L., and Wright, P. B., Global temperature variations between 1861 and 1984, *Nature*, v. 322, p. 430–434, 1986a.

Jones, P. D., Raper, S. C. B., Bradley, R. S., Diaz, H. F., Kelly, P. M., and Wigley, T. M. L., Northern hemisphere surface air temperature variations: 1851–1984, *Journal of Climate and Applied Meteorology*, v. 25, p. 161–179, 1986b.

Jones, P. D., Wigley, T. M. L., Folland, C. K., Parker, D. E., Angell, J. K., Lebedeff, S., and Hansen, J. E., Evidence for global warming in the past decade, *Nature*, v. 332, 790 p., 1988.

Keeling, C. D., The concentration and isotopic abundances of atmospheric carbon dioxide in rural areas, *Geochimica et Cosmochimica Acta*, v. 13, p. 322–334, 1958.

Keeling, C. D., The concentration and isotopic abundances of carbon dioxide in rural and marine air, *Geochimica et Cosmochimica Acta*, v. 24, p. 277–298, 1961.

Keeling, C. D., Carbon dioxide in surface ocean waters: 4. Global distribution, *Journal of Geophysical Research*, v. 73, p. 4543–4553, 1968.

Keeling, C. D., The carbon dioxide cycle: Reservoir models to depict the exchange of atmospheric carbon dioxide with the oceans and land plants, in *Chemistry of the Lower Atmosphere*, edited by S. I. Rasool, chap. 6, p. 251–329, Plenum Press, New York, 1973a.

Keeling, C. D., Industrial production of carbon dioxide from fossil fuels and limestone, *Tellus*, v. 25, p. 174–198, 1973b.

Keeling, C. D., The influence of Mauna Loa Observatory on the development of atmospheric $CO_2$ research, in *Mauna Loa Observatory a 20th Anniversary Report*, edited by J. Miller, p. 36–54, National Oceanographic and Atmospheric Administration, Special Report, 1978.

Keeling, C. D., Adjustments to Applied Physics infrared analyzer data to allow for differences in response of the various detectors used, 71 p., Scripps Institution of Oceanography, La Jolla, CA, 1988.

Keeling, C. D., and Heimann, M., Meridional eddy diffusion model of the transport of atmospheric carbon dioxide: 2. Mean annual carbon cycle, *Journal of Geophysical Research*, v. 91, p. 7782–7796, 1986.

Keeling, C. D., and Revelle, R., Effects of El Niño/Southern Oscillation on the atmospheric content of carbon dioxide, *Meteoritics*, v. 20, p. 437–450, 1985.

Keeling, C. D., Rakestraw, N. W., and Waterman, L. S., Carbon dioxide in surface waters of the Pacific Ocean: 1. Measurements of the distribution, *Journal of Geophysical Research*, v. 70, p. 6087–6097, 1965.

Keeling, C. D., Harris, T. B., and Wilkins, E. M., Concentration of atmospheric carbon dioxide at 500 and 700 millibars, *Journal of Geophysical Research*, v. 3, p. 4511–4528, 1968.

Keeling, C. D., Bacastow, R. B., Bainbridge, A. E., Ekdahl, C. A., Jr., Guenther, P. R., Waterman, L. S., and Chin, J. F. S., Atmospheric carbon dioxide variations at Mauna Loa Observatory, Hawaii, *Tellus*, v. 28, p. 538–551, 1976a.

Keeling, C. D., Adams, J. A., Jr., Ekdahl, C. A., Jr., and Guenther, P. R., Atmospheric carbon dioxide variations at the South Pole, *Tellus*, v. 28, p. 552–564, 1976b.

Keeling, C. D., Adams, J. A., Jr., and Ekdahl, C. A., Jr., Antarctic carbon dioxide project, Report 5, 94 p., Scripps Institution of Oceanography, La Jolla, CA, 1976c. (See footnote in Keeling et al. [1976b], p. 561).

Keeling, C. D., Mook, W. G., and Tans, P., Recent trends in the $^{13}C/^{12}C$ ratio of atmospheric carbon dioxide, *Nature*, v. 277, p. 121–123, 1979.

Keeling, C. D., Bacastow, R. B., and Tans, P., Predicted shift in the $^{13}C/^{12}C$ ratio of atmospheric carbon dioxide, *Geophysical Research Letters*, v. 7, p. 505–508, 1980.

Keeling, C. D., Bacastow, R. B., and Whorf, T. P., Measurements of the concentration of carbon dioxide at Mauna Loa Observatory, Hawaii, in *Carbon Dioxide Review: 1982*, edited by W. C. Clark, p. 377–385, Oxford University Press, 1982.

Keeling, C. D., Carter, A. F., and Mook, W. G., Seasonal, latitudinal, and secular variations in the abundance and isotopic ratios of atmospheric carbon dioxide: 2. Results from oceanographic cruises in the tropical Pacific Ocean, *Journal of Geophysical Research*, v. 89, p. 4615–4628, 1984.

Keeling, C. D., Guenther, P. R., and Moss, D. J., Scripps reference gas calibration system for carbon dioxide-in-air standards: Revision of 1985. Report No. 4 of the Environmental Monitoring Programme of the World Meteorological Organization, Geneva, 34 p. and Addendum, 43 p., 1986.

Keeling, C. D., Guenther, P. R., and Whorf, T. P., An analysis of the concentration of atmospheric carbon dioxide at fixed land stations, and over the oceans based on discrete samples and daily averaged continuous measurements, 451 p., Scripps Institution of Oceanography, La Jolla, CA, 1989a.

Keeling, C. D., Piper, S. C., and Heimann, M., A three-dimensional model of atmospheric $CO_2$ transport based on observed winds: 4. Mean annual gradients and interannual variations, in *Aspects of Climate Variability in the Pacific and the Western Americas*, edited by D. H. Peterson, this volume, American Geophysical Union, Washington, DC, 1989b.

Kelley, J. J., Jr., An analysis of Carbon Dioxide in the Arctic Atmosphere near Barrow, Alaska 1961 to 1967, *Contract N00014–67–A–0103–0007 NR 307–252*, 172 p., Scientific Report of the United States Office of Naval Research, 1969.

Kohlmaier, G. H., Siré, E., Janecek, A., Keeling, C. D., Piper, S. C., and Revelle, R., Modelling the seasonal contribution of a $CO_2$ fertilization effect of the terrestrial vegetation to the amplitude increase in atmospheric $CO_2$ at Mauna Loa Observatory, *Tellus*, in press, 1989.

Komhyr, W. D., Gammon, R. H., Harris, T. B., Waterman, L. S., Conway, T. J., Taylor, W. R., and Thoning, K. W., Global atmospheric $CO_2$ distribution and variations from 1968–1982 NOAA/GMCC $CO_2$ flask sample data, *Journal of Geophysical Research*, v. 90, p. 5567–5596, 1985.

Lange, O. L., Nobel, P. S., Osmond, C. B., Ziegler, H. (editors), *Physiological Plant Ecology II*, 747 p., Springer-Verlag, Berlin, 1982.

Lowe, D. C., Guenther, P. R., and Keeling, C. D., The concentration of atmospheric carbon dioxide at Baring Head, New Zealand, *Tellus*, v. 31, p. 58–67, 1979.

Maier-Reimer, E., and Hasselmann, K., Transport and storage in the ocean - An inorganic ocean-circulation carbon cycle model, *Climate Dynamics*, v. 2, p. 63–90, 1987.

Manning, M. R., and Pohl, K. P., A review of $CO_2$ in air calibration gas mixtures used at Baring Head, New Zealand, *Report INS–R–351*, 10 p., Institute of Nuclear Sciences, Department of Scientific & Industrial Research, Lower Hutt, New Zealand, 1986.

Marland, G., Fossil fuel $CO_2$ emissions: Three countries account for 50% in 1986, in CDIAC Communications, Oak Ridge National Laboratory, Oak Ridge, TN, p. 1–4, winter 1989.

Marland, G., and Rotty, R. M., Carbon dioxide emissions from fossil fuels: A procedure for estimation and results for 1950–1982, *Tellus*, v. 36B, p. 232–261, 1984.

Marland, G., R. M. Rotty, and Treat, N. L., $CO_2$ from fossil fuel

burning: Global distribution of emissions, *Tellus*, v. 37B, p. 243–258, 1985.

Meehl, G. A., The annual cycle and interannual variability in the tropical Pacific and Indian ocean regions, *Monthly Weather Review*, v. 115, p. 27–50, 1987.

Menard, H. W., and Smith, S. M., Hypsometry of ocean basin provinces, *Journal of Geophysical Research*, v. 81, p. 4305–4325, 1966.

Mitchell, J. F. B., The "Greenhouse" effect and climate change, *Reviews of Geophysics*, v. 27, p. 115–139, 1989.

Mook, W. G. and Grootes, P. M., The measuring procedure and corrections for the high-precision mass-spectrometric analysis of isotopic abundance ratios, especially referring to carbon, oxygen and nitrogen, *International Journal of Mass Spectrometry and Ion Physics*, v. 12, p. 273–298, 1973.

Mook, W. G., and Jongsma, J., The measurement of the $N_2O$ correction for $^{13}C/^{12}C$ ratios of atmospheric $CO_2$ by the removal of $N_2O$, *Tellus*, v. 39B, p. 96–99, 1987.

Mook, W. G., and Van der Hoek, S., The $N_2O$ correction in the carbon and oxygen isotopic analysis of atmospheric $CO_2$, *Isotope Geoscience*, v. 1, p. 237–242, 1983.

Mook, W. G., J. C. Bommerson, and Staverman, W. H., Carbon isotope fractionation between dissolved bicarbonate and gaseous carbon dioxide, *Earth and Planetary Science Letters*, v. 22, p. 169–176, 1974.

Mook, W. G., Koopmans, M., Carter, A. F., and Keeling, C. D., Seasonal, latitudinal, and secular variations in the abundance and isotopic ratios of atmospheric carbon dioxide: 1. Results from land stations, *Journal of Geophysical Research*, v. 88, p. 10915–10933, 1983.

Namias, J., Yuan, X., and Cayan, D. R., Persistence of north Pacific sea surface temperature and atmospheric flow patterns, *Journal of Climate*, v. 1, p. 682–703, 1988.

Neftel, A., Moor, E., Oeschger, H., and Stauffer, B., Evidence from polar ice cores for the increase in atmospheric $CO_2$ in the past two centuries, *Nature*, v. 315, p. 45–47, 1985.

Newell, N. E., Newell, R. E., Hsiung, J, and Zhongxiang, W., Global marine temperature variation and the solar magnetic cycle, *Geophysical Research Letters*, v. 16, p. 311–314, 1989.

Newell, R. E., Navato, A. R., and Hsiung, J., Long-term global sea surface temperature fluctuations and their possible influence on atmospheric $CO_2$ concentrations, *Pure and Applied Geophysics*, v. 116, p. 351–371, 1978.

Oeschger, H., Siegenthaler, U., Schotterer, U., and Gugelmann, A., A box diffusion model to study the carbon dioxide exchange in nature, *Tellus*, v. 27, p. 168–192, 1975.

O'Leary, M. H., Carbon isotope fractionation in plants, *Phytochemistry*, v. 20, p. 553–567, 1981.

Olsson, I. U., (editor), *Radiocarbon Variations and Absolute Chronology*, Twelth Nobel Symposium, Wiley-Interscience, New York, 1970.

Oort, A. H. and Pan, Y. H., Diagnosis of historical ENSO events, *Proceedings of the First WMO Workshop on the Diagnosis and Prediction of Monthly and Seasonal Atmospheric Variations over the Globe, Technical Document No. 87*, World Meteorological Organization, Geneva, p. 249–258, 1986.

Pearman, G. I., Pre-industrial atmospheric carbon dioxide levels: A recent assessment, *Search*, v. 15, p. 42–45, 1984.

Pearman, G. I., and Beardsmore, D. J., Atmospheric carbon dioxide measurements in the Australian region: ten years of aircraft data, *Tellus*, v. 36B, p. 1–24, 1984.

Peterson, B. J., and Melillo, J. M., The potential storage of carbon caused by eutrophication of the biosphere, *Tellus*, v. 37B, p. 117–127, 1985.

Prentice, K. C., The influence of the terrestrial biosphere on seasonal atmopsheric carbon dioxide: An empirical model, Ph.D. Thesis, 247 p., Columbia University, NY, 1986.

Rasmusson, E. M., El Niño: The ocean/atmosphere connection, *Oceanus*, v. 27, p. 5–12, 1984.

Rasmusson, E. M., and Carpenter, T. H., Variations in tropical sea surface temperature and surface wind fields associated with the southern oscillation/El Niño, *Monthly Weather Review* v. 110, p. 354–384, 1982.

Rasmusson, E. M., and Wallace, J. M., Meteorological aspects of the El Niño/Southern Oscillation, *Science*, v. 222, p. 1195–1202, 1983.

Reid, G. C., Influence of solar variability on global sea surface temperature, *Nature*, v. 329, p. 142–143, 1987.

Reinsch, C. H., Smoothing by spline functions, *Numerische Mathematik*, v. 10, p. 177–183, 1967.

Rotty, R. M., A look at 1983 $CO_2$ emissions from fossil fuels (with preliminary data for 1984), *Tellus*, v. 39B, p. 203–208, 1987.

Rust, B. W., Rotty, R. M., and Marland, G., Inferences drawn from atmospheric $CO_2$ data, *Journal of Geophysical Research*, v. 84, p. 3115–3122, 1979.

SCEP (Study of Critical Environmental Problems), *Man's Impact on the Global Environment*, Carroll L. Wilson, SCEP Director, 819 p., MIT Press, Cambridge, MA, 1970.

Schönwiese, C. -D., Northern hemisphere temperature statistics and forcing Part B: 1579–1980 AD, *Archives for Meteorology Geophysics and Bioclimatology*, Ser. B 35, p. 155–178, 1984.

Schönwiese, C. -D., and Malcher, J., The $CO_2$ temperature response. A comparison of the results from general circulation models with statistical assessments, *Journal of Climatology*, v. 7, p. 215–229, 1987.

Seitz, F., Bendetsen, K., Jastrow, R., and Nierenberg, W. A., *Scientific Perspectives on the Greenhouse Problem*, Technical Report, 35 p., George C. Marshall Institute, Washington, DC, 1989.

Semazzi, F. H. M., Mehta, V., and Sud, Y. C., An investigation of the relationship between sub-Saharan rainfall and global sea surface temperature, *Atmosphere-Ocean*, v. 26, p. 118–138, 1988.

Siegenthaler, U., Uptake of excess $CO_2$ by an outcrop-diffusion model of the ocean, *Journal of Geophysical Research*, v. 88, p. 3599–3608, 1983.

Siegenthaler, U., and Münnich, K. O., $^{13}C/^{12}C$ fractionation during $CO_2$ transfer from air to sea, in *SCOPE 16: Carbon Cycle Modelling*, edited by B. Bolin, p. 249–257, John Wiley and Sons, Chichester, 1981.

Siegenthaler, U. and Oeschger, H., Predicting future atmospheric carbon dioxide levels, *Science*, v. 199, p. 388–395, 1978.

Siegenthaler, U., and Oeschger, H., Biospheric $CO_2$ sources emissions during the past 200 years reconstructed by deconvolution of ice core data, *Tellus*, v. 39B, p. 140–154, 1987.

Singh, J. S., and Gupta, S. R., Plant decomposition and soil respiration in terrestrial ecosystems, *The Botanical Review*, v. 43, p. 449–528, 1977.

Stoeckenius, T., Interannual variations of tropical precipitation pat-

terns, *Monthly Weather Review,* v. 109, p. 1233–1247, 1981.

Strain, B. R., and Armentano, T., *Response of "Unmanaged" Ecosystems. Environmental and Societal Consequences of Carbon Dioxide Induced Climate Change,* (DOE/EV/10019–12), v. II, pt. 12, 45 p., U.S. Department of Energy, Washington, DC, available from NTIS, Springfield, VA, 1982.

Strain, B. R., and Cure, J. D., *Direct Effects of Increasing Carbon Dioxide on Vegetation,* (DOE/ER–0238), 286 p., U.S. Department of Energy, Washington, DC, available from NTIS, Springfield, VA, 1985.

Takahashi, T., Broecker, W. S., and Bainbridge, A. E., The alkalinity and total carbon dioxide concentration in the world oceans, in *SCOPE 16: Carbon Cycle Modelling,* edited by B. Bolin, p. 271–286, John Wiley and Sons, Chichester, 1981.

Tanaka, M., Nakazawa, T., and Aoki, S., Time and space variations of tropospheric carbon dioxide over Japan, *Tellus,* v. 39B, p. 3-12, 1987a.

Tanaka, M., Nakazawa, T., and Aoki, S., Seasonal and meridional variations of atmospheric carbon dioxide in the lower troposphere of the northern and southern hemispheres, *Tellus,* v. 39B, p. 29–41, 1987b.

Tanaka, M., Nakazawa, T., Shiobara, M., Ohshima, H., Aoki, S., Kawaguchi, S., Yamanouchi, T., Makino, Y., and Murayama, H., Variations of atmospheric carbon dioxide concentration at Syowa Station, Antarctica, *Tellus,* v. 39B, p. 72–79, 1987c.

Tans, P., $^{13}C/^{12}C$ of industrial $CO_2$, in *SCOPE 16: Carbon Cycle Modelling,* edited by B. Bolin, p. 127–129, John Wiley and Sons, Chichester, 1981.

Thompson, M. L., Enting, I. G., Pearman, G. I., and Hyson, P., Interannual variation of atmospheric $CO_2$ concentration, *Journal of Atmospheric Chemistry,* v. 4, p. 125–155, 1986.

Thoning, K. W., Tans, P., and Komhyr, W. D., Atmospheric carbon dioxide at Mauna Loa Observatory: 2. Analysis of the NOAA GMCC data, 1974–1985, *Journal of Geophysical Research,* v. 94, p. 8549–8565, 1989.

U.S. Department of Commerce, Solar Geophysical Data Prompt Report, no. 535, pt. 1, p. 11, 1989.

van Loon, H., The southern oscillation. Part III: Associations with the trades and with the trough in the westerlies of the South Pacific Ocean, *Monthly Weather Review,* v. 112, p. 947–954, 1984.

Verniani, F., The total mass of the earth's atmosphere. *Journal of Geophysical Research,* v. 71, p. 385–391, 1966.

Wagner, A. J., Seasonal climate summary: The global climate of March–May 1987: Moderately strong mature phase of ENSO with highly persistent monthly and seasonal temperature anomalies over the United States, *Monthly Weather Review,* v. 115, p. 3166–3187, 1987.

Weiss, R. F., Carbon dioxide in water and sea water: The solubility of a non-ideal gas, *Marine Chemistry,* v. 2, p. 203–215, 1974.

Weiss, R. F., The temporal and spatial distribution of tropospheric nitrous oxide, *Journal of Geophysical Research,* v. 86, p. 7185–7195, 1981.

WMO, Summary report on the status of the WMO background air pollution monitoring network as at (sic) May 1984, *Technical Document WMO/TD No. 13,* 21 p., The World Meteorological Organization, Geneva, 1984.

WMO, Provisional daily atmospheric carbon dioxide concentrations as measured at BAPMoN sites for the year 1983, *Technical Document WMO/TD No. 77,* Environmental Pollution Monitoring Programme, The World Meteorological Organization, Geneva, 53 p., 1985.

Woodwell, G. M., The Carbon Dioxide Problem, in *The Role of Terrestrial Vegetation in the Global Carbon Cycle,* edited by G. M. Woodwell, p. 3–17, John Wiley and Sons, New York, 1984.

Woodwell, G. M., Hobbie, J. E., Houghton, R. A., Melillo, J. M., Moore, B., Peterson, B. J., and Shaver, G. R., Global deforestation: Contribution to atmospheric carbon dioxide, *Science,* v. 22, p. 1081–1086, 1983.